Simulating Landscape and National Scale Carbon Fluxes in Canada's Terrestrial Ecosystems Using C-CLASS Model

By

Bin Chen

A Thesis
Submitted to the School of Graduate Studies
In Partial Fulfillment of the Requirements
for the Degree
Doctor of Philosophy

McMaster University

DOCTOR OF PHILOSOPHY (2012)
(Biogeosciences)

McMaster University
School of Geography
and Earth Sciences
Hamilton, Ontario, Canada

TITLE: Simulating Landscape and National Scale Carbon Fluxes in Terrestrial Ecosystems Using C-CLASS model

AUTHOR: Bin Chen

SUPERVISOR: Professor M. Altaf Arain

NUMBER OF PAGES: 286

ABSTRACT

Landscape-level understanding of forest carbon (C) dynamics is required to quantify the net contribution of forest biomes to the global C cycle and to help forest managers to understand the impacts of forest management activities to the C sequestration in forests. Landscape-level estimation of C exchanges in various ecosystems is also crucial for the validation of the Moderate Resolution Imaging Spectroradiometer (MODIS) derived Gross Primary Productivity (GPP) which may help in improving MODIS GPP algorithm and the estimation of national-scale C budget to meet Canada's international greenhouse gas inventory reporting obligations.

In this study, Carbon version of Canadian Land Surface Scheme (C-CLASS) was used to simulate historic C dynamics of a 2500 ha temperate Douglas fir forest landscape in Oyster River area of Vancouver Island in British Columbia from 1920 to 2005 and a 6275 ha boreal black spruce forest landscape at Chibougamau, Quebec from 1928 to 2005. The impacts of disturbance history and the climate variability on the landscape-level C stocks and fluxes were also investigated. The disturbance matrix of the Carbon Budget Model of the Canadian Forest Sector v3 (CBM-CFS3) was incorporated into C-CLASS to account for the removal of the C stocks by disturbance events. Study results indicate that GPP and autotrophic respiration (R_a) in the temperate Douglas fir forest landscape are sensitive to the air temperature variability. Stand replacing disturbance events can remove large amounts of C in the disturbed year, however, it takes a long period of time for the recovery of landscape-level total ecosystem carbon (TEC) to the initial state, which depends on forest age and the effects of historic climate variability. Our analysis further showed that in undisturbed forest landscape, simulated annual net ecosystem productivity (NEP) deviations were positively related to daily minimum and maximum temperatures in spring, while they were not sensitive to summer temperatures. Study results also showed that simulated landscape-level NEP is less sensitive to the changes in air temperature compared to other simulated C fluxes such as GPP, R_a and and heterotrophic respiration (R_h). Simulated landscape-level C stocks (aboveground biomass, belowground biomass, dead organic matter and soil organic matter) are sensitive to the changes in air temperature. This work suggests that the C-CLASS model can be used to investigate the impacts of climate variability and disturbance events on the historic C dynamics of forest landscapes. This study has also made it possible to analyze the importance of climate drivers and the development of methods for including climate sensitivity into inventory-based models.

In addition, C-CLASS simulated GPP over Canada's landmass (at 1-km resolution) in 2003 and its comparison with the MODIS GPP product (MOD17) indicated overestimation of MODIS GPP compared to the C-CLASS upscaled GPP over Canada's landmass. This overestimation was attributed to the limitations in the components of MODIS GPP algorithm. It further suggests that the parameterization of light use efficiency in MODIS GPP algorithm is amenable to improvement based on observations of light use efficiency at eddy covariance flux tower sites or the photochemical reflectance index derived from satellite remote sensing data.

This study would be helpful in calculating Canada's national terrestrial ecosystem C budget which is important for making environmental policies and ecosystem management for enhancing the terrestrial C sink.

ACKNOWLEDGEMENTS

I would like to thank my supervisor Dr. Altaf Arain for providing me opportunity and funding to pursue my Ph. D program. I am grateful for his instructions, patience, encouragement and constructive comments on the manuscripts. I appreciate his adivice and help in preparing me for my future academic career.

I would like to thank my committee members Dr. Jing Chen and Dr. Mike Waddington for their encouragement, valuable comments and criticism. I am especially grateful to Dr. Jing Chen for providing me all the input datasets needed for the C-CLASS model simulation over Canada's landmass. Advice and helpful comments from Dr. Paulin Coulibaly and William Morris for my Ph. D comprehensive exam are also acknowledged.

I would like to thank Dr. Sergey Mashchenko from the Department of Physics and Astronomy, McMaster University for his help in compiling and establishing C-CLASS model at the SHARCNET.

I would like to thank all the collegues from the McMaster Hydrometeorology and Climatology Research Group for all the funny talks we had in the lab. Specifically, I would like to thank Suo Huang and Jason Brodeur for their valuable support in Matlab scripts and modeling issues. Also, my several trips to Turkey Point sites with Matthias Peichl, Myroslava Khomik, Jason Brodeur and Samantha Mackay for help in field work were fun and a different learning experience.

I also would like to give thanks to the staff in SGES main office for their friendly assistance in administrative matters and Patrick De Luca for his GIS technical assistance. In addition, I appreciate Ric Hamiton for the help in printing my posters for every conference I attended and Mike Malott from Research and High-Performance Computing Support, McMaster University for his help in the maintenance and backup of my datasets.

I appreciate the financial support from the Canadian Foundation for Climate and Atmospheric Sciences (CFCAS) and the National Sciences and Engineering Research Council (NSERC) through Fluxnet Canada Research Network (FCRN) and Canadian Carbon Program (CCP) and Ontario Ministry of Environment. I am thankful for graduate scholarship and teaching/research assistantships. I also acknowledge to Shared Hierarchical Academic Research Computing Network (SHARCNET) for its sufficient computing resources provided for the support of my research.

Thanks to all my friends at the Hamilton Grace Mandarin Alliance Church. Becoming a Christian is one of the most important things in my life. I really enjoyed all the happy time in the church.

Finally, I would like to thank my parents, Baosen Chen and Huirong Li for giving me encouragement, love and support so that I can freely pursue my dream in Canada.

TABLE OF CONTENTS

LIST OF FIGURES

LIST OF TABLES

PREFACE

This thesis consists of three manuscripts. In addition, two model inter-comparison papers included in the appendix A and B have already been published. This candidate performed C-CLASS model simulation for these model inter-compariosn papers and provided comments on several versions of manuscripts. Although, there is some overlap in description of methodology, each manuscript contains additional information which is specific and relevant to the respective study and each chapter provides unique results. Because of the extensive amount of data and effort required in this type of research, all work in this thesis represents a collaborative effort from a number of contributors. The specific contribution from the Ph. D candidate and from co-authors is described below:

Chapter 2
Title: Evaluating the impacts of disturbance regimes and climate variability on the historic carbon budget of a Pacific Northwestern Forest Landscape

Authorship: Bin. Chen, M. Altaf Arain, Jagadeesh Yeluripati, Ziyu Wang, Robert F. Grant, G. Stinson, Werner. A. Kurz, J. A. Trofymow

Status: To be submitted to Forest Ecology and Managment

Candidate's contribution: The Ph.D candidate contributed to the processing of the soil, disturbance and meteorological data and the preparation of initialization files for C-CLASS model simulation. He incorporated the disturbance matrix of Carbon Budget Model of the Canadian Forest Sector (CBM-CFS3) into C-CLASS model. He performanced of model simulation, analyzed model results and write manuscript. Altaf Arain secured funding for the research and provided valuable feedback on the manuscript. Jagadeesh Yeluripati contributed in initial model input data and MATLAB scripts to used in data preprocessing. Ziyu Wang was responsible for the maintenance of FTP which provided all the input data required in this paper. Dr. Grant, Dr. Stinson, Dr. Kurz and Dr. Trofymow provided intellectual and editorial input to this manuscript.

Chapter 3
Title: Historic Carbon Dynamics of an Eastern Boreal Black Spruce Forest Landscape in Canada

Authorship: Bin Chen, M. Altaf Arain, Ziyu Wang, Robet F. Grant, Werner A. Kurz, Pierre Bernier, Luc Guindon, David Price

Status: To be submitted to Ecological Modeling.

Candidate's contribution: The Ph.D candidate contributed to the processing of the soil, disturbance and meteorological data and the preparation of initial files for C-CLASS model simulation. He incorporated the disturbance matrix of Carbon Budget Model of the Canadian Forest Sector (CBM-CFS3) into C-CLASS model. He conducted model simulations, analyzed model results and wrote manuscript. Altaf Arain secured funding for the research and provided valuable criticism on the manuscript. Ziyu Wang maintenanced FTP archive which provided all

the input data required in this paper. Dr. Grant, Dr. Werner Kurz, Dr. Pierre Bernier, Dr. Luc Guindon and Dr. David Price provided intellectual input to this manuscript.

Chapter 4
Title: Scaling Gross Primary Productivity (GPP) over Canada's Landmass in support of MODIS GPP product validation

Authorship: Bin Chen, M. Altaf Arain, Jing M. Chen, Gang Mo, Jane Liu

Status: To be submitted to Remote Sensing of Environment.

Candidate's contribution: The Ph. D candidate contributed to the input data processing and the preparation of initial files for C-CLASS model simulations. He established C-CLASS model at the Shared Hierarchical Academic Research Computing Network (SHARCNET) cluster in serial farming mode, performed mode simulations, analyszed model results and wrote manuscript. Dr. Jing Chen provided the esential spatial input data sets, including forcing data, soil data, leaf area index and ecozone map for C-CLASS model simulation over Canada's landmass. Gang Mo from Dr. Jing Chen's group helped in processing NCEP meteorological data and provided the C3/C4 spatial distribution data. Jane Liu from Dr. Jing Chen's group helped in the input/output data projections and ecozone map of Canada. Dr. Jing Chen also gave constructive comments on the manuscript. Altaf Arain secured funding for the research and provided feedback on the manuscript.

Appendix A
Title: Evaluating weather effects on interannual variation in net ecosystem productivity of a coastal temperate forest landscape: a model intercomparison

Authorship: Ziyu Wang, Robert F. Grant, M. Altaf Arain, Bin Chen, N. Coops, Robbie Hember, Werner A. Kurz, David T. Price, G. Stinson, J. A. Trofymow, J. Yeluripati, Baozhang Chen

*Status:*Published in Ecological Modelling, 222(17): 3236-3249 (2011).

Candidate's contribution: The Ph.D candidate contributed to the processing of the soil, disturbance and meteorological data and the preparation of initial files for C-CLASS model simulations. He incorporated the disturbance matrix of Carbon Budget Model of the Canadian Forest Sector (CBM-CFS3) into C-CLASS model. He was responsible for the performance of C-CLASS model simulation. Ziyu Wang had the lead role in the *ecosys* model simulations, the interpretation of different model results and manuscript write up. J. A. Trofymow was responsible for the CBM-CFS3 model simulations. David T. Price was responsible for the Can-IBIS model simulations. Robbie Hember was responsible for the 3PG model simulations. Robert Grant, Altaf Arain, N. Coops, Werner Kurz, G. Stinson, J. Yeluripati and Baozhang Chen provided intellectual input to this paper.

Appendix B
Title: Model intercomparison to evaluate climate and disturbance effects on interannual variation in net ecosystem productivity of a boreal forest landscape

Authorship: Ziyu Wang, Robert F. Grant, Altaf Arain, Pierre Bernier, Bin Chen, Jing Chen, Ajit Govind, L. Guindon, Werner A. Kurz, Changhui Peng, David T. Price, G. Stinson, Jianfeng Sun, J. A. Trofymow, J. Yeluripati

Status: Submitted to Ecological Modelling and is under review (2011).

Candidate's contribution: In this paper, the Ph.D candidate contributed by processing the soil, disturbance and meteorological data and the preparation of initial files for C-CLASS model simulations. He incorporated the disturbance matrix of Carbon Budget Model of the Canadian Forest Sector (CBM-CFS3) into C-CLASS model. He was responsible for the performance of C-CLASS model simulation. Ziyu Wang had the lead role of the *ecosys* model simulations, the interpretation of different model results and manuscript write up. Pierre Bernier was responsible for the CBM-CFS3 model simulations. David T. Price was responsible for the Can-IBIS model simulations. Ajit Govind was responsible for the InTEC model simulations. Jianfeng Sun was responsible for the TRIPLEX model simulations. Robert Grant, Altaf Arain, Jing Chen, L. Guindon, Werner Kurz, Changhui Peng, G. Stinson, J. Yeluripati and J. A. Trofymow provided intellectual contributions.

CHAPTER 1:
INTRODUCTION

1.1 Overview of Global Carbon Cycle

Carbon cycling is one of the most important terrestrial ecosystem processes which have been intensively studied. The knowledge and understanding of the Earth's contemporary carbon budget have advanced significantly since the Intergovernmental Panel on Climate Change (IPCC) Fourth Assessment Report (Solomon et al., 2007). Efforts to control climate change require the stabilization of atmospheric CO_2 concentrations, which can only be achieved through a drastic reduction of global CO_2 emissions. Yet fossil fuel emissions increased by 29% between 2000 and 2008, , due to production and international trade of goods and services in both developed and emerging economies and from the use of coal and gas as primary fuel sources (Le Quere et al., 2009). In contrast, emissions from land-use changes (LUC) were nearly constant (Houghton, 2003; Mouillot and Field, 2005; van der Werf et al., 2006; Canadell et al., 2007). In the past 50 years, the fraction of CO_2 emissions that remains in the atmosphere each year has increased from about 40% to 45%, and models suggested that this trend was caused by a decrease in the uptake of CO_2 by the terrestrial carbon sinks in response to climate change and variability (Le Quere et al., 2009). Changes in the terrestrial C sinks are highly uncertain, but they could have a significant influence on future atmospheric CO_2 levels (Solomon et al., 2007). Thus, it is crucial to reduce the uncertainties in estimating terrestrial carbon sinks.

Observations of atmospheric oxygen concentrations and carbon isotopes have helped to constrain the magnitude of global-scale carbon uptake by oceans and terrestrial ecosystems

(Rayner et al., 1999; Battle et al., 2000). CO_2 inversion studies using atmospheric-transport models indicate that temperate and boreal region of the Northern Hemisphere was a carbon sink of 0.6-2.7 Pg C yr^{-1} during the mid 1980s and mid 1990s (Rayner et al., 1999; Bousquet et al., 2000; Battle et al., 2000). Ciais et al. (2010) estimated the northern hemisphere (NH) terrestrial carbon sink by comparing four recent atmospheric inversion model estimates with land-based carbon accounting data for six large northern regions (Canada, USA, Mexico, Europe, Russia and China). They found that the mean NH terrestrial CO_2 sink from the inversion models is 1.7 Pg C yr^{-1} over the period of 2000-2004 and the inversion estimates agreed, within their uncertainty limits, across the Earth's longitude, with Russia being the largest sink. (Rodenbeck et al., 2003; Peylin et al., 2005; Peters et al., 2007; Peters et al., 2010). These results confirmed the continued critical role of NH terrestrial ecosystems in slowing down the atmospheric accumulation of anthropogenic CO_2 (Ciais et al., 2010).

In addition, national forest inventories can be used to provide complementary, ground-based estimation of large-scale carbon budgets that can help to identify the location of carbon sources and sinks. Using forest inventory data and long-term ecosystem carbon studies, Pan et al. (2011) estimated a global net forest sink of 1.11 ± 0.82 Pg C yr^{-1} during the period of 1990-2007 which was the residue of a total carbon sink of 2.41 ± 0.42 Pg C yr^{-1} in the global established forest and a tropical land-use change emission of 1.30 ± 0.70 Pg C yr^{-1} with tropical carbon sink/source estimates having the largest uncertainties (Pan et al., 2011).

Beer et al. (2010) provided an observation-based estimation of terrestrial gross primary production (GPP) of 123 ± 8 Pg C yr^{-1} using eddy covariance flux data and various diagnostic models. This study also indicated that tropical forests and savannahs accounted for 60% of global

terrestrial GPP (Beer et al., 2010). They found that GPP over 40% of the vegetated land has strong correlation with precipitation (Beer et al., 2010).

Mahecha et al. (2010) approximated the sensitivity of terrestrial ecosystem respiration to air temperature (Q_{10}) across 60 FLUXNET sites using a methodology that circumvented confounding effects of environmental constraints (i.e. physical protection, chemical protection, drought, flooding and freezing) (Mahecha et al., 2010; Davidson and Janssens, 2006) . Mahecha et al. (2010) suggested that Q_{10} which is independent of mean annual temperature, do not differ among biomes and is confined to values around 1.4 ± 0.1 and this results may partly explain a less pronounced climate-carbon cycle feedback than suggested by current carbon cycle climate models (Mahecha et al., 2010).

Piao et al. (2009) evaluated how climate change, rising atmospheric CO_2 concentration, and land use change influenced the terrestrial carbon cycle of the 20th century using a process-oriented terrestrial biosphere model (ORCHIDEE). Piao et al. estimated that about 129 Pg of C was emitted to the atmosphere from the land use change over the last century (Piao et al., 2009). However, about 76% (98 Pg C) of this emission was offset by net carbon uptake on land that was driven by climate changes and rising atmospheric CO_2 concentration. Piao et al. further suggested that the modeled net release of carbon from the terrestrial ecosystems to the atmosphere over 1901-2002 was about 31 Pg C. Piao et al. (2008) used the ORCHIDEE model and satellite vegetation greenness index observations to investigate the observed seasonal response of northern ecosystems to autumn warming (Piao et al., 2008). They found that both photosynthesis and respiration increased during autumn warming, but the increase in respiration is greater while warming increases photosynthesis more than respiration in spring (Piao et al., 2008). This study indicated that northern terrestrial ecosystems may currently lose CO_2 in response to autumn

warming, with a sensitivity of about 0.2 Pg C $^{\circ}C^{-1}$, offsetting 90% of the increased CO_2 uptake during spring (Piao et al., 2008). Piao et al. (2008) concluded that the carbon sequestration ability of northern ecosystems may be diminished earlier than previously suggested if future autumn warming occurs at a faster rate than in spring (Piao et al., 2008).

The greenhouse gas balance of Canada's managed forests is strongly affected by naturally occurring fire with high inter-annual variability in the area burned and by cyclical insect outbreaks (Kurz et al., 2008). Taking these disturbances into account, Kurz et al. (2008) used the Carbon Budget Model of the Canadian Forest Sector (CBM-CFS3) to project that Canada's managed forests could be a carbon source of between 30 and 245 Mt CO_2 yr^{-1} during the first Kyoto Protocol commitment period (2008-2012). This study also indicated a recent transition of carbon sink to source in Canada's forests which was the result of large insect outbreaks (Kurz et al., 2008). Metsaranta et al. (2010) further used the CBM-CFS3 model to make probabilistic forecasts of the recovery of carbon sinks in Canada's managed forest between 2010 and 2100 under two assumptions about future area burned by wildfire: (1) no increase relative to levels observed in the last half of the 20th century and (2) linear increases by a factor of two or four (depending on region) from 2010 and 2100. This study indicated that the recovery of strong carbon sinks in Canada's managed forest will be delayed until at least the 2030s because of insect outbreaks, even if predicted increases in area annually burned do not occur (Metsaranta et al., 2010). After 2050, this study project an annual sink near 70% with no increase in area burned and 35% with increasing area burned (Metsaranta et al., 2010). In this study, all simulations projected a cumulative carbon source from 2010-2100, even if annual area burned does not increase (Metsaranta et al., 2010).

Chen et al. (2003) used Integrated Terrestrial Ecosystem Carbon (InTEC) model to estimate the annual spatial distributions of carbon sources and sinks in Canada's forests at 1-km resolution

from 1901 to 1998 (Chen et al., 2003). Their study indicated large spatial variations in the carbon sink and source strength of Canada's forests corresponding to the patchiness of recent fire scars and productive forests. They are found a general south-to-north gradient of decreasing carbon sink strength and increasing carbon source which resulted mostly from differential effects of temperature increase on growing season length, nutrient mineralization and heterotrophic respiration at different latitudes as well as due to uneven nitrogen deposition (Chen et al., 2003). Ju et al. (2006) incorporated a three-dimensional hydrological module and an explicit parameterization of wetlands into the Integrated Terrestrial Ecosystem Carbon-budget model (InTEC V3.0) and used this model to study the hydrological effects on carbon cycles of Canada's forests and wetlands (Ju et al., 2006). It was found that the inclusion of the hydrological module considerably improved the model's ability to simulate carbon content and balances in different ecosystems and the InTEC V3.0 model predicted an annual net carbon uptake of 111.9 Tg C yr^{-1} by Canada's forests and wetlands over 1901-1998 of (Ju et al., 2006). In addition, Ju et al. (2008) conducted six simulations with different input scenarios of climate, CO_2 and nitrogen deposition to study the changes of soil carbon content in Canada's forests and wetlands. The simulated total carbon stored in Canada's forest and wetland soils was 164.5 Pg C and accounted for 7% of the global total carbon estimate of 2400 Pg C over 2 m depth (Ju and Chen, 2008). This study indicated that the climate influenced growing conditions, growing season length, net N mineralization, and N fixation and therefore the climate variability was the biggest driver of the increase in total soil carbon content of Canada's forests and wetlands during 1901-2000, followed by CO_2 fertilization and N deposition (Ju and Chen, 2008).

These measurement and modeling studies indicate that overall, the temporal patterns of global carbon fluxes are now relatively well understood but spatial patterns are more poorly resolved, with considerable variation among various studies.

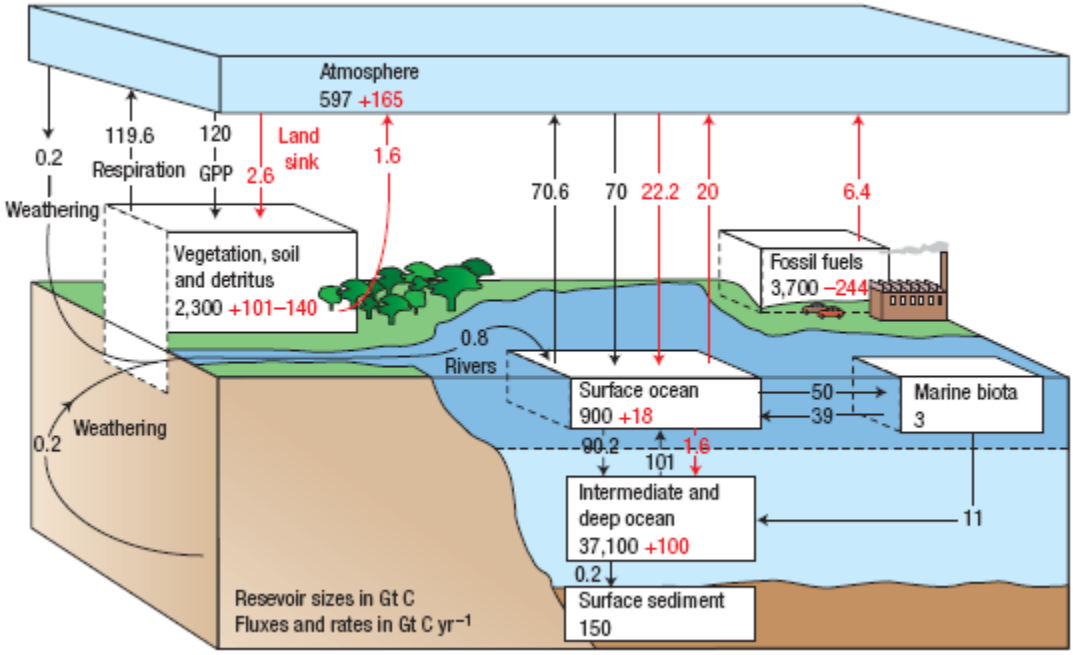

Figure 1. 1 The global carbon cycle in the 1990s. This shows the main annual fluxes in units of Gt C yr-1, with pre-industrial 'natural' fluxes in black and 'anthropogenic' fluxes in red. The net terrestrial loss is inferred from cumulative fossil fuel emissions minus atmospheric increase minus ocean storage. Gross fluxes generally have uncertainties of more than ±20%. Atmospheric C content and all cumulative fluxes since 1750 are as of the end of 1994, from IPCC 2007.

1.2 Carbon Cycle and Climate Change

The main goal of the carbon cycle research community in responding to the climate change challenge is to understand the role of the natural and managed carbon cycle in the dynamics of the climate system (Canadell et al., 2010). That requires quantifying the effect of human activities on the carbon cycle (Raupach and Canadell, 2010); determining the response of natural systems to these disturbances; projecting future behavior of carbon pools and fluxes; and exploring pathways

to atmospheric stabilization through the management of the carbon-climate-human system (Canadell et al., 2010).

The coupled carbon-climate modeling studies reported in the literature demonstrate a positive feedback between terrestrial carbon cycles and climate warming (Friedlingstein et al., 2001; Friedlingstein et al., 2003; Friedlingstein et al., 2006). A primary mechanism underlying the modeled positive feedback is the sensitivity of photosynthesis and respiration processes to temperature. Field studies, however, suggest much diverse mechanisms driving ecosystem responses to climate warming, including extended growing seasons, enhanced nutrient availability, shift in disturbance regimes and species composition, and altered ecosystem-water dynamics. These mechanisms work at different temporal and spatial scales and introduce more possibilities of carbon-climate feedbacks. Qian et al. (2010) investigated the terrestrial carbon storage in the northern high latitudes (NHL; poleward of 60˚N) based on 10 models from the Coupled Carbon Cycle Climate Model Intercomparison Project (C4MIP). It was found that both CO_2 fertilization and warming enhance vegetation growth in the NHL (Qian et al., 2010). Although the intense warming there enhances SOM decomposition, soil organic carbon (SOC) storage continues to increase in 21st century due to more litterfall into the soil resulting from higher vegetation productivity (Qian et al., 2010). However, the projected growth rate of SOC begins to level off after 2060 when SOM decomposition accelerates at high temperature and then catches up with the increasing input from vegetation turnover (Qian et al., 2010). Such competing mechanisms may lead to a switch of the NHL SOC pool from a sink to a source after 2100 under more intense warming, but large uncertainty exists due to our incomplete understanding of processes such as the strength of the CO_2 fertilization effect, permafrost, and the role of soil moisture (Qian et al., 2010). Unlike the CO_2 fertilization effect that enhances vegetation productivity across the world,

global warming increases the productivity at high latitudes but tends to reduce it in the tropics and mid-latitudes and these effects are further enhanced as a result of positive carbon cycle-climate feedbacks due to additional CO_2 and warming (Qian et al., 2010).

Climate models are necessary tools to simulate and understand these feedbacks and ecosystem responses to climate change. However, we have not developed necessary insights and modeling algorithms to adequately simulate ecosystem responses to climate change. Also to further constrain simulations of carbon-climate feedbacks, more empirical data sets are required across a wide range of biomes and closer interactions between models and field experiments (Luo, 2007).

1.3 Modeling of Carbon Dynamics in Terrestrial Ecosystems

Eddy covariance flux towers and eco-physiological measurements can provide process level understanding of ecosystem function. However, there will not be enough eddy covariance flux towers or field measurements which can adequately characterize spatial patterns and temporal dynamics of terrestrial ecosystems. Ecosystem models must then be used to upscale the eddy covariance flux measurements in time and space (Running et al., 1999). Therefore, models are critical tools for making regional and global assessments of the changes in the terrestrial biosphere (Waring and Running, 1998). Process-based models also have the potential for predicting how ecosystems will respond to elevated atmospheric CO_2 concentration and various future climate change scenarios. Therefore, simulations of C dynamics in terrestrial ecosystems have been the primary objective of various modeling groups across the world. In the past thirty years, a wide variety of ecosystem models have emerged in order to elucidate regional and global terrestrial ecosystem processes (Pitman, 2003). The current biosphere models can be categorized as follows:

1. Land Surface Models (LSM) which is an important component of General Circulation Models (GCMs) represents the processes coupling the land surface to the atmosphere. Land surface models simulate energy, water, momentum and CO_2 exchange of the soil-vegetation-atmosphere system and are specifically used in large-scale climate applications (Verseghy, 2000).

2. Terrestrial biogeochemistry models (e.g. TEM (Tian et al., 1999), CENTURY (Parton et al., 1987) and BGC (Running and Coughlan, 1988)) simulate the flow of carbon and mineral nutrients within and between vegetation, detritus, and soil organic matter pools. These models usually operate with geographically prescribed vegetation and soil types to examine global patterns of net primary productivity, carbon storage and nutrient cycling (Foley et al., 1996).

3. Dynamic Global Vegetation Models (DGVMs) are used to simulate vegetation structure and biogeography in response to climate change and its feedbacks. These types of model (e.g. LPJ (Sitch et al., 2003), IBIS (Foley et al., 1996), CLM-DVGM (Levis et al., 2004), TRIFFID (Cox, 2001), ORCHIDEE (Gervois et al., 2004) and CTEM (Arora and Boer, 2005)) includes mechanistic formulations of biogeochemical fluxes as well as transient vegetation dynamics, including: establishment, productivity and competition for resources, resource allocation, growth, disturbance and mortality.

Canadian Land Surface Scheme (CLASS; (Verseghy, 1991; Verseghy et al., 1993; Verseghy, 2000) is used as land boundary in the Canadian Global Climate Model (CGCM) – one of the global climate models used in IPCC assessments. CLASS can also be run in uncoupled or offline mode with meteorological data from a separate atmospheric system or from observational data.

CLASS identifies up to five vegetation or land cover types in each grid cell i.e. needleleaf trees, broadleaf trees, crops, grasses and urban areas. The soil profiles are divided into three layers (0.10, 0.25 and 3.75 m thick), while snow is treated as an analogous of the fourth soil layer with variable depth.

CLASS has been further improved by incorporating the two-leaf (sun-lit and shaded) canopy conductance and photosynthesis modules and soil and plant respiration algorithms (Arain et al., 2002; Kothavala et al., 2005) and plant-soil nitrogen algorithms to address the carbon and nitrogen coupled processes in the vegetation ecosystems (Arain et al., 2006; Yuan et al., 2007). This model is named as the Carbon and Nitrogen coupled Canadian Land Surface Scheme (CN-CLASS; Arain et al., 2006). Carbon and nitrogen algorithms of CN-CLASS and their testing over various ecosystems have provided necessary insights and formulations to further develop and improve carbon dynamics in CGCM and CTEM models (Huang et al., 2011).

In the past, C-CLASS or CN-CLASS have been extensively used in site-specific and site-level synthesis studies for simulating land-atmosphere exchanges of energy, water and carbon fluxes for a range of terrestrial ecosystems and to investigate the role of primary climatic controls and site specific carbon stocks on carbon dynamics of various terrestrial ecosystems (Arain et al., 2002; Arain et al., 2006; Kothavala et al., 2005; Yuan et al., 2007; Yuan et al., 2008). However, the C-CLASS model has not been tested over large spatial scales, including landscape and national scales. The development of spatial explicit datasets for ecosystem model testing and validation is a challenging and intensive task and very few such datasets exist. Recently, in the historical carbon modeling project, the detailed and spatial explicit record of forest conditions and disturbance events have been compiled at the Oyster River forest landscape, Vancouver Island, British Columbia (Trofymow et al., 2008) and the Chibougamau forest landscape, Quebec

(Bernier et al., 2010). Recent advances in satellite remote sensing provide regional and global spatial coverage of terrestrial carbon dynamics at 1-km spatial resolution such as the Moderate Resolution Imaging Spectroradiometer (MODIS) GPP product (Running et al., 2000). Using landscape or national scale spatial explicit datasets, the ecosystem models such as C-CLASS can have the capability of simulating the carbon cycle of terrestrial ecosystems. In return, well calibrated ecosystem models may also help to validate and improve the MODIS GPP algorithms (Running et al., 2000).

In this thesis, C-CLASS model was used to study the impacts of disturbance regimes and climate variability on the historical carbon dynamics in two forested landscapes in Canada and the gross primary productivity (GPP) of Canada's landmass at 1-km resolution in order to evaluate and validate MODIS GPP product. Eddy covariance measured flux data from Fluxnet-Canada Research Network (FCRN) tower sites were also used to calibrate the C-CLASS model before the performance of model simulation.

1.4 Study Objectives

The specific objectives of this thesis are to:

1) Investigate the impact of climate variability on the historic carbon dynamics over the past several decades at a temperate Douglas-fir forest landscape in western Canada at the Oyster River in British Columbia and a boreal black spruce forest landscape at Chibougamau, Quebec using C-CLASS model.

2) Explore the impact of historic disturbance events on the variations in carbon fluxes and carbon stocks at both temperate and boreal forest landscapes.

3) Provide high resolution and spatially explicit process-based model simulated C stock and flux maps of forest landscapes at the Oyster River and Chibougamau study area.

4) Simulate gross primary productivity (GPP) over the Canadian landmass at 1-km resolution.

5) Compare C-CLASS simulated GPP with MODIS derived GPP at national scale to validate MODIS GPP algorithms and to explore the possible improvement of MODIS GPP parameterization.

1.5 Study areas

The Oyster River study area is located in the Georgia Basin, on the eastern side of Vancouver Island, British Columbia, Canada within the Coastal Western Hemlock very dry maritime biogeoclimatic subzone (CWHxm). The 5 km × 5 km (2500 ha) study area is bisected by the Oyster River and is the location of two of the three flux tower sites (DF49, intermediate aged second-growth stand established in 1949; HDF00, recent third-growth clear-cut established in 2000; HDF88, juvenile third-growth pole/sapling stand established in 1988) that make up the Fluxnet Canada coastal BC flux station (Trofymow et al., 2008).

The Chibougamau forest landscape is located southeast of Chibougamau, Quebec, Canada. This 6275 ha boreal forest landscape is the location of a Fluxnet Canada Research Network (FCRN) eddy covariance flux tower in operation since 2003 (Bernier et al., 2010). Canada's landmass is 8,179,928 km^2 of which there are 3,153,046 km^2 forests, 493,580 km^2 shrubland, 480,217 km^2 cropland, 958,226 km^2 grassland, 36,001 km^2 wetland and 3,058,858 km^2 non-productive areas (burnt area, barren land, snow/ice and urban area).

1.6 Carbon Cycle terminologies

1.6.1 Gross primary productivity (GPP)

Gross primary productivity (GPP) is the sum of the photosynthesis by all leaves measured at the ecosystem scale. It is typically integrated over time periods of days to a year (g C m^{-2} yr^{-1}) and is the process by which carbon and energy enter ecosystems. GPP is generally simulated from ecosystem models rather than measured directly, because it is impossible to measure the net carbon exchange of all the leaves in the canopy in isolation from other ecosystem components of carbon fluxes (e.g. autotrophic respiration from the plant and heterotrophic respiration in the soil) and without modifying the vertical gradient in environment. Ecosystem differences in GPP are determined primarily by leaf area index and the duration of the photosynthetic season and secondarily by the environmental controls over photosynthesis (Chapin III et al., 2002).

1.6.2 Net primary productivity (NPP)

Net primary productivity (NPP) is the net carbon gain by vegetation and it is the balance between the carbon gained by gross primary productivity and carbon released by plant mitochondrial respiration.

$$NPP = GPP - R_{plant} \quad (1.1)$$

Like GPP, NPP is generally measured at the ecosystem scale, usually over relatively long time intervals, such as a year (g C m^{-2} yr^{-1}). NPP includes the new biomass produced by plants, the soluble organic compounds that diffuse or are secreted by roots into the soil (root exudation), the carbon transfers to microbes that are symbiotically associated with roots (e.g. mycorrhizae and

nitrogen-fixing bacteria), and the volatile emissions that are lost from leaves to the atmosphere (Clark et al., 2001). Most field measurements of NPP document only the new plant biomass produced and therefore probably underestimate the true NPP by at least 30% (Chapin III et al., 2002). A frequent objective of measuring NPP, for instance, is to estimate the rate of biomass increment. Root exudates, transfers to symbionts, losses to herbivores, and volatile emissions are lost from plants and therefore do not directly contribute to biomass increment. Consequently, failure to measure these components of NPP does not bias estimates of biomass accumulation (Chapin III et al., 2002). However, these losses of NPP from plants fuel other ecosystem processes such as herbivory, decomposition, and nutrient turnover and so are important components of the overall carbon dynamics of ecosystems and a critical carbon source for microbes.

1.6.3 Net ecosystem productivity (NEP)

Net ecosystem productivity (NEP) is the net accumulation of carbon by an ecosystem. It is the balance between carbon entering and leaving the ecosystem. Most carbon enters the ecosystem as gross primary productivity and leaves through several processes, including plant autotrophic respiration and heterotrophic respiration in the soil, leaching, plant volatile emissions and methane flux (Chapin III et al., 2002). NEP equals to NPP minus heterotrophic respiration (R_h)

$$NEP = NPP - R_h \quad (1.2)$$

NEP is ecologically important because it represents the increment in carbon stored by an ecosystem. When integrated globally, NEP determines the impact of the terrestrial biosphere on the atmospheric CO_2 concentration, which strongly affects climate and the amount of carbon transferred to oceans (Chapin III et al., 2002). In ecosystems that have not recently experienced disturbance, NEP is a small net difference between two large fluxes: (1) photosynthetic carbon

gain and (2) carbon loss through respiration (primarily plants and microbes) and leaching. During the season of peak plant growth, NEP is positive because photosynthesis exceeds respiration. In winter, when photosynthesis is low, NEP is negative and is mainly due to heterotrophic respiration. Thus, carbon uptake seldom balances carbon loss from ecosystems at any point in the season cycle.

1.6.4 Net biome productivity (NBP)

Net biome productivity (NBP) is the net ecosystem carbon balance (NECB) estimated at large temporal and spatial scales. This concept was developed to account for many of the fluxes seldom measured by net ecosystem exchange (NEE or -NEP) and explicitly includes disturbances such as fire that remove carbon from the ecosystem via nonrespiratory processes in addition to disturbances that redistribute carbon from the biomass into detrital carbon pools (Chapin et al., 2006). Therefore, net biome productivity can be viewed as the spatial and temporal average of NECB over a heterogeneous landscape:

$$NBP = \frac{\iint_{TA} NECB(x,t)dxdt}{T \cdot A} \tag{1.3}$$

where A is the land surface area considered, T is the temporal extent of the integration, and x and t are the spatial and temporal coordinates.

1.7 References

Arain, M.A., Black, T.A., Barr, A.G., Jarvis, P.G., Massheder, J.M., Verseghy, D.L., Nesic, Z., 2002. Effects of seasonal and interannual climate variability on net ecosystem productivity of boreal deciduous and conifer forests. Canadian Journal of Forest Research 32(5): 878-891.

Arain, M.A., Yuan, F., Andrew Black, T., 2006. Soil-plant nitrogen cycling modulated carbon exchanges in a western temperate conifer forest in Canada. Agric. Forest Meteorol. 140(1-4): 171-192.

Arora, V.K., Boer, G.J., 2005. Fire as an interactive component of dynamic vegetation models. J. Geophys. Res. 110.

Battle, M., Bender, M.L., Tans, P.P., White, J.W.C., Ellis, J.T., Conway, T., Francey, R.J., 2000. Global Carbon Sinks and Their Variability Inferred from Atmospheric O2 and 13C. Science 287(5462): 2467-2470.

Beer, C., Reichstein, M., Tomelleri, E., Ciais, P., Jung, M., Carvalhais, N., Rodenbeck, C., Arain, M.A., Baldocchi, D., Bonan, G.B., Bondeau, A., Cescatti, A., Lasslop, G., Lindroth, A., Lomas, M., Luyssaert, S., Margolis, H., Oleson, K.W., Roupsard, O., Veenendaal, E., Viovy, N., Williams, C., Woodward, F.I., Papale, D., 2010. Terrestrial Gross Carbon Dioxide Uptake: Global Distribution and Covariation with Climate. Science 329(5993): 834-838.

Bernier, P.Y., Guindon, L., Kurz, W.A., Stinson, G., 2010. Reconstructing and modelling 71 years of forest growth in a Canadian boreal landscape: a test of the CBM-CFS3 carbon accounting model. Canadian Journal of Forest Research 40(1): 109-118.

Bousquet, P., Peylin, P., Ciais, P., Quere, C.L., Friedlingstein, P., Tans, P.P., 2000. Regional Changes in Carbon Dioxide Fluxes of Land and Oceans since 1980. Science 290(5495): 1342-1346.

Canadell, J.G., Ciais, P., Dhakal, S., Dolman, H., Friedlingstein, P., Gurney, K.R., Held, A., Jackson, R.B., Le Quere, C., Malone, E.L., Ojima, D.S., Patwardhan, A., Peters, G.P., Raupach, M.R., 2010. Interactions of the carbon cycle, human activity, and the climate system: a research portfolio. Current Opinion in Environmental Sustainability 2(4): 301-311.

Chapin, F., Woodwell, G., Randerson, J., Rastetter, E., Lovett, G., Baldocchi, D., Clark, D., Harmon, M., Schimel, D., Valentini, R., Wirth, C., Aber, J., Cole, J., Goulden, M., Harden, J., Heimann, M., Howarth, R., Matson, P., McGuire, A., Melillo, J., Mooney, H., Neff, J., Houghton, R., Pace, M., Ryan, M., Running, S., Sala, O., Schlesinger, W., Schulze, E.D., 2006. Reconciling Carbon-cycle Concepts, Terminology, and Methods. Ecosystems 9(7): 1041-1050.

Chapin III, F.S., Pamela, A.M., Harold, A.M., 2002. Principles of terrestrial ecosystem ecology, Springer.

Chen, J.M., Weimin, J., Josef, C., David, P., Jane, L., Wenjun, C., Jianjun, P., Andy, B., Alan, B., 2003. Spatial distribution of carbon sources and sinks in Canada's forests. Tellus B 55(2): 622-641.

Ciais, P., Canadell, J.G., Luyssaert, S., Chevallier, F., Shvidenko, A., Poussi, Z., Jonas, M., Peylin, P., King, A.W., Schulze, E.-D., Piao, S., Rodenbeck, C., Peters, W., Breon, F.-M., 2010.

Can we reconcile atmospheric estimates of the Northern terrestrial carbon sink with land-based accounting? Current Opinion in Environmental Sustainability 2(4): 225-230.

Clark, D.A., Brown, S., Kicklighter, D.W., Chambers, J.Q., Thomlinson, J.R., Ni, J., 2001. Measuring Net Primary Production in Forests: Concepts and Field Methods. Ecological Applications 11(2): 356-370.

Cox, P.M., 2001. Description of the TRIFFID dynamic global vegetation model, Hadley Centre Tech. Note 24, 16pp.,. Hadley Centre, Bracknell, U.K.

Foley, J.A., Prentice, I.C., Ramankutty, N., Levis, S., Pollard, D., Sitch, S., Haxeltine, A., 1996. An Integrated Biosphere Model of Land Surface Processes, Terrestrial Carbon Balance, and Vegetation Dynamics. Global Biogeochem. Cycles 10: 603-628.

Friedlingstein, P., Bopp, L., Ciais, P., Dufresne, J.L., Fairhead, L., LeTreut, H., Monfray, P., Orr, J., 2001. Positive Feedback between Future Climate Change and the Carbon Cycle. Geophysical Research Letters 28: 1543-1546.

Friedlingstein, P., Cox, P., Betts, R., Bopp, L., von Bloh, W., Brovkin, V., Cadule, P., Doney, S., Eby, M., Fung, I., Bala, G., John, J., Jones, C., Joos, F., Kato, T., Kawamiya, M., Knorr, W., Lindsay, K., Matthews, H.D., Raddatz, T., Rayner, P., Reick, C., Roeckner, E., Schnitzler, K.G., Schnur, R., Strassmann, K., Weaver, A.J., Yoshikawa, C., Zeng, N., 2006. Climate-carbon Cycle Feedback Analysis: Results from the C4MIP Model Intercomparison. Journal of Climate 19(14): 3337-3353.

Friedlingstein, P., Dufresne, J.L., Cox, P.M., Rayner, P., 2003. How positive is the feedback between climate change and the carbon cycle? Tellus B 55(2): 692-700.

Gervois, S., de Noblet-Ducoudre, N., Viovy, N., Ciais, P., Brisson, N., Seguin, B., Perrier, A., 2004. Including Croplands in a Global Biosphere Model: Methodology and Evaluation at Specific Sites. Earth Interactions 8(16): 1-25.

Huang, S., Arain, M.A., Arora, V.K., Yuan, F., Brodeur, J., Peichl, M., 2011. Analysis of nitrogen controls on carbon and water exchanges in a conifer forest using the CLASS-CTEMN+ model. Ecological Modelling 222(20-22): 3743-3760.

Ju, W., Chen, J.M., 2008. Simulating the effects of past changes in climate, atmospheric composition, and fire disturbance on soil carbon in Canada's forests and wetlands. Global Biogeochem. Cycles 22(3): GB3010.

Ju, W., Chen, J.M., Black, T.A., Barr, A.G., McCaughey, H., Roulet, N.T., 2006. Hydrological effects on carbon cycles of Canada's forests and wetlands. Tellus B 58(1): 16-30.

Kothavala, Z., Arain, M.A., Black, T.A., Verseghy, D.L., 2005. The simulation of energy, water vapor and carbon dioxide fluxes over common crops by the Canadian Land Surface Scheme (CLASS). Agricultural and forest meteorology 133: 89-108.

Kurz, W.A., Stinson, G., Rampley, G.J., Dymond, C.C., Neilson, E.T., 2008. Risk of natural disturbances makes future contribution of Canada's forests to the global carbon cycle highly uncertain. Proc. Natl. Acad. Sci. U.S.A. 105(5): 1551-1555.

Le Quere, C., Raupach, M.R., Canadell, J.G., Marland, G., et al., 2009. Trends in the sources and sinks of carbon dioxide. Nature Geosci 2(12): 831-836.

Levis, S.G., Bonan, B., Vertenstein, M., Oleson, K.W. (2004). The Community Land Model's Dynamic Global Vegetation Model (CLM-DGVM): Technical Description and User's Guide. NCAR Tech. Note TN-459+IA. National Center for Atmospheric Research, Boulder, Colorado**:** 50.

Luo, Y., 2007. Terrestrial Carbon-Cycle Feedback to Climate Warming. Annual Review of Ecology, Evolution, and Systematics 38: 683-712.

Mahecha, M.D., Reichstein, M., Carvalhais, N., Lasslop, G., Lange, H., Seneviratne, S.I., Vargas, R., Ammann, C., Arain, M.A., Cescatti, A., Janssens, I.A., Migliavacca, M., Montagnani, L., Richardson, A.D., 2010. Global Convergence in the Temperature Sensitivity of Respiration at Ecosystem Level. Science 329: 838-840.

Metsaranta, J.M., Kurz, W.A., Neilson, E.T., Stinson, G., 2010. Implications of future disturbance regimes on the carbon balance of Canada's managed forest (2010–2100). Tellus B 62(5): 719-728.

Pan, Y., Birdsey, R.A., Fang, J., Houghton, R., Kauppi, P.E., Kurz, W.A., Phillips, O.L., Shvidenko, A., Lewis, S.L., Canadell, J.G., Ciais, P., Jackson, R.B., Pacala, S.W., McGuire, A.D., Piao, S., Rautiainen, A., Sitch, S., Hayes, D., 2011. A Large and Persistent Carbon Sink in the World's Forests. Science 333(6045): 988-993.

Parton, W.J., Schimel, D.S., Cole, C.V., Ojima, D.S., 1987. Analysis of Factors Controlling Soil Organic Matter Levels in Great Plains Grasslands. Soil Sci Soc Am J 51(5): 1173-1179.

Piao, S., Ciais, P., Friedlingstein, P., de Noblet-Ducoudr, N., Cadule, P., Viovy, N., Wang, T., 2009. Spatiotemporal patterns of terrestrial carbon cycle during the 20th century. Global Biogeochem. Cycles 23(4): GB4026.

Piao, S., Ciais, P., Friedlingstein, P., Peylin, P., Reichstein, M., Luyssaert, S., Margolis, H., Fang, J., Barr, A., Chen, A., Grelle, A., Hollinger, D.Y., Laurila, T., Lindroth, A., Richardson, A.D., Vesala, T., 2008. Net carbon dioxide losses of northern ecosystems in response to autumn warming. Nature 451(7174): 49-52.

Pitman, A.J., 2003. The evolution of, and revolution in, land surface schemes designed for climate models. International Journal of Climatology 23(5): 479-510.

Qian, H., Joseph, R., Zeng, N., 2010. Enhanced terrestrial carbon uptake in the Northern High Latitudes in the 21st century from the Coupled Carbon Cycle Climate Model Intercomparison Project model projections. Global Change Biology 16(2): 641-656.

Raupach, M.R., Canadell, J.G., 2010. Carbon and the Anthropocene. Current Opinion in Environmental Sustainability 2(4): 210-218.

Rayner, P.J., I.G. Enting, R.J.F., Langenfelds, R., 1999. Reconstructing the recent carbon cycle from atmospheric CO_2, ^{13}C and O_2/N_2 observations. Tellus 51B(2): 213-232.

Running, S.W., Baldocchi, D.D., Turner, D.P., Gower, S.T., Bakwin, P.S., Hibbard, K.A., 1999. A Global Terrestrial Monitoring Network Integrating Tower Fluxes, Flask Sampling, Ecosystem Modeling and EOS Satellite Data. Remote Sensing of Environment 70(1): 108-127.

Running, S.W., Coughlan, J.C., 1988. A general model of forest ecosystem processes for regional applications I. Hydrologic balance, canopy gas exchange and primary production processes. Ecological Modelling 42(2): 125-154.

Running, S.W., Thornton, P.E., Nemani, R., Glassy, J.M., 2000. Global terrestrial gross and net primary productivity from the Earth observing system. In O. E. Sala, R. B. Jackson, H. A. Mooney, R. W. Howarth, (Eds.), Methods in ecosystem science (pp. 44-57). New York, Springer-Verlag.

Sitch, S., B.Smith, I.C.Prentice, A.Arneth, A.Bondeau, W.Cramer, J.O.Kaplan, S.Levis, W.Lucht, M.T.Sykes, K.Thonicke, S.Venevsky, 2003. Evaluation of ecosystem dynamics, plant geography and terrestrial carbon cycling in the LPJ dynamic global vegetation model. Global Change Biology 9(2): 161-185.

Solomon, S., Qin, D., Manning, M., Marquis, M., Averyt, K., Tignor, M.M.B., Miller, H.L., Chen, Z., 2007. Climate Change 2007: The Physical Science Basis. Working Group I

Contribution to the Fourth Assessment Report of the Intergovernmental Panel on Climate Change, Cambridge University Press.

Tian, H., Melillo, J.M., Kicklighter, D.W., McGUIRE, A.D., Helfrich, J., 1999. The sensitivity of terrestrial carbon storage to historical climate variability and atmospheric CO2 in the United States. Tellus B 51(2): 414-452.

Trofymow, J.A., Stinson, G., Kurz, W.A., 2008. Derivation of a spatially explicit 86-year retrospective carbon budget for a landscape undergoing conversion from old-growth to managed forests on Vancouver Island, BC. Forest Ecology and Management 256(10): 1677-1691.

Verseghy, D.L., 1991. CLASS - a Canadian land surface scheme for GCMs. I. Soil model. International Journal of Climatology 11: 111-113.

Verseghy, D.L., 2000. The Canadian Land Surface Scheme (CLASS): Its History and Future. Atmosphere-Ocean 38(1): 1-13.

Verseghy, D.L., McFarlane, N.A., Lazare, M., 1993. CLASS - a Canadian land surface scheme for GCMs. II. Vegetation model and coupled runs. International Journal of Climatology 13: 347-370.

Waring, R.H., Running, S.W., 1998. Forest Ecosystems: Analysis at Multiple Scales. San Diego, Academic Press.

Yuan, F., Arain, M.A., Alan, G.B., Black, T.A., Charles, P.A.B., Carole, C., Hank, A.M., McCAUGHEY, J.H., Steven, C.W., 2008. Modeling analysis of primary controls on net ecosystem productivity of seven boreal and temperate coniferous forests across a continental transect. Global Change Biology 14(8): 1765-1784.

Yuan, F., Arain, M.A., Black, T.A., Morgenstern, K., 2007. Energy and water exchanges modulated by soil-plant nitrogen cycling in a temperate Pacific Northwest conifer forest. Ecological Modelling 201(3-4): 331-347.

CHAPTER 2:

EVALUATING THE IMPACTS OF DISTURBANCE REGIMES AND CLIMATE VARIABILITY ON THE HISTORIC CARBON BUDGET OF A PACIFIC NORTHWESTERN FOREST LANDSCACPE

2.1 Abstract

The effects of disturbance regimes and climate variability on the carbon dynamics of a Pacific Northwest temperate conifer forest landscape (2500 ha) were studied from 1920 to 2005 using a process-based land surface model, known as the carbon and nitrogen coupled Canadian Land Surface Scheme (C-CLASS). Disturbance matrices from the Carbon Budget Model of the Canadian Forest Sector (CBM-CFS3) were incorporated into C-CLASS to improve its capabilities to simulate disturbance impacts on forest carbon dynamics. The model was driven using hourly meteorological data from historic climate records. Site-scale maps of soil characteristics, topography, vegetation and disturbance type (logging and fires) were provided by the historic carbon modelling project of the Canadian Carbon Program (CCP). Simulated carbon fluxes suggest that landscape was close to C neutral with annual net ecosystem productivity (NEP) of 0.008 Mg C ha^{-1} yr^{-1} in 1920 until it was disturbed. During the disturbance period, the landscape became a significant carbon source and the disturbance type and intensity determined the magnitude of the carbon source. Mass balance calculation indicated that the conversion of 2500 ha of old-growth forests to managed forests in the study area from 1920 through 2005 induced 7.3×10^5 Mg loss of total ecosystem carbon as simulated by C-CLASS compared to 7.2×10^5 Mg simulated by CBM-CFS3 model. In 2005, the landscape was a C sink with NEP value of 1.65 Mg

C ha^{-1} yr^{-1}. Among the landscape-level carbon fluxes, net primary productivity was most sensitive to air temperature effects, due to the relatively high temperature sensitivity of autotrophic respiration in C-CLASS model. Among carbon pools, changes in dead organic carbon pools were more sensitive to air temperature than biomass carbon pools. Overall, landscape-level carbon fluxes and changes of carbon stocks appeared to be less sensitive to precipitation than air temperature. This study will enhance our understanding of the impacts of future climate variability and disturbance regimes on landscape-level carbon dynamics.

2.2 Introduction

Forest ecosystems play an important role in the global carbon (C) cycle by storing large amounts of carbon. There are about 4.17 billion hectares of forests (larger than 15 years old) on the Earth which are renewed by afforestation and deforestation. The world's forests (tropical, temperate and boreal forests) store around 359 Pg C in the vegetation and around 787 Pg C in the soil, (Dixon et al., 1994). However, at the intermediate spatial scale (~10 km^2), forest landscapes significantly vary in their species composition and age structure and C dynamics at this scale have not been fully studied by the scientific community. Therefore, better knowledge of C flux dynamics and C stock changes is required to understand the current state of the C cycle in forest landscapes and how it might evolve with the variability of disturbance regimes and climatic conditions.

In recent years, significant progress has been made in simulating landscape level C budgets and how they might be impacted by various disturbance regimes. For example, Harmon et al. (1990) used a model to track the C dynamics in old-growth and second-growth young forests and suggested that timber harvest converted 5×10^6 ha of old-growth forests to younger plantations

in Western Oregon and Washington State in US in the past 100 years. During this period, 1.5×10^9 to 1.8×10^9 Mg C was released to the atmosphere. Kurz et al. (1997) used Carbon Budget Model of Canadian Forest Sector (CBM-CFS2) to investigate the impact of disturbance regimes (frequency, intensity and disturbance types) on landscape-level C stocks and fluxes in 6 representative forest landscapes (100,000 ha each) during their conversion from unmanaged to managed forest landscapes. Kurz et al. (1997) suggested that disturbance frequency, age-dependence of the disturbance probabilities and the disturbance-specific impacts on ecosystem C content are major factors that considerably affect the landscape-level ecosystem C stocks. Song et al. (2003) used a regional forest ecosystem C budget model to study the influences of forest age structure and land use history on regional C fluxes of the forests in the Pacific Northwest of the United States. They found that a forest stand can be a carbon sink for up to 200 years old with a peak at 30-40 years old and old-growth forests (older than 200 years old) are carbon neutral to the atmosphere in the long term (Song and Woodcock, 2003). Moreover, Smithwick et al. (2007) used a process-based model to investigate the impact of two contrasting disturbance types (fire and forest harvest) on landscape-level net biome productivity (NBP). Their model explicitly describes C stock changes as a function of disturbance regimes including disturbance interval, disturbance intensity and the relative abundance of stands in the landscape with unique disturbance histories (Smithwick et al., 2007). Their study suggested that landscape-level C stocks were higher for random than for regular disturbance intervals, and C stocks increased as the mean disturbance interval increased and as disturbance intensity decreased (Smithwick et al., 2007). Therefore, disturbance and forest age structure needs to be taken into account to improve the accuracy of forest C stocks estimates over large areas due to the high spatial variability of stand ages caused by disturbance.

Inclusion of disturbance subroutines in the process-based land surface model (such as Carbon and Nitrogen coupled Canadian Land Surface Scheme, C-CLASS (Arain et al, 2006) provides capabilities of studying both the impact of climate variability and the effects of disturbance regimes on the C dynamics of forest landscapes. Land surface models are a key component of global and regional climate models that represent water and energy fluxes between the land surface and the atmosphere. Over the last two decades, C components (photosynthesis and respiration algorithms) have been added into many commonly used land surface models to enhance their capabilities to simulate the C exchanges between terrestrial ecosystems and the atmosphere (Bonan, 1995; Foley et al., 1996; Sellers et al., 1996; Sellers et al., 1997; Dickinson et al., 1998; Kucharik et al., 2000; Arain et al., 2002; Wang et al., 2002; Wang, 2002; Kothavala et al., 2005). Moreover, a few models have further included nitrogen processes as a way of including the effects of nutrient limitation on C and water fluxes in vegetation ecosystems (Wang et al., 2001; Liu et al., 2005; Arain et al., 2006; Yuan et al., 2007). However, most land surface models still need to consider the episodic non-respiratory direct CO_2 emissions (disturbances) to calculate the long term C balance or net biome productivity (NBP) in disturbed forest ecosystems because disturbances (i.e. fire, forest harvest, insect outbreaks and wind storm) are the major mechanism that convert forest ecosystems from C sinks to sources in short term (a few hours to about 3 years).

In this study, we incorporated CBM-CFS3 disturbance matrices into C-CLASS and applied it over a 2500 ha forest landscape in the Oyster River study area for several decades (1920-2005) to investigate its historic C budget by considering both disturbance regimes and climate variability. The specific objectives of this study are (i) to investigate the impact of different disturbance events on the variations in C fluxes and C stocks at landscape level; (ii) to

explore the impacts of climate variability on landscape-level C dynamics over the past several decades i.e. 1920-2005.

2.3 Materials and Methods

2.3.1 Study area

The study landscape ($49^{\circ}52'8.2''N$, $125^{\circ}20'7.2''W$) is located on the eastern side of Vancouver Island, British Columbia, Canada. It covers a 5 km × 5 km (2500 ha) area with UTM co-ordinates NAD83 (Zone 10, NW corner 331126E, 5529894N; SE corner 336117E, 5524893N). The study area is bisected by the Oyster River and has two flux tower sites (DF49, in an intermediate aged second-growth Douglas-fir stand established in 1949; HDF00, in a regenerating third-growth Douglas-fir stand clearcut and planted in 2000) (Trofymow et al., 2008). The elevation of this landscape varies from about 499 m in the southwest to around 120 m in the northeast. Presently, the majority of the study area (1863 ha) is dominated by even-aged, second-growth forest stands of Douglas-fir (*Pseudotsuga menziesii*) among which there are 1426 ha pure Douglas-fir forest stand and around 437 ha Douglas fir stands are mixed with Western Red Cedar (*Thuja plicata*), Red Alder (*Alnus rubra*), Western Hemlock (*Tsuga heterophylla*).

The study area has 12 different soil types, which are Arrowsmith, Bowser, Cassidy, Dashwood, Fairbridge, Hawarth, Hiller/Piggott, Honeymoon, Kye, Quinsam, Quimper and Rossiter/Cullite based on the Canadian system of soil classification. These soil types range from very gravely textured duric humo-ferric podzols of fluvial origin at low elevations, to gravely sandy loam textured duric humo-ferric and ferro-humic podzols of morainal origin at intermediate elevations and shallow stony ortho hum-ferric podzols on colluvium on higher elevation hilltops

(Jungen, 1985). Overall this region is located in the Coastal Western Hemlock very dry maritime biogeoclimatic subzone (CWHxm) (Pojar et al. 1991). Mean annual precipitation is 1460 mm and the mean annual temperature is 8.3 ˚C. About 75% of precipitation falls between October and March. July and August are the warmest months, with mean monthly temperature of 16.9 ˚C. January is the coldest month, with mean monthly temperature of 1.3 ˚C.

2.3.2 Study area disturbance history

Based on the historic disturbance data reconstructed and compiled by Trofymow et al. (2008), there was no substantial logging in the study area before 1920, except a widespread wildfire in the region in the late 1600s (Mackie, 2000). Most of the forest land in the study area was purchased by private timber companies in the late 1890s (Trofymow et al., 2008). Timber cruises were completed before 1920 by three timber companies operating in the area: Comox Logging and Railway Company, Elk River Timber Company and International Timber Company (Trofymow et al., 2008).

From 1928 to 1944, intensive forest harvest activities occurred in this area. A large portion of wood was left on site after the logging and most of it was slash burned. In 1938, the Bloedel/Sayward wildfire burned part of the northeast corner of this study area (Trofymow et al., 2008). Natural regeneration was limited and so forest planting began in the 1940s for much of this area and is practiced in all recent harvest areas. Planting activities continued in 1950s and even into the 1970s for blocks with insufficient stocking. Productive second growth forest eventually re-established over most of the study area when harvesting of 40-60-year-old second growth stands started in 1989 (Trofymow et al., 2008).

2.3.3 Carbon and Nitrogen coupled Canadian Land Surface Scheme (C-CLASS)

2.3.3.1 Model overview

Carbon and Nitrogen coupled Canadian Land Surface Scheme (C-CLASS) was developed from Canadian Land Surface Scheme (CLASS) which is a physically based land surface model to simulate energy and water fluxes from the land surface (Verseghy, 1991; Verseghy et al., 1993; Verseghy, 2000). CLASS was originally developed for coupling with Canadian Global Climate Model (CGCM) and Canadian Regional Climate Model (CRCM). CLASS can also be run in uncoupled or offline mode with meteorological data from a separate atmospheric system or from observational data. The model used in this study was version 3.0 of CLASS, in which the land surfaces are classified into four subareas for the surface flux calculation: bare soil, vegetation covered soil, snow covered bare soil, or vegetation and snow covered soil (Verseghy, 2000). CLASS identifies up to five vegetation or land cover types in each grid cell i.e. needleleaf trees, broadleaf trees, crops, grasses and urban areas. The soil profiles are divided into three layers (0.10, 0.25 and 3.75 m thick), while snow is treated as an analogous of the fourth soil layer with variable depth.

CLASS has been developed to incorporate the two-leaf (sun-lit and shaded) canopy conductance and photosynthesis modules and soil and plant respiration algorithms and is named as C-CLASS (Arain et al., 2002; Kothavala et al., 2005). C-CLASS was further improved by incorporating plant-soil nitrogen algorithms to address the C and nitrogen coupled processes in the vegetation ecosystems (Arain et al., 2006; Yuan et al., 2007). Recently, C-CLASS was used to investigate the role of primary climatic controls and site specific C stocks on the net ecosystem productivity (NEP) of seven intermediate-aged to mature coniferous forest sites across an east–

west continental transect in Canada to help evaluate the impact of future climatic changes on C uptake and loss in forest ecosystems growing in diverse environments (Yuan et al., 2008).

2.3.3.2 Carbon allocation

In the C budget module of C-CLASS, gross primary productivity (GPP) is allocated to four plant C pools (i.e. photosynthate, leaf, wood and root). Leaf maintenance respiration depends on leaf area index (LAI), base leaf respiration rate at a reference temperature (15 ˚C) and leaf temperature as a function of the Q_{10} coefficient. Assuming no respiration from the heartwood, sapwood maintenance respiration is calculated as a function of sapwood volume, base sapwood respiration rate at reference temperature and leaf temperature. Root maintenance respiration is calculated as the sum of coarse root and fine root maintenance respiration which depend on their respective biomass C pools, the base respiration at reference temperature and the temperature of first soil layer. Total plant maintenance respiration is the sum of leaf, wood and root maintenance respiration and it has the first priority than the C allocation to photosynthate pool. Leaf growth respiration is assumed to be 15% of net photosynthesis or leaf net primary productivity (NPP). After C allocation of GPP into the photosynthate pool, leaf NPP and leaf growth respiration, the rest of assimilated C is available for wood and root growth and their growth respirations. Wood and root growth respiration are also estimated as 15% of the wood and root NPP, respectively. An allometry module is used to estimate the new heartwood and coarse root biomass after the growth of wood and root. Heterotrophic respiration (R_h) are estimated as the sum of ground surface litter respiration, dead roots respiration, short-lived soil organic matter (SOM) respiration and stable SOM respiration. R_h of these different C pools are described as a function of organic C per unit ground area, base respiration rate at a reference

temperature (10 ˚C), root zone temperature (0.1 or 0.25 m) with a temperature sensitivity defined by a Q_{10} coefficient and the soil water content in the upper and subsurface soil layer (Kothavala et al., 2005; Arain et al., 2006). Stem and branch turnover rate is estimated as 0.02 μmol kg^{-1} C s^{-1} and root turnover rate is estimated as 0.08 μmol kg^{-1} C s^{-1} for coast Douglas-fir in this study.

2.3.3.3 Disturbance Matrices

For this study, the C budget subroutine of the model as described above was modified to incorporate a module describing C transfers among different C pools for different disturbance types. The values used for the C transfers among C pool module were the same as used in the CBM-CFS3 model's disturbance matrices (Kurz et al., 2009). Twelve disturbance types are identified in the landscape history and parameterized by the disturbance matrices including historic harvest, historic harvest with slashburn, historic harvest with partial slashburn, historic harvest with ground fire, clearcut and broadcast burn, clearcut and pile burn, partial burn, slash burn, ground burn, partial slashburn, total burn and fertilization. The disturbance matrices define flow of C from donating (pre-disturbance) to receiving (post-disturbance) C pools as ratios of the C stocks in each pool at the time of disturbance (Trofymow et al., 2008). Post-disturbance pools involve C pools of forest ecosystems and atmosphere and forest product sector. Each C pool of the forest ecosystem was updated after the disturbance event. Further details of disturbance matrices used for this study can be found in Trofymow et al. (2008).

In C-CLASS, annual minimum LAI was set to 1.0 for disturbance year and the expected maximum LAI for disturbed year was set empirically to 2.2 which mostly represents the understory (Grant et al., 2007). C-CLASS model assumed that it takes around 30 years for the

expected annual maximum LAI to reach the original level after the stand-replacing disturbances. After that, expected annual maximum LAI was calculated as 60% of the product of sapwood transaction area (cm^2) at diameter at breast height (DBH, 1.37 m) and plant density (Gower et al., 1997; Turner et al., 2000).

2.3.4 Model Input Data

The meteorological data used to drive the time series of the model from 1920 to 1997 were derived from nearby daily climate station records (Campbell River Airport and Cumberland) which had been interpolated to the DF49 eddy covariance flux tower site (Morgenstern et al., 2004). From 1998 to 2005, the observed meteorology data from DF49 tower site were used. This long term historic weather dataset (1920-1997) had been adjusted to match the tower measurements based on the comparison of concurrent records (1998-2005) from Campbell River Airport and DF49 tower. The area historic daily weather record from 1920 – 1997 were further interpolated to estimate hourly values for use in the model. Although the correlations are high, the inconsistency of the meteorological forcing dataset may cause a systematic bias in the modeling outputs. Specifically, solar radiation was interpolated over calculated day length to obtain hourly values using a sine function. Hourly air temperature data was also interpolated using sine function with the daily minimum temperature at dawn and maximum temperature at 3 hours after solar noon.

Historic annual atmospheric CO_2 concentration data was originated from Canadian Integrated BIosphere Simulator (Can-IBIS; Liu et al, 2005) model run (1765-2100) under CO_2 emission scenario (SRES-a2). The soil map of Oyster River study area was derived from the soil map of Jungen (1985). Soil characteristics data includes information about all 12 soil types and

soil depth for each layer, soil texture, soil organic C content, soil total N content and the drainage information. Topography data was built from 1:20000 Terrain Resource Information Management (TRIM) digital elevation data (DEM) and it has 3 m horizontal spatial resolution. Initial inventory data and disturbance matrices were provided by CBM-CFS3 model and the further details can be found in Trofymow et al. (2008).

Trofymow et al. (2008) reconstructed the complex disturbance history of this study area by compiling spatial data and historic air photos. GIS coverages of current forest inventories (circa 1999) were compiled and overlaid with digitized historic disturbance maps, a 1919 timber cruise map and a series of historic orthophotographs to produce a GIS coverage of forest cover polygons with unique disturbance histories dating back to 1920 (Trofymow et al., 2008). Further details of study area history and the compilation of spatial data sources can be found in Trofymow et al. (2008).

2.3.5 Model initialization, parameterization and sensitivity analysis

The study area was a Dougalus-fir dominant old-growth forest (around 350 years old) in 1920 (Trofymow et al., 2008). In this study, initial (1920) aboveground biomass (AGB) data was provided by CBM-CFS3 model using information derived from 1919 timber cruise map (Trofymow et al., 2008). The ratio of belowground biomass (BGB) to aboveground biomass was assumed to be 0.222 (Li et al., 2003). Initial total ecosystem C stock (TEC) was also estimated by CBM-CFS3 assuming a long-term historic disturbance regime of stand-replacing fire every 300 years on average prior to 1920 (Trofymow et al., 2008). The residue of TEC minus total biomass (AGB and BGB) is necromass including 50% of soil organic matter (SOM), 20% of dead wood, 18.9% of forest floor litter and 11.1% of dead root (Sun et al., 2004; Trofymow et al., 2008).

Initial minimum and maximum LAI of old-growth Dougalus-fir forest was assumed to be 8.2 and 9.3, respectively (Thomas and Winner, 2000). Initial canopy and soil temperature and soil moisture were derived from a 5-year model spin-up run, using observed meteorology data (2003-2004).

Table 2 shows the key parameters used to run C-CLASS model over the Oyster River forest landscape. For the model runs, the Oyster River forest landscape was resolved into 2500 grid cells of 100 m × 100 m (1 ha) each. The soils, inventory, forest cover types and disturbance data in these 2500 grid cells were then aggregated into 1146 unique combinations of soils, inventory, forest cover types and disturbances, each of which was represented by one model simulation.

Eight scenarios were run on the simulation period of 1920-2005 over the whole landscape to test the impact of disturbance, environmental change (CO_2 concentration) and climate variability on the historic dynamics of C fluxes and stocks. These scenarios were (1) Full: base simulation; (2) No_CO_2: no anthropogenic-driven increase in atmospheric CO_2 concentration with time (use CO_2 concentration in 1820-1905 for the simulation period of 1920-2005); (3) No_dis: no disturbance (forest harvest, planting and fire); (4) No_dis/CO_2: no CO_2 fertilization and no disturbance; (5) No_Clim: no interannual variability in climate variables and CO_2 (repeating 1920 climate); (6) No_Clim/CO_2: no climate variability and no CO_2 fertilization; (7) No_Clim/Dis: no climate variability and no disturbance; (8) No_Clim/CO_2/Dis: no climate variability, no CO_2 fertilization and no disturbance.

In order to evaluate the relative influences of climatic variables on historic C dynamics in the landscape, model sensitivity tests were conducted for the whole simulation period. For climate variables, the sensitivity was assessed by increasing/decreasing hourly values of (i) air temperature by ±1.0 ˚C and ±2.0 ˚C; (ii) precipitation by ±10% and ±25%, respectively. In order

to isolate the compounding effects of climatic forcing on C budget, we changed one variable at a time, while all others were kept unchanged during the sensitivity model runs.

2.4 Results

2.4.1 Annual landscape-level C stock changes and C fluxes

The disturbance history of the Oyster River landscape originated from the compilation of various spatial data sources (Trofymow et al., 2008). Four distinct periods in the study area's disturbance history can be identified as shown in Figure 2.1, i.e. (a) the period before large-scale forest clearing and fire events (1920-1927); (b) the period of intensive forest logging, slash burn, fire and planting (1928-1949); (c) the regeneration period in which there were very few disturbance events except some small-scale plantings (1950-1989); and (d) the period of second-growth forest harvest (1990-2005). In 1920, initial landscape-level above-ground tree biomass (AGB) (leaf , wood and bark biomass) and below-ground biomass (BGB) (live fine and coarse root biomass) was estimated as 284.87 Mg C ha^{-1} and 57.50 Mg C ha^{-1}, respectively (Figure 2.2). In the following intensive disturbance period (1928-1949), simulated AGB and BGB experienced large decline, and reached the lowest value of 16.54 Mg C ha^{-1} and 6.89 Mg C ha^{-1} in 1943, respectively. After that, the simulated AGB and BGB gradually increased to 162.19 Mg C ha^{-1} and 54.57 Mg C ha^{-1} in 1997, respectively, until the second-growth forest cut in the late 1990s. In 2005, simulated landscape-level AGB and BGB were decreased to 123.02 Mg C ha^{-1} and 39.00 Mg C ha^{-1}, respectively, due to the clear cut and burning events in the second growth forest stands. Thus, the C-CLASS modeled landscape-level AGB and BGB in 2005 were lower than the initial value in 1920. Simulated initial landscape-level dead organic matter (DOM) (forest floor litter, dead wood and belowground dead roots) and soil organic matter (SOM) (short-lived soil organic matter and

stable soil organic matter) were 205.57 Mg C ha^{-1} and 210.29 Mg C ha^{-1}, respectively. DOM were close to constant until the period of intensive disturbance in 1928-1949 during which, DOM was decreased by the fire burning and increased when fires and logging killed the trees leaving the residues on site. Simulated landscape-level DOM declined steadily for many decades after the original forest cover was removed and reached the lowest value of 52.84 Mg C ha^{-1} in 1971 because DOM decomposition exceeds the input of litter fall and the wood/root turnover in young forest stands. After that, DOM gradually recovered and reached 98.60 Mg C ha^{-1} in 2005 when young forests became mature and litter fall and the wood/root turnover overpass the DOM decomposition. Simulated landscape-level SOM was slightly reduced from 210.29 Mg C ha^{-1} in 1920 to 207.30 Mg C ha^{-1} in 2005 during the whole simulation period which was much less influenced by the disturbance events compared to DOM.

C-CLASS simulated a significant reduction of total ecosystem C stocks following conversion from old-growth stands to second growth (or third growth) managed forests in the Oyster River study area. Mass balance calculation indicated that the conversion of 2500 hectares of old-growth forests to managed forests in the study area from 1920 through 2005 induced 7.26×10^5 Mg loss of total ecosystem carbon (TEC) as simulated by C-CLASS

Figure 2.3 shows C-CLASS simulated annual landscape-level C fluxes throughout the simulation period. It suggests that forest ecosystems in the study were close to C neutral (NBP of 0.008 Mg C ha^{-1} yr^{-1} in 1920) until they were disturbed. During the disturbance period, the landscape became a significant C source and the disturbance type and intensity determined the magnitude of the C source in the year when disturbance occurred (Figure 2.3). Following disturbance, the landscape was nearly C neutral for many years, eventually becoming a net C sink when C uptake from forest re-growth exceeded C losses due to decomposition of logged and other

disturbance residues. The landscape became C source since late 1990s because of the logging of second growth forest (Figure 2.3).

In 1920, simulated landscape-level GPP and NPP was 20.32 Mg C ha^{-1} yr^{-1} and 8.80 Mg C ha^{-1} yr^{-1}, respectively. Both GPP and NPP started to decrease in the following period of intensive disturbance and reached relatively low level, 8.57 Mg C ha^{-1} yr^{-1} and 5.89 Mg C ha^{-1} yr^{-1}, in 1944 and 1938, respectively (Figure 2.3). They gradually recovered from 1951 to 1997 which had less disturbance events and reaching 21.02 and 9.18 Mg C ha^{-1} yr^{-1}, respectively, in 1997 (Figure 2.3). After that, harvest of second-growth forests reduced simulated landscape-level GPP and NPP to 16.30 and 7.58 Mg C ha^{-1} yr^{-1}, respectively, in 2005 (Figure 2.3). In 1920, C-CLASS simulated landscape-level NEP was 0.008 Mg C ha^{-1} yr^{-1}. C-CLASS simulated NEP started to declined in 1922 and reached the minimum value, -5.24 Mg C ha^{-1} yr^{-1} in 1938 (Figure 2.3). Then it recovered and increased to above zero in 1946. In the following period, climate variability had more impact on NEP than disturbance until late 1990s when second-growth forests were harvested. In 2005, landscape-level NEP was 1.65 Mg C ha^{-1} yr^{-1} (Figure 2.3).

Spatial standard deviation (σ) was calculated to elaborate the dynamics of spatial heterogeneity in AGB and NBP during the simulation period (1920-2005). σ was determined as:

$$\sigma = \sqrt{\frac{1}{N-1}\sum_{i=1}^{N}(x_i - \bar{x})^2} \quad (1)$$

where x_i is simulated AGB or NBP at one pixel, $\bar{x}$ is the mean value of AGB or NBP over the whole landscape, and N is the total number of pixels in the landscape. Oyster River landscape AGB standard deviations were in the range of 81-89 Mg C ha^{-1} from 1920-1927, during which there was no large-scale disturbance on the landscape and the spatial heterogeneity of old-growth forest AGB was determined by the stand age-class structure and site fertility (Figure 2.4). AGB

standard deviation increased to 102.50 Mg C ha^{-1} in 1928 because a small patch of forest stands (131 ha) were harvested in 1928 which increased the spatial heterogeneity of landscape AGB (Figure 2.4). AGB standard deviation continued to increase when more forests were cut or burnt and it reached the highest value (159.71 Mg C ha^{-1}) in 1934. After that, standard deviations of AGB started to decrease because most of the landscape was disturbed and it reached the lowest value (16.55 Mg C ha^{-1}) in 1943 when all the landscape had been disturbed and converted from old-growth forests to second-growth forests. AGB standard deviation was kept at a low level (16-31 Mg C ha^{-1}) in the following regeneration period, during which there were very few disturbance events. Finally, the harvest of second-growth forests in the late 1990s began to increase the AGB standard deviation indicating the increase of spatial heterogeneity of landscape AGB (Figure 2.4). Landscape NBP standard deviations were low (3-9 Mg C ha^{-1} yr^{-1}) during the period when there were no or very few disturbance events and landscape NBP were considerably heterogeneous (high standard deviation) during the period of intensive disturbance (1928-1943) and the logging of second-growth forests (1990-2005) (Figure 2.5).

2.4.2 Climate variability and carbon fluxes

Relationship between C-CLASS simulated seven year mean (moving average) C flux deviations and mean daily minimum or maximum air temperature for the whole study area during the undisturbed period (1963-1984) is shown in Figure 6. Over this period, mean daily minimum air temperature (T_{min}) ranged from 0 to 5 ^{o}C in spring (March, April and May) while the mean daily maximum air temperature (T_{max}) was around 8 to 13 ^{o}C (Figure 2.6). Over the same period, mean daily T_{min} in summer (June, July and August) was between 9 and 13 ^{o}C while mean daily T_{max} in the summer was between 15 and 22 ^{o}C (Figure 2.6). Generally, landscape-level GPP deviation

appears to be positively related T_{min} and T_{max} in spring while negatively related to T_{min} and T_{max} in summer (R^2 values shown in each figure panel). Landscape-level annual photosynthesis rate increased with air temperature in spring when the air temperature was relatively low. In summer, the air temperature was too high and landscape-level GPP decreased with the temperature. Meanwhile, annual landscape-level ecosystem respiration (Re) deviation appears to be positively related to air temperature (T_{min} and T_{max}) in both spring and summer (Figure 2.6b; Figure 2.6e; Figure 2.6h; Figure 2.6k). Annual landscape-level NEP deviation were negatively related to T_{min} and T_{max} in summer (Figure 2.6f and Figure 2.6l) because GPP deviation decreases with air temperature and R_e increases with air temperature in the summer.

Annual landscape-level GPP, Re and NEP did not show significant relationship with the total precipitation in spring (Figure 2.7). However, GPP, Re and NEP deviations showed some correlation with summer precipitation (Figure 2.7) since the study area is located in the coastal temperate rainforest zone of the Pacific Northwest and can experience moisture limitations in the summer (Arain et al., 2006; Trofymow et al., 2008). Annual landscape-level GPP deviation increased with summer precipitation when summer precipitation is lower than about 203 mm and reached the maximum value when summer precipitation was about 203 mm and then it started to decrease with summer precipitation when summer precipitation was higher than 203 mm. R_e deviations initially decreased with summer precipitation when summer precipitation was lower than 183 mm and reached the minimum value when summer precipitation was about 183 mm. Similarly, annual landscape-level NEP deviations increased with summer precipitation when it was lower than 193 mm and then decreased with further increase in summer precipitation (Figure 2.7).

2.4.3 Model Scenarios and climate sensitivity analysis

Differences in ecosystem C stocks in 2005 across the model run scenarios reveal the long-term impact of disturbance and rising atmospheric CO_2 concentration and climate variability. Simulated forest AGB, BGB and DOM were 1.08-1.12, 1.14-1.16 and 1.07-1.15 times larger, respectively, with increased CO_2 than without (Table 2.3). Simulated forest AGB, BGB, and DOM were 2.82-2.94, 1.49-1.51 and 2.12-2.29 times larger, respectively, without disturbance than with (Table 2.3), indicating the significant impacts of disturbance (forest harvest, fire and planting) on the forest ecosystem C stocks. Simulated forest AGB, BGB, and DOM were 1.00-1.12, 1.01-1.18, 1.03-1.18 times larger, respectively, without interannual climate variability than with (Table 2.3). However, simulated SOM were insensitive with increasing atmospheric CO_2, disturbance and interannual climate variability because SOM was assumed to be constant throughout the simulation period.

Annual GPP, NPP, NEP and Re averaged over 1998-2005 showed that each scenario impacted these C fluxes differently (Table 2.4). Simulated forest GPP, NPP, NEP and Re were 1.10-1.12, 1.14-1.16, 1.27, 1.06-1.10 times larger, respectively, with increased CO_2 than without (Table 2.4). Simulated forest GPP was 1.12-1.14 times larger without disturbance than with (Table 2.4), owing to the higher LAI in old-growth forest. Simulated forest Re was 1.43-1.48 times larger without disturbance than with (Table 2.4), due to the lack of carbon removal by harvest and fire. On the contrary, simulated NPP and NEP were smaller without disturbance than with (Table 2.4), owing to the faster growth in younger forests. Simulated forest GPP, NPP and NEP were 1.02-1.14, 1.10-1.34, 1.35-1.72 times larger, respectively, without interannual climate variability than with (Table 2.4). However, interannual climate variability did not have significant impact on the simulated ecosystem respiration (Table 2.4).

The sensitivity of simulated landscape-level C fluxes and stocks to the changes of air temperature is shown in Figure 2.8. In the model, foliage respiration is calculated using leaf or canopy temperature which may be more related to air temperature. Therefore, autotrophic respiration (R_a) is more sensitive to changes in air temperature. However, heterotrophic respiration (R_h) including detritus respiration and SOM respiration was calculated from upper soil layer temperature and subsurface soil layer temperature, respectively, which was less sensitive to the changes in air temperature. Thus, R_h was less sensitive to the changes in air temperature. When air temperature was decreased by 2 ˚C, simulated GPP became much lower than the control simulation. Except this, modelled GPP appeared to be less sensitive to air temperature compared to R_a. Because NPP equals to GPP minus R_a, therefore, we can expect that NPP would be sensitive to air temperature. In the model, DOM is updated by C input from foliage, wood and root turnovers and C loss through DOM decomposition. The turnover rates of foliage, wood and root are based on their biomass which is related to NPP. Thus, the air temperature sensitivity of DOM should be attributed to the air temperature sensitivity of foliage, wood and root turnover rate which are related to the air temperature sensitivity of NPP. Also, SOM is calculated from C input of DOM turnover and the C loss of its decomposition. Therefore, both SOM and DOM are also sensitive to the change of air temperature.

Figure 2.9 shows the sensitivity of C-CLASS simulated landscape-level C fluxes and stocks to the change of precipitation. It shows that simulated C fluxes and stocks are not sensitive to the change of precipitation.

2.5 Discussion

In this study, we used aboveground biomass in 1920 provided by CBM-CFS3 to initialize C-CLASS. CBM-CFS3 takes the information that is commonly available in contemporary forest inventory growth and yield plots as the basis of estimating the growth of aboveground tree biomass C stocks (Trofymow et al., 2008). However, the digitized 1919 Timber Cruise map of total merchantable volume which was used to estimate aboveground tree biomass in 1920 by CBM-CFS3 does not provide merchantable volumes for all species or all trees and other information that is commonly seen in contemporary forest inventories, although some valuable information on forest species composition and spatial distribution of the cruise volume for the area were obtained (Trofymow et al., 2008). This different nature of volume information in 1919 timber cruise forced CBM-CFS3 to make some assumptions to bring the data up to current inventory standards. These issues have contributed to the uncertainty in the estimated initial aboveground biomass in 1920.

On the other hand, old-growth forests on Vancouver Island and in the Pacific Northwest can have very high biomass C stocks (Table 2.5), and therefore have a lot to lose in the event of disturbance. Although there is uncertainty about the biomass C stocks in the Oyster River study landscape prior to large-scale disturbance, the biomass estimates of C-CLASS are not higher than those values reported in the literature of other research on other Pacific Northwest old-growth forest stands (Table 2.5). However, C-CLASS estimates of old-growth DOM and SOM appear to be high (Table 2.5). The reason is that C-CLASS used DOM and SOM in 1920 provided by CBM-CFS3 for the model initialization and the CBM-CFS3's high estimates are attributed to initialized DOM and SOM C pools generated using a model spin-up procedure that simulated a long-term stand replacing disturbance regime without considering other disturbances (i.e. ground

fires) that can significantly reduce the DOM and SOM accumulation in the model (Trofymow et al., 2008). In the historic records of Oyster River study area, there was no documentation or evidence of extensive logging with large amount of debris left on site prior to 1920, but historical information indicates that there was a wide spread wild fire in the region in the late 1600s (Mackie, 2000). Stand-destroying wild fire frequency before the settlement of Europeans in this region is estimated to have ranged from 150 to 350 years (Hamilton and Nicholson, 1990). Old-growth DOM and surface SOM may also be consumed in the wild fire and are less possible to reach high values estimated by CBM-CFS3. However, the SOM value estimated by C-CLASS is close to the measurements by Smithwick et al. (2002) in Olympic National Park, Washington, USA. Compared to measurements of DOM and SOM in western Vancouver Island old-growth forests, the measurements in eastern side of the island appear to be lower, which can be attributed to the lower fire frequency on the wetter and windward west side of the island (Trofymow and Blackwell, 1998).

Old-growth forests in Oyster River study landscape in 1920 were estimated by C-CLASS to be very productive, with a landscape-level average NPP of 8.80 Mg C ha^{-1} yr^{-1}. This NPP value is higher than published estimates for an old-growth forest at Wind River Experimental Forest, Washington, USA (Harmon et al., 2004) and old-growth Douglas fir stands of a Western Oregon Watershed, USA (Grier and Logan, 1977) (see Table 2.6). Measurements of belowground component of NPP (BNPP) at the Wind River Experimental Forest and H.J. Andrew Experimental Forest only accounted for coarse and fine root increments and the coarse and fine roots mortality, ignoring root loss to herbivores, root exudates and carbohydrate export to symbionts which probably underestimate the true NPP by at least 30% (Clark et al., 2001; Chapin III et al., 2002). If the previously published belowground NPP estimates are recalculated using the model

developed by Coble et al. (2001) for high-productivity Douglas-fir stands (BNPP = 0.6333*ANPP + 431.63, where ANPP and BNPP are expressed in kg C ha^{-1} yr^{-1}, respectively), then we can see first that Coble's model agrees well with the C-CLASS simulated old-growth below-ground NPP and second that the recalculated total NPP estimates for old-growth stands at the Wind River and H.J. Andrew Experimental Forest are close to C-CLASS estimates for both DF49 tower site and the whole landscape.

Forest productivity following conversion from old-growth to second-growth forest as simulated by C-CLASS for the Oyster River study area can be evaluated by examining the patterns of GPP, Re and NEP in relation to forest stand age. GPP simulated by C-CLASS for the DF49 site pixel through its regeneration after harvesting agrees well with estimates based on data from the HDF00-HDF88-DF49 tower sites by Schwalm et al. (2007) as well as those reported by Jassal et al. (2007) for DF49 (Figure 2.10). The general pattern of GPP with stand age reported by C-CLASS, with GPP peaking at around 40 years old, is consistent with that simulated for the chronosequence of coastal Douglas-fir forest stands using a process-based model, ecosys (Grant et al., 2007). The NEP pattern shown in Figure 7 is also similar to the pattern described by, Pregitzer and Euskirchen (2004), with NEP reaching its maximum while the forest stand is still quite young (Pregitzer and Eugenie, 2004). NEP estimates for the HDF00-HDF88-DF49 tower sites indicate that these ecosystems act as net C sources for at least 17 years following clearcut harvesting (Schwalm et al., 2007). C-CLASS estimated that DF49 first became a net C sink at age 4. However, age is not a perfect proxy for time-since-disturbance for DF49 since this stand was not immediately regenerated following disturbance (Trofymow et al., 2008). The historic disturbance data indicate that the stand was not planted until 12 years after the site was harvested in 1937. The number of years during which the stand was a net C source after disturbance estimated by C-

CLASS is actually very similar to the period inferred from the estimates reported by Schwalm et al. (2007) and is also consistent with the estimate reported by Grant et al. (2007). Additionally, the HDF00-HDF88-DF49 tower sites are not a true chronosequence. The HDF00 and HDF88 sites are in third-growth stands which were clearcut, broadcast burned and planted within one year, while DF49 site is a second-growth stand that was harvested in 1937, slash burned in 1939 and planted in 1949 (12 years' regeneration delay). Therefore, more dead organic matter were left in HDF00 and HDF88 than in DF49, which would lead to a higher Re and lower NEP (Figure 2.7), a demonstration of the legacy effects of differences in disturbance history on a site's recent C budget (Trofymow et al., 2008).

When we refer to C-CLASS estimates for the DF49 stand in this study, it refers to the results generated by the model for 1 ha pixel where DF49 tower is located. The footprint of the flux tower covers a far larger area than this single pixel, and within this footprint are stands that have a range of different disturbance and planting histories (and are represented by different pixels in C-CLASS model run). Thus, some of the differences between tower-based estimates and C-CLASS simulation may be attributed to this spatial heterogeneity within the tower footprint area. However, the comparisons between model estimates from C-CLASS and the estimates calculated using tower measurement data are still helpful although the interpretation of these is not entirely straight-forward. In the future, we are going to make comparisons between tower-based measurements of C fluxes, ground plot C stock change measurements, and the C-CLASS simulation by developing more accurate methods to define and weight the flux tower footprints (Trofymow et al., 2008; Chen et al., 2009).

2.6 Study Significance and Conclusions

This study demonstrates that if carefully parameterized, land surface models can be used to investigate the impacts of climate variability and disturbance history on long term carbon balance of forest landscapes. Such parameterization is only possible where systematic and consistent spatial data are available, as these are essential to the study of landscape-level carbon budgets using process-based models such as C-CLASS. When required input data have been gridded on the same spatial area, then disturbance history, initial inventory and historic weather data can be used to examine the possible biases in inventory-based carbon budget models, e.g. CBM-CFS3. Such studies make it possible to analyze the importance of climate drivers and the development of methods for including climate variability in inventory-based models.

Our results showed that landscape-level net primary productivity among carbon fluxes is more sensitive to air temperate due to the relatively high sensitivity of autotrophic respiration to air temperature. Among carbon pools, changes in dead organic carbon pools are more sensitive to air temperature than biomass carbon pools. All landscape-level carbon fluxes and changes of carbon stocks appear less sensitive to precipitation.

This study resulted in the improvement of C-CLASS model by incorporating CBM-CFS3's approach to simulate disturbance impacts by the model. It also provided historic carbon dynamics at landscape level using the improved C-CLASS model. These improvements will enable future studies using C-CLASS to enhance our understanding of the impacts of future climate variability and disturbance regimes on landscape-level carbon dynamics.

In the future, as carbon takes on economic value and forest managers are required to monitor and track the carbon implications of their silvicultural and harvesting activities – either as part of Criteria and Indicators reporting, or to support carbon credit trading, integration of multiple

methodologies (e.g. biometric and eddy covariance measurement, remote sensing observation, inventory-based and process-based modeling, atmospheric inverse modeling) will be required to ensure that the carbon benefits of sustainable forest management are adequately quantified and understood at all relevant spatial and temporal scales.

2.7 References

Arain, M.A., Black, T.A., Barr, A.G., Jarvis, P.G., Massheder, J.M., Verseghy, D.L., Nesic, Z., 2002. Effects of seasonal and interannual climate variability on net ecosystem productivity of boreal deciduous and conifer forests. Canadian Journal of Forest Research 32(5): 878-891.

Arain, M.A., Yuan, F., Andrew Black, T., 2006. Soil-plant nitrogen cycling modulated carbon exchanges in a western temperate conifer forest in Canada. Agric. Forest Meteorol. 140(1-4): 171-192.

Bonan, G.B., 1995. Land-atmosphere CO2 exchange simulated by a land surface process model coupled to an atmospheric general circulation model. J. Geophys. Res. 100: 2817-2831.

Chapin III, F.S., Pamela, A.M., Harold, A.M., 2002. Principles of terrestrial ecosystem ecology, Springer.

Chen, B., Black, T., Coops, N., Hilker, T., Trofymow, J., Morgenstern, K., 2009. Assessing Tower Flux Footprint Climatology and Scaling Between Remotely Sensed and Eddy Covariance Measurements. Boundary-Layer Meteorology 130(2): 137-167.

Clark, D.A., Brown, S., Kicklighter, D.W., Chambers, J.Q., Thomlinson, J.R., Ni, J., 2001. Measuring Net Primary Production in Forests: Concepts and Field Methods. Ecological Applications 11(2): 356-370.

Coble, D.W., Milner, K.S., Marshall, J.D., 2001. Above- and below-ground production of trees and other vegetation on contrasting aspects in western Montana: a case study. Forest Ecology and Management 142(1-3): 231-241.

Dickinson, R.E., Shaikh, M., Bryant, R., Graumlich, L., 1998. Interactive Canopies for a Climate Model. Journal of Climate 11: 2823-2836.

Dixon, R.K., Solomon, A.M., Brown, S., Houghton, R.A., Trexier, M.C., Wisniewski, J., 1994. Carbon Pools and Flux of Global Forest Ecosystems. Science 263(5144): 185-190.

Foley, J.A., Prentice, I.C., Ramankutty, N., Levis, S., Pollard, D., Sitch, S., Haxeltine, A., 1996. An Integrated Biosphere Model of Land Surface Processes, Terrestrial Carbon Balance, and Vegetation Dynamics. Global Biogeochem. Cycles 10: 603-628.

Gower, S.T., Vogel, J.G., Norman, J.M., Kucharik, C.J., Steele, S.J., Stow, T.K., 1997. Carbon distribution and aboveground net primary production in aspen, jack pine, and black spruce stands in Saskatchewan and Manitoba, Canada. J. Geophys. Res. 102.

Grant, R.F., Black, T.A., Humphreys, E.R., Morgenstern, K., 2007. Changes in net ecosystem productivity with forest age following clearcutting of a coastal Douglas-fir forest: testing a mathematical model with eddy covariance measurements along a forest chronosequence. Tree Physiology 27: 115-131.

Grier, C.C., Logan, R.S., 1977. Old-Growth Pseudotsuga menziesii Communities of a Western Oregon Watershed: Biomass Distribution and Production Budgets. Ecological Monographs 47(4): 373-400.

Hamilton, E., Nicholson, A. (1990). Old-Growth Forests Problem Analysis. Victoria, BC Ministry of Forests**:** 104.

Harmon, M.E., Bible, K., Ryan, M.G., Shaw, D.C., Chen, H., Klopatek, J., Li, X., 2004. Production, Respiration, and Overall Carbon Balance in an Old-growth Pseudotsuga-Tsuga Forest Ecosystem. Ecosystems 7(5): 498-512.

Jassal, R.S., Black, T.A., Cai, T., Morgenstern, K., Li, Z., Gaumont-Guay, D., Nesic, Z., 2007. Components of ecosystem respiration and an estimate of net primary productivity of an intermediate-aged Douglas-fir stand. Agricultural and forest meteorology 144(1-2): 44-57.

Jungen, J.R. (1985). Soils of Southern Vancouver Island. BC Soil Survey Report. Victoria, BC, BC Ministry of Environment.

Kothavala, Z., Arain, M.A., Black, T.A., Verseghy, D.L., 2005. The simulation of energy, water vapor and carbon dioxide fluxes over common crops by the Canadian Land Surface Scheme (CLASS). Agricultural and forest meteorology 133: 89-108.

Kucharik, C.J., Foley, J.A., Delire, C., Fisher, V.A., Coe, M.T., Lenters, J.D., Young-Molling, C., Ramankutty, N., Norman, J.M., Gower, S.T., 2000. Testing the Performance of a Dynamic Global Ecosystem Model: Water Balance, Carbon Balance, and Vegetation Structure. Global Biogeochemical Cycles 14(3): 795-825.

Kurz, W., Beukema, S., Apps, M., 1997. Carbon budget implications of the transition from natural to managed disturbance regimes in forest landscapes. Mitigation and Adaptation Strategies for Global Change 2(4): 405-421.

Kurz, W.A., Dymond, C.C., White, T.M., Stinson, G., Shaw, C.H., Rampley, G.J., Smyth, C., Simpson, B.N., Neilson, E.T., Trofymow, J.A., Metsaranta, J., Apps, M.J., 2009. CBM-CFS3: A model of carbon-dynamics in forestry and land-use change implementing IPCC standards. Ecological Modelling 220(4): 480-504.

Li, Z., Kurz, W.A., Apps, M., Beukema, S., 2003. Belowground biomass dynamics in the Carbon Budget Model of the Canadian Forest Sector: recent improvements and implications for the estimation of NPP and NEP. Canadian Journal of Forest Research 33: 126-136.

Liu, J., Price, D.T., Chen, J.M., 2005. Nitrogen controls on ecosystem carbon sequestration: a model implementation and application to Saskatchewan, Canada. Ecological Modelling 186(2): 178-195.

Mackie, R.S., Ed. 2000. Island Timber. Victoria, BC, Sono Nis Press.

Morgenstern, K., Andrew Black, T., Humphreys, E.R., Griffis, T.J., Drewitt, G.B., Cai, T., Nesic, Z., Spittlehouse, D.L., Livingston, N.J., 2004. Sensitivity and uncertainty of the carbon balance of a Pacific Northwest Douglas-fir forest during an El Nino/La Nina cycle. Agricultural and forest meteorology 123(3-4): 201-219.

Pojar, J., Klinka, K., Demarchi, D.A., 1991. Chapter 6: Coastal Western Hemlock Zone. In: Meidinger, D., Pojar, J. (Eds.). Ecosystems of British Columbia. BC Special Report Series No. 6. BC Ministry of Forests. Victoria, pp. 95-111.

Pregitzer, K.S., Eugenie, S.E., 2004. Carbon cycling and storage in world forests: biome patterns related to forest age. Global Change Biology 10(12): 2052-2077.

Schwalm, C.R., Black, T.A., Kai, M., Elyn, R.H., 2007. A method for deriving net primary productivity and component respiratory fluxes from tower-based eddy covariance data: a case study using a 17-year data record from a Douglas-fir chronosequence. Global Change Biology 13(2): 370-385.

Sellers, P.J., Dickinson, R.E., Randall, D.A., Betts, A.K., Hall, F.G., Berry, J.A., Collatz, G.J., Denning, A.S., Mooney, H.A., Nobre, C.A., Sato, N., Field, C.B., Henderson-Sellers, A., 1997. Modeling the Exchanges of Energy, Water, and Carbon Between Continents and the Atmosphere. Science 275(5299): 502-509.

Sellers, P.J., Los, S.O., Tucker, C.J., Justice, C.O., Dazlich, D.A., Collatz, G.J., Randall, D.A., 1996. A Revised Land Surface Parameterization (SiB2) for Atmospheric GCMS. Part II: The Generation of Global Fields of Terrestrial Biophysical Parameters from Satellite Data. Journal of Climate 9: 706-737.

Smithwick, E., Harmon, M., Domingo, J., 2007. Changing Temporal Patterns of Forest Carbon Stores and Net Ecosystem Carbon Balance: the Stand to Landscape Transformation. Landscape Ecology 22(1): 77-94.

Smithwick, E.A.H., Harmon, M.E., Remillard, S.M., Acker, S.A., Franklin, J.F. (2002). POTENTIAL UPPER BOUNDS OF CARBON STORES IN FORESTS OF THE PACIFIC NORTHWEST. **12:** 1303-1317.

Song, C., Woodcock, C.E., 2003. A regional forest ecosystem carbon budget model: impacts of forest age structure and landuse history. Ecological Modelling 164(1): 33-47.

Sun, O.J., Campbell, J., Law, B.E., Wolf, V., 2004. Dynamics of carbon stocks in soils and detritus across chronosequences of different forest types in the Pacific Northwest, USA. Global Change Biology 10(9): 1470-1481.

Thomas, S.C., Winner, W.E., 2000. Leaf area index of an old-growth Douglas-fir forest estimated from direct structural measurements in the canopy. Canadian Journal of Forest Research 30: 1922-1930.

Trofymow, J.A., Blackwell, B.A., 1998. Changes in ecosystem mass and carbon distributions in coastal forest chronosequences. Northwest Science 72(2): 40-42.

Trofymow, J.A., Stinson, G., Kurz, W.A., 2008. Derivation of a spatially explicit 86-year retrospective carbon budget for a landscape undergoing conversion from old-growth to managed forests on Vancouver Island, BC. 6th North American Forest Ecology Workshop: From science to sustainability 256(10): 1677-1691.

Trofymow, J.A., Stinson, G., Kurz, W.A., 2008. Derivation of a spatially explicit 86-year retrospective carbon budget for a landscape undergoing conversion from old-growth to managed forests on Vancouver Island, BC. Forest Ecology and Management 256(10): 1677-1691.

Turner, D.P., Acker, S.A., Means, J.E., Garman, S.L., 2000. Assessing alternative allometric algorithms for estimating leaf area of Douglas-fir trees and stands. Forest Ecology and Management 126(1): 61-76.

Verseghy, D.L., 1991. CLASS - a Canadian land surface scheme for GCMs. I. Soil model. International Journal of Climatology 11: 111-113.

Verseghy, D.L., 2000. The Canadian Land Surface Scheme (CLASS): Its History and Future. Atmosphere-Ocean 38(1): 1-13.

Verseghy, D.L., McFarlane, N.A., Lazare, M., 1993. CLASS - a Canadian land surface scheme for GCMs. II. Vegetation model and coupled runs. International Journal of Climatology 13: 347-370.

Wang, S., Grant, R.F., Verseghy, D.L., Black, T.A., 2001. Modelling plant carbon and nitrogen dynamics of a boreal aspen forest in CLASS - the Canadian Land Surface Scheme. Ecological Modelling 142(1-2): 135-154.

Wang, S., Grant, R.F., Verseghy, D.L., Black, T.A., 2002. Modelling Carbon Dynamics of Boreal Forest Ecosystems Using the Canadian Land Surface Scheme. Climatic Change 55(4): 451-477.

Wang, S.R.F.G.D.L.V.T.A.B., 2002. Modelling carbon-coupled energy and water dynamics of a boreal aspen forest in a general circulation model land surface scheme. International Journal of Climatology 22(10): 1249-1265.

Yuan, F., Arain, M.A., Alan, G.B., Black, T.A., Charles, P.A.B., Carole, C., Hank, A.M., McCAUGHEY, J.H., Steven, C.W., 2008. Modeling analysis of primary controls on net ecosystem productivity of seven boreal and temperate coniferous forests across a continental transect. Global Change Biology 14(8): 1765-1784.

Yuan, F., Arain, M.A., Black, T.A., Morgenstern, K., 2007. Energy and water exchanges modulated by soil-plant nitrogen cycling in a temperate Pacific Northwest conifer forest. Ecological Modelling 201(3-4): 331-347.

Table 2. 1 Initial C/N characteristics of soil and vegetation used in C-CLASS simulations at the Oyster River landscape.

Characteristics	**Value**
Tree density (trees m^{-2})[a]	0.11
Initial LAI (m^2 m^{-2})	8.2
Specific leaf area (m^2 kg^{-1} C)[b]	15
C in reserved pool (kg C m^{-2})	0.01
N:C ratio in plant labile reservoir	0.1
N:C ratio in heartwood tissue	0.001
N:C ratio in fine roots	0.02
N:C ratio in coarse roots	0.01
N:C ratio in surface litter	0.0125
N:C ratio in root litter	0.01
N:C ratio in fresh SOM	0.04
N:C ratio in stable SOM	0.03

[a] Assigned from Drewitt et al. (2002)
b Assigned from Warren et al. (2003a,b)
c Assigned from CBM-CFS3 output

Table 2. 2 Photosynthesis and respiration parameters used in C-CLASS simulation at the Oyster River landscape.

Parameters	**Value**
Maximum carboxylation rate, V_{cmax} (μmol m^{-2} s^{-1})	39.0
Empirical constant related to intercellular CO_2 concentration, a_1	3.9
Empirical parameter for stomatal sensitivity to VPD, D_0 (Pa)	1000
Extinction coefficient for canopy nitrogen	0.14
Maximum transfer rate of assimilate to leaf structure, k_p (s^{-1})	5.0×10^{-6}
Quantum efficiency of RuBP regeneration (mol e mol^{-1} quanta)	0.2
Leaf respiration rate at reference condition, R_{ref} at 15 ˚C (μmol m^{-2} s^{-1})	0.3
Living wood respiration rate at reference condition at 15 ˚C (μmol m^{-3} s^{-1})	2.5
Fine root respiration rate at reference condition at 15 ˚C (μmol kg^{-1} C s^{-1})	0.5
Coarse root respiration rate at reference condition at 15 ˚C (μmol kg^{-1} C s^{-1})	0.3
Base litter respiration rate at 10 ˚C (μmol kg^{-1} C s^{-1})	0.15
Base dead wood respiration rate at 10 ˚C (μmol kg^{-1} C s^{-1})	0.10
Base dead root respiration rate at 10 ˚C (μmol kg^{-1} C s^{-1})	0.08
Base short-lived SOM respiration rate at 10 ˚C (μmol kg^{-1} C s^{-1})	0.20
Base stable SOM respiration rate at 10 ˚C (μmol kg^{-1} C s^{-1})	0.08
Relative change in stem/coarse root respiration for 10 ˚C (Q_{10})	2.0
Relative change in leaf/fine root respiration for 10 ˚C (Q_{10})	2.0
Q_{10} in soil/litter respiration when temperature in 10 – 30 ˚C	2.0
Q_{10} in soil/litter respiration when temperature is under 10 ˚C	6.0
Q_{10} in soil/litter respiration when temperature is over 30 ˚C	2.0
One-half field capacity water content	0.20
One-half saturated water content (porosity)	0.23
Wood turnover rate (μmol kg^{-1} C s^{-1})	0.02
Root turnover rate (μmol kg^{-1} C s^{-1})	0.08

Table 2. 3 C-CLASS simulated landscape carbon stocks in 2005 for the eight model run (1920-2005) scenarios, showing the impact of disturbance, CO_2 fertilization and climate variability on carbon stocks.

Scenario	CO_2 change	Disturbance	Climate Variability	AGB	BGB	DOM	SOM
Full	yes	yes	yes	123.02	39.00	98.60	207.30
No_CO_2		yes	yes	109.58	34.30	85.71	206.22
No_Dis	yes		yes	346.91	59.04	209.09	210.29
No_Dis/CO_2			yes	322.26	50.97	196.28	210.29
No_Clim	yes	yes		123.24	39.30	101.55	207.43
No_Clim/CO_2		yes		123.24	39.30	101.55	207.43
No_Clim/Dis	yes			353.18	60.29	222.36	210.29
No_Clim/CO_2/Dis				353.18	60.29	222.36	210.29

Unit is Mg C ha^{-1}.
No_CO_2 denotes pre-Industrial CO_2/no CO_2 fertilization.
No_Dis denotes no disturbance.
No_Clim denotes no interannual variability in climate variables and CO_2.
AGB denotes aboveground tree biomass.
BGB denotes belowground tree biomass.
DOM denotes dead organic matter including dead wood, dead root and forest floor litter.
SOM denotes soil organic matter.

Table 2. 4 C-CLASS simulated annual GPP, NPP, NEP and Re averaged over 1998-2005 for the eight model run scenarios.

Scenario	GPP	NPP	NEP	Re
Full	17.67	7.82	2.51	15.16
No_CO_2	15.81	6.86	1.97	13.84
No_Dis	19.83	7.28	-1.89	21.72
No_Dis/CO_2	18.00	6.26	-2.53	20.53
No_Clim	18.08	8.64	3.39	14.69
No_Clim/CO_2	18.08	8.64	3.39	14.69
No_Clim/Dis	20.31	8.38	-0.59	20.90
No_Clim/CO_2/Dis	20.31	8.38	-0.59	20.90

Unit is Mg C ha^{-1} yr^{-1}.
No_CO_2 denotes pre-Industrial CO_2/no CO_2 fertilization.
No_Dis denotes no disturbance.
No_Clim denotes no interannual variability in climate variables and CO_2.

Table 2. 5 Carbon stocks (Mg C ha^{-1}) in old-growth forests of Vancouver Island and the Pacific Northwest including aboveground biomass (AGB), belowground biomass (BGB), total biomass ($Biomass_{TOT}$), dead wood (DW), dead root (DR), dead organic C in litter (DOM_L), total dead organic matter (DOM_{TOT}), soil organic matter (SOM) and total ecosystem carbon (TEC).

	AGB	**BGB**	**$Biomass_{TOT}$**	**DW**	**DR**	**DOM_L**	**DOM_{TOT}**	**SOM**	**TEC**
OR	285	57	342	85	46	75	206	210	758
DF49	291	59	350	70	37	61	168	170	688
EVI	-	-	417	-	-	-	49	47	513
WVI	-	-	532	-	-	-	178	89	799
WR	313	85	398	87	-	41	128	93	619
HJA	359	76	435	107	-	26	133	56	625
ONP	364	122	485	103	-	36	139	195	819

OR: Old-growth landscape average C stock simulated by C-CLASS for Oyster River study area in 1920 (prior to any logging).

DF49: Old-growth site C stocks in 1920 (prior to any logging) simulated by C-CLASS for the stand where the DF49 flux tower is now located

EVI: Measured eastern Vancouver Island old-growth forests C stocks (Trofymow and Blackwell, 1998).

WVI: Measured western Vancouver Island old-growth forests C stocks (Trofymow and Blackwell, 1998).

WR: Wind River Experimental Forest in Washington (Harmon et al., 2004).

HJA: H.J. Andrews Experimental Forest in Oregon (Grier and Logan, 1977).

ONP: Olympic National Park in Washington (Smithwick et al., 2002).

Table 2. 6 Estimated net primary productivity of old-growth forests at Oyster River in 1920 and the Pacific Northwest (Mg C ha^{-1} yr^{-1}) including above-ground net primary productivity (ANPP) and below-ground net primary productivity (BNPP) and total NPP.

Location	ANPP	BNPP	NPP
C-CLASS simulated landscape average in 1920	5.73	3.07 (4.06)	8.80 (9.79)
C-CLASS simulated DF49 tower site stand in 1920	5.72	2.95 (4.05)	8.67 (9.77)
Wind River Exp. Forest, WA[a]	4.55	1.42 (3.31)	5.97 (7.86)
H.J. Andrews Exp. Forest, OR[b]	3.99	1.45 (2.96)	5.44 (6.95)

[a] Harmon et al. (2004)
[b] Grier and Logan (1977)
Values in parentheses were calculated by estimating BNPP as a function of ANPP using the model (Coble et al., 2001): BNPP = 0.6333*ANPP + 431.63, where ANPP and BNPP are expressed in kg C ha^{-1} yr^{-1}.

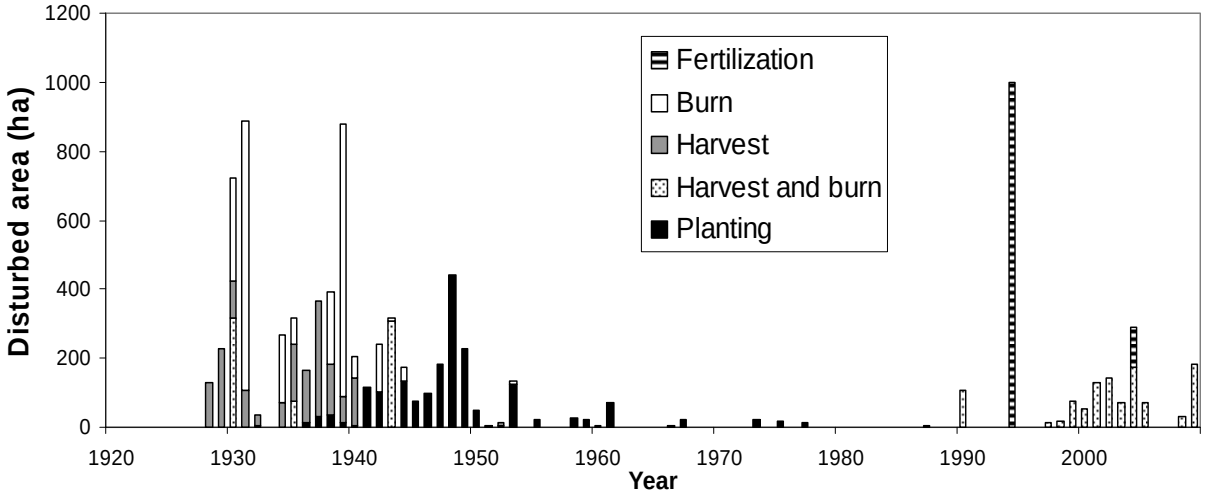

Figure 2. 1 The disturbance events and total area covered by these events in the Oyster River landscape from 1920-2005.

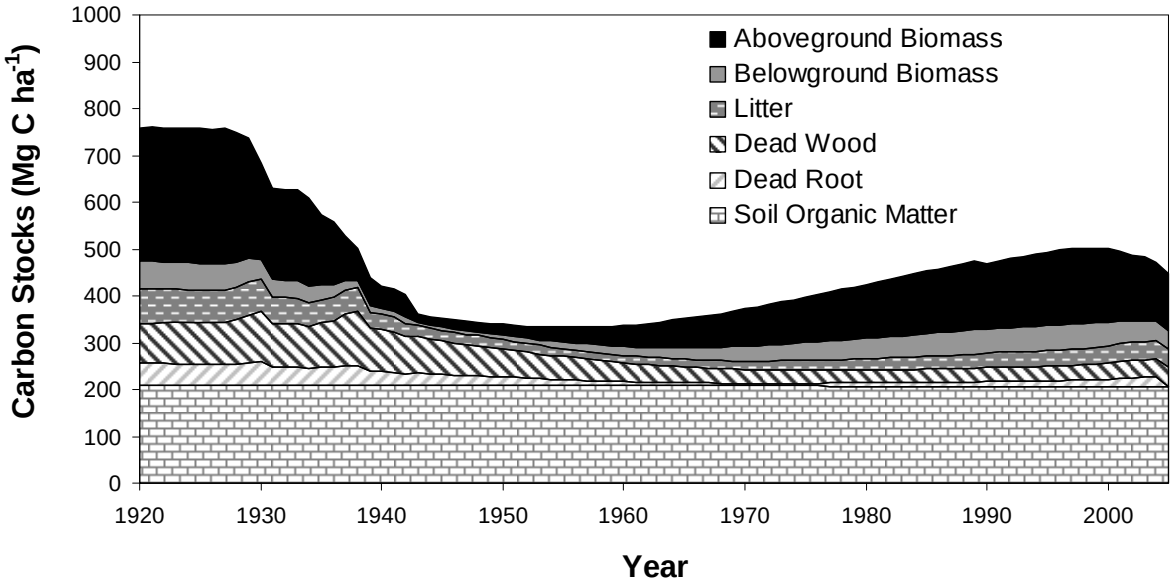

Figure 2.2 C-CLASS simulated annual average landscape carbon stocks categorize in Intergovernmetal Panel on Climate Change (IPCC) specified carbon pools from 1920-2005.

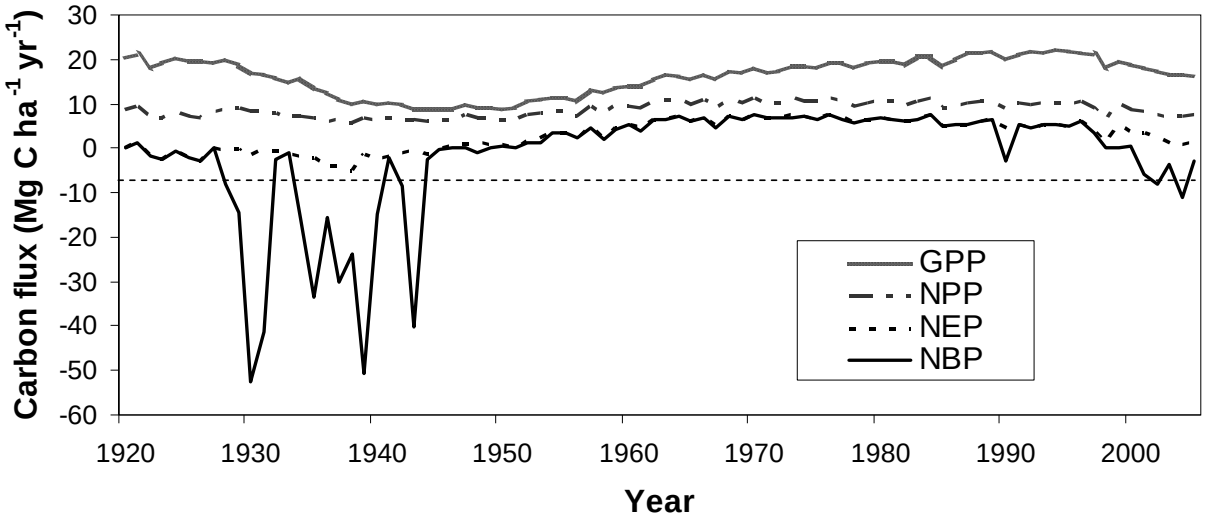

Figure 2. 3 C-CLASS simulated annual average landscape carbon fluxes: gross primary productivity (GPP), net primary productivity (NPP), net ecosystem productivity (NEP) and net biome productivity (NBP) from 1920-2005. Positive values are carbon sinks and negative values are carbon sources.

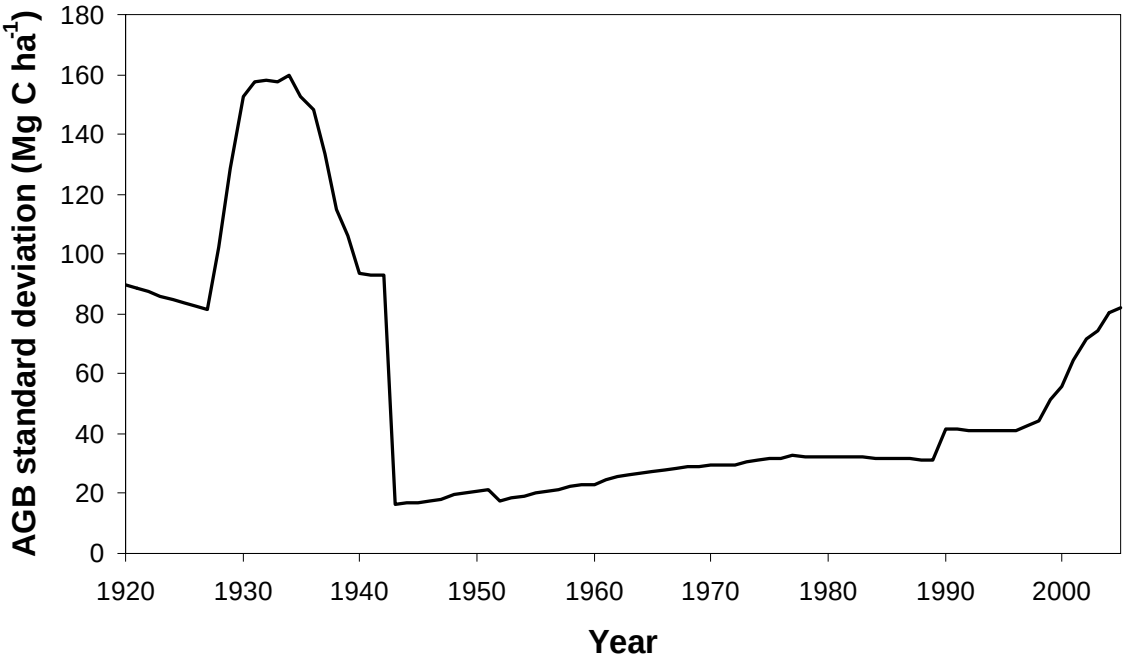

Figure 2. 4 C-CLASS simulated standard deviations of aboveground biomass (AGB) in the Oyster River landscape from 1920-2005.

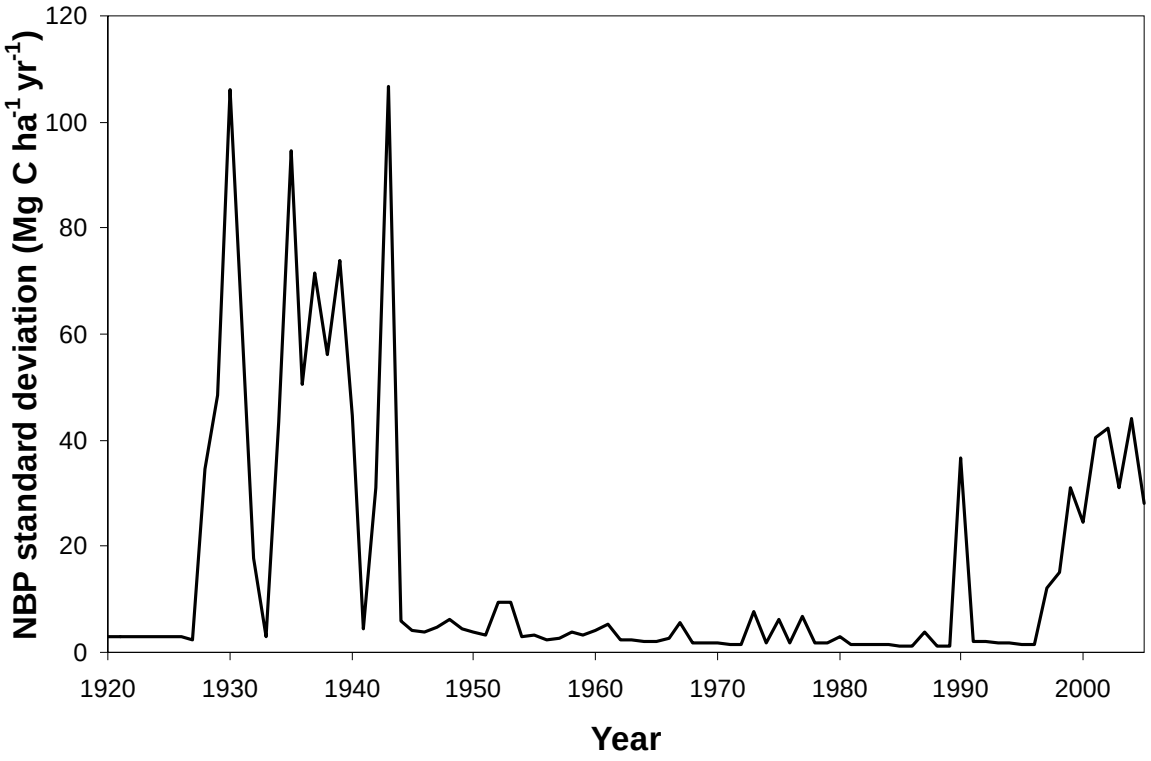

Figure 2. 5 C-CLASS simulated standard deviations of net biome productivity (NBP) in the Oyster River landscape from 1920-2005.

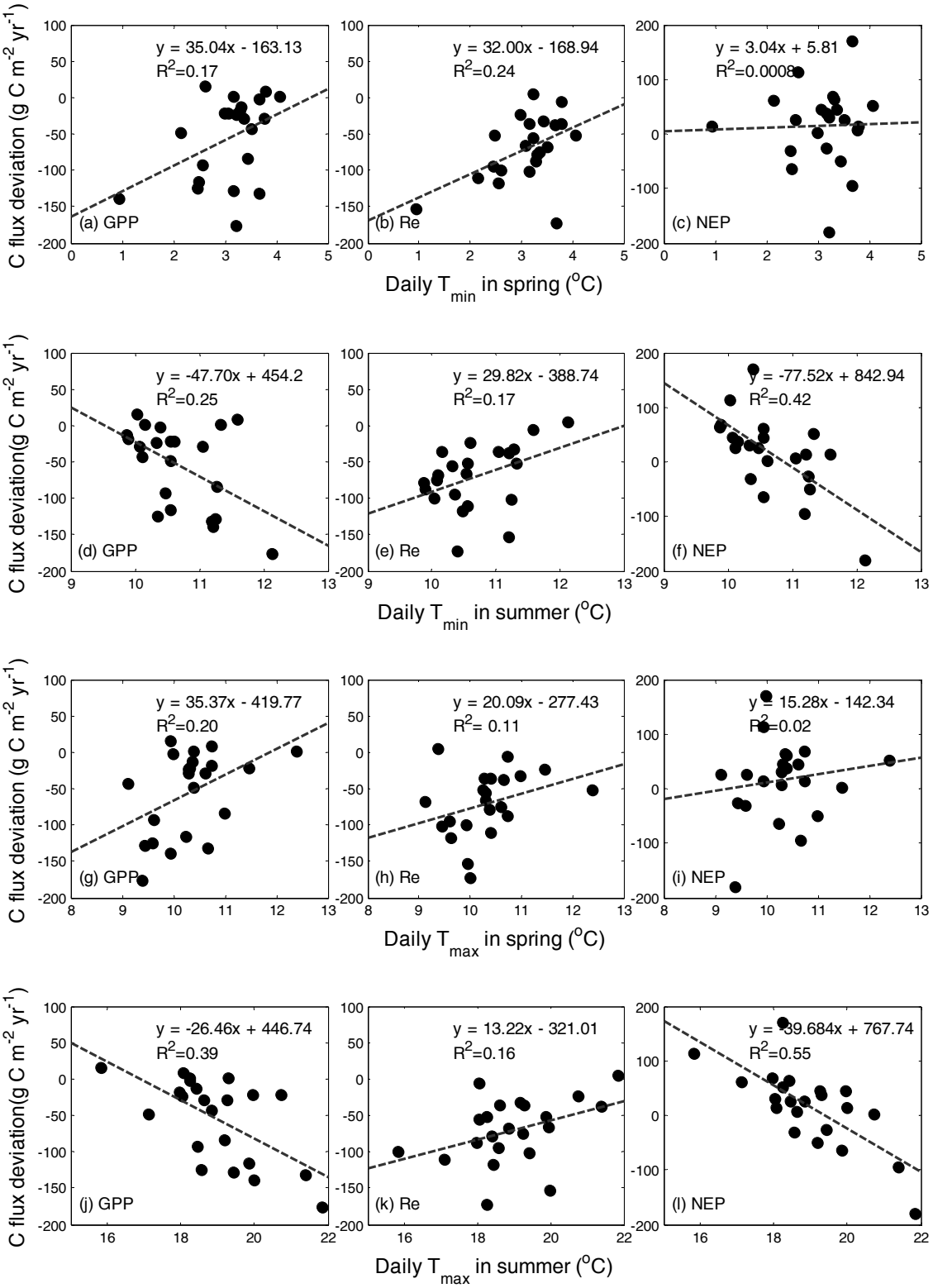

Figure 2. 6 Relationship between C-CLASS simulated deviations in 7-year mean gross primary productivity (GPP), ecosystem respiration (Re), net ecosystem productivity (NEP) and daily maximum and minimum temperature in spring and summer in the Oyster River landscape from 1963-1984.

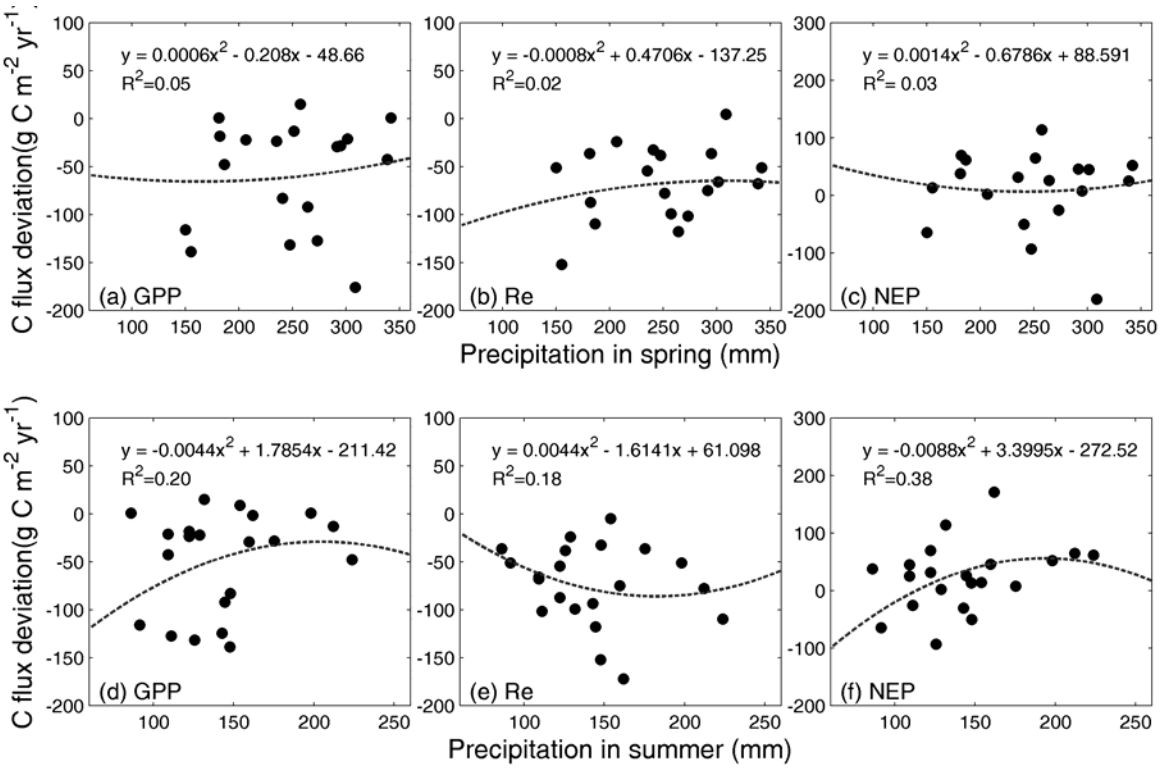

Figure 2. 7 Relationship between C-CLASS simulated deviations in 7-year mean gross primary productivity (GPP), ecosystem respiration (Re), net ecosystem productivity (NEP) and total precipitation in spring or summer in the Oyster River landscape from 1963-1984.

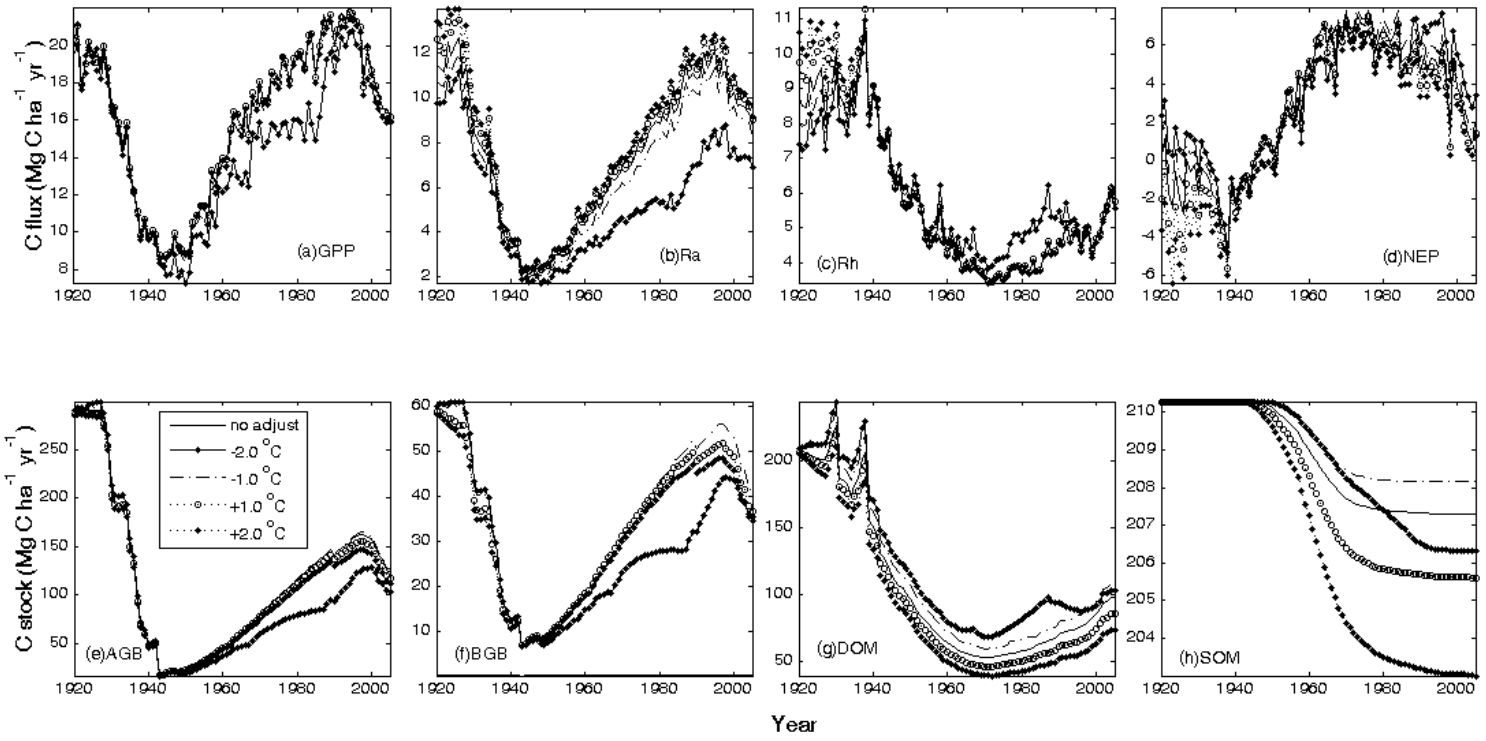

Figure 2. 8 Sensitivity of C-CLASS simulated landscape-level carbon fluxes and stocks to air temperature. GPP, gross primary productivity; R_a, autotrophic respiration; R_h, heteorotrophic respiration; NEP, net ecosystem productivity; AGB, aboveground biomass; BGB, belowground biomass; DOM, dead organic matter; SOM, soil organic matter.

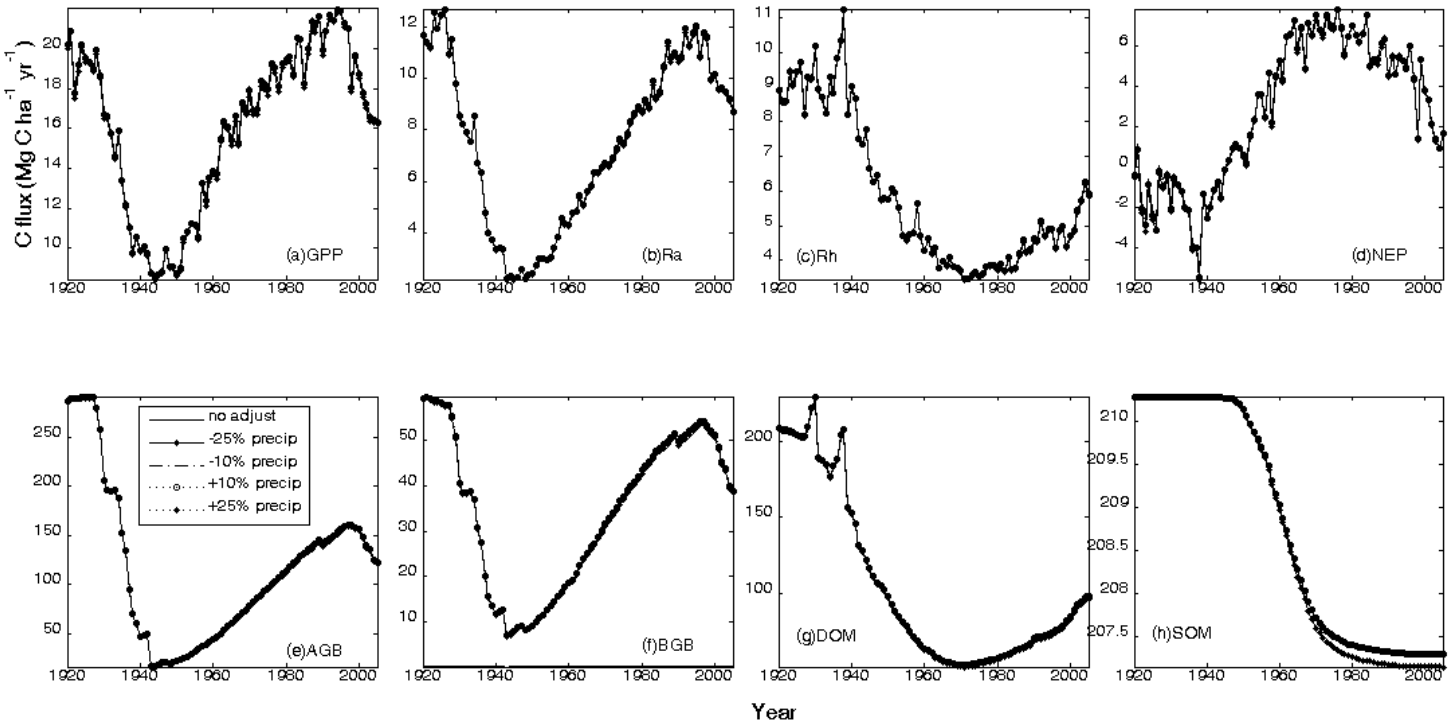

Figure 2. 9 Sensitivity of C-CLASS simulated landscape-level carbon fluxes and stocks to precipitation. GPP, gross primary productivity; R_a, autotrophic respiration; R_h, heterotrophic respiration; NEP, net ecosystem productivity; AGB, aboveground biomass; BGB, belowground biomass; DOM, dead organic matter; SOM, soil organic matter.

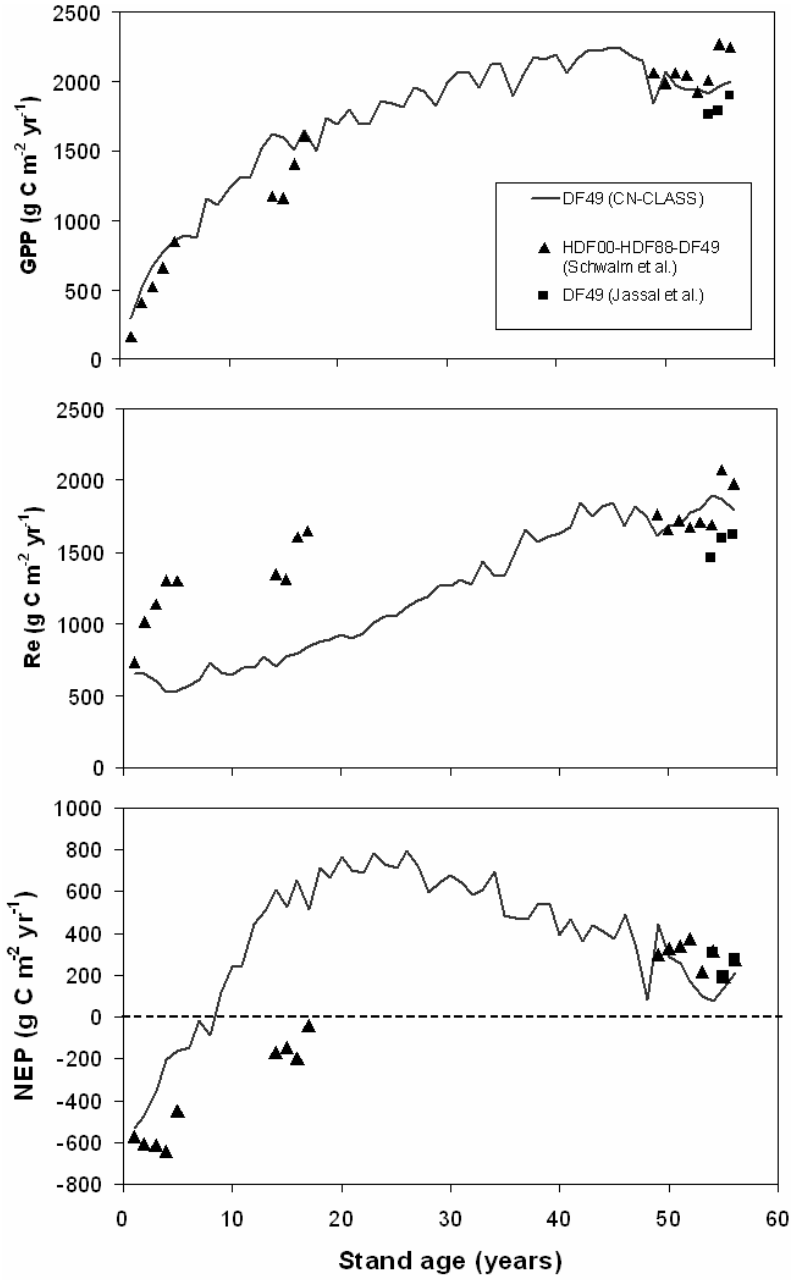

Figure 2. 10 Stand-level (A) GPP, (B) Re, and (C) NEP plotted against stand age. C-CLASS estimates for the 1 ha pixel containing the flux tower at the DF49 site are shown, with the comparison to the estimates based on flux measurements for DF49 by Jassal et al. (2007) and for the HDF00-HDF88-DF49 tower sites by Schwalm et al. (2007).

CHAPTER 3:

HISTORIC CARBON DYNAMICS OF AN EASTERN BOREAL BLACK SPRUCE FOREST LANDSCAPE IN CANADA

3.1 Abstract

Black spruce stands constitute a large portion of Canadian boreal forest landscape and have been increasingly impacted by both anthropogenic and natural disturbances over the last century. In this study, Carbon and Nitrogen coupled Canadian Land Surface Scheme (C-CLASS) was used to simulate the historic carbon stocks and fluxes in a 6275 ha forested landscape in Chibougamau, Quebec, Canada to evaluate the impact of disturbance regimes and climate variability on the carbon budget of the eastern Canadian boreal forests. The disturbance matrix of Carbon Budget Model of Canadian Forest Sector (CBM-CFS3) was used to represent the impact of different disturbance events on the carbon fluxes from different pools. Landscape maps of soil texture, topography, forest types, stand density, stand age and inventory data in 1928 and historic disturbance data were provided by historic carbon modeling project of Canadian Carbon Program (CCP). Hourly meteorology data input constructed from climate

records was used to drive the model timeseries to simulate forest productivity from 1928 to 2005.

Over the study period, C-CLASS suggests a 19.27 Mg C ha^{-1} increase in total ecosystem carbon (TEC) as compared to 12.11 Mg C ha^{-1} increase estimated by the inventory based CBM-CFS3 model. In 1963, about 689 ha forest area was disturbed, of which 608 ha was clear cut, 75 ha partial cut and 6 ha was partially defoliated by insects. During these events, a large amount of carbon was released from the forest and the landscape-level net biome productivity (NBP) in 1963 and 1964 was -4.10 and -3.31 Mg C ha^{-1} yr^{-1}, respectively. The landscape was a strong C source in these two years. From 1970 to 2005, there were very few disturbance events in the region and the landscape-level TEC increased from 76.70 to 94.66 Mg C ha^{-1}. During this period, C-CLASS simulated NBP ranged from -0.08 Mg C ha^{-1} yr^{-1} in 2005 to 0.89 Mg C ha^{-1} yr^{-1} in 1977, and these differences were mostly determined by inter-annual climate variability. Our analysis further showed that in undisturbed forest landscape simulated annual NEP deviations were positively related to mean daily minimum and maximum air temperature in spring. This study will help to explore the impact of forest management and future climate change on boreal forest landscapes.

3.2 Introduction

The world's boreal forests cover circumpolar areas in the Northern Hemisphere in both North America and Eurasia. They occupy 16.6 million km^2 area worldwide covering around 10 percent of the Earth's total landmass (Canadian Forest Service, 2005). About half of the terrestrial biosphere's carbon (C) stocks exist in the boreal forests. There are 3.3 million km^2 boreal forests in Canada and they occupy around 37% of the country's landmass which is about 77% of Canada's forested land (Brandt, 2009). Canada's boreal forest had about 335.5 Mg C ha^{-1} in 1989 (Kurz and Apps, 1999).

Disturbance events such as wild fire, insect outbreak and logging are not only damaging but also renewing agents of Canadian boreal forest landscape. On a 10-year average basis, approximately 7500 forest fires including intentional fires (e.g. fuel management in national parks) occur in Canada each year for the period of 1995-2004, burning around 2.8 million ha of forests (Canadian Forest Service, 2005). These fires usually remove the fine materials such as leaf biomass and understory vegetation, leaving behind coarse woody residues of the forest stands (Amiro et al., 2006). In Canadian boreal forests, these fire induced dead and charred woody debris will eventually fall on the colder and wetter forest floors and will then be buried and covered by the ground vegetation and moss growth (Litvak et al., 2003).

In fire affected stands, gross primary productivity (GPP) initially declines because of the decrease in leaf area and then, it gradually recovers within a few years after the fire event (Odum, 1969). Similarly, ecosystem respiration (Re) initially increases after the fire event due to increased decomposition of fire debris (Litvak et al., 2003) and then it gradually declines when fire residues is lost through decomposition (Odum, 1969). Therefore, net ecosystem productivity (NEP) of post-fire boreal stands depend on relative contribution of GPP and Re variation, with most recently disturbed boreal forests being a large C source for a few years (Litvak et al., 2003; Amiro et al., 2006).

Besides the natural disturbances (e.g. wildfire and insect outbreak), human activities such as logging also have significant impacts on the structure and function of boreal forest ecosystems. In the early 20th century, forest harvest was only a minor fraction of disturbance in Canada's boreal forests, following wild fires and insect outbreaks (Kurz & Apps, 1999). However, in the late 20th and 21st century, the demand of forest products increased dramatically due to the rapid economic development of the world. Currently, about 0.9 M ha yr^{-1} of forests are harvested in Canada, the largest proportion of which is in the boreal region (Canadian Forest Service, 2005). Therefore, understanding and quantifying how different types of disturbance regimes impact the C budget of Canada's boreal forests is essential and critical for determining appropriate forest management policy and methods.

Black spruce (*Picea mariana* (*Mill.*) *B.S.P.*) stands constitute a large portion of Canadian boreal forest landscapes. Over the last few decades, they have been impacted by both natural and anthropogenic disturbances. There has been some research conducted on the impact of various disturbance regimes on the C cycle of boreal black spruce forests. Bergeron et al. (2008) compared carbon dioxide fluxes of a mature black spruce stand (EOBS) with a site that was harvested in 2000 (HBS00) near Chibougamau, Quebec, Canada. They found that the C budget of boreal black spruce forests much more depends on the disturbance regime (i.e. stand age) than the between-year climate variability. Bond-Lamberty et al. (2004) measured net primary productivity (NPP) and net ecosystem productivity (NEP) in seven black spruce sites which comprise a boreal forest wildfire chronosequence near Thompson, Manitoba, Canada. This study demonstrated the profound impact of wildfire on the rate of C exchange between forest and atmosphere and the need to account for soil drainage, bryophyte production and species succession when modeling boreal C fluxes. However, most of these studies in literature are stand specific and there are hardly any studies that have investigated the impact of disturbance on the historic C dynamics of boreal forests at landscape scale, in particular the black spruce landscape which dominates the Canadian boreal forests.

The long-term changes in climate also have a significant impact on the net exchange of C between the forest and the atmosphere. For instance, warmer

springs tend to increase the yearly CO_2 uptake due to the earlier beginning of the growing season (Tanja et al., 2003; Barr et al., 2004; Bergeron et al., 2007). In contrast, autumn warming tends to enhance respiration more than photosynthesis and thus decreases the yearly CO_2 uptake of the forest ecosystem (Piao et al., 2008).

Thus, in order to quantify the relative influences of stand-age class structure, disturbances, forest regrowth and inter-annual variability of environmental conditions on a landscape-level historic C dynamics, Fluxnet Canada Research Network (FCRN) launced a model intercomparison project which involves a inventory-based model (CBM-CFS3), a number of process-based models (ecosys, Can-IBIS, C-CLASS, InTEC and TRIPLEX), flux-tower measurements of ecosystem C exchange and long-term observations of changes in biomass and disturbance to carry out model validation and assessment over the boreal forest landscape near Chibougamau, Quebec. Bernier et al. (2010) used the CBM-CFS3 C accounting model to simulate the historic C dynamics of a boreal forest landscape in eastern Canada based on the reconstructed dataset of forest growth and disturbances for a 71-year period (1928-1998). Their simulation indicated an increase in total ecosystem C of 11.9 Mg C ha^{-1} which was driven primarily by the increase in biomass C (Bernier et al., 2010). However, the impacts of long-term trends in climate and atmospheric composition were not considered in the study.

This study, as a part of the model intercomparison project, incorporated the disturbance matrix of the Carbon Budget Model of the Canadian Forest Sector (CBM-CFS3) model into the Carbon and Nitrogen coupled Canadian Land Surface Scheme (C-CLASS) and applied it to a 6275 ha forest landscape in Chibougamau, Quebec in eastern Canada from 1928 to 2005.

The specific objectives of this study are (i) to investigate the impact of different disturbance events on the variations in C fluxes and C stocks at landscape level in a boreal forest; (ii) to explore the impacts of climate variability on the C budget of undisturbed forest landscape; and (iii) to provide high resolution and spatially explicit process-based model simulated C stock and flux maps of Chibougamau landscape over the past several decades i.e. 1928-2005.

3.3 Materials and methods

3.3.1 Study landscape

The Chibougamau study area (centered at 49˚41'32.9" N, 74˚20'31.3" W) is located about 30 km south of Chibougamau, Quebec, Canada and is dominated by black spruce forests. Most of the forests in Chibougamau area were originated from major forest fires in late 1800s, although about 22 ha of 120-year old stands of balsam fir (*Abies balsamea* (L.) Mill), which is considered relatively fire-resistant, are still present in the study area. The study landscape covers 6275 ha

area with UTM co-ordinates (Zone 18, NAD 83). The elevation of the study area varies from 368 m in the southwest to 444 m in the north. The major soil types in the study area include fluvio-glacial deposits, deep glacial till, shallow glacial till, deep organic and shallow organic. The drainage of these soil types ranges from well drained fluvio-glacial to very poor drained organic soils. The 30-year (1971-2000) mean annual air temperature and precipitation are 0.0 ˚C and 961 mm at Chapais which is less than 30 km away from Eastern Old Black Spruce Flux Station (EOBS) main tower site located in this landscape (Coursolle et al., 2006; Bergeron et al., 2007; Bergeron et al., 2008).

3.3.2 Model details

C-CLASS is the carbon and nitrogen coupled version of Canadian Land Surface Scheme, CLASS which was originally developed for coupling with the Canadian Global Climate Model, CGCM (Verseghy, 1991; Verseghy et al., 1993; Verseghy, 2000). Similar to other 'second generation' land surface schemes developed for GCMs, original version of CLASS focused on the integrated simulation of energy and water fluxes only over different land surface types (i.e. bare soil, vegetation covered soil, snow covered bare soil, or vegetation and snow covered soil) forward in time from an initial starting points, making use of meteorological forcing data to drive the simulation (Verseghy, 2009). CLASS

may have up to five surface/vegetation types in each grid cell including needleleaf trees, broadleaf trees, crops, grasses and urban areas. The soil column is divided into three layers (0.10, 0.25 and 3.75 m thick) and snow is treated as an analogous fourth layer with variable depth. In order to address the interactions between the climate and biogeochemical systems, the ecosystem carbon and nitrogen algorithms were implemented in CLASS version 3.0, yielding C-CLASS model (Arain et al., 2002; Arain et al., 2006).

C-CLASS includes modules for photosynthesis (sun-lit and shaded leaves), canopy conductance, autotrophic respiration, live biomass allocation (i.e. photosynthate, leaf, wood and root pools), short-lived and stable soil C pools dynamics and heterotrophic respiration (R_h) which is estimated as the sum of ground surface litter respiration, dead roots respiration, short-lived soil organic matter (SOM) respiration and stable SOM respiration. A simple tree allometry module with dynamic leaf phenology was also incorporated in C-CLASS when the model was applied to seven boreal and temperate conifer forests across Canadian continental transect (Arora and George, 2005; Yuan et al., 2008). In order to evaluate the historic carbon dynamics of the Chibougamau landscape, the disturbance matrix from CBM-CFS3 model (Kurz et al., 2009) was incorporated into C-CLASS to calculate the carbon fluxes between different ecosystem carbon pools after the specific disturbance event occurred in the landscape. In C-CLASS, ten disturbance types can be identified and parameterized including clear cut, light

damage due to insect epidemy and eight different percentages of partial cut. The disturbance matrices define flow of C from donating (pre-disturbance) to receiving (post-disturbance) C pools as ratios of the C stocks in each pool at the time of disturbance. Each C pool of the forest ecosystem was updated after the disturbance event. A fixed time of year was prescribed for each disturbance event in every disturbed pixel.

3.3.3 Disturbance history and initialization data

The historic disturbance data of Chibougamau forest landscape in Quebec was created and validated at Laurentian Forestry Centre of Canadian Forest Service (Bernier et al., 2010). Six intermediate mosaics of black and white aerial photos (taken during survey flights in 1953-54, 1959, 1965, 1967-68, 1969-70 and 1982) were interpreted to retrieve the disturbance layers (clear cut, partial cut, insect defoliation and infrastructure) for the period of 1928-2003. Moreover, three decennial provincial forest inventory maps (1970-2005) and Quickbird Pansharped Multispectral images (2003) with 0.6 m resolution were also used to obtain more precise disturbance information after mid 1970s. There was no wood exploitation in this area until 1950s. The study area was extensively disturbed from 1950 onwards. Major disturbance events include partial cuts (25-75% forest crown density removal) in 1950, 1953, 1957 and 1963 in about 130, 14, 11 and 75

ha areas, respectively (Figure 3.1). In 1950s, about 155 ha forest were partially cut (<75% removal) and 11 ha forest was clear cut (> 75% removal). In 1963, around 683 ha forest was harvested in this landscape, of which 608 ha was clear cut and 75 ha was partial cut. Also, in the same year, approximately 6 ha forest was affected by mild insect defoliation. From 1966 to 1969, about 95 ha forest was clear cut. From 1982 to 1991, 12 ha forest was clear cut, of which 10 ha forest was clear cut with regeneration protection. Approximately, 222 ha stands were converted into infrastructure development (Bernier et al., 2010). Infrastructure development caused the permanent reduction of forest area (deforestation) and these grid cells were not included in the simulations.

Currently, the majority of this disturbed landscape (4601 ha) is dominated by different-aged forest stands of black spruce, among which there are 3857 ha pure black spruce stands and around 744 ha black spruce stands are mixed with trembling aspen (*Populus tremuloides*). In the rest of the landscape, there are 123 ha pure trembling aspen forest stands, 984 non-productive area and 455 ha is covered by water (Figure 3.1). In 2005, area-weighted mean stand age was 121 and 43 years for undisturbed and disturbed stands, respectively. This was determined from the photointerpretation of the 1998 provincial forest cover map at 1:20 000 scale (Bernier et al., 2010).

In the model, initial above-ground biomass was prescribed from CBM-CFS3's output. Above ground biomass (AGB) from the 1928 inventory was used

to initialize the C-CLASS model. The initial wood biomass, heartwood biomass, root biomass and fine root biomass in the model was assumed as 80%, 60%, 20% and 10% of AGB in 1928, respectively. Other initial conditions such as photosynthetic C pool, litter, fast mineralized SOM, stable SOM, canopy temperature, soil temperature and soil moisture were set arbitrarily and modified by the model spin-up.

Soil texture parameters and soil drainage conditions for each soil type were derived from the layer files of Soil Landscapes of Canada (SLC Version 3.1) in the CanSIS National Soil Database (CanSIS, 2006). Forest age and disturbance data (in GIS format) were provided by the historic carbon modeling project of CCP. The weather data used to drive the time series of C-CLASS model from 1928 to 2003 were derived from climate archives from Great Lakes Forestry Centre, Canadian Forest Service, Natural Resources Canada which had been interpolated to the EOBS eddy covariance flux tower site. From 2004 to 2005, the observed meteorology data from EOBS tower site were used. The historic daily weather record from 1928-2003 were further interpolated to calculate hourly values for use in C-CLASS model. Specifically, daily shortwave radiation was interpolated over calculated day length to obtain hourly values using a sine function. Hourly air temperature was also interpolated using sine function with the daily minimum temperature at dawn and maximum temperature occurring three hours after solar noon.

The forest landscape was resolved into 6275 one ha grid cells. The soils, inventory, forest cover types and disturbance data in these grid cells were then aggregated into 319 unique combinations of soils, inventory, forest cover types and disturbances, each of which was represented by one model simulation. The model was spun-up from the year when the stand age is 1 based on the stand age data in 1928 using the same meteorology forcing data (2004 and 2005 meteorology data) repetitively and resetting the wood biomass, litter and total C content in stable SOM each year to their initial values to keep model pre-running in a steady forest before starting formal simulations on January 1st, 1928 and completing on December 31st, 2005.

Influence of climatic factors on the annual C balances of Chibougamau forest landscape was also assessed by performing a climate sensitivity analysis over the study period by increasing/decreasing hourly values of air temperature by ±0.5 ˚C, ±1.0 ˚C and ±2.0 ˚C.

3.4 Results and discussion

Total aboveground tree biomass (AGB) simulated by C-CLASS in the study area showed an increase of 30-50 Mg C ha^{-1} between 1928 and 2005 over much of the landscape but a slight net decrease in the forest stands that were harvested during the simulation period of 1928-2005 (Figure 3.2). Overall, C-

CLASS simulated an increase of 118573 Mg C (31 Mg C ha^{-1} or 0.397 Mg C ha^{-1} yr^{-1}) in aboveground tree biomass over the 3825 ha forested area in the landscape during the 78 year period (Table 3.3).

C-CLASS used the AGB inventory conducted in 1928 as the input to the model. The AGB inventory of 3825 ha forest stands in the study area was 88059 Mg C, which was 35% lower than the value (135265 Mg C) derived from Fournier et al. (2003) lookup table (Table 3.3). The photointerpretation of forest cover map revealed that in 1928 this landscape was covered with different age forests, which included 478, 1564, 1627, 476, 577 and 22 ha stands that were 10, 30, 50, 70 and 90 years old, respectively. The area-weighted mean stand age was 47 years in 1928 indicating relatively younger age of forests in the Chibougamau landscape. Younger forests were underrepresented in the sample plot due to the operational sampling bias toward older stands and the low prevalence of fires in Quebec's boreal forests during most of the 20th century (Bergeron et al., 2006; Bernier et al., 2010). This underrepresentation has resulted in a possible bias in the strata-level estimates of aboveground biomass in 1928 (Bernier et al., 2010).

C-CLASS simulated AGB increased faster than the estimates of CBM-CFS3 (Figure 3.3). The reason is that two models use different algorithms to calculate the wood biomass. CBM-CFS3 uses yield curve to derive wood biomass from merchantable volume (Bernier et al., 2010). C-CLASS calculates the gross primary productivity (GPP) with two-leaf (sunlit and shaded) photosynthesis

model which is driven by solar radiation, air temperature and atmospheric CO_2 concentration (Wang and Leuning, 1998; Arain et al., 2002). Then, a fraction of GPP is allocated to drive the growth of aboveground biomass after the maintenance respiration which is calculated from Q_{10} model (Arain et al., 2002). Therefore, the long-term trends of increasing air temperature and atmospheric CO_2 concentration, which have not been considered explicitly by CBM-CFS3, may contribute to the faster increase of AGB simulated by C-CLASS than CBM-CFS3.

C-CLASS simulation also provides an estimate of the 78-year historic dynamics of landscape-level major C stocks throughout the simulation period of 1928-2005 (Figure 3.4). Initial landscape-level biomass C stocks were estimated to be 35 Mg C ha^{-1} on average in 1928. These stocks showed a modest increase during most years of the simulation period, but a slight net decrease in 1963 when 683 ha forests were harvested in the landscape. C-CLASS simulated dead organic matter (DOM) declined significantly from 4 Mg C ha^{-1} to 2 Mg C ha^{-1} in the first 5 years of the simulation period and then it gradually increased to 3 Mg C ha^{-1}. The intensive disturbance in 1963 made the simulated DOM increase to 4 Mg C ha^{-1}. After that, simulated DOM decreased to 2.6 Mg C ha^{-1} and then gradually increased to 3.7 Mg C ha^{-1} in 2005. C-CLASS simulated soil organic matter (SOM) C stocks declined continuously from 35 Mg C ha^{-1} to 24 Mg C ha^{-1} in the period of 1928-1962. Then, the disturbance in 1963 increased the simulated SOM

to 29 Mg C ha^{-1}. After that, the simulated SOM gradually decreased to 19 Mg C ha^{-1} in 2005 (Figure 3.4).

C-CLASS simulated landscape-level C fluxes (Figure 3.5) suggest that forest ecosystems in the study area were close to C neutral in most of the years before the disturbance in 1963. Following disturbance, the landscape continued to act as a net C source for several years, eventually becoming a small net C sink when uptake from forest growth exceeded losses from decomposition of forest cut and other disturbance residues. The forests of the landscape as a whole acted as a net C source from 1963 to 1967, losing 9.5 Mg C ha^{-1} on average, for a total loss of 0.04 Mt C from the study area's forest during this period. After 1967, the forest landscape acted as a net C sink during most years, with total ecosystem C stocks recovering to 95 Mg C ha^{-1} by 2005, including 72 Mg C ha^{-1} in biomass (Figure 3.4).

Comparisons between model estimates of monthly NEP from C-CLASS and estimates calculated using EC tower (EOBS) data have been made for two years (2004 and 2005). The tower fetch area corresponds to an approximately 500 m radius centered on the tower (Bergeron et al., 2007). Model roughly captured the seasonal variation of monthly NEP from 2004 to 2005, although simulated NEP was overestimated at the beginning of each year and underestimated at the end of each year as compared to observed values (Fig 3.6). This is attributed to the overestimation of GEP at the beginning of the year and the underestimation of

GEP at the end of the year which result from the temperature sensitivity of photosynthesis rate. It seems that the photosynthesis is dormant at the beginning of the growing season and the occasional pulse of high air temperature cannot significantly raise the GEP. On the other hand, the photosynthesis is still active at the end of the growing season and the occasional pulse of low air temperature cannot significantly reduce the GEP. Our model has not reflected this kind of ecosystem processes.

At the mature black spruce stand (EOBS), C-CLASS simulated annual NEP values were -9.36 g C m^{-2} yr^{-1} in a cooler, wetter year (2004) and -14.5 g C m^{-2} yr^{-1} in a warmer, drier year (2005). Meanwhile, over the same period C-CLASS simulated landscape level NEP was between -46.33 and 103.33 g C m^{-2} yr^{-1} (2004) or between -49.91 and 115.51 g C m^{-2} yr^{-1} (2005) within Chibougamau landscape. The mean difference of annual NEP within the landscape was much greater than the mean difference between years. Thus, the C fluxes such as NEP of this boreal black spruce forests are much more influenced by stand development stage (i.e. stand age) than by inter-annual climate variability which is consistent with the findings of Bergeron et al. (2008).

The correlation between simulated seven-year mean C flux deviations and the meteorological variables in undisturbed areas of the landscape from 1928-1999 was explored. Seven-year average was taken to remove the age effect on the C fluxes. Over this period, mean daily minimum air temperature (T_{min}) ranged

from -8 to 1 ^{o}C in spring (April and May) while the mean daily maximum air temperature (T_{max}) was around 2 to 14 ^{o}C in spring (Figure 3.7). Over the same period, mean daily T_{min} in summer (June, July and August) was between 6 and 12 ^{o}C while mean daily T_{max} in the summer was between 17 and 23 ^{o}C (Figure 3.7).

Generally, GEP deviation of undisturbed forest showed positive relationship with daily T_{min} and T_{max} in spring while GEP was not sensitive to daily T_{min} or T_{max} in summer (Figure 3.7a, d, g and j; R^2 values shown in each figure panel). Landscape-level annual photosynthesis rate increased with air temperature in spring when the air temperature was relatively low. In summer, the weather is warm and the air temperature was not a major factor that limits the photosynthesis rate. Meanwhile, ecosystem respiration (R_e) deviation of undisturbed forests was positively related to air temperature (T_{min} and T_{max}) in both spring and summer (Figure 3.7b, 3.7e, 3.7h and 3.7k). Annual NEP deviation of undisturbed forests showed positive relationship with daily T_{min} and T_{max} in spring (Figure 3.7c and 3.7i) because the increase in GEP with air temperature was faster as compared to R_e.

The sensitivity of C-CLASS simulated landscape-level C fluxes and C stocks to the changes in air temperature is shown in Figure 3.9. Simulated GPP, autotrophic respiration (R_a) and heterotrophic respiration (R_h) was more sensitive to changes in air temperature as compared to NEP, while simulated AGB, BGB, DOM and SOM was sensitive to the change in air temperature. Higher

temperatures resulted in smaller simulated aboveground biomass and larger simulated belowground biomass because more allocation of NPP to belowground biomass than aboveground biomass in warm climate. Simulated higher dead C pools (such as DOM and SOM) with the higher air temperature was attributed to the higher litter fall due to higher simulated NPP values during warm temperatures. Generally, the landscape-level C stocks were sensitive to the air temperature, which suggest that the C stocks in boreal forest landscape may increase due to global warming in the future under various IPCC 2007 CO_2 emission scenarios.

3.5 Conclusions

Results of this study showed 19.27 Mg C ha^{-1} increase in C-CLASS simulated total ecosystem carbon as compared to 12.11 Mg C ha^{-1} increase estimated by the inventory based CBM-CFS3 model. In 1963, about 689 ha forest stands were disturbed, of which 608 ha were clear cut, 75 ha partial cut and 6 ha were partially defoliated by insects. During these events, a large amount of carbon was released from the forest and the landscape-level net biome productivity in 1963 and 1964 was -4.10 and -3.31 Mg C ha^{-1} yr^{-1}, respectively. From 1970 to 2005, there were very few disturbance events in the region and the landscape-level total ecosystem carbon increased from 76.70 to 94.66 Mg C ha^{-1}. During this period, C-CLASS

simulated net biome productivity ranging from -0.08 Mg C ha^{-1} yr^{-1} in 2005 to 0.89 Mg C ha^{-1} yr^{-1} in 1977, and these differences were mostly determined by inter-annual climate variability. Our analysis further showed that in undisturbed forest landscape simulated annual NEP deviations were positively related to daily T_{min} and T_{max} in spring, while they were not sensitive to daily T_{min} and T_{max} in summer. Study results also show that simulated landscape-level NEP is less sensitive to the changes in air temperature compared to other simulated carbon fluxes (gross primary productivity, autotrophic respiration and heterotrophic respiration). Also, C-CLASS simulated landscape-level carbon stocks (aboveground biomass, belowground biomass, dead organic matter and soil organic matter) are sensitive to the change of air temperature. This study will help to explore the impact of forest management and future climate change on boreal forest productivity in eastern Canada.

3.6 References

Amiro, B.D., Barr, A.G., Black, T.A., Iwashita, H., Kljun, N., McCaughey, J.H., Morgenstern, K., Murayama, S., Nesic, Z., Orchansky, A.L., Saigusa, N., 2006. Carbon, energy and water fluxes at mature and disturbed forest sites, Saskatchewan, Canada. Advances in Surface-Atmosphere Exchange - A Tribute to Marv Wesely 136(3-4): 237-251.

Arain, M.A., Black, T.A., Barr, A.G., Jarvis, P.G., Massheder, J.M., Verseghy, D.L., Nesic, Z., 2002. Effects of seasonal and interannual climate variability on net ecosystem productivity of boreal deciduous and conifer forests. Canadian Journal of Forest Research 32(5): 878-891.

Arain, M.A., Yuan, F., Andrew Black, T., 2006. Soil-plant nitrogen cycling modulated carbon exchanges in a western temperate conifer forest in Canada. Agric. Forest Meteorol. 140(1-4): 171-192.

Arora, V.K., Boer, G.J., 2005. Fire as an interactive component of dynamic vegetation models. J. Geophys. Res. 110.

Arora, V.K., George, J.B., 2005. A parameterization of leaf phenology for the terrestrial ecosystem component of climate models. Global Change Biology 11(1): 39-59.

Baldocchi, D. (1994). An analytical solution for coupled leaf photosynthesis and stomatal conductance models. **14:** 1069-1079.

Barr, A.G., Black, T.A., Hogg, E.H., Griffis, T.J., Morgenstern, K., Kljun, N., Theede, A., Nesic, Z., 2007. Climatic controls on the carbon and water balances of a boreal aspen forest, 1994–2003. Global Change Biology 13(3): 561-576.

Barr, A.G., Black, T.A., Hogg, E.H., Kljun, N., Morgenstern, K., Nesic, Z., 2004. Inter-annual variability in the leaf area index of a boreal aspen-hazelnut forest in relation to net ecosystem production. Agricultural and forest meteorology 126(3-4): 237-255.

Barton, C.V.M., North, P.R.J., 2001. Remote sensing of canopy light use efficiency using the photochemical reflectance index: Model and sensitivity analysis. Remote Sensing of Environment 78(3): 264-273.

Beer, C., Reichstein, M., Tomelleri, E., Ciais, P., Jung, M., Carvalhais, N., Rodenbeck, C., Arain, M.A., Baldocchi, D., Bonan, G.B., Bondeau, A., Cescatti, A., Lasslop, G., Lindroth, A., Lomas, M., Luyssaert, S., Margolis, H., Oleson, K.W., Roupsard, O., Veenendaal, E., Viovy, N., Williams, C., Woodward, F.I., Papale, D., 2010. Terrestrial Gross Carbon Dioxide Uptake: Global Distribution and Covariation with Climate. Science 329(5993): 834-838.

Bergeron, O., Hank A, M., T. Andrew, B., Carole, C., Allison L, D., Alan G, B., Steven C, W. (2007). Comparison of carbon dioxide fluxes over three boreal black spruce forests in Canada. **13:** 89-107.

Bergeron, O., Margolis, H.A., Coursolle, C., Giasson, M.-A., 2008. How does forest harvest influence carbon dioxide fluxes of black spruce ecosystems in eastern North America? Agricultural and forest meteorology 148(4): 537-548.

Bergeron, Y., Cyr, D., Drever, C.R., Flannigan, M., Gauthier, S., Kneeshaw, D., Lauzon, E., Leduc, A., Le Goff, H., Lesieur, D., Logan, K., 2006. Past, current, and future fire frequencies in Quebec's commercial forests: implications for the cumulative effects of harvesting and fire on age-class structure and natural disturbance-based management. Canadian Journal of Forest Research 36(11): 2737-2744.

Bernier, P.Y., Guindon, L., Kurz, W.A., Stinson, G., 2010. Reconstructing and modelling 71 years of forest growth in a Canadian boreal landscape: a test of the CBM-CFS3 carbon accounting model. Canadian Journal of Forest Research 40(1): 109-118.

Bonan, G.B., 1995. Land-atmosphere CO2 exchange simulated by a land surface process model coupled to an atmospheric general circulation model. J. Geophys. Res. 100: 2817-2831.

Brandt, J.P., 2009. The extent of the North American boreal zone. Environ. Rev. 17: 101-161.

Chapin, F., Woodwell, G., Randerson, J., Rastetter, E., Lovett, G., Baldocchi, D., Clark, D., Harmon, M., Schimel, D., Valentini, R., Wirth, C., Aber, J., Cole, J., Goulden, M., Harden, J., Heimann, M., Howarth, R., Matson, P., McGuire, A., Melillo, J., Mooney, H., Neff, J., Houghton, R., Pace, M., Ryan, M., Running, S., Sala, O., Schlesinger, W., Schulze, E.D., 2006. Reconciling Carbon-cycle Concepts, Terminology, and Methods. Ecosystems 9(7): 1041-1050.

Chapin III, F.S., Pamela, A.M., Harold, A.M., 2002. Principles of terrestrial ecosystem ecology, Springer.

Chen, B., Black, T., Coops, N., Hilker, T., Trofymow, J., Morgenstern, K., 2009. Assessing Tower Flux Footprint Climatology and Scaling Between Remotely Sensed and Eddy Covariance Measurements. Boundary-Layer Meteorology 130(2): 137-167.

Chen, J.M., Chen, W., Liu, J., Cihlar, J., 2000. Annual carbon balance of Canada's forests during 1895-1996. Global Biogeochemical Cycles 14(3): 839-850.

Chen, J.M., Feng, D., Mingzhen, C., 2006. Locally adjusted cubic-spline capping for reconstructing seasonal trajectories of a satellite-derived surface parameter. Geoscience and Remote Sensing, IEEE Transactions on 44(8): 2230-2238.

Chen, J.M., Leblanc, S., 1997. A 4-scale bidirectional reflection model based on canopy architecture. IEEE Transactions on Geoscience and Remote Sensing 35: 1316-1337.

Chen, J.M., Leblanc, S.G., 2001. Multiple-scattering scheme useful for hyperspectral geometrical optical modelling. IEEE Transactions on Geoscience and Remote Sensing 39(5): 1061-1071.

Chen, J.M., Liu, J., Cihlar, J., Goulden, M.L., 1999. Daily canopy photosynthesis model through temporal and spatial scaling for remote sensing applications. Ecological Modelling 124(2-3): 99-119.

Chen, J.M., Weimin, J., Josef, C., David, P., Jane, L., Wenjun, C., Jianjun, P., Andy, B., Alan, B., 2003. Spatial distribution of carbon sources and sinks in Canada's forests. Tellus B 55(2): 622-641.

Chen, W.J., Chen, J.M., Liu, J., Cihlar, J., 2000. Approaches for reducing uncertainties in regional forest carbon balance. Global Biogeochemical Cycles 14(3): 827-838.

Ciais, P., Canadell, J.G., Luyssaert, S., Chevallier, F., Shvidenko, A., Poussi, Z., Jonas, M., Peylin, P., King, A.W., Schulze, E.-D., Piao, S., Rodenbeck, C., Peters, W., Breon, F.-M., 2010. Can we reconcile atmospheric estimates of the Northern terrestrial carbon sink with land-based accounting? Current Opinion in Environmental Sustainability 2(4): 225-230.

Clark, D.A., Brown, S., Kicklighter, D.W., Chambers, J.Q., Thomlinson, J.R., Ni, J. (2001). MEASURING NET PRIMARY PRODUCTION IN FORESTS: CONCEPTS AND FIELD METHODS. **11:** 356-370.

Coble, D.W., Milner, K.S., Marshall, J.D., 2001. Above- and below-ground production of trees and other vegetation on contrasting aspects in western Montana: a case study. Forest Ecology and Management 142(1-3): 231-241.

Collatz, G.J., Ball, J.T., Grivet, C., Berry, J.A., 1991. Physiological and environmental regulation of stomatal conductance, photosynthesis and transpiration: a model that includes a laminar boundary layer. Agricultural and forest meteorology 54(2-4): 107-136.

Coursolle, C., Margolis, H.A., Barr, A.G., Black, T.A., Amiro, B.D., McCaughey, J.H., Flanagan, L.B., Lafleur, P.M., Roulet, N.T., Bourque, C.P.-A., Arain, M.A., Wofsy, S.C., Dunn, A., Morgenstern, K., Orchansky, A.L., Bernier, P.Y., Chen, J.M., Kidston, J., Saigusa, N., Hedstrom, N., 2006. Late-summer carbon fluxes from Canadian forests and peatlands along an east-west continental transect Canadian Journal of Forest Research 36(3): 783-800.

Cox, P.M., 2001. Description of the TRIFFID dynamic global vegetation model, Hadley Centre Tech. Note 24, 16pp.,. Hadley Centre, Bracknell, U.K.

Deng, F., Chen, J.M., Plummer, S., Mingzhen, C., Pisek, J. (2006). Algorithm for global leaf area index retrieval using satellite imagery. Geoscience and Remote Sensing, IEEE Transactions on. 44: 2219-2229.

Dickinson, R.E., Shaikh, M., Bryant, R., Graumlich, L., 1998. Interactive Canopies for a Climate Model. Journal of Climate 11: 2823-2836.

Dixon, R.K., Solomon, A.M., Brown, S., Houghton, R.A., Trexier, M.C., Wisniewski, J., 1994. Carbon Pools and Flux of Global Forest Ecosystems. Science 263(5144): 185-190.

Farquhar, G.D., Caemmerer, S.V., Berry, J.A., 1980. A biochemical model of photosynthetic CO2 assimilation in leaves of C-3 species. Planta 149: 78-90.

Farquhar, G.D., von Caemmerer, S., 1982. Modelling of photosynthetic response to environmental conditions. Berlin, Spring Verlag.

Foley, J.A., Prentice, I.C., Ramankutty, N., Levis, S., Pollard, D., Sitch, S., Haxeltine, A., 1996. An Integrated Biosphere Model of Land Surface Processes, Terrestrial Carbon Balance, and Vegetation Dynamics. Global Biogeochem. Cycles 10: 603-628.

Friedlingstein, P., Bopp, L., Ciais, P., Dufresne, J.L., Fairhead, L., LeTreut, H., Monfray, P., Orr, J., 2001. Positive Feedback between Future Climate Change and the Carbon Cycle. GEOPHYSICAL RESEARCH LETTERS 28: 1543-1546.

Friedlingstein, P., Cox, P., Betts, R., Bopp, L., von Bloh, W., Brovkin, V., Cadule, P., Doney, S., Eby, M., Fung, I., Bala, G., John, J., Jones, C., Joos, F., Kato, T., Kawamiya, M., Knorr, W., Lindsay, K., Matthews, H.D., Raddatz, T., Rayner, P., Reick, C., Roeckner, E., Schnitzler, K.G., Schnur, R., Strassmann, K., Weaver, A.J., Yoshikawa, C., Zeng, N., 2006. Climate-carbon Cycle Feedback Analysis: Results from the C4MIP Model Intercomparison. Journal of Climate 19(14): 3337-3353.

Friedlingstein, P., Dufresne, J.L., Cox, P.M., Rayner, P., 2003. How positive is the feedback between climate change and the carbon cycle? Tellus B 55(2): 692-700.

Gamon, J.A., Penuelas, J., Field, C.B., 1992. A narrow-waveband spectral index that tracks diurnal changes in photosynthetic efficiency. Remote Sensing of Environment 41(1): 35-44.

Gervois, S., de Noblet-Ducoudre, N., Viovy, N., Ciais, P., Brisson, N., Seguin, B., Perrier, A., 2004. Including Croplands in a Global Biosphere Model: Methodology and Evaluation at Specific Sites. Earth Interactions 8(16): 1-25.

Gower, S.T., Vogel, J.G., Norman, J.M., Kucharik, C.J., Steele, S.J., Stow, T.K., 1997. Carbon distribution and aboveground net primary production in

aspen, jack pine, and black spruce stands in Saskatchewan and Manitoba, Canada. J. Geophys. Res. 102.

Grant, R.F., Black, T.A., Humphreys, E.R., Morgenstern, K., 2007. Changes in net ecosystem productivity with forest age following clearcutting of a coastal Douglas-fir forest: testing a mathematical model with eddy covariance measurements along a forest chronosequence. Tree Physiology 27: 115-131.

Grier, C.C., Logan, R.S., 1977. Old-Growth Pseudotsuga menziesii Communities of a Western Oregon Watershed: Biomass Distribution and Production Budgets. Ecological Monographs 47(4): 373-400.

Hamilton, E., Nicholson, A. (1990). Old-Growth Forests Problem Analysis. Victoria, BC Ministry of Forests**:** 104.

Harmon, M.E., Bible, K., Ryan, M.G., Shaw, D.C., Chen, H., Klopatek, J., Li, X., 2004. Production, Respiration, and Overall Carbon Balance in an Old-growth Pseudotsuga- Tsuga Forest Ecosystem. Ecosystems 7(5): 498-512.

Huang, S., Arain, M.A., Arora, V.K., Yuan, F., Brodeur, J., Peichl, M., 2011. Analysis of nitrogen controls on carbon and water exchanges in a conifer forest using the CLASS-CTEMN+ model. Ecological Modelling 222(20-22): 3743-3760.

Ju, W., Chen, J.M., 2008. Simulating the effects of past changes in climate, atmospheric composition, and fire disturbance on soil carbon in Canada's forests and wetlands. Global Biogeochem. Cycles 22(3): GB3010.

Ju, W., Chen, J.M., Black, T.A., Barr, A.G., McCaughey, H., Roulet, N.T., 2006. Hydrological effects on carbon cycles of Canada's forests and wetlands. Tellus B 58(1): 16-30.

Jungen, J.R. (1985). Soils of Southern Vancouver Island. BC Soil Survey Report. Victoria, BC, BC Ministry of Environment.

Kothavala, Z., Arain, M.A., Black, T.A., Verseghy, D.L., 2005. The simulation of energy, water vapor and carbon dioxide fluxes over common crops by the Canadian Land Surface Scheme (CLASS). Agricultural and forest meteorology 133.

Krishnan, P., Black, T.A., Grant, N.J., Barr, A.G., Hogg, E.H., Jassal, R.S., Morgenstern, K., 2006. Impact of changing soil moisture distribution on net ecosystem productivity of a boreal aspen forest during and following drought. Agricultural and forest meteorology 139(3 欽?): 208-223.

Kucharik, C.J., Foley, J.A., Delire, C., Fisher, V.A., Coe, M.T., Lenters, J.D., Young-Molling, C., Ramankutty, N., Norman, J.M., Gower, S.T., 2000. Testing the Performance of a Dynamic Global Ecosystem Model: Water Balance, Carbon Balance, and Vegetation Structure. Global Biogeochemical Cycles 14(3): 795-825.

Kurz, W.A., Apps, M.J., 1999. A 70-YEAR RETROSPECTIVE ANALYSIS OF CARBON FLUXES IN THE CANADIAN FOREST SECTOR. Ecological Applications 9(2): 526-547.

Kurz, W.A., Dymond, C.C., White, T.M., Stinson, G., Shaw, C.H., Rampley, G.J., Smyth, C., Simpson, B.N., Neilson, E.T., Trofymow, J.A., Metsaranta, J., Apps, M.J., 2009. CBM-CFS3: A model of carbon-dynamics in forestry and land-use change implementing IPCC standards. Ecological Modelling 220(4): 480-504.

Kurz, W.A., Stinson, G., Rampley, G.J., Dymond, C.C., Neilson, E.T., 2008. Risk of natural disturbances makes future contribution of Canada's forests to the global carbon cycle highly uncertain. Proc. Natl. Acad. Sci. U.S.A. 105(5): 1551-1555.

Latifovic, R., Zhu, Z.-L., Cihlar, J., Giri, C., Olthof, I., 2004. Land cover mapping of North and Central America -Global Land Cover 2000. Remote Sensing of Environment 89(1): 116-127.

Le Quere, C., Raupach, M.R., Canadell, J.G., Marland, G., et al., 2009. Trends in the sources and sinks of carbon dioxide. Nature Geosci 2(12): 831-836.

Leuning, R., Kelliher, F.M., Pury, D.G.G., Schulze, E.D., 1995. Leaf nitrogen, photosynthesis, conductance and transpiration: scaling from leaves to canopies. Plant, Cell and Environment 18(10): 1183-1200.

Levis, S.G., Bonan, B., Vertenstein, M., Oleson, K.W. (2004). The Community Land Model's Dynamic Global Vegetation Model (CLM-DGVM): Technical Description and User's Guide. NCAR Tech. Note TN-459+IA. National Center for Atmospheric Research, Boulder, Colorado**:** 50.

Li, Z., Kurz, W.A., Apps, M., Beukema, S., 2003. Belowground biomass dynamics in the Carbon Budget Model of the Canadian Forest Sector: recent improvements and implications for the estimation of NPP and NEP. Canadian Journal of Forest Research 33: 126-136.

Litvak, M., Miller, S., Wofsy, S.C., Goulden, M., 2003. Effect of stand age on whole ecosystem CO2 exchange in the Canadian boreal forest. J. Geophys. Res. 108.

Liu, J., Chen, J.M., Cihlar, J., Chen, W., 2002. Net primary productivity mapped for Canada at 1-km resolution. Global Ecology & Biogeography 11(2): 115-129.

Liu, J., Price, D.T., Chen, J.M., 2005. Nitrogen controls on ecosystem carbon sequestration: a model implementation and application to Saskatchewan, Canada. Ecological Modelling 186(2): 178-195.

Luo, Y., 2007. Terrestrial Carbon-Cycle Feedback to Climate Warming. Annual Review of Ecology, Evolution, and Systematics 38: 683-712.

Mackie, R.S., Ed. 2000. Island Timber. Victoria, BC, Sono Nis Press.

Mahecha, M.D., Reichstein, M., Carvalhais, N., Lasslop, G., Lange, H., Seneviratne, S.I., Vargas, R., Ammann, C., Arain, M.A., Cescatti, A., Janssens, I.A., Migliavacca, M., Montagnani, L., Richardson, A.D., 2010. Global Convergence in the Temperature Sensitivity of Respiration at Ecosystem Level. Science 329: 838-840.

Metsaranta, J.M., Kurz, W.A., Neilson, E.T., Stinson, G., 2010. Implications of future disturbance regimes on the carbon balance of Canada's managed forest (2010–2100). Tellus B 62(5): 719-728.

Morisette, J.T., Privette, J.L., Justice, C.O., 2002. A framework for the validation of MODIS Land products. Remote Sensing of Environment 83(1-2): 77-96.

Norman, J.M., 1982. Simulation of microclimates. New York, Academic Press.

Odum, E.P., 1969. The strategy of ecosystem development. Science 164: 262-270.

Pan, Y., Birdsey, R.A., Fang, J., Houghton, R., Kauppi, P.E., Kurz, W.A., Phillips, O.L., Shvidenko, A., Lewis, S.L., Canadell, J.G., Ciais, P., Jackson, R.B., Pacala, S.W., McGuire, A.D., Piao, S., Rautiainen, A., Sitch, S., Hayes, D., 2011. A Large and Persistent Carbon Sink in the World's Forests. Science 333(6045): 988-993.

Parton, W.J., Schimel, D.S., Cole, C.V., Ojima, D.S., 1987. Analysis of Factors Controlling Soil Organic Matter Levels in Great Plains Grasslands. Soil Sci Soc Am J 51(5): 1173-1179.

Piao, S., Ciais, P., Friedlingstein, P., de Noblet-Ducoudr, N., Cadule, P., Viovy, N., Wang, T., 2009. Spatiotemporal patterns of terrestrial carbon cycle during the 20th century. Global Biogeochem. Cycles 23(4): GB4026.

Piao, S., Ciais, P., Friedlingstein, P., Peylin, P., Reichstein, M., Luyssaert, S., Margolis, H., Fang, J., Barr, A., Chen, A., Grelle, A., Hollinger, D.Y., Laurila, T., Lindroth, A., Richardson, A.D., Vesala, T., 2008. Net carbon dioxide losses of northern ecosystems in response to autumn warming. Nature 451(7174): 49-52.

Pisek, J., Chen, J.M., 2007. Comparison and validation of MODIS and VEGETATION global LAI products over four BigFoot sites in North America. Remote Sensing of Environment 109(1): 81-94.

Pitman, A.J., 2003. The evolution of, and revolution in, land surface schemes designed for climate models. International Journal of Climatology 23(5): 479-510.

Pregitzer, K.S., Eugenie, S.E., 2004. Carbon cycling and storage in world forests: biome patterns related to forest age. Global Change Biology 10(12): 2052-2077.

Qian, H., Joseph, R., Zeng, N., 2010. Enhanced terrestrial carbon uptake in the Northern High Latitudes in the 21st century from the Coupled Carbon Cycle Climate Model Intercomparison Project model projections. Global Change Biology 16(2): 641-656.

Rahman, H., Dedieu, G. (1994). SMAC: a simplified method for the atmospheric correction of satellite measurements in the solar spectrum, Taylor & Francis. **15:** 123 - 143.

Reich, P.B., 2010. The Carbon Dioxide Exchange. Science 329(5993): 774-775.

Running, S.W., Baldocchi, D.D., Turner, D.P., Gower, S.T., Bakwin, P.S., Hibbard, K.A., 1999. A Global Terrestrial Monitoring Network Integrating Tower Fluxes, Flask Sampling, Ecosystem Modeling and EOS Satellite Data. Remote Sensing of Environment 70(1): 108-127.

Running, S.W., Coughlan, J.C., 1988. A general model of forest ecosystem processes for regional applications I. Hydrologic balance, canopy gas exchange and primary production processes. Ecological Modelling 42(2): 125-154.

Running, S.W., Thornton, P.E., Nemani, R., Glassy, J.M., 2000. Global terrestrial gross and net primary productivity from the Earth observing system. In O. E. Sala, R. B. Jackson, H. A. Mooney, R. W. Howarth, (Eds.), Methods in ecosystem science (pp. 44-57). New York, Springer-Verlag.

Schut, P., Shields, J., Tarnocai, C., Coote, D., Marshall, I. (1994). Soil Landscapes of Canada - An Environmental Reporting Tool. Canadian Conference on GIS Proceedings, Ottawa.

Schwalm, C.R., Black, T.A., Kai, M., Elyn, R.H., 2007. A method for deriving net primary productivity and component respiratory fluxes from tower-based eddy covariance data: a case study using a 17-year data record from a Douglas-fir chronosequence. Global Change Biology 13(2): 370-385.

Sellers, P.J., Berry, J.A., Collatz, G.J., Field, C.B., Hall, F.G., 1992. Canopy reflectance, photosynthesis, and transpiration. III. A reanalysis using improved leaf models and a new canopy integration scheme. Remote Sensing of Environment 42(3): 187-216.

Sellers, P.J., Dickinson, R.E., Randall, D.A., Betts, A.K., Hall, F.G., Berry, J.A., Collatz, G.J., Denning, A.S., Mooney, H.A., Nobre, C.A., Sato, N., Field, C.B., Henderson-Sellers, A., 1997. Modeling the Exchanges of Energy, Water, and Carbon Between Continents and the Atmosphere. Science 275(5299): 502-509.

Sellers, P.J., Los, S.O., Tucker, C.J., Justice, C.O., Dazlich, D.A., Collatz, G.J., Randall, D.A., 1996. A Revised Land Surface Parameterization (SiB2) for Atmospheric GCMS. Part II: The Generation of Global Fields of Terrestrial Biophysical Parameters from Satellite Data. Journal of Climate 9: 706-737.

Shields, J.A., Tarnocai, C., Valentine, K.W.G., MacDonald, K.B., 1991. Soil Landscapes of Canada - Procedures Manual and User's Handbook. Ottawa., Ontario, Canada, Agriculture Canada.

Sitch, S., B.Smith, I.C.Prentice, A.Arneth, A.Bondeau, W.Cramer, J.O.Kaplan, S.Levis, W.Lucht, M.T.Sykes, K.Thonicke, S.Venevsky, 2003. Evaluation of ecosystem dynamics, plant geography and terrestrial carbon cycling in the LPJ dynamic global vegetation model. Global Change Biology 9(2): 161-185.

Smithwick, E., Harmon, M., Domingo, J., 2007. Changing Temporal Patterns of Forest Carbon Stores and Net Ecosystem Carbon Balance: the Stand to Landscape Transformation. Landscape Ecology 22(1): 77-94.

Smithwick, E.A.H., Harmon, M.E., Remillard, S.M., Acker, S.A., Franklin, J.F. (2002). POTENTIAL UPPER BOUNDS OF CARBON STORES IN FORESTS OF THE PACIFIC NORTHWEST. **12:** 1303-1317.

Song, C., Woodcock, C.E., 2003. A regional forest ecosystem carbon budget model: impacts of forest age structure and landuse history. Ecological Modelling 164(1): 33-47.

Still, C.J., Berry, J.A., Collatz, G.J., DeFries, R.S., 2003. Global distribution of C3 and C4 vegetation: Carbon cycle implications. Global Biogeochem. Cycles 17(1): 1006.

Sun, O.J., Campbell, J., Law, B.E., Wolf, V., 2004. Dynamics of carbon stocks in soils and detritus across chronosequences of different forest types in the Pacific Northwest, USA. Global Change Biology 10(9): 1470-1481.

Tanja, S., Berninger, F., Vesala, T., Markkanen, T., Hari, P., Mäkelä, A., Ilvesniemi, H., Hänninen, H., Nikinmaa, E., Huttula, T., Laurila, T., Aurela, M., Grelle, A., Lindroth, A., Arneth, A., Shibistova, O., Lloyd, J., 2003. Air temperature triggers the recovery of evergreen boreal forest photosynthesis in spring. Global Change Biology 9(10): 1410-1426.

Thomas, S.C., Winner, W.E., 2000. Leaf area index of an old-growth Douglas-fir forest estimated from direct structural measurements in the canopy. Canadian Journal of Forest Research 30: 1922-1930.

Tian, H., Melillo, J.M., Kicklighter, D.W., McGUIRE, A.D., Helfrich, J., 1999. The sensitivity of terrestrial carbon storage to historical climate variability and atmospheric CO2 in the United States. Tellus B 51(2): 414-452.

Trofymow, J.A., Blackwell, B.A., 1998. Changes in ecosystem mass and carbon distributions in coastal forest chronosequences. Northwest Science 72(2): 40-42.

Trofymow, J.A., Stinson, G., Kurz, W.A., 2008. Derivation of a spatially explicit 86-year retrospective carbon budget for a landscape undergoing conversion from old-growth to managed forests on Vancouver Island, BC. 6th North American Forest Ecology Workshop: From science to sustainability 256(10): 1677-1691.

Trofymow, J.A., Stinson, G., Kurz, W.A., 2008. Derivation of a spatially explicit 86-year retrospective carbon budget for a landscape undergoing

conversion from old-growth to managed forests on Vancouver Island, BC. Forest Ecology and Management 256(10): 1677-1691.

Turner, D.P., Acker, S.A., Means, J.E., Garman, S.L., 2000. Assessing alternative allometric algorithms for estimating leaf area of Douglas-fir trees and stands. Forest Ecology and Management 126(1): 61-76.

Turner, D.P., Ritts, W.D., Cohen, W.B., Gower, S.T., Running, S.W., Zhao, M., Costa, M.H., Kirschbaum, A.A., Ham, J.M., Saleska, S.R., Ahl, D.E., 2006. Evaluation of MODIS NPP and GPP products across multiple biomes. Remote Sensing of Environment 102(3-4): 282-292.

Turner, D.P., Ritts, W.D., Cohen, W.B., Gower, S.T., Zhao, M., Running, S.W., Wofsy, S.C., Urbanski, S., Dunn, A.L., Munger, J.W., 2003. Scaling Gross Primary Production (GPP) over boreal and deciduous forest landscapes in support of MODIS GPP product validation. Remote Sensing of Environment 88(3): 256-270.

Verseghy, D. (2009). CLASS - The Canadian Land Surface Scheme (Version 3.4), Environment Canada.

Verseghy, D.L., 1991. CLASS - a Canadian land surface scheme for GCMs. I. Soil model. International Journal of Climatology 11: 111-113.

Verseghy, D.L., 2000. The Canadian Land Surface Scheme (CLASS): Its History and Future. Atmosphere-Ocean 38(1): 1-13.

Verseghy, D.L., McFarlane, N.A., Lazare, M., 1993. CLASS - a Canadian land surface scheme for GCMs. II. Vegetation model and coupled runs. International Journal of Climatology 13: 347-370.

Wang, S., Grant, R.F., Verseghy, D.L., Black, T.A., 2001. Modelling plant carbon and nitrogen dynamics of a boreal aspen forest in CLASS - the Canadian Land Surface Scheme. Ecological Modelling 142(1-2): 135-154.

Wang, S., Grant, R.F., Verseghy, D.L., Black, T.A., 2002. Modelling Carbon Dynamics of Boreal Forest Ecosystems Using the Canadian Land Surface Scheme. Climatic Change 55(4): 451-477.

Wang, S.R.F.G.D.L.V.T.A.B., 2002. Modelling carbon-coupled energy and water dynamics of a boreal aspen forest in a general circulation model land surface scheme. International Journal of Climatology 22(10): 1249-1265.

Wang, Y.P., Leuning, R., 1998. A two-leaf model for canopy conductance, photosynthesis and partitioning of available energy. I. Model description and comparison with a multi-layered model. Agricultural and forest meteorology 91: 89-111.

Wang, Z., Grant, R.F., Arain, M.A., Chen, B.N., Coops, N., Hember, R., Kurz, W.A., Price, D.T., Stinson, G., Trofymow, J.A., Yeluripati, J., Chen, Z., 2011. Evaluating weather effects on interannual variation in net ecosystem productivity of a coastal temperate forest landscape: A model intercomparison. Ecological Modelling In Press, Corrected Proof.

Waring, R.H., Running, S.W., 1998. Forest Ecosystems: Analysis at Multiple Scales. San Diego, Academic Press.

Wullschleger, S.D. (1993). Biochemical Limitations to Carbon Assimilation in C3 Plants - A Retrospective Analysis of the A/Ci Curves from 109 Species. 44**:** 907-920.

Yuan, F., Arain, M.A., Alan, G.B., Black, T.A., Charles, P.A.B., Carole, C., Hank, A.M., McCAUGHEY, J.H., Steven, C.W., 2008. Modeling analysis of primary controls on net ecosystem productivity of seven boreal and temperate coniferous forests across a continental transect. Global Change Biology 14(8): 1765-1784.

Yuan, F., Arain, M.A., Black, T.A., Morgenstern, K., 2007. Energy and water exchanges modulated by soil-plant nitrogen cycling in a temperate Pacific Northwest conifer forest. Ecological Modelling 201(3-4): 331-347.

Zhao, M., Running, S.W., 2010. Drought-Induced Reduction in Global Terrestrial Net Primary Production from 2000 Through 2009. Science 329(5994): 940-943.

Table 3. 1 Initial C/N characteristics of soil and plant used to run the model.

Characteristics	**Value**	**Note**
Initial LAI (m^2 m^{-2})	1.0	Initial values assigned by pre-run
Specific leaf area (m^2 kg^{-1} C)	15.0	Assigned from Warren et al. (2003a,b)
C in reserved pool (kg C m^{-2})	0.01	Initial values assigned by pre-run
C in litter layer (kg C m^{-2})	0.81	Initial values assigned by pre-run
C in dead roots (kg C m^{-2})	0.20	Initial values assigned by pre-run
C in fast mineralized soil OM (kg C m^{-2})	1.0	Initial values assigned by pre-run
C in stable soil OM (kg C m^{-2})	3.50	Initial values assigned by pre-run
N : C ratio in plant labile reservoir	0.1	Initial values assigned by pre-run
N : C ratio in heartwood tissue	0.001	Initial values assigned by pre-run
N : C ratio in fine roots	0.020	Initial values assigned by pre-run
N : C ratio in coarse roots	0.01	Initial values assigned by pre-run
N : C ratio in surface litter materials	0.0125	Initial values assigned by pre-run
N : C ratio in root litter materials	0.01	Initial values assigned by pre-run
N : C ratio in fresh SOM	0.04	Initial values assigned by pre-run
N : C ratio in stable SOM	0.03	Initial values assigned by pre-run

Table 3. 2 Primary parameters used to run the model.

Parameters	**Value**
Empirical constant related to intercellular CO_2 concentration, a_1	3.9
Empirical parameter for stomatal sensitivity to VPD, D_0	1000.0
Maximum value of V_{cmax}, α ($\mu molm^{-2}s^{-1}$)	38.0
Extinction coefficient for canopy nitrogen	0.14
Quantum efficiency of RuBP regeneration	0.2
Rubisco-N exponential decay coefficient, k_n	0.25
Maximum transfer rate of assimilate to leaf structure, k_p	$5.0\times10^{-6}s^{-1}$
Leaf respiration rate at reference condition, R_{ref}	0.3 μmol m^{-2} s^{-1}
Sapwood base respiration rate at reference condition	2.0 μmol m^{-2} s^{-1}
Fine root respiration rate at reference condition	2.0 μmol kg^{-1} Cs^{-1}
Coarse root respiration rate at reference condition	0.3 μmol kg^{-1} Cs^{-1}
Maximum leaf relative growth rate	0.015 degree day^{-1}
Transition time of leaf exponential to linear growth, t_b	300 degree-days
Reference value for ET	$2.0\times10^{-4}mms^{-1}$
Ideal N:C ratio for leaf growth, NC_{lf}	0.024 g g^{-1}
Ideal N:C ratio for fine root growth, NC_{fr}	0.020 g g^{-1}
Ideal N:C ratio for living wood growth, NC_{sw}	0.002 g g^{-1}
N reallocation fraction of old tissues to new ones, frea	0.5

Table 3. 3 Values of aboveground biomass for 1928, 1998 and 2005 as obtained from inventory method, look-up table method and CBM-CFS3 and C-CLASS models.

	Disturbed	**Undisturbed**	**All**
Area (ha)	962	2863	3825
Total aboveground biomass (Mg C)			
1928			
Inventory[1]	30744	57315	88059
Lookup[2]	39699	95566	135265
1998			
Inventory[1]	26477	113883	140341
Lookup[2]	32730	132075	164805
CBM-CFS3	24181	108317	132498
C-CLASS	35693	159222	194915
2005			
CBM-CFS3	26400	107994	134395
C-CLASS	39235	164971	204206

[1] Bernier et al, 2010

[2] Fournier et al, 2003

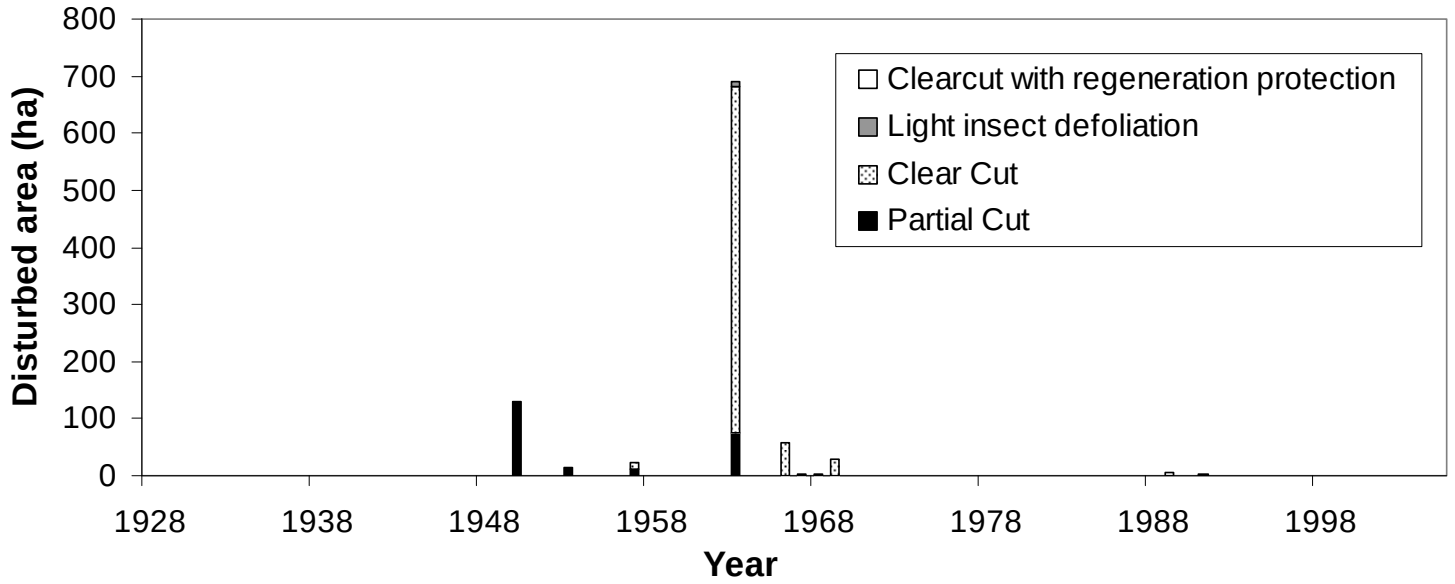

Figure 3. 1 Disturbed area in Chibougamau forest landscape (6275 ha) by the disturbance events type for the 1928-2005 simulation period.

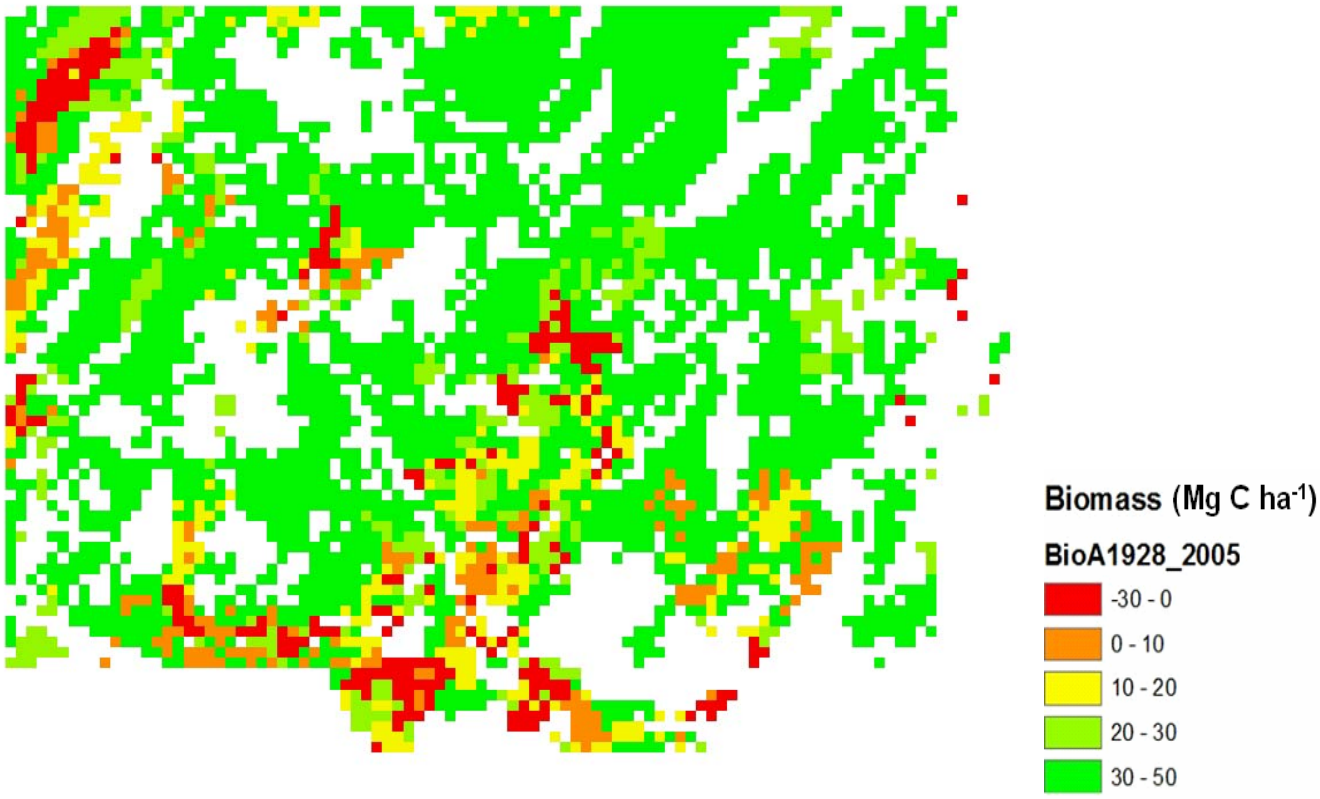

Figure 3. 2 Changes in C-CLASS simulated aboveground biomass in the study area between 2005 and 1928. Changes were calculated for all the forested grid cells (3825 ha) which remain productive throughout the 78 years.

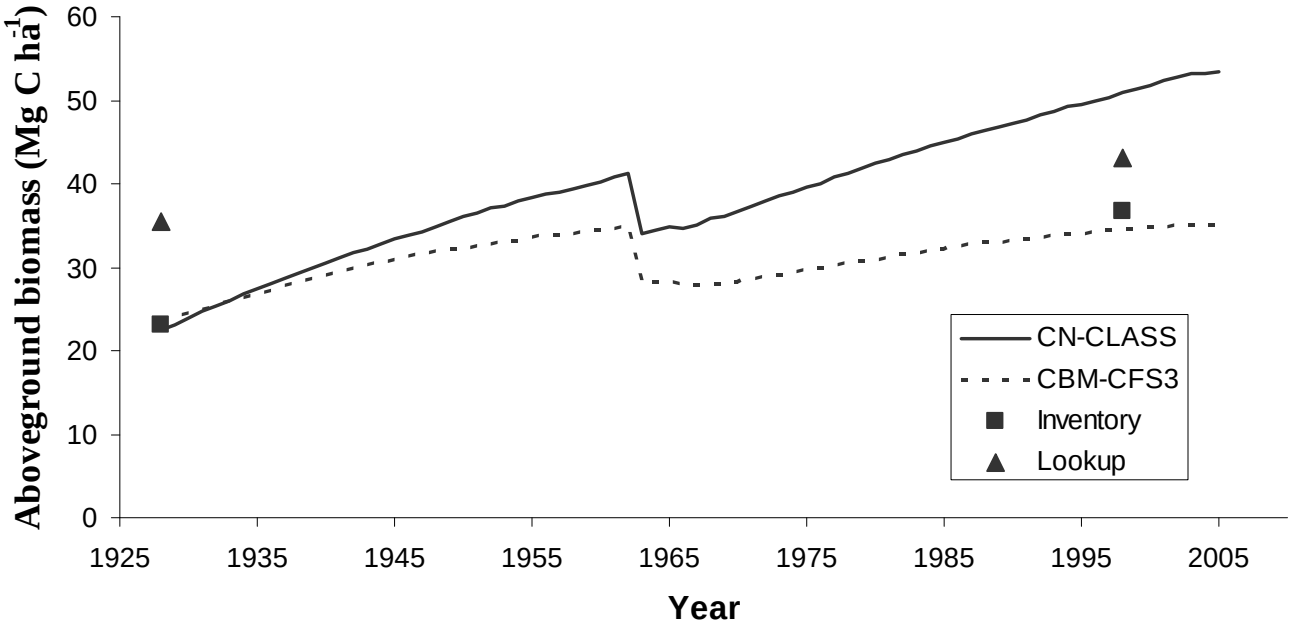

Figure 3. 3 Historic dynamics of aboveground biomass C stock changes between 1928 and 2005 for the 3825 ha forests in the study area as estimated by C-CLASS (simulated), CBM-CFS3 (simulated), the forest inventory (the 1928 forest inventory was used as input to both CBM-CFS3 and C-CLASS), and the Fournier et al. (2003) lookup tables.

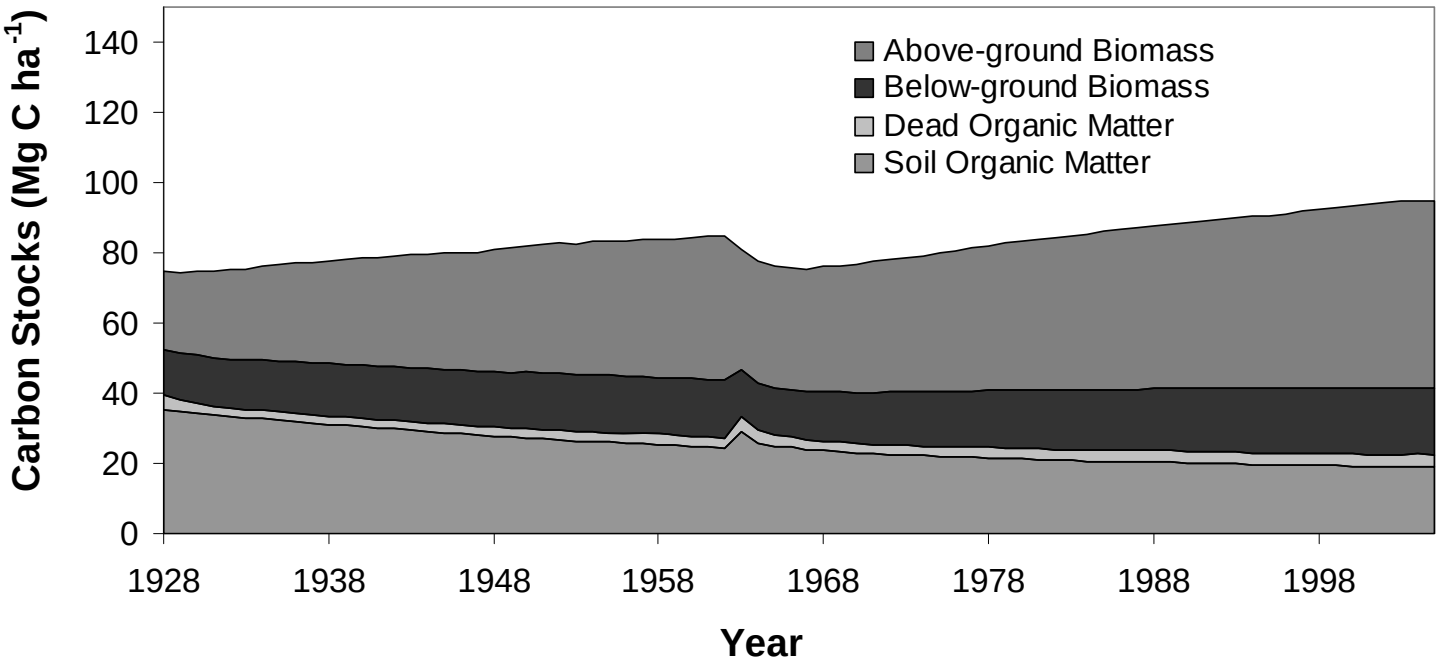

Figure 3. 4 C-CLASS simulated annual average landscape carbon stocks in the four Intergovernmetal Panel on Climate Change (IPCC) carbon pools for the 1928-2005 simulation period.

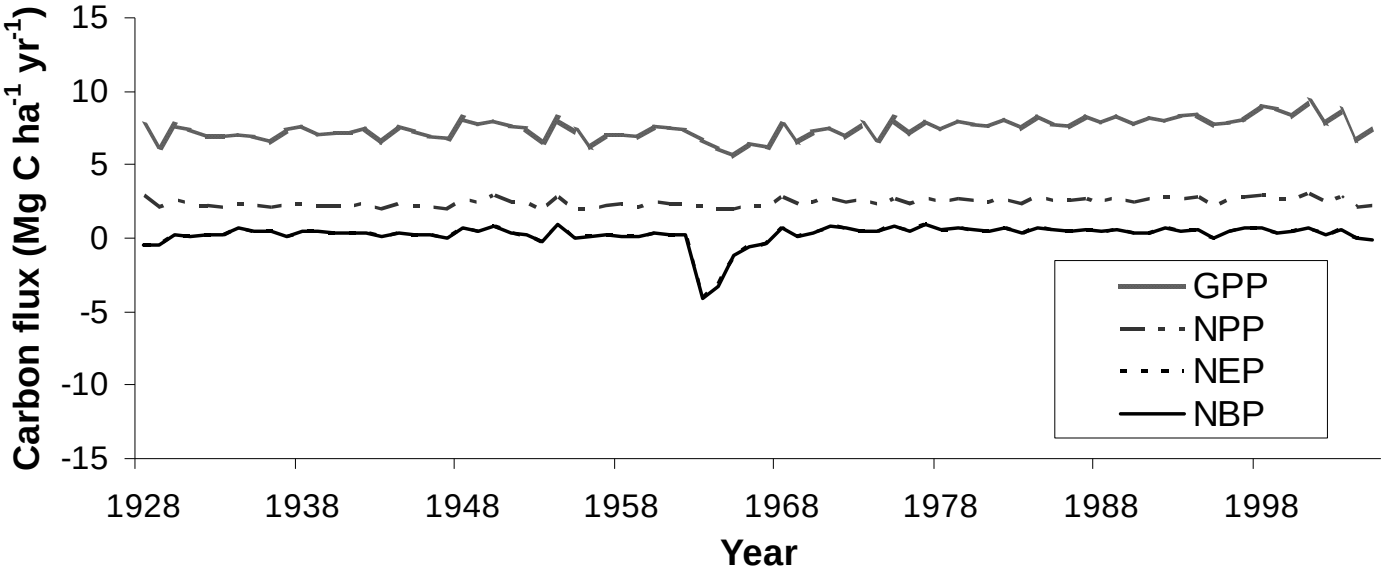

Figure 3. 5 C-CLASS simulated annual average landscape carbon fluxes: gross primary productivity (GPP), net primary productivity (NPP), net ecosystem productivity (NEP) and net biome productivity (NBP) for the 1928-2005 simulation period.

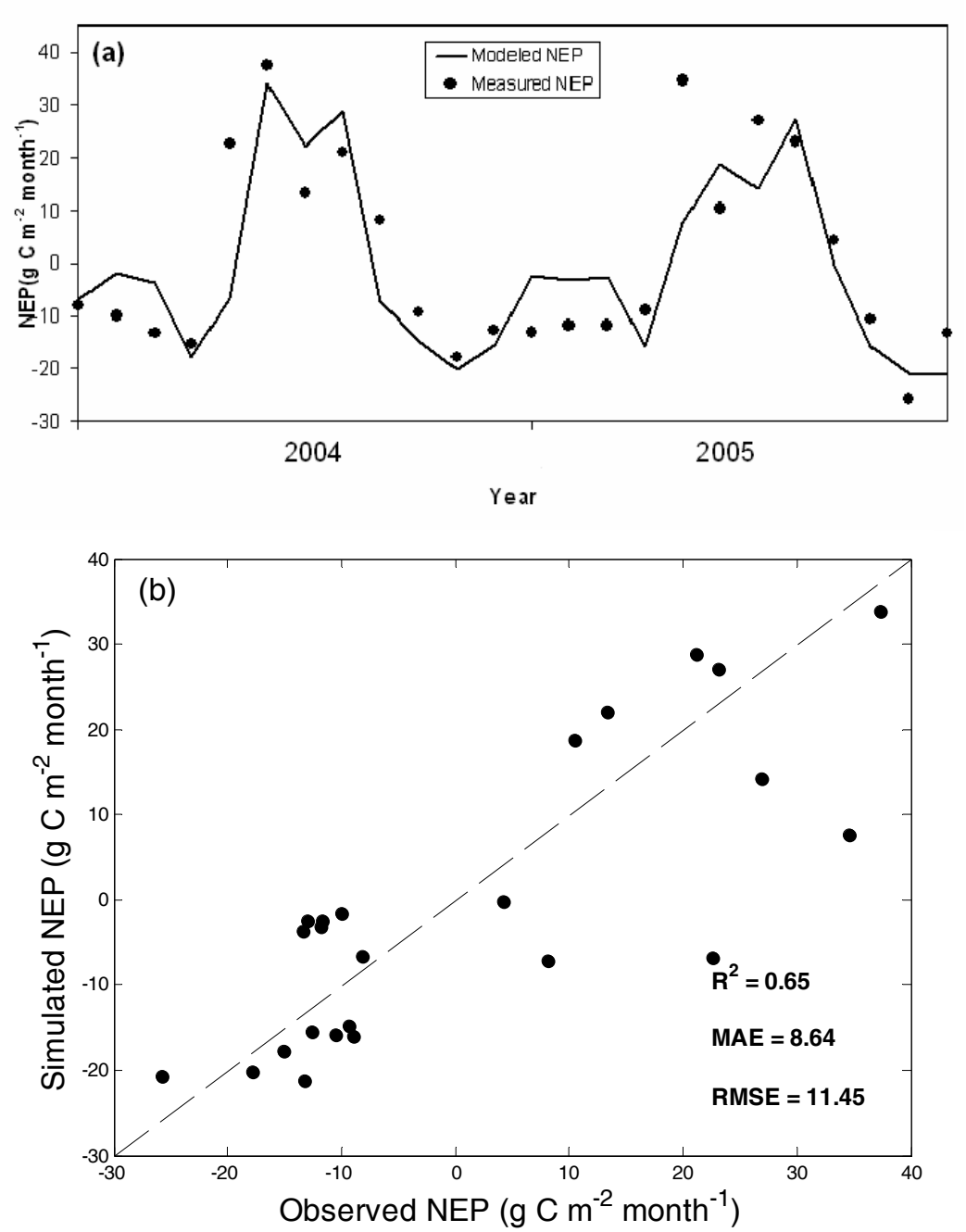

Figure 3. 6 Comparison of eddy covariance measured and C-CLASS simulated monthly net ecosystem productivity (NEP) from 2004-2005.

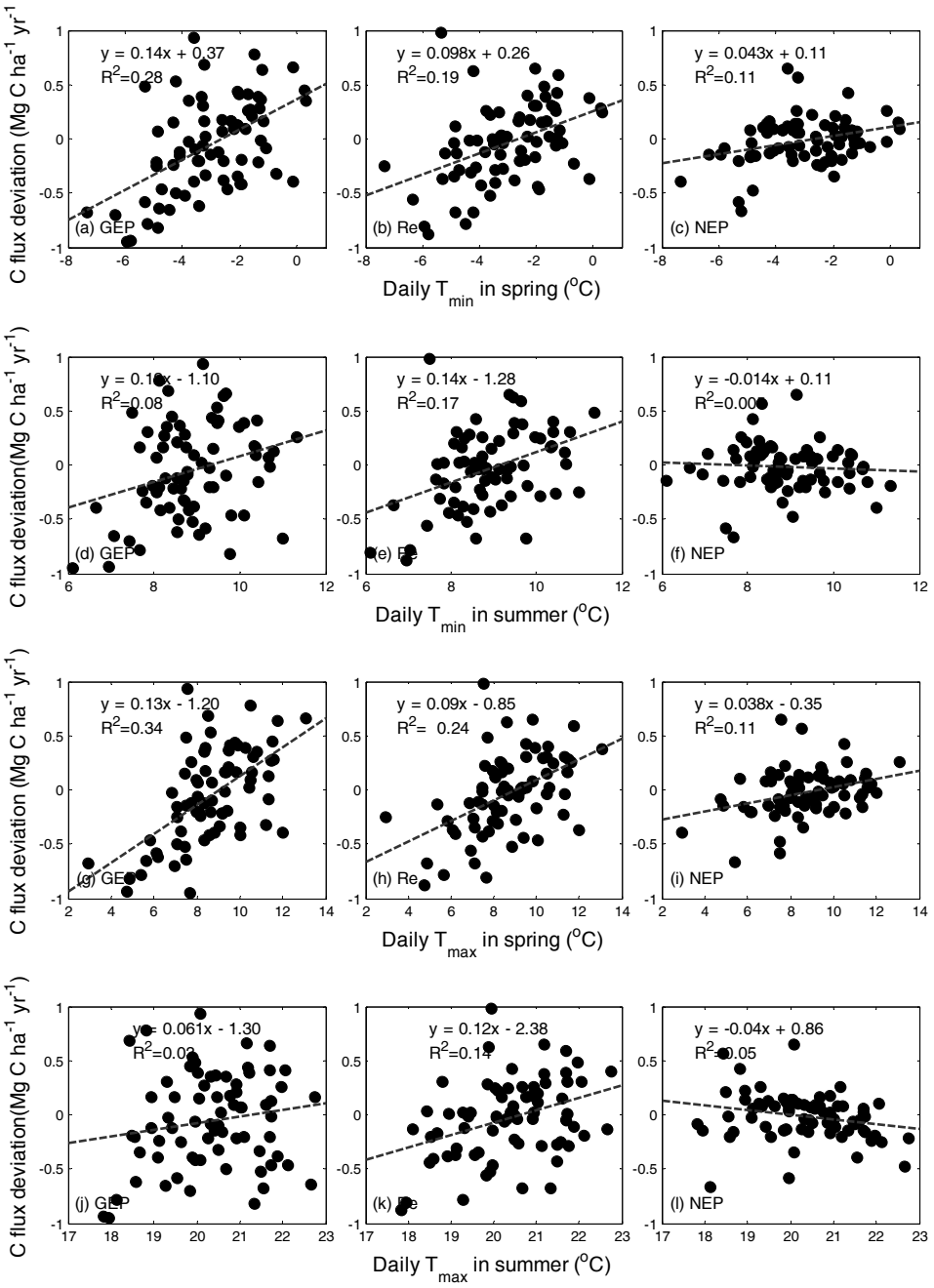

Figure 3. 7 Relationship between C-CLASS simulated deviations in 7-year mean gross primary productivity (GPP), ecosystem respiration (Re), net ecosystem productivity (NEP) and daily maximum and minimum temperature in spring and summer in Chibougamau undisturbed forest landscape from 1928-1999.

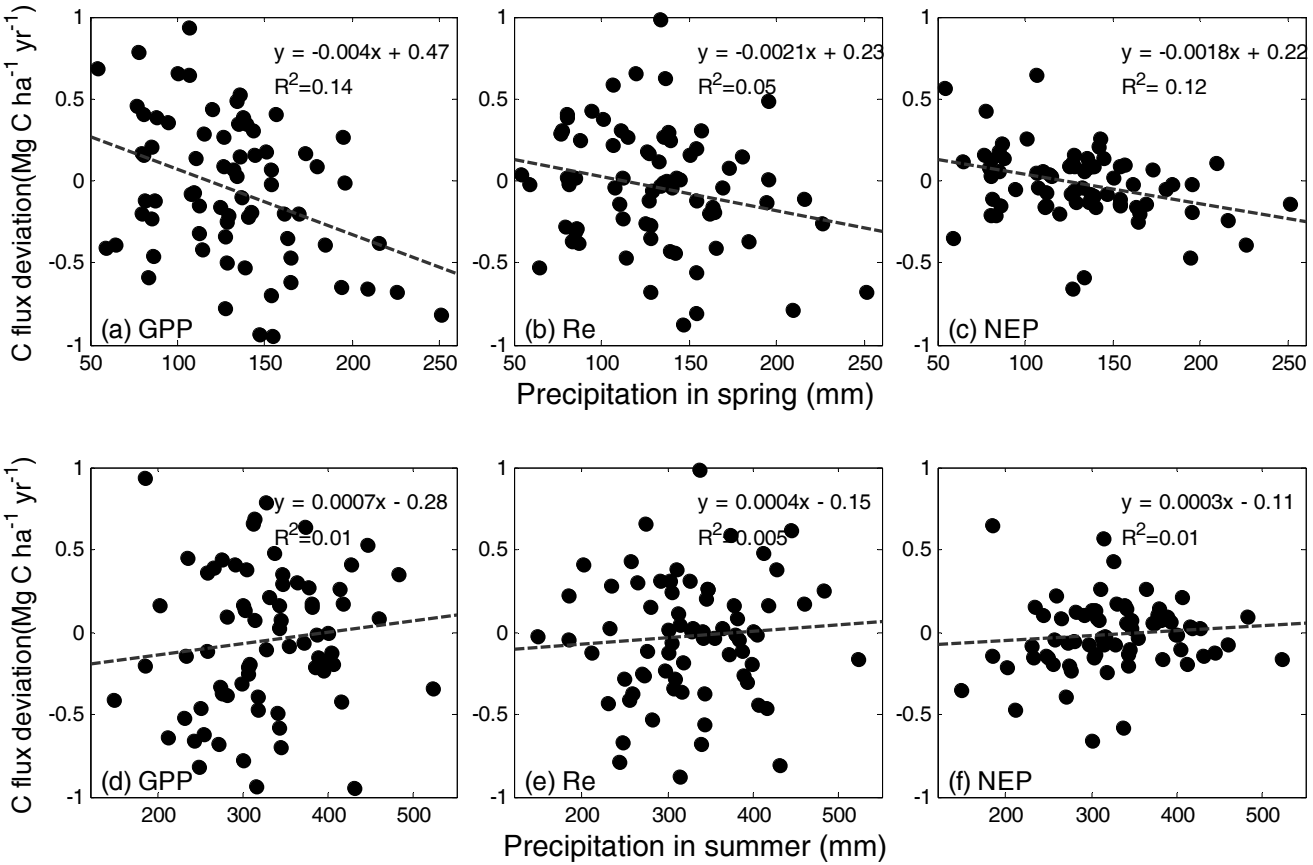

Figure 3. 8 Relationship between C-CLASS simulated deviations in 7-year mean gross primary productivity (GPP), ecosystem respiration (Re), net ecosystem productivity (NEP) and total precipitation in spring or summer in Chibougamau undisturbed forest landscape from 1928-1999.

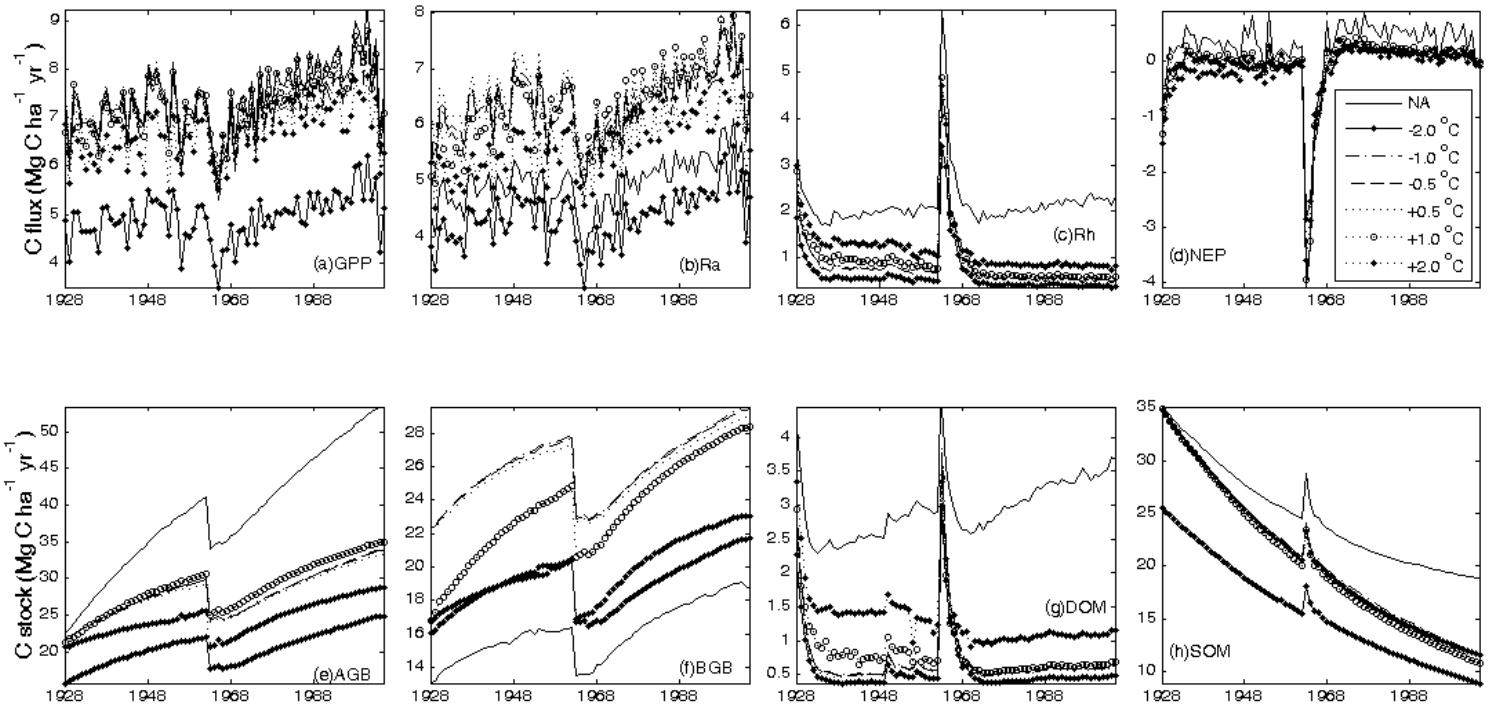

Figure 3. 9 Sensitivity of C-CLASS simulated landscape-level carbon fluxes and stocks to air temperature. [GPP, gross primary productivity; R_a, autotrophic respiration; R_h, heterotrophic respiration; NEP, net ecosystem productivity; AGB, aboveground biomass; BGB, belowground biomass; DOM, dead organic matter; SOM, soil organic matter; NA, no adjustment].

CHAPTER 4:

SIMULATING GROSS PRIMARY PRODUCTIVITY OVER CANADA'S LANDMASS FOR EVALUATING THE MODIS GPP PRODUCT

4.1 Abstract

The Moderate Resolution Imaging Radiometer (MODIS) is a primary instrument in the National Aeronautics and Space Administration (NASA) Earth Observing System (EOS) which is designed for monitoring the seasonality of global terrestrial vegetation. MODIS provides global estimates of 8-day mean gross primary productivity (GPP) at 1-km spatial resolution. In this study, annual GPP from MODIS was compared with the Integrated Carbon-Canadian Land Surface Scheme (IC-CLASS) simulated GPP over Canadian landmass in 2003. The North American land cover map (GLC 2000-NCA) compiled using SPOT VGT sensor was used to describe land cover types and to derive the leaf area index used in the model. The model was run at 1-km spatial resolution using hourly time series of meteorological data from medium range forecast of the National Center for Environmental Prediction (NCEP) available for 1^o x 1^o grids across the globe. GPP simulated by IC-CLASS was first corroborated with the annual GPP estimates at seven eddy covariance flux tower sites across Canada. IC-CLASS GPP for whole Canadian landmass was 3134.8 Mt C yr^{-1} as compared to 3906.3

Mt C yr^{-1} derived from the MODIS GPP product. Seasonal dynamics of the simulated GPP indicated high summer values during a short (April-October) growing season due to Canada's northern location. Overall, monthly mean values of simulated and MODIS-derived GPP values in conifer forest, deciduous forest, mixed forest, cropland and grassland followed similar patterns. However, IC-CLASS simulated GPP were higher than MODIS values in deciduous forest, while they were lower in mixed forest and grassland during most of the growing season. The overestimation of MODIS annual GPP over Canada's landmass compared to IC-CLASS simulation may be attributed to the limitations of MODIS GPP algorithm and the calculation method of light use efficiency used to produce MODIS GPP product.

4.2 Introduction

Terrestrial plants fix carbon dioxide (CO_2) through photosynthesis, a carbon (C) flux also known as gross primary productivity (GPP) at the ecosystem level (Beer et al., 2010). GPP data are useful in many applications, such as the global C cycle and climate change research (Bonan, 1995; Chen et al., 2000; Beer et al., 2010; Reich, 2010). Although photosynthesis at the leaf and canopy levels is quite well understood, only tentative observation-based estimates of regional and global terrestrial GPP have been possible so far (Beer et al., 2010). With the advancement of satellite technologies, remote sensing data have become a primary means to derive regional and global estimates of the terrestrial C cycle (Running et al., 1999; Turner et al., 2003).

The Moderate Resolution Imaging Spectroradiometer (MODIS) sensor of the National Aeronautics and Space Administration (NASA), Earth Observing System (EOS), was designed partly for this purpose and continuous global estimates of 8-day composite GPP are now being produced (Running et al., 2000). The estimation of MODIS GPP is based on a light use efficiency model. The model computes GPP for each 1-km^2 pixel for each day using the absorbed photosynthetic active radiation (APAR) multiplied by the light use efficiency (ε). This algorithm contains three fundamental assumptions, i.e. (i) plant GPP is directly related to APAR, (ii) a correlation exists between FPAR and satellite-

derived spectral indices of vegetation, and (iii) there are biophysical reasons for the reduction of ε below its theoretical potential value. Therefore, validation of MODIS-derived GPP with observed data is critical for accurate and credible usage of this dataset (Morisette et al., 2002; Turner et al., 2003; Turner et al., 2006). However, observed flux data are available at a limited number of sites in each biome across the world (Baldocchi et al., 2001; Baldocchi 2008). Therefore, process-based ecosystem models, in combination with observed flux measurements may play a crucial role in validating MODIS data products, including GPP. The process-based models have many advantages for estimating GPP because they are theoretically based and has the ability to handle interactions and feedbacks between different canopy processes (Liu et al., 2002).

Turner et al. (2003) compared the 2001 MODIS GPP with the GPP estimates derived from a process-based model (Biome-BGC) over boreal and deciduous forest landscapes (25 km^2) (Turner et al., 2003). Later, Turner et al. (2006) validated MODIS GPP and net primary productivity (NPP) at 9 sites with varying biome types and land use, including arctic tundra, boreal forest, temperate hardwood forest, temperate conifer forest, tropical rain forest, tall grass prairie, desert grassland and cropland using Biome-BGC model integrated over a 25 km^2 areas at each site for effective comparisons with MODIS products (Turner et al., 2006). Although these validations of MODIS GPP with the ground-based estimates have improved the confidence in these products but there have been

very few studies in literature where MODIS GPP were validated at a large spatial scale (Zhang et al., 2012). Such large scale comparisons are necessary to improve the confidence in regional and continental C exchange estimates derived using MODIS indices. These comparisons may also help to improve the formulation and parameterization of MODIS GPP algorithm.

The primary objective of this study is to simulate GPP over Canadian landmass at 1-km resolution using a process-based model, the Integrated Carbon-Canadian Land Surface Scheme (IC-CLASS) and to compare it with MODIS-derived GPP for each key biome type. The secondary objective of this study is to explore the possible improvements in the formulation of MODIS GPP algorithm.

4.3 Materials and Methods

4.3.1 Model Input data

Land cover type is among the basic state variables determining the terrestrial ecosystem structure and the magnitude of ecosystem carbon pool (Liu et al., 2002). The land cover map used in this study is derived from the land cover map of North and Central America for the year 2000 (GLC 2000-NCA). This land cover map was compiled using the Satellite pour 1' observation de la terre (SPOT) VEGETATION (VGT) sensor during 2000 growing season at 1-km spatial resolution (Latifovic et al., 2004). There were 28 land cover types based on

modified Federal Geographic Data Committee/Vegetation Classification Standard (FGDC-VCS) system, which were compiled into 11 land cover types including conifer forest, broadleaf forest, mixed forest, cropland, grassland, shrubland, barren land, urban area, burnt area, wetland and snow/ice (Figure 4.1). The statistics of 1-km land cover classification across Canada are given in Table 4.1.

The spatial distribution of C3 and C4 plants is required to accurately simulate CO_2, water and energy exchanges between the land surface and atmosphere (Still et al., 2003). The global C3/C4 vegetation distribution map at 1-degree spatial resolution was used in combinations with the GLC-2000 land cover map for model initialization in this study. Due to the different spatial resolutions of these land cover and C3/C4 vegetation distribution maps, C3 crop pixels were randomly chosen by the fraction. This is the best we can do to solve the sub-grid issue although it may still introduce some uncertainties.

Leaf area index (LAI) maps used in this study were retrieved from 2003 global LAI product at 1-km resolution derived from SPOT synthesis images (Deng et al., 2006; Pisek and Chen, 2007). The simplified method for atmospheric correction (SMAC) was used to adjust the atmospheric effect in 10-day composite (VGT S10) images (Rahman and Dedieu, 1994). The cloud effects were screened using the standard VGT formulas and the maximum normalized difference vegetation index (NDVI) criterion for selecting the best date of measurements in each pixel to form the 10-day composites. Moreover, a procedure named locally

adjusted cubic-spline capping (LACC) was used to reconstruct the seasonal trajectory of LAI pixel by pixel so that residual cloud effects can be further minimized (Chen et al., 2006; Deng et al., 2006). The Four-Scale model with a multiple scattering scheme was used to simulate the relationships between LAI and reflectance of the three spectral bands (red, near infrared and shortwave infrared) separately for different plant functional types based on GLC-2000 land cover datasets (Chen and Leblanc, 1997; Chen and Leblanc, 2001; Deng et al., 2006). Deng et al. (2006) developed a new algorithm to fit the key coefficients in the bidirectional reflectance distribution function (BRDF) kernels with Chebyshev polynomials. This algorithm considered the BRDF explicitly and it solved the problem of no analytical solution to directly drive LAI from reflectance data through developing a simple iteration procedure (Deng et al., 2006). The detail of the theoretical basis of this algorithm and the derivation and accuracy assessments of LAI maps can be found in Deng et al. (2006).

Soil texture data on silt and clay fraction were obtained from the version 2 of the Soil Landscapes of Canada (SLC) database, which is the best soil database currently available for Canada (Shields et al., 1991; Schut et al., 1994). The original vector data in SLC were mosaiced, rasterized and reprojected into a 1-km resolution grids using a standard Lambert conformal conic (LCC) projection with 49° and 77º N standard parallels and a 95º W meridian. Soil carbon density was derived from the International Satellite Land Surface Climatology Project

(ISLSCP) initiative II data that has 1-degree spatial resolution. The soil organic carbon (SOC) map derived from Integrated Terrestrial Ecosystem C-budget model (InTEC) at 1-km spatial resolution was used to fill gaps in the ISLSCP II soil C density map.

Meteorological data used in this study were retrieved from the median range forecast (MRF) global flux archives of the National Center for Environmental Prediction (NCEP), distributed by the National Center for Atmospheric Research (NCAR). Downward shortwave radiation, precipitation, specific humidity, air temperature and wind speed at one degree spatial resolution were used to drive the model at hourly time step.

4.3.2. Coupled canopy photosynthesis and conductance sub-model

The original C-CLASS model calculate the total radiation absorptions by sunlit and shaded leaf groups and treat each group as a big leaf, and therefore this type of model is a two-big-leaf model (Arain et al., 2002; Chen et al., 2012). In this study, the canopy radiation routine of the Boreal Ecosystem Productivity Simulator (BEPS) was introduced into the original C-CLASS model in order to calculate the incident irradiances on representative sunlit and shaded leaves, and in this way the problem of CO_2 flow distortion associated with big-leaf formulation can be entirely avoided (Chen et al., 2012). The canopy radiation

routine of the BEPS model has reduced some radiation transfer physics into simple equations through numerical experiments, and therefore it is suitable for regional and global applications using remote sensing data (Chen et al., 2012). The original C-CLASS model calculate canopy-level photosynthesis rate as the sum of two big-leaves, and therefore its vertical integrations result in the total accumulated values of photosynthesis capacity for the two big-leaves (Arain et al., 2006). In order to avoid using the big-leaf formulation, the leaf-to-canopy up-scaling methodology of photosynthesis capacity in the original C-CLASS model was improved by first calculating the photosynthesis values of a representative sunlit leaf and a representative shaded leaf separately and multiplying them with their respective LAI (Chen et al., 2012).

4.3.2.1 Instantaneous leaf-level gross photosynthesis

The instantaneous leaf-level gross photosynthesis for C3 plant is calculated as the minimum of (Farquhar et al., 1980; Arain et al., 2002):

$$W_c = V_m \frac{C_i - \Gamma}{C_i + K} \tag{1a}$$

and

$$W_j = J \frac{C_i - \Gamma}{4C_i + 8\Gamma} \tag{1b}$$

where W_c (μmol m^{-2} s^{-1}) is ribulose-bisphosphate carboxylase-oxygenase (Rubisco) limited gross photosynthesis rate, W_j (μmol m^{-2} s^{-1}) is light limited gross photosynthesis rate. V_m is the maximum carboxylation rate in μmol m^{-2} s^{-1}; J is the electron transport rate in μmol m^{-2} s^{-1}; C_i is the intercellular CO_2 concentration; Γ is the CO_2 compensation point without dark respiration; K is a function of enzyme kinetics. The dimension for C_i, Γ and K is in Pa. Both Γ and K are temperature dependent parameters (Collatz et al., 1991; Sellers et al., 1992). Γ can be expressed as:

$$\Gamma = 1.92 * 10^{-4} O_2 * 1.75^{(T-25)/10} \quad (2)$$

where O_2 is the oxygen concentration in the atmosphere and O_2 = 0.21*P. P is the atmospheric pressure in Pa and it is assumed that O_2 occupies 21% of the air by volume. T is the leaf temperature in °C. K is given by:

$$K = K_c (1 + O_2/K_o) \quad (3)$$

where K_c and K_o are Michaelis-Menten constants for CO_2 and O_2, respectively in Pa. $K_c = 30*2.1^{(T - 25)/10}$, and $K_o = 30{,}000*1.2^{(T - 25)/10}$ (Collatz et al., 1991). V_m can be expressed as a function of both temperature and leaf nitrogen content (Bonan, 1995):

$$V_m = V_{m25} * 2.4^{(T-25)/10} f(T) f(N) \quad (4)$$

where V_{m25} is V_m at 25°C, and is a variable depending on vegetation type; $f(T)$ and $f(N)$ are temperature and nitrogen limitation terms defined as (Bonan, 1995):

$$f(T) = \left\{1 + \exp[\frac{-220{,}000 + 710(T+273)}{8.314(T+273)}]\right\}^{-1} \quad (5)$$

Leaf nitrogen content per unit leaf area $N(L)$ generally decreases exponentially from the top to the bottom of a canopy (Leuning et al., 1995; De Pury and Farquhar, 1997; Kattge et al., 2009) and can be expressed as (Chen et al., 2012):

$$N(L) = N_0 e^{-k_n L} \quad (6)$$

where N_0 is the nitrogen content at the top of the canopy, and k_n is the leaf nitrogen content decay rate with increasing depth into the canopy, i.e., LAI(L). In this study, we assumed $k_n = 0.3$ (De Pury and Farquhar, 1997). The leaf maximum carboxylation rate at 25 ˚C (V_{m25} or V_{cmax}) is generally proportional to leaf nitrogen content and therefore is also a function of L (Chen et al., 2012):

$$V_{c\max}(L) = V_{c\max,0} * \chi_n * N(L) \quad (7)$$

where $V_{c\max,0}$ is $V_{c\max}$ at the top of the canopy (i.e., $L = 0$), and χ_n is the relative change of $V_{c\max}$ with N. N has a unit of g m^{-2} and χ_n has a unit of m^2 g^{-1}. The values of χ_n, N and $V_{c\max,0}$ for the various vegetation types are provided in Table 4.2.

The fractions of sunlit and shaded leaf areas to the total leaf area vary with the depth into the canopy and can be described as (Chen et al., 2012):

$$f_{sun}(L) = e^{-kL} \tag{8}$$

and

$$f_{sh}(L) = 1 - e^{-kL} \tag{9}$$

where k = G(θ)Ω/cosθ, where G(θ) is the projection coefficient, usually taken as 0.5 for spherical leaf angle distribution, Ω is the clumping index, and θ is the solar zenith angle.

Because these fractions vary with L, the mean values of leaf nitrogen content for sunlit and shaded leaves and their corresponding $V_{c\max}$ values can be obtained by vertical integrations with respect to L (Chen et al., 2012):

$$V_{c\max,sun} = \frac{\int_0^L V_{c\max,0}\chi_n N(L) f_{sun}(L) dL}{\int_0^L f_{sun}(L) dL}$$

$$= V_{c\max,0}\chi_n N_0 \frac{\int_0^L e^{-k_n L} e^{-kL} dL}{\int_0^L e^{-kL} dL}$$

$$= V_{c\max,0}\chi_n N_0 \frac{k[1 - e^{-(k_n + k)L}]}{(k_n + k)(1 - e^{-kL})} \tag{10}$$

and

$$V_{c\max,sh} = \frac{\int_0^L V_{c\max,0}\chi_n N(L) f_{sh}(L) dL}{\int_0^L f_{sh}(L) dL}$$

$$= V_{c\max,0}\chi_n N_0 \frac{\int_0^L e^{-k_n L}(1-e^{-kL}) dL}{\int_0^L (1-e^{-kL}) dL}$$

$$= V_{c\max,0}\chi_n N_0 \frac{\frac{1}{k_n}(1-e^{-k_n L}) - \frac{1}{k_n+k}[1-e^{-(k_n+k)L}]}{L - \frac{1}{k}(1-e^{-kL})} \quad (11)$$

Equations (10) and (11), therefore, represent the mean V_{cmax} values for the representative sunlit and shaded leaves, respectively, obtained through weighting against sunlit and shaded leaf occurrence probabilities (Chen et al., 2012).

The electron transport rate (J) is dependent on photosynthetic photon flux density (PPFD) absorbed by the leaf (Farquhar and von Caemmerer, 1982; Chen et al., 1999) and is given by:

$$J = J_{\max} * PPFD/(PPFD + 2.1 * J_{\max}) \quad (12)$$

where J_{max} (μmol m^{-2} s^{-1}) is the light-saturated rate of electron transport in the photosynthetic carbon reduction cycle in leaf cell. After V_{cmax} values for the representative sunlit and shaded leaves are obtained, J_{max} for the sunlit and shaded leaves are obtained from (Wullschleger, 1993; Chen et al., 1999):

$$J_{\max,sun} = 29.1 + 1.64 * V_{m,sun} \quad (13)$$

and

$$J_{\max,sh} = 29.1 + 1.64 * V_{m,sh} \quad (14)$$

In this way, the effects of the vertical nitrogen gradient in the canopy on both the maximum carboxylation rate and the maximum electron transport rate are considered.

Then, leaf net photosynthesis rate (A) is given by:

$$A = \min(W_c, W_j) - R_d \quad (15)$$

where R_d is daytime leaf dark respiration (μmol m^{-2} s^{-1}) and is given by (Collatz et al., 1991):

$$R_d = 0.015 * V_m \quad (16)$$

4.3.2.2 Stomatal conductance

The internal CO_2 concentration (C_i) can be described in the form (Baldocchi, 1994):

$$C_i = C_s - \frac{A}{g_{sc}} \quad (17)$$

where C_s is the CO_2 concentration at the leaf surface (Pa). g_{sc} is leaf stomatal conductance for CO_2 (μmol m^{-2} s^{-1} Pa^{-1}). C_s can be further expressed in terms of the atmospheric CO_2 concentration (C_a) in Pa and the conductance for CO_2 across the laminar boundary layer of a leaf (g_{bc}) in μmol m^{-2} s^{-1} Pa^{-1} (Baldocchi, 1994):

$$C_s = C_a - \frac{A}{g_{bc}} \tag{18}$$

The stomatal conductance model in the original C-CLASS model was used in this study (Leuning et al., 1995; Arain et al., 2002):

$$g_{sc} = b' + \frac{m f_w A}{(C_s - \Gamma)(1 + \frac{D_s}{D_0})} \tag{19}$$

where the coefficient m is a dimensionless slope, D_s is water vapor pressure deficit (VPD) at the leaf surface (Pa), b' is the zero intercept (μmol m^{-2} s^{-1} Pa^{-1}) when A is equal to or less than zero and D_0 is an empirical parameter determining stomatal sensitivity to vapor pressure deficit (Pa) (Arain et al., 2002). The empirical function f_w describes the effect of soil water supply on stomatal conductance and it is expressed as follows (Wang and Leuning, 1998; Arain et al., 2002):

$$f_w = \min(1.0, \frac{10(\theta_s - \theta_{\min})}{3(\theta_{\max} - \theta_{\min})}) \tag{20}$$

where θ_s is the volumetric soil water content of the root zone and θ_{min} and θ_{max} are the volumetric soil water content at wilting point and field capacity, respectively.

4.3.2.3 The derivation of coupled leaf photosynthesis and stomatal conductance sub-model

Now that the set of working equations has been articulated, our goal is to derive an equation describing A that is independent of C_s, C_i and g_{sc}. The term C_s is eliminated by inserting equation (18) into equation (17) and (19). Subsequently, the term g_{sc} is eliminated by inserting equation (19) into equation (17). After algebraic manipulation, an expression for C_i is derived:

$$C_i = \frac{A^2(\frac{b'\varepsilon}{g_b} - mf_w + \varepsilon) + A[-\varepsilon C_a b' - \varepsilon b'(C_a - \Gamma) + g_b C_a mf_w - \varepsilon g_b C_a + \varepsilon g_b \Gamma] + \varepsilon g_b C_a b'(C_a - \Gamma)}{A(g_b mf_w - \varepsilon b') + \varepsilon g_b b'(C_a - \Gamma)} \tag{21}$$

$$\varepsilon = 1 + \frac{D_s}{D_0} \tag{22}$$

Further algebraic manipulation yields a cubic equation dependent on A:

$$0 = e\alpha A^3 + A^2(e\beta + b\theta - a\alpha + e\alpha R_d) + A(eC_a\gamma + b\gamma - a\beta + ad\theta + R_d b\theta + eR_d\beta) - a\gamma C_a + R_d e\gamma C_a + \gamma R_d b + \gamma ad \tag{23}$$

The variables a, b, d and e are coefficients from equation (1). If W_c is minimal, these coefficients correspond to:

$$W_c = V_m \frac{C_i - \Gamma}{C_i + K} = \frac{aC_i - ad}{eC_i + b} \tag{24}$$

If W_j is minimal, the a, b, d and e coefficients correspond to:

$$W_j = J \frac{C_i - \Gamma}{4C_i + 8\Gamma} = \frac{aC_i - ad}{eC_i + b} \tag{25}$$

Other terms in equation (23) are defined in the following equations:

$$\alpha = mf_w - \frac{b'\varepsilon}{g_b} - \varepsilon \tag{26}$$

$$\beta = 2\varepsilon C_a b' - \varepsilon b'\Gamma - g_b C_a m f_w + \varepsilon g_b C_a - \varepsilon g_b \Gamma \tag{27}$$

$$\gamma = \varepsilon g_b b'(\Gamma - C_a) \tag{28}$$

$$\theta = \varepsilon b' - g_b m f_w \tag{29}$$

4.3.2.3 The solution of coupled leaf photosynthesis and stomatal conductance sub-model

The solution of the cubic equation was taken from Press et al. (1989). In brief, if equation (23) is manipulated into the form:

$$x^3 + px^2 + qx + r = 0 \tag{30}$$

Three roots for the cubic equation are

$$x_1 = -2\sqrt{Q}\cos(\frac{\theta}{3}) - \frac{p}{3}$$

$$x_2 = -2\sqrt{Q}\cos(\frac{\theta + 2\pi}{3}) - \frac{p}{3}$$

$$x_3 = -2\sqrt{Q}\cos(\frac{\theta + 4\pi}{3}) - \frac{p}{3} \tag{31}$$

Terms in equation (31) are defined as:

$$Q = \frac{p^2 - 3q}{9}$$

$$R = \frac{2p^3 - 9pq + 27r}{54}$$

and

$$\theta = a\cos(\frac{R}{\sqrt{Q^3}}) \tag{32}$$

The root corresponding to leaf net photosynthesis rate (A) is chosen as the smaller root which is larger than zero (Baldocchi, 1994).

4.3.2.4 Boundary layer conductance to CO_2 (g_{bc})

Total boundary layer conductance to heat (g_{bH}) for one side of a leaf can be expressed as (Leuning et al., 1995):

$$g_{bH} = g_{bHw} + g_{bHf} \tag{33}$$

where g_{bHw} is the boundary layer conductance for one side of a leaf resulting from forced convection and it can be calculated as follows (Monteith 1973):

$$g_{bHw} = 0.003(\frac{U}{w_l})^{1/2} \tag{34}$$

where U is the wind speed (m s^{-1}) and w_l is the leaf width (= 0.01 m). The wind speed within the canopy was assumed to decrease exponentially with depth in the canopy according to:

$$U(L) = U_0 e^{(-k_u L)} \tag{35}$$

where U_0 is the wind speed just above the canopy in m s^{-1}. k_u is the extinction coefficient for wind speed (= 0.5 m^2 ground m^{-2} leaf). The mean values of wind

speed for sunlit and shaded leaves can be obtained through vertical integrations with respect to L:

$$U_{sun} = \frac{\int_0^L U_0 e^{-k_u L} f_{sun}(L) dL}{\int_0^L f_{sun}(L) dL} = U_0 \frac{\int_0^L e^{-k_u L} e^{-kL} dL}{\int_0^L e^{-kL} dL} = U_0 \frac{k[1 - e^{-(k_u + k)L}]}{(k_u + k)(1 - e^{-kL})} \tag{36}$$

$$U_{sh} = \frac{\int_0^L U_0 e^{-k_u L} f_{sh}(L) dL}{\int_0^L f_{sh}(L) dL} = U_0 \frac{\int_0^L e^{-k_u L} (1 - e^{-kL}) dL}{\int_0^L (1 - e^{-kL}) dL} = U_0 \frac{\frac{1}{k_u}(1 - e^{-k_u L}) - \frac{1}{k_u + k}[1 - e^{-(k_u + k)L}]}{L - \frac{1}{k}(1 - e^{-kL})} \tag{37}$$

The leaf boundary layer conductance for free convection (g_{bHf}) is calculated as (Monteith 1973):

$$g_{bHf} = \frac{0.5 D_H Gr^{1/4}}{w_l} \tag{38}$$

where D_H is the molecular diffusivity for heat and the Grashof number is:

$$Gr = 1.6 \times 10^8 \left| T_l - T_a \right| w_l^3 \tag{39}$$

where T_l is the leaf temperature. We did not consider the difference between T_l and T_a in this study and we assumed that $g_{bHf} \approx 0$. Thus, $g_{bH} \approx g_{bHw}$.

Water and CO_2 are assumed to be lost from one side of the leaf only (Sellers et al., 1996). The boundary layer conductance to water vapor (g_{bw}) can be expressed as:

$$g_{bw} = 1.075 g_{bH} \tag{40}$$

The boundary layer conductance to CO_2 (g_{bc}) can be expressed as:

$$g_{bc} = \frac{g_{bw}}{1.56} \tag{41}$$

where the factor 1.56 is the ratio of molecular diffusivities for water vapor and CO_2 in air. Thus, g_{bc} can be expressed as:

$$g_{bc} = \frac{1.075 g_{bH}}{1.56} \approx \frac{1.075 * 0.003 (\frac{U}{w_l})^{1/2}}{1.56} = 0.002 (\frac{U}{w_l})^{1/2} \tag{42}$$

After the wind speed values for the representative sunlit and shaded leaves are obtained, the boundary layer conductance to CO_2 for the sunlit and shaded leaves are obtained from:

$$g_{bc,sun} = 0.002 (\frac{U_{sun}}{w_l})^{1/2} \tag{43}$$

and

$$g_{bc,sh} = 0.002 (\frac{U_{sh}}{w_l})^{1/2} \tag{44}$$

The units of g_{bH}, g_{bHf}, g_{bHw}, g_{bw} and g_{bc} are m s^{-1}. The boundary layer conductance to CO_2 (g_{bc}) in m s^{-1} can be converted to the unit of μmol m^{-2} s^{-1} by multiplying by 42400 at 15 ˚C (Korner et al., 1979).

4.3.2.5 Sunlit and shaded GPP modeling

With the separation of sunlit and shaded leaf groups, the total canopy photosynthesis (A_{canopy}) can be calculated as (Norman, 1982; Chen et al., 1999):

$$A_{canopy} = A_{sun} * LAI_{sun} + A_{shade} * LAI_{shade} \quad (45)$$

where the subscripts 'sun' and 'shade' denote the sunlit and shaded components of photosynthesis and LAI. The method of Norman (1982) with the modification of considering the effect of foliage clumping index (Ω) on the canopy radiation regime was used in this study to calculate LAI_{sun} and LAI_{shade} (Chen et al., 1999):

$$LAI_{sun} = 2\cos\theta(1 - \exp(-0.5\Omega LAI / \cos\theta)) \quad (46a)$$

$$LAI_{shade} = LAI - LAI_{sun} \quad (46b)$$

where θ is the solar zenith angle.

The detailed description of canopy radiation routine can be found in Chen et al. (1999). The equations for C4 photosynthesis pathway follow the coupled photosynthesis-stomatal conductance model of Collatz et al. (1992) and it is described in Kothavala et al. (2005). Key photosynthesis parameters used in the IC-CLASS model are given in Table 4.2.

4.3.3 MODIS GPP and its evaluation

The MODIS GPP product used in this study was downloaded from the Numerical Terradynamic Simulation Group (NTSG) (http://www.ntsg.umt.edu). This global dataset is gridded to a common equal-angle latitude/longitude grid,

where the coordinates of the upper left corner of the map are at 180° W, 80° N and the lower right corner coordinate is located at 180° E, 60° S. The data is in GEOTIFF format with a spatial resolution of 0.00833 degree (≈1 km). The IC-CLASS model scaled GPP is in the Lambert Conformal Conic (LCC) projection. For the purpose of MODIS GPP product validation with the IC-CLASS model simulated GPP over Canada's landmass, an area ranging from 41-80° N, 143-49° W was retrieved from the global MODIS GPP map.

The IC-CLASS model simulated GPP were compared with eddy covariance (EC) measured GPP at seven Canadian Carbon Program (CCP) flux tower sites (Coursolle et al., 2006). These sites include a grassland site in Alberta (AB-GRA) (Flanagan et al., 2002), three boreal conifer forest sites in Saskatchewan and Manitoba (southern old jack pine (SK-SOJP), southern old black spruce (SK-SOBS), northern old black spruce (MB-NOBS)) (Kljun et al., 2006; Dunn et al., 2007), a boreal deciduous forest site in Saskatchewan (SK-SOA) (Krishnan et al., 2006; Barr et al., 2007), a mixedwood forest site in Ontario, ON-OMW (McCaughey et al., 2006) and a temperate Douglas-fir forest site in British Columbia (BC-DF49) (Morgenstern et al., 2004; Chen et al., 2009).

4.4 Results and Discussion

4.4.1 Site-level validations

Comparison of simulated and measured annual GPP values indicated good agreement for all six forest sites (Figure 4.2; Table 4.3). However, simulated GPP was 49% and 59% higher than measured GPP at the SK-SOJP and the temperate grassland site (AB-GRA), respectively (Table 4.3). Overall the mean difference between simulated and measured GPP values for all seven sites was 17%.

A similar comparison was conducted between MODIS-derived and EC-measured annual GPP values (Figure 4.3; Table 4.3). Good agreement was found at the five boreal forest sites (Figure 4.3). However, MODIS GPP was 129% higher than EC measurement at AB-GRA site and 40% lower than measured value at BC-DF49 site (Table 4.3). The mean difference between simulated and measured GPP values for all seven sites was 23%.

4.4.2 GPP distribution across Canada

The spatial distribution of annual MODIS GPP over Canada for 2003 is shown in Figure 4.4a. High GPP values appear in the forested areas across Canada. The highest GPP values (> 1400 g C m^{-2} yr^{-1}) were recorded in the western and southern parts of the Vancouver Island in British Columbia and in the northern parts of Nova Scotia. GPP values of about 1000 g C m^{-2} yr^{-1} were recorded in the

west coast and interior parts of British Columbia, central and northern Alberta, and southern parts of Manitoba, Ontario and Quebec and New Brunswick. In the far north, with mainly snow, ice and barren land, GPP values were very low (< 50 g C m^{-2} yr^{-1}).

IC-CLASS simulated annual GPP values across Canada for 2003 are shown in Figure 4.4b. High GPP values were again associated with forested areas across the country. The highest GPP (> 1400 g C m^{-2} yr^{-1}) was simulated in most areas of Vancouver Island, southern parts of Haida Gwaii Island in British Columbia and southern parts of Ontario. Areas with GPP values around 1000 g C m^{-2} yr^{-1} were located in interior British Columbia, central and northern parts of Alberta and southern areas on Manitoba, Ontario and Quebec. In northern parts of the country, GPP was very low (< 10 g C m^{-2} yr^{-1}) due to colder temperatures.

4.4.3 GPP distribution for major land cover types

The magnitudes of simulated and MODIS-derived GPP values depend on land cover types. A comparison between simulated and MODIS-derived mean annual GPP values for whole Canada for major land cover types is shown Figure 4.5 and Table 4.4. The relative contribution of simulated and MODIS-derived total GPP from different land cover types is shown in Figure 4.6. Overall, deciduous forests had the highest capacity to absorb C followed by mixed forests, conifer forests,

cropland, shrubland, and grassland (Figure 4.5). The national mean annual GPP in forested areas was 722 and 764 g C m^{-2} yr^{-1} for IC-CLASS and MODIS, respectively. The national mean annual GPP in deciduous forests was underestimated by the MODIS (1050 g C m^{-2} yr^{-1}) as compared to the simulated value (1417 g C m^{-2} yr^{-1}). Overall, the simulated and MODIS-derived national mean annual GPP for the whole Canadian landmass was 400 and 557 g C m^{-2} yr^{-1}, respectively (Table 4.4).

Conifer forests were only about half as productive as deciduous forests (Figure 4.5). However, the conifer forests, as a whole, contributed the greatest portion (49.6% vs 38.3% from IC-CLASS and MODIS, respectively) to the country's annual total GPP because of their large spatial coverage and longer growing season (Figure 4.6, Tables 4.1 and 4.4). Mixed forests showed the second largest GPP contribution (12.9% vs 17.6%), followed by the deciduous forest (10.2% vs 5.9%) from the IC-CLASS and MODIS, respectively. Cropland, grassland and shrubland made 7.4%, 8.5% and 7.1% contributions, respectively, to the country's total annual GPP as simulated by the IC-CLASS. Contributions based on MODIS GPP were 8.5, 11.3 and 7.7%, respectively. Total national GPP in 2003 was estimated to be 3134.8 Mt C by the IC-CLASS model compared to 3906.3 Mt C by the MODIS (Table 4.6).

4.4.4 GPP by ecozone

IC-CLASS simulated and MODIS derived GPP for each Canadian ecozone are summarized in Table 4.5 and Table 4.6. MODIS derived and IC-CLASS simulated mean GPP values in the Boreal shield and plains, Atlantic maritime, Mixedwood plains, Pacific maritime and Montane cordillera were >600 g C m^{-2} yr^{-1} and >500 g C m^{-2} yr^{-1}, respectively, due to the large coverage of forested areas and/or their southern locations (Table 4.5). MODIS derived and IC-CLASS simulated mean GPP values in the Taiga Plains, Taiga Shield, Prairies, Taiga Cordillera, Boreal Cordillera and Hudson Plains ranged from 200 to 600 g C m^{-2} yr^{-1} and 100 to 500 g C m^{-2} yr^{-1}, respectively (Table 4.5). Further north, in Arctic Cordillera, Northern Arctic and Southern Arctic, MODIS derived and IC-CLASS simulated mean GPP values were < 200 g C m^{-2} yr^{-1} and < 100 g C m^{-2} yr^{-1}, respectively (Table 4.5).

Overall Boreal Shield was larger than all other ecozones with IC-CLASS simulated and MODIS derived total GPP values of 1184 and 1252 Mt C yr^{-1}, respectively, followed by the Boreal Plains that had respective total GPP values 410 and 535 Mt C yr^{-1} (Table 4.6). Simulated total GPP in the rest of ecozones ranged between 30 and 250 Mt C yr^{-1} as simulated by the IC-CLASS model and between 60 and 400 Mt C yr^{-1} as derived by the MODIS GPP product, except for Arctic Cordillera and Northern Arctic where GPP values were very low (Table 4.6).

4.4.5 Seasonal variation of GPP

Because of Canada's northern location, short growing season and high summer GPP are apparent in the seasonal dynamics of IC-CLASS simulated and MODIS derived GPP values (Figure 4.7 and 4.8). In most areas, the growing season started in April and ended in October in forests (Figure 4.7). For crops and grasslands, start of the growing season simulated by the IC-CLASS model was one month late in May (Figure 4.8). Both IC-CLASS simulated and MODIS derived GPP of conifer, deciduous and mixed forest peaked in July (Figure 4.7).

Overall, monthly values of IC-CLASS simulated and MODIS-derived GPP in conifer, deciduous, mixed forest and cropland and grassland followed similar patterns (Figure 4.7 and 4.8). Especially for conifer forest, IC-CLASS simulated GPP fits very well with MODIS GPP trends except in May when MODIS derived GPP was much lower than the IC-CLASS simulated value (Figure 4.7a). This underestimation of MODIS GPP compared to the IC-CLASS simulated value in May also occurred in mixed and deciduous forest (Figure 4.7b and 4.7c). Moreover, simulated GPP of deciduous forests in summer (June-August) were higher than the MODIS GPP values (Figure 4.7b). Conversely, simulated GPP for mixed forest in summer and autumn (June-October) were lower than the MODIS derived GPP (Figure 4.7c). For cropland and grassland, MODIS-derived GPP are larger than IC-CLASS simulated values in the summer months (June-August) (Figure 4.8).

4.5 Conclusion

IC-CLASS simulated GPP used a wide array of ground-based and satellite measured input data that constrained these simulations. Simulated GPP has spatial and temporal resolutions that are compatible with the MODIS-derived values. Our study is the first of such study in which a process-based model (IC-CLASS) has been run at hourly time step to produce daily and annual GPP maps for whole Canada at 1-km spatial resolution. IC-CLASS used a two-leaf (sunlit and shaded) canopy photosynthesis model (Chen et al., 1999) which performs separate photosynthesis and stomatal conductance calculations for each of the sunlit and shaded portions of the canopy and calculates the weighted means for whole canopy. Therefore, IC-CLASS is capable of integrating and analyzing the effects of several factors such as climate, vegetation types and soil texture on the terrestrial ecosystems and their photosynthetic uptake. Because it is a process-based model, it avoids problems experienced by the empirical formulations that are most often used in continental and global studies. In addition, IC-CLASS simulated GPP was compared to eddy covariance flux measurements to avoid any systematic biases in simulated GPP. Results presented in this study give us confidence in the IC-CLASS simulated spatial patterns and the seasonal variations of GPP across Canada's landmass, which is a mosaic of diverse climates and biomes.

The stream of satellite imagery provided by the MODIS and the development of associated systems for data processing and archiving has initiated a new era in observing and monitoring the Earth's ecosystem and their carbon exchanges. MODIS GPP products (MOD17) used in this study are among the highest order products of this Earth observing satellite. MODIS-derived GPP estimates rely on other MODIS products as well such as land cover (MOD12), FPAR/LAI (MOD15A2) and meteorological variables including daily downward shortwave solar radiation, vapour pressure and daily mean and minimum air temperatures generated by the NCEP reanalysis II initiative (Zhao and Running, 2010). The MODIS GPP products also depend on the accurate parameterization of the light use efficiency model (Zhao and Running, 2010). These inputs may cause a great deal of uncertainty in the MODIS-derived GPP estimates. Therefore validation of MODIS GPP over a range of biomes and climate zones is a critical step before its application.

Our study revealed a number of key differences in seasonal dynamics of MODIS derived GPP and IC-CLASS simulated GPP. For example, MODIS hugely overestimated GPP in grasslands and crops, while it showed small underestimation in deciduous forest across Canada. The differences between measured and MODIS derived GPP at the seven EC flux tower sites are largely attributed to the mismatch in spatial scales (~100 km) and possible limitations of the NCEP meteorological input data (Zhao and Running, 2010). Therefore, in

future the use of new version of NCEP meteorology data would be a reasonable improvement to the MODIS derived GPP and its algorithm. The MODIS light use efficiency (ε) parameterization is perhaps the most feasible and appropriate of the algorithms' components to modification because it relies on a simple look-up table approach (Zhao and Running, 2010). The original biome-specific ε maxima and scalar parameterizations were based on model outputs rather than ε observations and there is potential for its improvement now because of the availability of eddy covariance observations from an extensive global network of flux tower sites (Running et al., 1999; Turner et al., 2003). As generalizations of ε become available across multiple flux tower sites and for multiple years in each biome, new parameterization can be developed and implemented in the MODIS GPP algorithm (Turner et al., 2003). ε may also be calculated using high spectral resolution sensors and a number of investigators have focused on this aspect (Gamon et al., 1992; Barton and North, 2001).

Overall, results of our study are of interest from the perspectives of both absolute annual values and seasonal dynamics of photosynthetic carbon uptake. Even if there are significant errors in the satellite-based annual values, seasonal dynamics of both IC-CLASS simulated and MODIS derived GPP provides useful information that may help to improve the MODIS GPP product (Zhao and Running, 2010). However, in order to improve confidence in regional and global carbon budgets, it is necessary to continue improving the relevant algorithms and

validation of the MODIS GPP product with ground-based measurements and developing scaling approaches that incorporate process-based ecosystem models.

4.6 References

Arain, M.A., Black, T.A., Barr, A.G., Jarvis, P.G., Massheder, J.M., Verseghy, D.L., Nesic, Z., 2002. Effects of seasonal and interannual climate variability on net ecosystem productivity of boreal deciduous and conifer forests. Canadian Journal of Forest Research 32(5): 878-891.

Arain, M.A., Yuan, F., Andrew Black, T., 2006. Soil-plant nitrogen cycling modulated carbon exchanges in a western temperate conifer forest in Canada. Agric. Forest Meteorol. 140(1-4): 171-192.

Baldocchi, D. (1994). An analytical solution for coupled leaf photosynthesis and stomatal conductance models. 14**:** 1069-1079.

Baldocchi, D., 2008. 'Breathing' of the terrestrial biosphere: lessons learned from a global network of carbon dioxide flux measurement systems. Australian Journal of Botany(56): 1-26.

Baldocchi, D., Falge, E., Gu, L., Olson, R., Hollinger, D., Running, S., Anthoni, P., Bernhofer, C., Davis, K., Evans, R., Fuentes, J., Goldstein, A., Katul, G., Law, B., Lee, X., Malhi, Y., Meyers, T., Munger, W., Oechel, W., Paw, K.T., Pilegaard, K., Schmid, H.P., Valentini, R., Verma, S., Vesala, T., Wilson, K., Wofsy, S., 2001. FLUXNET: A New Tool to Study the Temporal and Spatial Variability of Ecosystem-scale Carbon Dioxide, Water Vapor, and Energy Flux Densities. Bulletin of the American Meteorological Society 82(11): 2415-2434.

Barr, A.G., Black, T.A., Hogg, E.H., Griffis, T.J., Morgenstern, K., Kljun, N., Theede, A., Nesic, Z., 2007. Climatic controls on the carbon and water balances of a boreal aspen forest, 1994–2003. Global Change Biology 13(3): 561-576.

Barton, C.V.M., North, P.R.J., 2001. Remote sensing of canopy light use efficiency using the photochemical reflectance index: Model and sensitivity analysis. Remote Sensing of Environment 78(3): 264-273.

Beer, C., Reichstein, M., Tomelleri, E., Ciais, P., Jung, M., Carvalhais, N., Rodenbeck, C., Arain, M.A., Baldocchi, D., Bonan, G.B., Bondeau, A., Cescatti, A., Lasslop, G., Lindroth, A., Lomas, M., Luyssaert, S., Margolis, H., Oleson, K.W., Roupsard, O., Veenendaal, E., Viovy, N., Williams, C., Woodward, F.I., Papale, D., 2010. Terrestrial Gross Carbon Dioxide Uptake: Global Distribution and Covariation with Climate. Science 329(5993): 834-838.

Bonan, G.B., 1995. Land-atmosphere CO2 exchange simulated by a land surface process model coupled to an atmospheric general circulation model. J. Geophys. Res. 100: 2817-2831.

Chen, B., Black, T.A., Coops, N.C., Krishnan, P., Jassal, R., BrÜMmer, C., Nesic, Z., 2009. Seasonal controls on interannual variability in carbon dioxide exchange of a near-end-of rotation Douglas-fir stand in the Pacific Northwest, 1997–2006. Global Change Biology 15(8): 1962-1981.

Chen, J.M., Chen, W., Liu, J., Cihlar, J., 2000. Annual carbon balance of Canada's forests during 1895-1996. Global Biogeochemical Cycles 14(3): 839-850.

Chen, J.M., Feng, D., Mingzhen, C., 2006. Locally adjusted cubic-spline capping for reconstructing seasonal trajectories of a satellite-derived surface parameter. Geoscience and Remote Sensing, IEEE Transactions on 44(8): 2230-2238.

Chen, J.M., Leblanc, S., 1997. A 4-scale bidirectional reflection model based on canopy architecture. IEEE Transactions on Geoscience and Remote Sensing 35: 1316-1337.

Chen, J.M., Leblanc, S.G., 2001. Multiple-scattering scheme useful for hyperspectral geometrical optical modelling. IEEE Transactions on Geoscience and Remote Sensing 39(5): 1061-1071.

Chen, J.M., Liu, J., Cihlar, J., Goulden, M.L., 1999. Daily canopy photosynthesis model through temporal and spatial scaling for remote sensing applications. Ecological Modelling 124(2-3): 99-119.

Chen, W.J., Chen, J.M., Liu, J., Cihlar, J., 2000. Approaches for reducing uncertainties in regional forest carbon balance. Global Biogeochemical Cycles 14(3): 827-838.

Chen, J.M., Mo, G., Pisek, J., Liu, J., Deng, F., Ishizawa, M., Chan, D., 2012. Effects of foliage clumping on the estimation of global terrestrial gross primary productivity. Global Biogeochem. Cycles 26(1): GB1019.

Collatz, G.J., Ball, J.T., Grivet, C., Berry, J.A., 1991. Physiological and environmental regulation of stomatal conductance, photosynthesis and transpiration: a model that includes a laminar boundary layer. Agricultural and forest meteorology 54(2-4): 107-136.

Collatz, G.J., Ribas-Carbo, M., Berry, J.A., 1992. Coupled photosynthesis-stomatal conductance model for leaves of C4 plants. Australian Journal of Plant Physiology 19(5): 519-538.

Coursolle, C., Margolis, H.A., Barr, A.G., Black, T.A., Amiro, B.D., McCaughey, J.H., Flanagan, L.B., Lafleur, P.M., Roulet, N.T., Bourque, C.P.-A., Arain, M.A., Wofsy, S.C., Dunn, A., Morgenstern, K., Orchansky, A.L., Bernier, P.Y., Chen, J.M., Kidston, J., Saigusa, N., Hedstrom, N., 2006. Late-summer carbon fluxes from Canadian forests and peatlands along an east-west continental transect Canadian Journal of Forest Research 36(3): 783-800.

De Pury, D.G.G., Farquhar, G.D., 1997. Simple scaling of photosynthesis from leaves to canopies without the errors of big-leaf models. Plant, Cell & Environment 20(5): 537-557.

Deng, F., Chen, J.M., Plummer, S., Mingzhen, C., Pisek, J. (2006). Algorithm for global leaf area index retrieval using satellite imagery. Geoscience and Remote Sensing, IEEE Transactions on. 44**:** 2219-2229.

Dunn, A.L., Barford, C.C., Wofsy, S.C., Goulden, M.L., Daube, B.C., 2007. A long-term record of carbon exchange in a boreal black spruce forest: means, responses to interannual variability, and decadal trends. Global Change Biology 13(3): 577-590.

Farquhar, G.D., Caemmerer, S.V., Berry, J.A., 1980. A biochemical model of photosynthetic CO2 assimilation in leaves of C-3 species. Planta 149: 78-90.

Farquhar, G.D., von Caemmerer, S., 1982. Modelling of photosynthetic response to environmental conditions. Berlin, Spring Verlag.

Flanagan, L.B., Wever, L.A., Carlson, P.J., 2002. Seasonal and interannual variation in carbon dioxide exchange and carbon balance in a northern temperate grassland. Global Change Biology 8(7): 599-615.

Gamon, J.A., Penuelas, J., Field, C.B., 1992. A narrow-waveband spectral index that tracks diurnal changes in photosynthetic efficiency. Remote Sensing of Environment 41(1): 35-44.

Kattge, J., Knorr, W., Raddatz, T., Wirth, C., 2009. Quantifying photosynthetic capacity and its relationship to leaf nitrogen content for global-scale terrestrial biosphere models. Global Change Biology 15(4): 976-991.

Kljun, N., Black, T.A., Griffis, T.J., Barr, A.G., Gaumont-Guay, D., Morgenstern, K., McCaughey, J.H., Nesic, Z., 2006. Response of Net Ecosystem Productivity of Three Boreal Forest Stands to Drought. Ecosystems 9(7): 1128-1144.

Körner, C., Scheel, J.A., Bauer, H., 1979. Maximum leaf diffusive conductance in vascular plants. Photosynthetica 13: 45-82.

Kothavala, Z., Arain, M.A., Black, T.A., Verseghy, D.L., 2005. The simulation of energy, water vapor and carbon dioxide fluxes over common crops by the Canadian Land Surface Scheme (CLASS). Agricultural and forest meteorology 133: 89-108.

Krishnan, P., Black, T.A., Grant, N.J., Barr, A.G., Hogg, E.H., Jassal, R.S., Morgenstern, K., 2006. Impact of changing soil moisture distribution on net ecosystem productivity of a boreal aspen forest during and following drought. Agricultural and forest meteorology 139: 208-223.

Latifovic, R., Zhu, Z.-L., Cihlar, J., Giri, C., Olthof, I., 2004. Land cover mapping of North and Central America -Global Land Cover 2000. Remote Sensing of Environment 89(1): 116-127.

Leuning, R., Kelliher, F.M., Pury, D.G.G., Schulze, E.D., 1995. Leaf nitrogen, photosynthesis, conductance and transpiration: scaling from leaves to canopies. Plant, Cell and Environment 18(10): 1183-1200.

Liu, J., Chen, J.M., Cihlar, J., Chen, W., 2002. Net primary productivity mapped for Canada at 1-km resolution. Global Ecology & Biogeography 11(2): 115-129.

McCaughey, J.H., Pejam, M.R., Arain, M.A., Cameron, D.A., 2006. Carbon dioxide and energy fluxes from a boreal mixedwood forest ecosystem in Ontario, Canada. Agricultural and forest meteorology 140(1-4): 79-96.

Monteith, J.L., 1973. Principles of Environmental Physics. Edward Arnold, London.

Morgenstern, K., Andrew Black, T., Humphreys, E.R., Griffis, T.J., Drewitt, G.B., Cai, T., Nesic, Z., Spittlehouse, D.L., Livingston, N.J., 2004. Sensitivity and uncertainty of the carbon balance of a Pacific Northwest Douglas-fir forest during an El Nino/La Nina cycle. Agricultural and forest meteorology 123(3-4): 201-219.

Morisette, J.T., Privette, J.L., Justice, C.O., 2002. A framework for the validation of MODIS Land products. Remote Sensing of Environment 83(1-2): 77-96.

Norman, J.M., 1982. Simulation of microclimates. New York, Academic Press.

Pisek, J., Chen, J.M., 2007. Comparison and validation of MODIS and VEGETATION global LAI products over four BigFoot sites in North America. Remote Sensing of Environment 109(1): 81-94.

Press, W.H., Flannery, B.P., Teukolsky, S.A., Vetterling, W.T., 1989. Numerical recipes: the art of scientific computing. Cambridge University Press, Cambridge, U.K., 992 p.

Rahman, H., Dedieu, G. (1994). SMAC: a simplified method for the atmospheric correction of satellite measurements in the solar spectrum, Taylor & Francis. 15: 123-143.

Reich, P.B., 2010. The Carbon Dioxide Exchange. Science 329(5993): 774-775.

Running, S.W., Baldocchi, D.D., Turner, D.P., Gower, S.T., Bakwin, P.S., Hibbard, K.A., 1999. A Global Terrestrial Monitoring Network Integrating Tower Fluxes, Flask Sampling, Ecosystem Modeling and EOS Satellite Data. Remote Sensing of Environment 70(1): 108-127.

Running, S.W., Thornton, P.E., Nemani, R., Glassy, J.M., 2000. Global terrestrial gross and net primary productivity from the Earth observing system. In O. E. Sala, R. B. Jackson, H. A. Mooney, R. W. Howarth, (Eds.), Methods in ecosystem science (pp. 44-57). New York, Springer-Verlag.

Schut, P., Shields, J., Tarnocai, C., Coote, D., Marshall, I. (1994). Soil Landscapes of Canada - An Environmental Reporting Tool. Canadian Conference on GIS Proceedings, Ottawa.

Sellers, P.J., Berry, J.A., Collatz, G.J., Field, C.B., Hall, F.G., 1992. Canopy reflectance, photosynthesis, and transpiration. III. A reanalysis using improved leaf models and a new canopy integration scheme. Remote Sensing of Environment 42(3): 187-216.

Sellers, P., Randall, D., Collatz, G., Berry, J., Field, C., Dazlich, D., Zhang, C., Collelo, G., Bounoua, L., 1996. A Revised Land Surface Parameterization (SiB2) for Atmospheric GCMS. Part I: Model Formulation. Journal of Climate 9: 676-705.

Shields, J.A., Tarnocai, C., Valentine, K.W.G., MacDonald, K.B., 1991. Soil Landscapes of Canada - Procedures Manual and User's Handbook. Ottawa., Ontario, Canada, Agriculture Canada.

Still, C.J., Berry, J.A., Collatz, G.J., DeFries, R.S., 2003. Global distribution of C3 and C4 vegetation: Carbon cycle implications. Global Biogeochem. Cycles 17(1): 1006.

Turner, D.P., Ritts, W.D., Cohen, W.B., Gower, S.T., Running, S.W., Zhao, M., Costa, M.H., Kirschbaum, A.A., Ham, J.M., Saleska, S.R., Ahl, D.E., 2006. Evaluation of MODIS NPP and GPP products across multiple biomes. Remote Sensing of Environment 102(3-4): 282-292.

Turner, D.P., Ritts, W.D., Cohen, W.B., Gower, S.T., Zhao, M., Running, S.W., Wofsy, S.C., Urbanski, S., Dunn, A.L., Munger, J.W., 2003. Scaling Gross Primary Production (GPP) over boreal and deciduous forest landscapes in support of MODIS GPP product validation. Remote Sensing of Environment 88(3): 256-270.

Wang, Y.P., Leuning, R., 1998. A two-leaf model for canopy conductance, photosynthesis and partitioning of available energy. I. Model description and comparison with a multi-layered model. Agricultural and forest meteorology 91: 89-111.

Wullschleger, S.D. (1993). Biochemical Limitations to Carbon Assimilation in C3 Plants - A Retrospective Analysis of the A/Ci Curves from 109 Species. 44: 907-920.

Zhang, F. M., J. M. Chen, C. M. Gough, D. Dragoni, T. Martin. Evaluating spatial and temporal patterns of MODIS GPP over the conterminous U.S. against flux measurements and a process model. Remote Sensing of Environment. (in review)

Zhao, M., Running, S.W., 2010. Drought-induced reduction in global terrestrial net primary production from 2000 through 2009. Science 329(5994): 940-943.

Table 4. 1 Land cover classification statistics for Canada at 1-km resolution**.**

Land cover type	Number of 1-km pixels	Land cover (%)
Conifer forest	2231203	27.28
Mixed forest	697084	8.52
Deciduous forest	224759	2.75
Shrubland	493580	6.03
Burnt area	119340	1.46
Barren land	2418745	29.60
Cropland	480217	5.87
Grassland	958226	11.71
Urban area	5526	0.068
Snow/ice	515247	6.29
Total land	8179928	100
Total forest	3153046	38.55

Table 4. 2 Major vegetation parameters for different Canadian land cover types used in IC-CLASS model.

Parameter	Conifer forest	Mixed forest	Deciduous forest	Shrub	Crop	Other	Reference
Maximum carboxylation rate at 25 ˚C (μmol CO_2 m^{-2} s^{-1})	38	48	58	58	90	33	Chen et al. (2012) Liu et al. (2002)
N_0 (g m^{-2})	1.75	1.75	1.74	1.86	1.69	1.69	Chen et al. (2012)
χ_n (m^2 g^{-1})	0.33	0.46	0.59	0.57	0.60	0.60	Chen et al. (2012)
Slope (m)	8.0	8.0	2.5	8.0	8.0	8.0	Leuning (1995)
Intercept (b'), mol m^{-2} s^{-1}	0.0011	0.0011	0.0011	0.0011	0.0011	0.0011	Leuning (1995)
Parameter for stomatal sensitivity to VPD (D_0), Pa	2000	2000	2000	2000	2000	3000	Leuning (1995)
LAI	3.05	3.10	3.14	1.49	1.64	1.64	Chen et al. (2012)
Clumping index	0.50	0.60	0.70	0.75	0.76	0.76	Liu et al. (2002) Chen et al. (2005)

Table 4. 3 Comparison of the IC-CLASS simulated and MODIS GPP with the EC measured GPP at seven flux tower sites across Canada.

Site	Longitude (degree)	Latitude (degree)	Modeled GPP (g C m^{-2} yr^{-1})	MODIS GPP (g C m^{-2} yr^{-1})	Measured GPP (g C m^{-2} yr^{-1})	Relative difference between modeled and measured GPP (%)	Relative difference between MODIS and measured GPP (%)
SK-SOJP	104.69 W	53.92 N	975	775	653	49.3	18.7
SK-SOBS	105.12 W	53.99 N	1037	958	875	18.6	9.5
MB-NOBS	98.48 W	55.879 N	934	852	692	35.0	23.1
SK-SOA	106.20 W	53.63 N	1180	1134	1038	13.7	9.2
ON-OMW	82.156 W	48.217 N	705	1194	1075	-34.5	11.1
BC-DF49	125.335 W	49.869 N	1624	1247	2078	-21.8	-40.0
AB-GRA	112.56 W	49.43 N	458	658	287	59.4	129.1
Mean			988	974	957	17.1	23.0

Table 4. 4 Comparison of simulated and MODIS derived mean GPP (±1 SD) for each land cover type.

Land cover type	**Simulated GPP** ($g\ C\ m^{-2}\ yr^{-1}$)	**MODIS GPP** ($g\ C\ m^{-2}\ yr^{-1}$)	**RMSE** ($g\ C\ m^{-2}\ yr^{-1}$)
Conifer forest	696 (270)	711 (252)	181
Deciduous forest	1417 (338)	1050 (197)	459
Mixed forest	579 (166)	1011 (190)	467
Cropland	480 (263)	698 (183)	282
Grassland	278 (160)	477 (209)	258
Shrubland	451 (283)	626 (291)	266
Barren land	63 (65)	240 (160)	208
Urban area	118 (117)	858 (278)	721
Burnt area	7 (22)	374 (191)	413
Wetland	270 (117)	712 (267)	499
Total land	400 (377)	557 (353)	264

Table 4. 5 Comparison of simulated and MODIS derived mean GPP (±1 SD) for each ecozone of Canada.

Ecozone	**Simulated GPP** ($g\ C\ m^{-2}\ yr^{-1}$)	**MODIS GPP** ($g\ C\ m^{-2}\ yr^{-1}$)	**RMSE** ($g\ C\ m^{-2}\ yr^{-1}$)
Arctic Cordillera	4 (16)	14 (48)	41
Northern Arctic	9 (14)	36 (52)	50
Southern Arctic	78 (68)	199 (70)	128
Taiga Plains	422 (249)	546 (236)	219
Taiga Shield	240 (177)	372 (153)	203
Boreal Shield	774 (350)	878 (233)	326
Atlantic Maritime	861 (409)	1141 (175)	511
Mixedwood Plains	875 (371)	954 (173)	320
Boreal Plains	650 (278)	875 (163)	352
Prairies	282 (198)	572 (140)	322
Taiga Cordillera	168 (152)	292 (133)	170
Boreal Cordillera	292 (199)	405 (182)	178
Pacific Maritime	529 (510)	655 (494)	331
Montane Cordillera	522 (321)	640 (247)	265
Hudson Plains	495 (223)	592 (192)	203
Canada land	400 (377)	557 (353)	264

Table 4. 6 Comparison of simulated and MODIS derived total GPP for each ecozone of Canada.

Ecozone	**Simulated GPP (Mt C yr^{-1})**	**MODIS GPP (Mt C yr^{-1})**
Arctic Cordillera	0.8	2.4
Northern Arctic	9.4	20.2
Southern Arctic	51.6	105.4
Taiga Plains	218.4	275.0
Taiga Shield	245.2	352.3
Boreal Shield	1184.4	1252.4
Atlantic Maritime	158.8	206.8
Mixedwood Plains	92.6	94.7
Boreal Plains	410.0	535.1
Prairies	126.1	253.9
Taiga Cordillera	39.7	68.2
Boreal Cordillera	113.1	155.7
Pacific Maritime	94.3	111.6
Montane Cordillera	231.6	279.0
Hudson Plains	162.1	188.3
Canada land	3134.8	3906.3

1 pixel $\approx$1 km^2. The bracket denotes the standard deviation (SD).

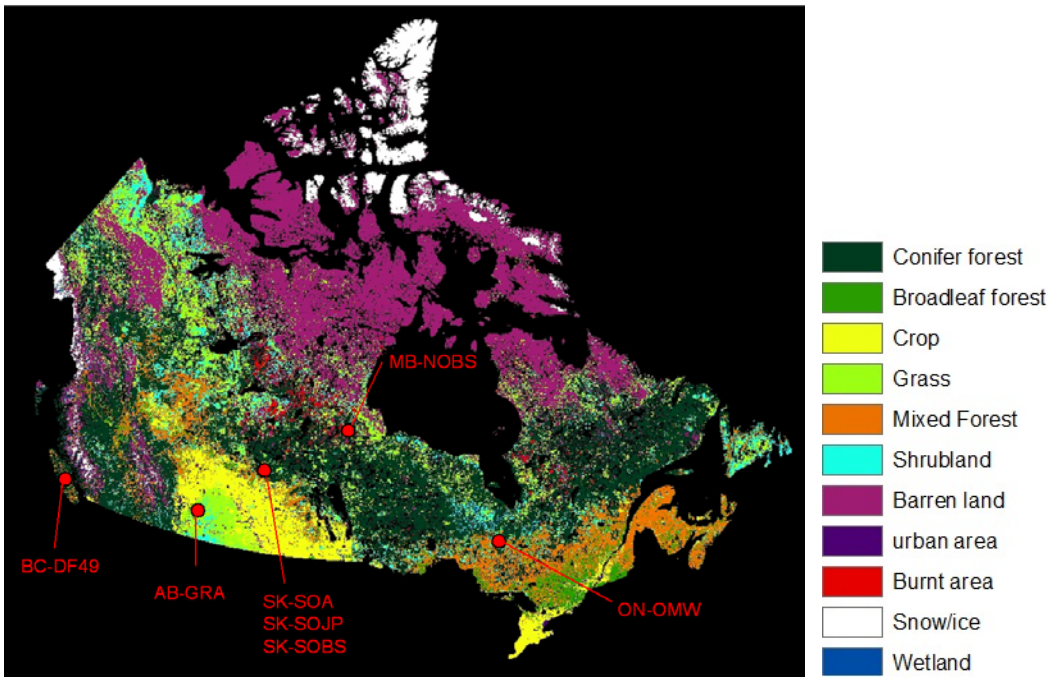

Figure 4. 1 Land cover map of Canada-wide landmass. Canadian Carbon Program (CCP) flux measurement sites are also shown.

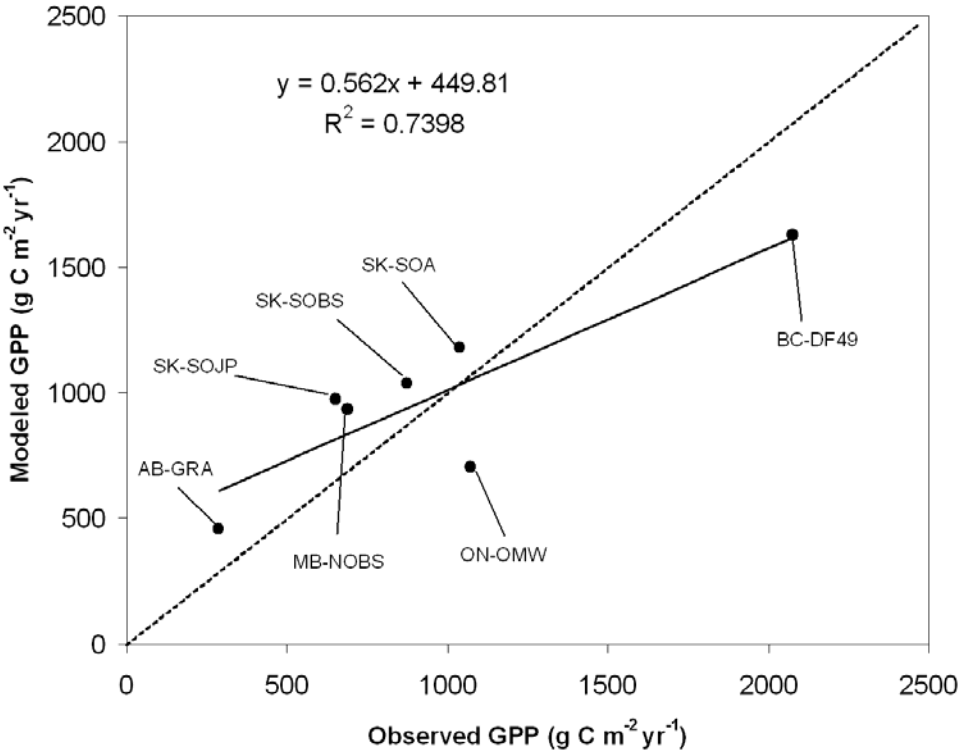

Figure 4. 2 Comparison of IC-CLASS simulated and measured gross primary productivity (GPP) values at seven Canadian Carbon Program (CCP) flux sites (i.e. SK-SOJP, SK-SOBS, MB-NOBS, SK-SOA, ON-OMW, BC-DF49 and AB-GRA).

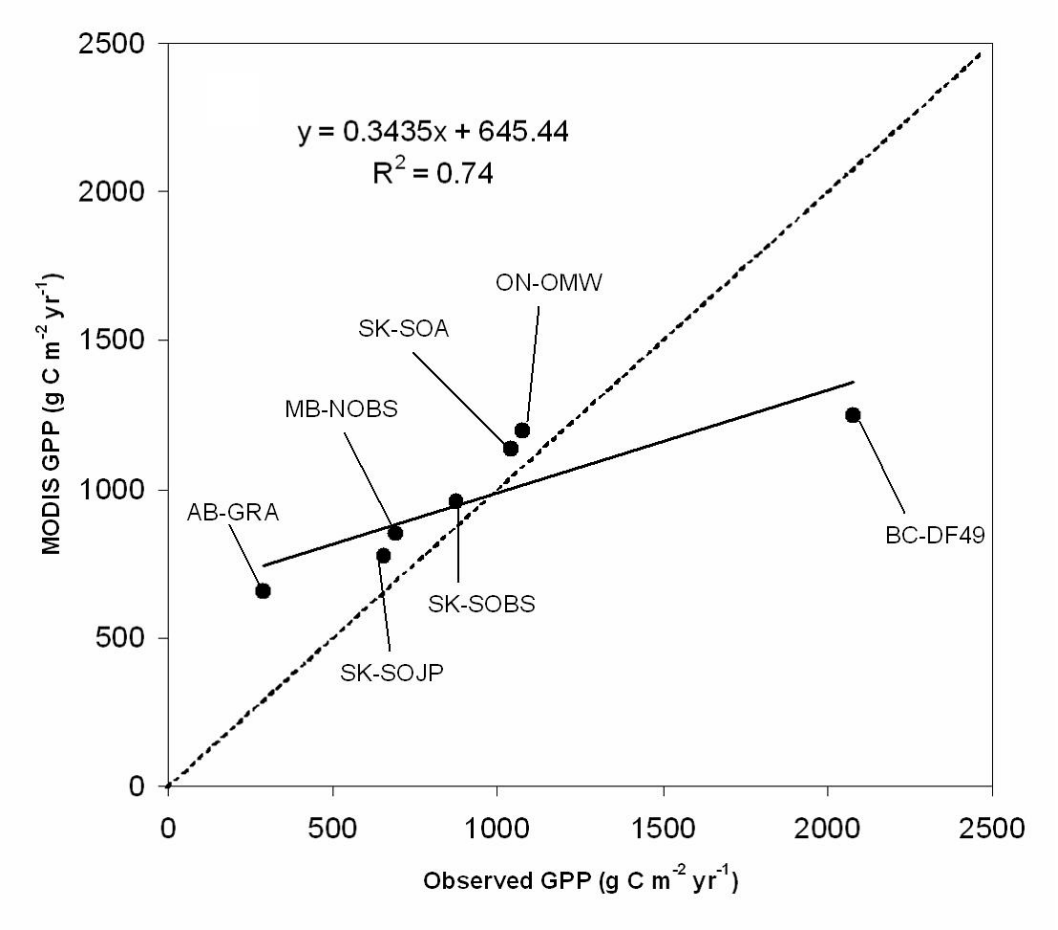

Figure 4. 3 Comparison of MODIS derived and measured Gross primary productivity (GPP) at seven Canadian Carbon Program (CCP) flux sites (i.e. SK-SOJP, SK-SOBS, MB-NOBS, SK-SOA, ON-OMW, BC-DF49 and AB-GRA).

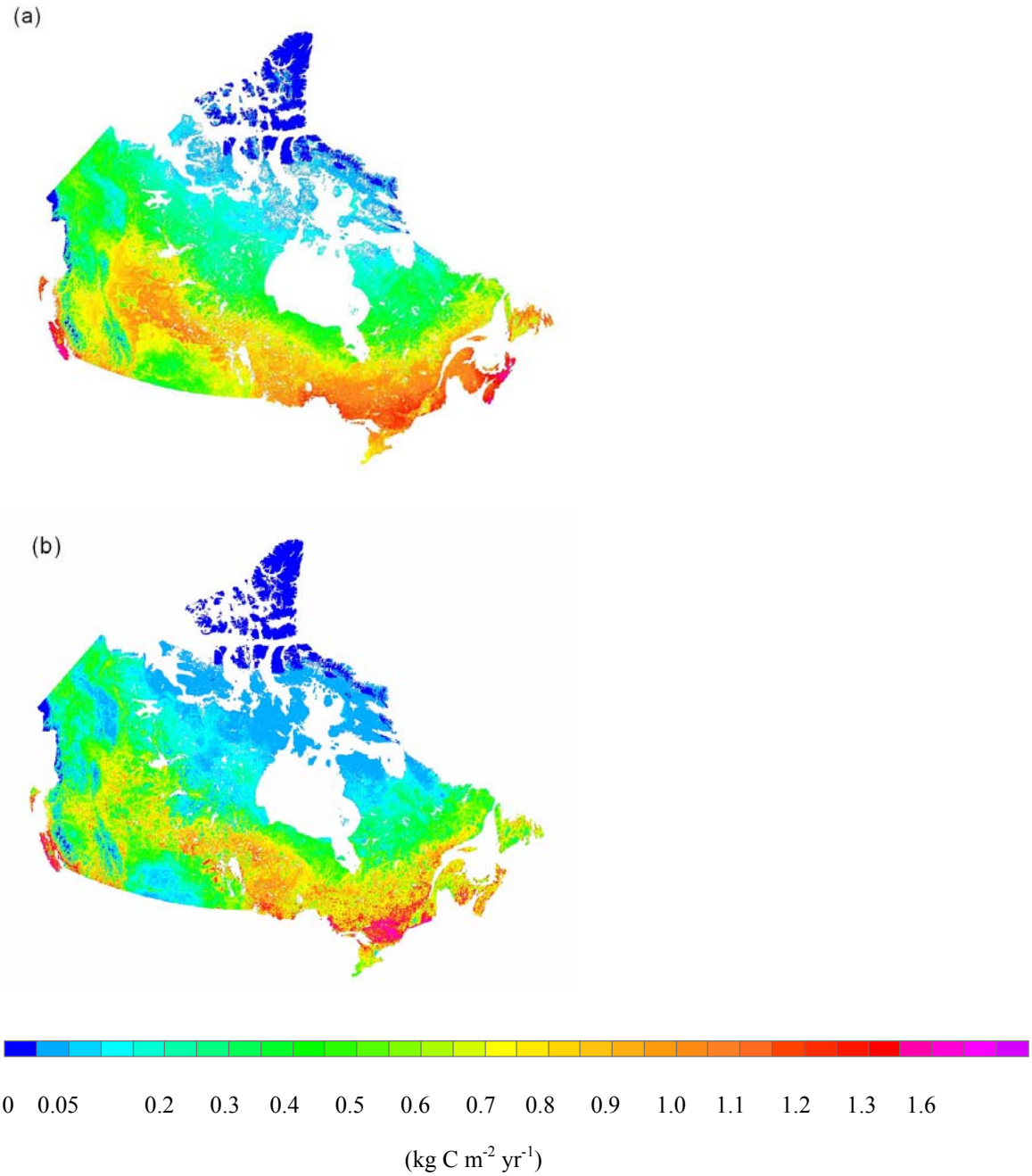

Figure 4. 4 Gross primary productivity (GPP) derived from MODIS (a) and simulated by the IC-CLASS model (b) over Canada's landmass in 2003.

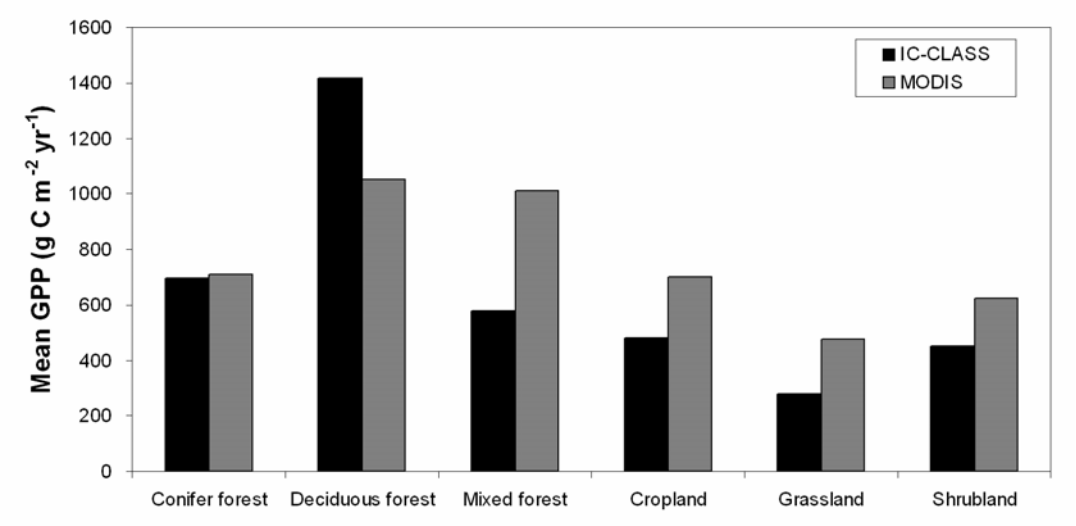

Figure 4. 5 Comparison of simulated and MODIS derived mean GPP for key Canadian land cover types in 2003.

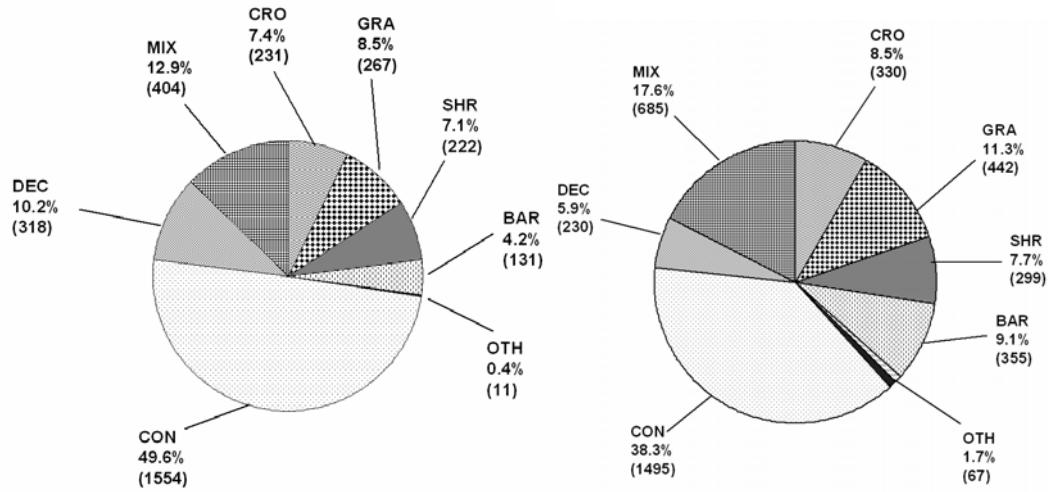

(a) IC-CLASS (b) MODIS

Figure 4. 6 Distribution of (a) simulated and (b) MODIS derived total annual GPP values for Canadian land cover types in 2003. Values in parenthesis are class total GPP values in Mt C yr^{-1}. CON = conifer forests, DEC = deciduous forests, MIX = mixed forests, CRO = cropland, GRA = grassland, SHR = shrubland, BAR = barren land, OTH = others, including urban area, burnt area and wetland.

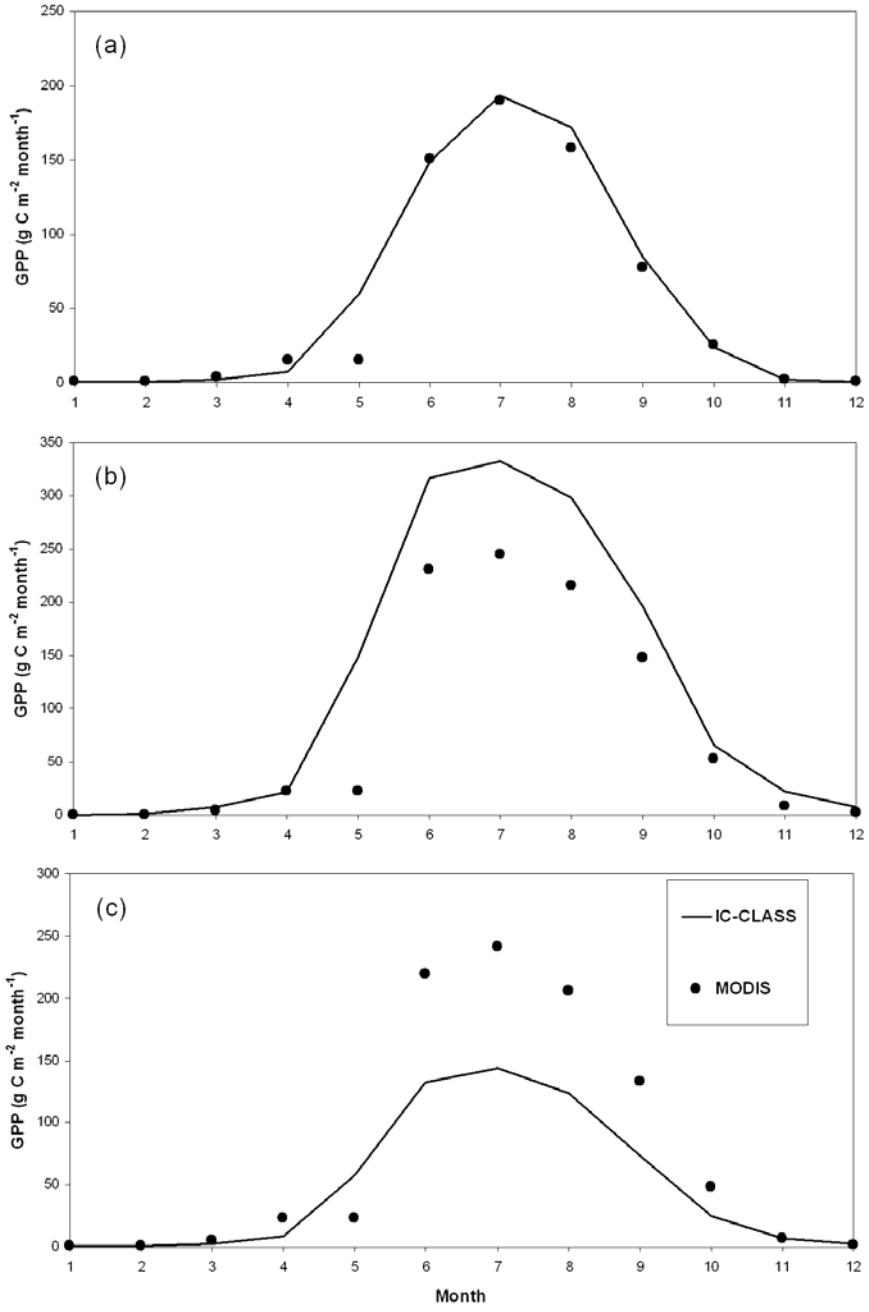

Figure 4. 7 Comparisons of simulated and MODIS derived monthly mean GPP values for (a) conifer forest, (b) deciduous forest and (c) mixed forest.

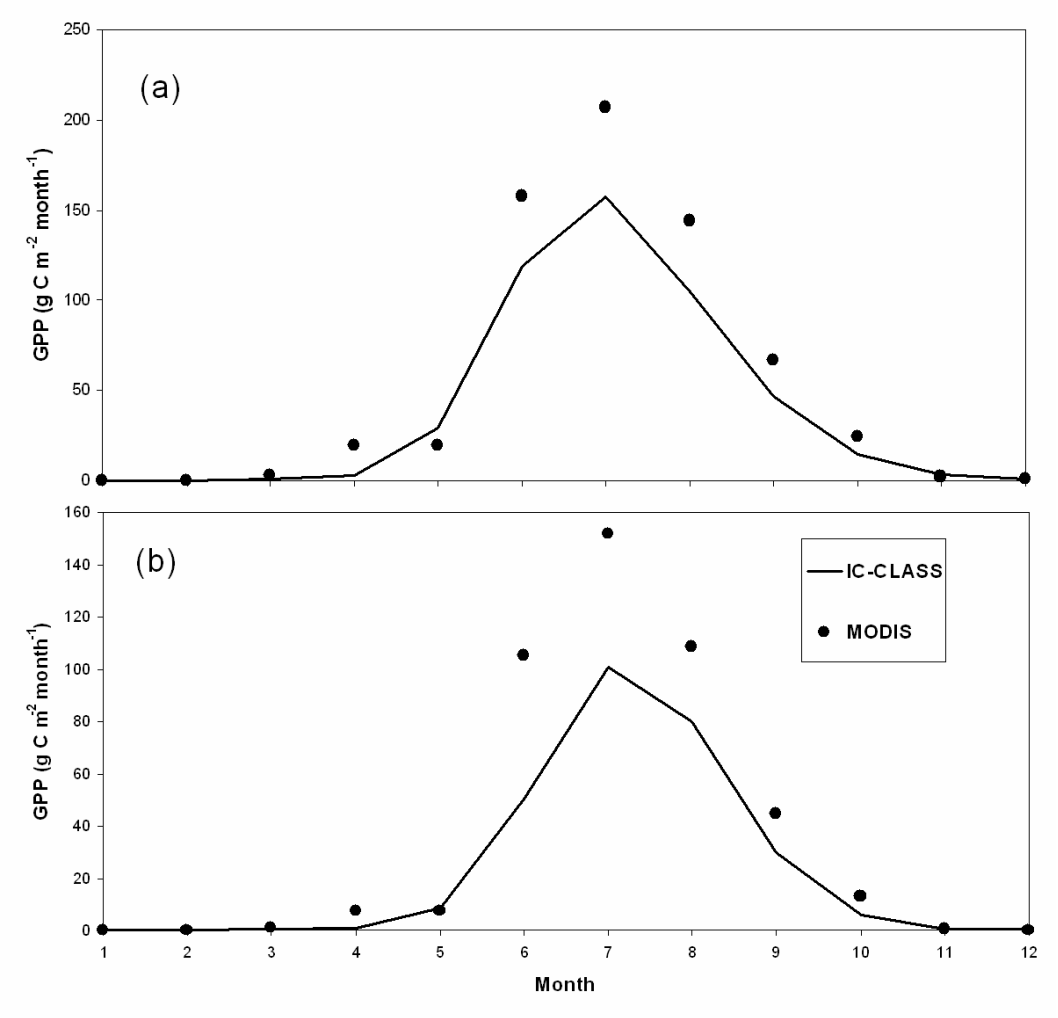

Figure 4. 8 Comparison of simulated and MODIS derived monthly mean GPP values for (a) cropland and (b) grassland.

CHAPTER 5:

SUMMARY AND CONCLUSIONS

5.1 Summary of results

This thesis uses C-CLASS model to simulate historic carbon dynamics of a temperate Douglas fir forest landscape in Oyster River area, Vancouver Island, British Columbia and a boreal black spruce forest landscape at Chibougamau, Quebec, Canada. The impacts of disturbance history and the climate variability on the landscape-level C stocks and fluxes were also investigated. The historic carbon stocks and fluxes in a 2500 ha Pacific Northwest temperate conifer forest landscape was simulated from 1920 to 2005. The historic carbon stocks and fluxes in a 6275 ha Eastern Canadian boreal forest landscape was simulated from 1928 to 2005. The disturbance matrix of the Carbon Budget Model of the Canadian Forest Sector (CBM-CFS3) was incorporated into C-CLASS to simulate the removal of the carbon stocks by disturbance events. In addition, C-CLASS model simulations were performed over Canada's landmass to simulate gross primary productivity at 1-km resolution for the year 2003 in support of MODIS GPP product validation. The main findings of this thesis have been described in various chapters as summarized below:

Chapter 2 concludes that if carefully parameterized, land surface model can be used to investigate the impacts of climate variability and disturbance history on long term carbon balance of forest landscapes. It further suggests that landscape-level net primary productivity among carbon fluxes is more sensitive to air temperate due to the relatively high sensitivity of autotrophic respiration to air temperature. Among carbon pools, changes in dead organic carbon pools are more sensitive to air temperature than biomass carbon pools. All landscape-level carbon fluxes and changes of carbon stocks appear less sensitive to precipitation.

Chapter 3 suggests that in undisturbed Chibougamau boreal forest landscape, simulated annual net ecosystem productivity deviations were positively related to daily minimum and maximum air temperatures in spring, while they were not sensitive to daily minimum and maximum air temperatures in summer. It concludes that simulated landscape-level net ecosystem productivity is less sensitive to the changes in air temperature compared to other simulated carbon fluxes (gross primary productivity, autotrophic respiration and heterotrophic respiration). The results further indicate that C-CLASS simulated landscape-level carbon stocks (aboveground biomass, belowground biomass, dead organic matter and soil organic matter) are sensitive to the change of air temperature. In combination with chapter 2, the thesis work concludes that by incorporating the

disturbance matrix of CBM-CFS3 model, C-CLASS model can be used to investigate the impacts of climate variability and disturbance events on the historic carbon dynamics of forest landscapes.

Chapter 4 assesses the MODIS derived gross ecosystem productivity acroos whole Canada in 2003 using an approach based on a spatially distributed ecosystem process-based model. It concludes that the overestimation of MODIS gross ecosystem productivity compared to the C-CLASS simulated gross ecosystem productivity can be attributed to the limitations in the components of MODIS GPP algorithm. It further suggests that the parameterization of light use efficiency of the MODIS GPP algorithm is particularly amenable for improvement based on observations of light use efficiency at eddy covariance flux towers or the photochemical reflectance index derived from satellite remote sensing data.

5.2 Significance of study

To date, few attempts have been made to investigate the impacts of climate variability and disturbance history on the historic C dynamics of a Pacific Northwest temperate conifer forest landscape and a boreal forest landscape in Canada (Trofymow et al., 2008; Bernier et al., 2010). This study is therefore

unique in simulating the effects of climate variability and disturbance events on historic C dynamics of forest landscapes using process-based model (C-CLASS) with the incorporation of disturbance matrix from CBM-CFS3 model. In addition, this study is able to provide C-CLASS simulated GPP of Canadian landmass at 1-km spatial resolution. This spatial scaling approach based on process-based model is essential to the validation of MODIS GPP product, helping the improvement of MODIS GPP algorithm.

Furthermore, this study has made it possible to analyze the importance of climate drivers and the development of methods for including climate sensitivity into inventory-based models. Although previous studies have investigated the influence of disturbance, age-class structure and land use on landscape-level carbon budgets for Oyster River and Chibougamau study areas using CBM-CFS3 model (Trofymow et al., 2008; Bernier et al., 2010), the effects of inter-annual variations in growing conditions were not considered, whereas this study refined our understanding of landscape level forest C budgets. It investigated the factors that are not currently represented in empirical models, such as CO_2 fertilization and climate change. Thus, this thesis work would enable future studies of using C-CLASS model for long-term projections into the future under a changing climate.

In this thesis, C-CLASS model simulation has been performed at 1 km resolution over whole Canada. These model results will be helpful to calculate the national terrestrial ecosystem C budgets which are fundamentally important for

making environmental policies and ecosystem management for enhancing the terrestrial C sink.

5.3 Future research suggestion

In the future, efforts should be made for comparisons between tower-based measurements of C fluxes, C stock change measurements, and the C-CLASS simulated C fluxes by developing more accurate methods to define and weight the flux tower foorprints (Trofymow et al., 2008; Chen et al., 2009).

The C-CLASS model simulation over Oyster River and Chibougamau forest landscapes were part of the historic carbon modeling project. The process models (Ecosys, Can-IBIS, C-CLASS and 3PG) generally agreed regarding climate sensitivity of NPP and NEP, indicating that ecozone-specific response functions for NPP to mean daily maximum air temperature during July-September could be incorporated into inventory-based model (CBM-CFS3) to capture effects of climate variability on forest C inventories (Wang et al., 2011). This new climate-sensitive version of the Carbon Budget Model of the Canadian Forest Sector (CBM-CFS4) will be further developed by incorporating a simple representation of vegetation succession in order to investigate the effects of vegetation dynamics on Canada's forest carbon budget projection in the context of future climate change.

C-CLASS model may contribute in incorporating the weather effects on the net primary productivity estamted by the Carbon Budget Model of the Canadian Forest Service under future climate scenarios to investigate climate change impacts on forest productivity.

C-CLASS model may also be used to analysized national-scale net ecosystem productivity and ecosystem respiration. Becasye, soil heterotrophic respiration is assumed to be equal to the long term average NPP ($\overline{NPP}$). Then, $\overline{NPP}$ can be used to constrain the fractions of four component soil carbon pools in C-CLASS model. Therefore, long-term simulation of model spin-up can be avoided and the NEP of Canada's landmass can be calculated afterwards.

5.4 References

Bernier, P.Y., Guindon, L., Kurz, W.A., Stinson, G., 2010. Reconstructing and modelling 71 years of forest growth in a Canadian boreal landscape: a test of the CBM-CFS3 carbon accounting model. Canadian Journal of Forest Research 40(1): 109-118.

Chen, B., Black, T., Coops, N., Hilker, T., Trofymow, J., Morgenstern, K., 2009. Assessing Tower Flux Footprint Climatology and Scaling Between Remotely Sensed and Eddy Covariance Measurements. Boundary-Layer Meteorology 130(2): 137-167.

Trofymow, J.A., Stinson, G., Kurz, W.A., 2008. Derivation of a spatially explicit 86-year retrospective carbon budget for a landscape undergoing conversion from old-growth to managed forests on Vancouver Island, BC. Forest Ecology and Management 256(10): 1677-1691.

Wang, Z., Grant, R.F., Arain, M.A., Chen, B.N., Coops, N., Hember, R., Kurz, W.A., Price, D.T., Stinson, G., Trofymow, J.A., Yeluripati, J., Chen, Z., 2011. Evaluating weather effects on interannual variation in net ecosystem productivity of a coastal temperate forest landscape: A model intercomparison. Ecological Modelling 222(17): 3236-3249.

Appendix A

Evaluating weather effects on interannual variation in net ecosystem productivity of a coastal temperate forest landscape: a model intercomparison

Z. Wang[a], R. F. Grant[a, 1], M. A. Arain[b], B.N. Chen[b], N. Coops[c], R. Hember[c], W. A. Kurz[d], D. T. Price[e], G. Stinson[d], J. A. Trofymow[d], J. Yeluripati[b, 2] and B.Z. Chen[c]

[a]*Department of Renewable Resources, University of Alberta, Edmonton, AB, Canada, T6G 2E3;*

[b]*School of Geography and Earth Sciences and McMaster Centre for Climate Change, McMaster University, Hamilton, Ont., Canada;*

[c]*Department of Forest Resources Management, University of British Columbia, Vancouver, BC, Canada;*

[d] *Natural Resources Canada, Canadian Forest Service, Victoria, BC, Canada;*

[e] *Natural Resources Canada, Canadian Forest Service, Edmonton, Alta., Canada*

Keywords: Ecosystem models; Carbon flux; Carbon budget; Forest productivity; Disturbance; *CBM-CFS3*; *ecosys*; *C-CLASS*; *Can-IBIS*; *3PG*

[1] Corresponding author. Tel.: +1 780 492 6609; fax: +1 780 492 1767.
E-mail address: Robert.grant@ales.ualberta.ca (R. Grant)
[2] Present address: School of Biological Science, University of Aberdeen, Aberdeen, UK.

Abstract

Forest productivity is strongly affected by seasonal weather patterns and by natural or anthropogenic disturbances. However weather effects on forest productivity are not currently represented in inventory-based models such as *CBM-CFS3* used in national forest C accounting programs. To evaluate different approaches to modelling these effects, a model intercomparison was conducted among four process models (*ecosys*, *C-CLASS, Can-IBIS* and *3PG*) and an inventory model (*CBM-CFS3*) over a 2500 ha landscape in the Oyster River (OR) area of British Columbia, Canada. The process models used local weather data to simulate net primary productivity (*NPP*), net ecosystem productivity (*NEP*) and net biome productivity (*NBP*) from 1920 to 2005. Other inputs used by the process and inventory models were generated from soil, land cover and disturbance records. During a period of intense disturbance from 1928 to 1943, simulated *NBP* diverged considerably among the models. This divergence was attributed to differences among models in the sizes of detrital and humus C stocks in different soil layers to which a uniform set of soil C transformation coefficients were applied during disturbances. After the disturbance period, divergence in modelled *NBP* among models was much smaller, and attributed mainly to differences in simulated *NPP* caused by different approaches to modelling weather effects on productivity. In spite of these differences, age-detrended variation in annual *NPP* and *NEP* of closed canopy forest stands was negatively correlated with mean daily maximum air temperature during July - September (T_{amax}) in all process models (R^2=0.4-0.6), indicating that these correlations were robust. The negative correlation between T_{amax} and *NEP* was attributed to different processes in different models, which were tested by comparing CO_2 fluxes from these models with those measured by eddy covariance (EC) under contrasting air temperatures (T_a). The general agreement in sensitivity of annual *NPP* to T_{amax} among the process models led to the development of a generalized

algorithm for weather effects on *NPP* of coastal temperate coniferous forests for use in inventory-based models such as CBM-CFS3: $NPP' = NPP - 57.1 (T_{amax} - 18.6)$, where *NPP* and *NPP′* are the current and temperature-adjusted annual *NPP* estimates from *CBM-CFS3*, 18.6 is the long-term mean daily maximum air temperature during July - September, and T_{amax} is the mean value for the current year. Our analysis indicated that the sensitivity of *NPP* to T_{amax} was nonlinear, so that this algorithm should not be extrapolated beyond the conditions of this study. However the process-based methodology to estimate weather effects on *NPP* and *NEP* developed in this study is widely applicable to other forest types and may be adopted for other inventory based forest carbon cycle models.

1. Introduction

Forests cover about 30% of the earth's land surface (Thornton et al., 2002) and sequester large amounts of global carbon (C) (Dixon et al., 1994). Interannual variation in forest productivity has been found to be very sensitive to seasonal changes in weather (e.g., Black et al., 2000; Grant et al., 2000; Barr et al., 2002; Chen et al., 2003; Morgenstern et al., 2004; Ciais et al., 2005; Bergeron et al., 2007; Turner et al., 2007; Chertov et al., 2009). This sensitivity is not currently represented in inventory-based models such as the Carbon Budget Model of the Canadian Forest Sector (*CBM-CFS3*) (Kurz et al., 2009), which simulate productivity from growth curves at annual time steps that typically capture climate effects only over periods of several decades or longer. A more process-based explanation of weather effects on interannual variation in forest productivity would therefore help inventory models to make more reliable projections of productivity with changes in climate.

Studies of weather and climate effects on forest productivity at seasonal to decadal time scales usually rely on ecosystem process models (e.g. Grant et al., 2007a,b; Chen et al., 2003; Peng et al., 2002; Arain et al., 2006). Such models can simulate seasonal effects of weather on forest productivity, summary forms of which could be used to simulate these effects in inventory models. However intercomparisons among process models to establish the consistency with which these effects are simulated are still limited in number (e.g. Grant et al., 2005; Schwalm et al., 2010). These intercomparisons have indicated that differing hypotheses among process models for weather effects on productivity often cause divergent results, so that process models require well-constrained testing against experimental observations before being used for prediction. Such observations are best provided by eddy covariance (EC) measurements of ecosystem CO_2 exchange, supported by surface chamber measurements of soil CO_2 exchange and

biometric measurements of changes in ecosystem C in various above- and below-ground stocks. However such measurements are scarce for the multi-annual, landscape-scale tests required to support model projections of changes in forest productivity with weather and climate.

The objectives of this study were to:

(1) investigate the basis for simulating seasonal effects of weather on forest productivity in process models by testing them against CO_2 exchange measured at an EC flux tower during changes in weather at hourly and daily time scales,

(2) determine whether changes in forest productivity in the fetch area of the flux tower modelled and measured with changes in weather at hourly and daily time scales in (1) affect those modelled and measured with changes in weather at the annual time scale at which inventory models function,

(3) aggregate weather effects on forest productivity from the tower fetch scale in (2) to the landscape scale at which these effects need to be estimated in inventory models, by conducting longer-term simulations of weather and disturbance effects on forest productivity in a complex landscape, using historical inventory, disturbance and climate data with inventory and process models

(4) determine whether the simulation of seasonal landscape-scale weather effects on annual forest productivity in (3) is sufficiently robust among process models to be summarized for use in an inventory model to help it account for the effects of seasonal changes in weather on future forest C stocks.

This study was conducted in the Oyster River (OR) area of Vancouver Island, British Columbia, Canada. This area is particularly well-suited to the objectives of this study because EC and biometric measurements have been made

at forest stands within this area since 1998 as part of the Fluxnet Canada Research Network (FCRN) and the Canadian Carbon Program (CCP) (Figure 1). Detailed inventory, soils, vegetation and disturbance maps were also available for this area (Trofymow et al., 2008), enabling the comparison of inventory and process models over a well-documented forest landscape with a diverse disturbance history. The methodology used to meet the objectives of this study was intended to be applicable to all forest types and site conditions.

2. Model Descriptions

Model intercomparisons for weather effects on forest productivity were conducted among an inventory model *CBM-CFS3* and four diverse process models *ecosys*, *C-CLASS*, *Can-IBIS* and *3PG*, described in more detail below. Key algorithms of each model that govern the response of productivity to weather are described in the text and listed in an Appendix included as Supplementary Material with this paper.

2.1. Carbon Budget Model of the Canadian Forest Sector (CBM-CFS3)

2.1.1. Background

The inventory-based model *CBM-CFS3* (Carbon Budget Model of the Canadian Forest Sector, Kurz et al., 2009, http://carbon.cfs.nrcan.gc.ca/CBM-CFS3_e.html) was developed to serve as the key component of Canada's National Forest C Monitoring Accounting and Reporting System (NFCMARS, Kurz and Apps, 2006) and to provide forest managers with a national, regional and operational-scale modelling tool that implements Intergovernmental Panel on Climate Change (IPCC) standards (IPCC, 1997, 2003). The *CBM-CFS3* modeling framework simulates the dynamics of all 5 IPCC forest ecosystem carbon stocks

(above- and below-ground biomass, litter, dead wood, and soils) in annual time steps by integrating forest inventory datasets and monitoring data with a submodel describing dead organic matter and soil C dynamics. The model inputs include forest inventory, merchantable wood volume yield curves, natural disturbance monitoring data, forest management, harvest and silvicultural activity schedules, land-use change monitoring data, and information describing disturbance impacts. The model does not currently simulate weather effects on forest biomass growth.

2.1.2. Ecosystem productivity simulations

Total live above-ground biomass is calculated from species- and region-specific volume-age curves of merchantable wood volume and then converted to component biomass stocks using a national system of volume-to-biomass models (Boudewyn et al., 2007) and a curve-smoothing algorithm to estimate above-ground biomass at low merchantable wood volumes. Below-ground biomass C (fine and coarse roots) is estimated as a function of above-ground biomass (Li et al., 2003). *DOM* stocks are divided into above-ground (snags, leaf and needle litter, fine woody debris, coarse woody debris, dead fine roots, forest floor humus) and below-ground (dead fine roots, dead coarse roots, humified soil C) components and compartmentalized according to their turnover rates. Carbon stock inputs to the *DOM* stocks are computed according to biomass turnover and litterfall transfer rates as well as disturbance mortality (Kurz et al., 2009). Losses of *DOM* are explicitly modeled through a stock- specific decay rate using a Q10 relationship based on mean annual air temperature (MAT) with a fraction transferred to the atmosphere and another fraction to a humified slow *DOM* stock with its own Q_{10} decay rate. *NPP* is calculated as the sum of net growth and litterfall at an annual time step. Heterotrophic respiration (R_h) is the sum of all *DOM* stock decomposition losses to the atmosphere. *NEP* is estimated as the difference of *NPP* and R_h. *NBP* integrated over time and space is calculated as

NEP minus C loss due to disturbances, such as direct emissions to the atmosphere in the event of fire, and transfers of C to the forest product sector in the event of timber harvesting.

2.2. ecosys

2.2.1. Background

The process-based model *ecosys* (https://portal.ales.ualberta.ca/ecosys/default.aspx; Grant, 2009a,b) was developed at the University of Alberta as a detailed, comprehensive model of terrestrial ecosystems. It is a multi-component model in which hourly rates of transfer processes for C, O, N, P, heat and water are controlled by a set of hypotheses derived from basic chemical, biological and biophysical theories. The model uses inputs for weather, basic plant and soil properties, and plant and soil management events to simulate C, O, N, P, heat and water cycling in terrestrial ecosystems at different timescales. *Ecosys* is used to estimate the impacts of weather, land-use practices and soil quality on primary productivity, water and atmospheric quality and associated resource requirements (e.g. water, fertilizer) at hourly to centennial timescales.

2.2.2. Ecosystem productivity simulations

The CO_2 fixation rate of each leaf surface (A.2.4 in Grant et al., 2005) is summed to arrive at a value for gross primary productivity (*GPP*), with set values for the maximum specific rubisco-limited CO_2 fixation rate (V_{rmax}) and the maximum specific electron transport rate (J_{max}) (A.1.1) (Grant et al., 2005). Canopy temperature (T_c) effects on rubisco-limited CO_2 fixation rate (V_r) and electron transport rate (J) follow Arrhenius functions with low and high temperature inactivation (A.1.2). Water stress effects on V_r and J are calculated

using an exponential function of canopy turgor potential (ψ_T) from the canopy water potential (ψ_C) at which the difference between energy-driven canopy transpiration and hydraulically-driven total water uptake from all rooted soil layers equals change in plant water content (A.1.3). Nitrogen effects on V_r and J are estimated through functions of leaf structural and non-structural N:C ratios arising from uptake vs. assimilation of C and N (A.1.4). Water stress effect on leaf conductance (g_l) is calculated using an exponential function of ψ_T (A.2.1) related to the water stress effect on V_r and J, aggregated by leaf area to a canopy conductance (g_c). Temperature effect on autotrophic respiration (R_a) follows an Arrhenius function of T_c or root temperature (A.3.1). Temperature effect on R_h is calculated with an Arrhenius function of soil temperature (T_s) (A.4.1) derived from a solution to the general heat flux equation driven by surface energy exchange. Water effect on R_h is estimated from the effects of soil water content on microbial O_2 uptake (A.4.2), and on specific microbial activity (A.4.2).

2.3. Modified version of Integrated Biosphere Simulator (Can-IBIS)

2.3.1. Background

Can-IBIS is a dynamic vegetation model developed by incorporating a soil nitrogen cycling model (Liu et al., 2005) and many other enhancements into the Integrated BIosphere Simulator (IBIS) of Foley et al. (1996). It features a hierarchical structure which simulates biophysical and physiological processes at hourly timescales, and generates outputs at daily to annual intervals over multiple centuries. Annual estimates of *NPP* are allocated to vegetation C stocks, with accumulations in woody and foliar biomass that determine dominant plant functional types (PFT) in upper (tree) and lower (shrub and herb) canopies, respectively. Model inputs are meteorological data and soil texture information, together with PFT-specific parameters for physiology, allocation and phenology.

2.3.2. Ecosystem productivity simulations

Photosynthesis is simulated following Farquhar et al. (1980; see also El Maayar et al., 2002), where V_{rmax} is specified for each PFT (A.1.1). Leaf temperature effect on V_r is calculated through a multiplier V_f (A.1.2). Water effects on V_r are estimated using an empirical function of available water content in rootable layers (A.1.3), while nitrogen effects are determined from the N:C ratio of leaves (A.1.4). Water effect on g_l is estimated through the effect on V_r (A.2.1). Temperature effects on R_a and R_h follow modified Arrhenius functions of tissue temperature (T_i) (A.3.1) and soil temperature (A.4.1), respectively. Soil temperature is simulated from energy balance and forcing climatology, including air temperature and net radiation. Water effect on R_h is estimated through a function of the available water content of ice-free soil pore space (θ_s) (A.4.2).

2.4. Carbon and Nitrogen Coupled Canadian Land Surface Scheme (C-CLASS)

2.4.1. Background

The process-based model Canadian Land Surface Scheme (*CLASS*) was originally developed by the Meteorological Service of Canada (MSC) for coupling into the Canadian Global Climate Model (*CGCM*) and the Regional Climate Model (Verseghy, 2000). The C- and N coupled version (*C-CLASS*) was developed by incorporating plant and soil carbon and nitrogen cycle algorithms in *CLASS* (Arain et al., 2006). *C-CLASS* simulates ecological, biophysical and physiological processes at half-hourly or hourly time step (Yuan et al., 2008). Data inputs include meteorological variables, soil textures, vegetation parameters, and disturbance types and intensities.

2.4.2. Ecosystem productivity simulations

In *C-CLASS*, canopy CO_2 fixation is derived by integrating fractional coverage of sunlit and shaded photosynthesis rates (Farquhar et al., 1980), while soil processes are simulated for three soil layers. The maximum fixation rate V_{rmax} is dependent on plant cover types and is a function of total rubisco-related nitrogen (N_{rub}), canopy N inverse decay distance (N_{id}), and leaf area index (*LAI*, with the threshold value of 1). Maximum electron transfer rate J_{max} is estimated through V_{rmax}. (A.1.1). Leaf temperature effects on V_r and J are estimated through a function of the minimum, optimal and maximum leaf temperature (T_{min}, T_{opt} and T_{max}) (A.1.2). Water effects on V_r and J are estimated through effect on g_c in A.2.1. Nitrogen effect on V_r is estimated through effect on V_{rmax} in A.1.1. Water effect on g_l is calculated using a function of root zone water content (θ) at wilting point and at field capacity (A.2.1). Temperature effect on R_a follows Q_{10} functions for leaf, wood and root (A.3.1). Temperature effect on R_h is computed using a Q_{10} function of soil temperature (A.4.1). Water effect on R_h is estimated through a function of θ, one-half field capacity water content (a_1), and one-half porosity (a_2) (A.4.2).

2.5. Physiological Principles Predicting Growth (3PG) Model

2.5.1. Background

The model Physiological Principles Predicting Growth (*3PG*) is a forest productivity model, originally developed by Landsberg and Waring (1997), to simulate total stem volume and biomass in managed evergreen forests. In order to simulate *NBP*, *3PG* was nested within a more comprehensive C cycle model, that adopted the C stock structure, internal C fluxes, and disturbance effects defined within *CBM-CFS3* (Kurz et al. 2009). In addition to *3PG*, a submodel was developed to simulate environmental controls on decomposition from *CBM-CFS3* detrital C stocks. Hence, model behaviour is similar to *CBM-CFS3*, with the exception that growth is driven by a nested process model (*3PG*) in place of

inventory yield curves. The model assumes that spatial units comprise a homogeneous, uniform-aged stand and simulates stand-average attributes. The canopy is represented by a single foliage layer (i.e., 'big leaf'). This implementation of the model therefore computes monthly *NPP*, C allocation, turnover, internal detrital C fluxes, and decomposition, while tree mortality and disturbance (emissions and removals) are computed annually.

Growth is controlled by site variables (i.e., species, soil depth, texture class, coarse fraction, and fertility index), species-specific physiological parameters, and monthly weather variables. Tree mortality was controlled exclusively by self-thinning. Species-specific parameters were compiled from published studies for three species, including Douglas-fir (*Pseudotsuga menziesii*), western redcedar (*Thuja plicata*), and western hemlock (*Tsuga heterophylla*). As the model does not simulate deciduous phenology, stands in the area covered by red alder (*Alnus rubra*) were simulated as Douglas-fir. Internal fluxes between dead C stocks, disturbance effects (i.e., emissions and removals) were controlled by ecozone-specific softwood parameters of *CBM-CFS3* (Kurz et al., 2009).

2.5.2. Ecosystem productivity simulations

In contrast to the other process models, *GPP* is computed from the product of absorbed photosynthetically active radiation (*APAR*) and gross photosynthetic efficiency (ε_g) (Landsberg and Waring, 1997; Coops et al., 2007; Hember et al., 2010), rather than from a biochemically-based submodel. *APAR* is estimated from incident PAR, adjusted for canopy reflectance and attenuation of radiation based on Beer's law. The water balance is simulated prior to *GPP* and is calculated as the difference between precipitation and evapotranspiration. Canopy interception is a function of *LAI* and precipitation. Environmental regulation of g_c is based on functions of radiation $f(APAR)$, vapor pressure deficit $f(D)$ and soil

water potential $f(\psi)$ (A.2.1). The value of ε_g is reduced by water stress exclusively through stomatal closure $f(C)$ (A.1.3). The value of ε_g may be further reduced by thermal stress caused by the combined effects of immediate temperature $f(T)$, antecedent heat availability $f(H)$, and frost damage $f(F)$. Temperature effects on R_a and R_h follow a Q_{10} function (A.3.1, A.4.1). Water effect on R_h is estimated through a function of relative volumetric soil water content $f(\theta_r)$ (A.4.2).

3. Modelling experiment

3.1. Study area

The Oyster River study area (49.899°-49.853°N; 125.352°-125.280°W) is located on the leeward eastern side of Vancouver Island, British Columbia (Figure 1), as part of the CCP/FCRN. The 5km × 5km study area is within the very dry maritime coastal western hemlock biogeoclimatic subzone (Pojar et al., 1991) with average annual precipitation of 1461 mm and MAT of 8.35 ^{o}C. This subzone has a maritime climate with typically cool summers and mild winters, though it can experience significant dry conditions during the summer (Trofymow et al., 2008). The study area spans the transition from the Nanaimo Lowlands and Leeward Island Mountain Ecosections, ranging in elevation from 120 m to 460 m, and is 10 to 15 km from the coast (Trofymow et al., 2008). Area characteristics are summarized in Table 4.1.

3.2. Input data

3.2.1. Weather

Half-hourly weather data during 1998-2005 were recorded at the Oyster River flux tower DF49, a CCP/FCRN flux site located in the study area (Figure 1). Daily records before 1998 were assembled from nearby meteorological stations operated by the Meteorological Service of Canada (MSC, 2006). Solar radiation

data during 1920-1959 were calculated from sunshine hours with calibration from solar and sunshine data during 1959-1980. Solar radiation for the years 1959-1997 were gap-filled using sunshine hour records at stations in Nanaimo and Vancouver, which were acquired from MSC (2006). Air temperature and precipitation data were acquired from MSC (2006) using data for Nanaimo during 1920-1922, based on regression with the Campbell River airport data; for Cumberland during 1922-1964 and for Campbell River airport during 1965-1997 (D. Spittlehouse BC Ministry of Forests and Range, unpublished data).

3.2.2. Soils

Soil associations, soil textures, parent material mode of deposition and phase were extracted from Jungen (1985). This dataset was used to create a GIS coverage that identified soil characteristics at a scale of 1:100,000 within Oyster River study area. Gridded soil types with 100 m spatial resolution are shown in Figure 2. Properties for each soil horizon used in the process models were taken from the Soil Landscapes of Canada (SLC Version 3.1) in the CanSIS National Soil Database (CanSIS, 2006). Most soils in the OR study area are humo-ferric podzols with variable surface organic horizons of 2-6 cm. Below LFH horizons, the soil texture is loamy sand and gravelly sand with rapid drainage (see also Jassal et al., 2009) and large coarse fragment fractions. Fairbridge is less sandy (sand content 40-90 g kg^{-1}) and hence less freely drained than Bowser, Cassidy, Dashwood, Hawarth, Hiller/Piggott, Honeymoon, Kye, Quinsam and Quimper (with sand contents of 540-900 g kg^{-1}). Arrowsmith is an organic soil with an O horizon of 1.6 m and poor drainage.

3.2.3. Vegetation

Current forest cover data obtained from TimberWest and Weyerhaeuser were compiled into a common polygonal GIS coverage (Trofymow et al. 2008).

The dominant tree species is Douglas-fir with site index of 12-47 m on dry to mesic sites. Secondary tree species found especially on wetter sites include western red cedar, western hemlock and red alder. Patches of alder-dominated or hardhack-sweet gale (*Spirea douglasii ssp. Douglasii-Myrica gale*) wetlands are also found throughout the area, especially at lower elevations. Second-growth stands regenerated naturally, or in some areas were planted after considerable regeneration delay following the clearcuts and slashburns occurring between 1928 and 1960 (Figure 3). Third-growth stands were all planted. Non-forested sites occupy 32 ha in roads, rivers, rocky areas, gravel pits, log sorting areas, and a small area of private pasture land. The density of the understory varies, with a sparse to moderate understory dominated by salal (*Gaultheria shallon*) and Oregon grape (*Berberis nervosa*) bushes in mostly closed canopy forest. Denser understories of sword fern (*Polystichum munitum*), bracken fern (*Pteridium aquilinum*), willow (*Salix sp*.), salal and red huckleberry (*Vaccinium parvifolium*) are found in sapling stands, while on recent cutovers moderate understories of salal, oregon-grape, sword fern, bracken fern, fireweed (*Epilobium angustifolium*), twinflower (Linnaea borealis L.), bedstraw (*Galium triflorum*), bearberry (*Arctostaphylos uva-ursi*), and various Rubus spp. occur (Humphreys et al. 2006).

3.2.4. Disturbance

A consolidated spatial disturbance history was compiled for the study area as a polygonal (vector) GIS coverage from a variety of historical sources with details as described in Trofymow et al. (2008). A number of different disturbances occurred within the study area between 1920 and 2005. Initial harvesting of old-growth forest during 1928-1960 was followed by various combinations of slash burning, partial slash burning, and human-caused partial and total burning, and more recently (1989-2005) by clear cut harvesting of second-growth stands with broadcast burning or pile burning (Figure 3). The areas harvested in 1928-1943

and 1952-1960 were derived from a digitization of a regeneration survey map from Godwin (1937), an Elk River Timber Company map from 1945, and digital orthophotomosaics prepared from air photos acquired from the British Columbia Air Photo Library (2003) and National Air Photo Library (2003) (Trofymow et al., 2008). Fire history coverages were derived from the digitized 1937 regeneration map (Godwin, 1937), 1920-1945 fire maps digitized as part of the BC Natural Disturbance Database project (Taylor, 2002), digitization of a paper map of the 1938 Bloedel Stewart fire from the BC Ministry of Forests and supplemented by the digitized orthophotomosaics (Trofymow et al., 2008). The areas harvested in 1990-2005 were obtained from Weyerhaeuser and TimberWest as GIS coverages.

3.3. Model runs

A 100 m resolution grid of the polygonal soil, topography, forest cover and disturbance mapping data was considered adequate to capture spatial variation for landscape-level simulations. The Oyster River area was resolved into 2500 grid cells of 100 m x 100 m, and attributes of soil, plant species and disturbances in these grid cells were extracted from the consolidated polygonal GIS coverages based on the attributes at the grid cells' centroids. In *CBM-CFS, 3PG* and *Can-IBIS*, model simulations were based on grid cells. In *ecosys* and *C-CLASS*, grid cell attributes were resolved into unique combinations, each of which was used in a single model run, results from which were then allocated to all grid cells with the attribute combination. All models thus simulated productivity in all grid cells so that model runs provided estimation of the carbon fluxes and stocks in the whole study area. All process models used coefficients from the CBM-CFS default disturbance matrices described in Kurz et al. (2009) and Trofymow et al. (2008) to estimate C removals and transfers among C stocks following stand-level disturbances such as fire or harvest. A more detailed description of each model's protocol follows:

3.3.1. CBM-CFS3

Initial dead organic matter (*DOM*) and soil C stocks in 1920 were estimated using a model spin-up procedure where each stand was grown and disturbed over multiple rotations according to the assumed historical disturbance regime until the slow (most stable) *DOM* stocks reached equilibrium (Kurz et al., 2009). Modeling parameters and assumptions used for *DOM* spin-up and modeling were reported in Trofymow et al. (2008). The above-ground biomass C (*AGC*) in 1920 was calculated using the digitized adjusted 1919 timber cruise volume (Trofymow et al. 2008) together with the model's built-in volume to biomass conversion algorithm, and used to initialize the model. Annual *NPP* from 1920 onwards was computed from growth curves for each forest inventory analysis unit, such as Douglas-fir, or mix of Douglas-fir and red alder, until a stand-replacing disturbance occurred (e.g., clear cut or stand-replacing fire) (Trofymow et al., 2008). A set of C transfer coefficients from the CBM-CFS3 disturbance matrices was used to define the transfer of C between different stocks, emitted to the atmosphere or exported off site as timber during forest disturbances, such as fire, clear cut with or without slash burning, clear cut following fire, insect disturbances, and stand mortality. After the stand-replacing disturbance, the stand age was reset to zero and existing or, if planted, new corresponding managed growth curves were used to simulate *NPP* in the regenerating second-growth stands. Annual R_h was calculated as the sum of *DOM* stock decomposition losses which were affected by the temperature modifier (Kurz et al., 2009).

3.3.2. Process models

In all process model simulations, *NPP* was calculated as *GPP* ($=\Sigma V_c$) minus R_a ($=R_m+R_g$ where R_m is maintenance respiration and R_g is growth respiration). *NEP* was calculated as *GPP* minus ecosystem respiration ($R_e = R_a$

$+R_h$ from (A.3) and (A.4)). *NBP* was computed as *NEP* minus carbon loss due to disturbances, using the *CBM-CFS3* transfer coefficients with for plant and litter C stocks specific to each process model. Process models were initialized with soil horizon characteristics taken from Soil Landscapes of Canada (SLC) Version 3.1 (CanSIS, 2006) and 1920 estimates of species composition from the GIS.

In *ecosys*, the starting year for each run was set between 1720 and 1880 to reproduce the *AGC* modelled in each grid cell by *CBM-CFS3* in 1920. *Ecosys* was seeded with PFTs representing Douglas-fir, red alder, and a deciduous bush as an understory species and then run under repeated sequences of weather data recorded at the DF49 flux tower until 1920, and then under site weather data until 2005. These three plant populations used biological attributes used in earlier studies of cool temperate C3 perennial species. The resulting range of stand ages in 1920 was consistent with that derived from the 1919 timber cruise (Trofymow et al., 2008). Prescribed thinning was applied monthly to simulate background mortality rate generally observed during forest regrowth.

In *Can-IBIS*, a historical spin-up from 1601 to 1920 was conducted to stabilize ecosystem C stocks, during which the soil biogeochemistry submodel in *Can-IBIS* performed an accelerated soil carbon accumulation procedure following Kucharik et al. (2000). To simulate historical fire effects, all grid cells were considered to have been burned in 1650 and 1750. At the start of the historical simulation period (1921), the biomass densities in every grid cell were adjusted to agree with the *AGC* values inferred from the 1920 inventory data. All other site variables were left unchanged.

In *C-CLASS*, vegetation cover type was specified as conifer forest. The soil profile was divided into 3 layers with thickness of 10 cm, 25 cm and 375 cm

with an assumed root depth of 2 m. Snow was treated as an analogous fourth layer of "soil" with variable depth. A spin-up run to 1920 was conducted to stabilize ecosystem carbon stocks, at which time *AGC* was re-initialized with values from *CBM-CFS3*. Tree heartwood biomass was assumed as 80% of total tree wood biomass. The transfer coefficients from *CBM-CFS3* disturbance matrices were incorporated into *C-CLASS* to calculate the C fluxes among different forest ecosystem carbon stocks (biomass, litter and soil) and *LAI* was updated after a specific disturbance event.

In *3PG*, initial stem density was set to 0.05 stems m^{-2}. Initial living C stocks were set so that total biomass equaled that of *CBM-CFS3* in 1920. Dead C stocks were initialized by a 20 ka spin-up simulation at the DF49 tower, forced with repeating randomly-selected 10-year sequences from the 1920–2006 climate record and a 400-year return interval of stand-replacing wildfire. Initial dead C stocks for the study area were set to those of the corresponding forest age during the last disturbance cycle of the spin-up simulation. Disturbed pixels were seeded at 0.25 stems m^{-2}.

Results from all models were checked for C conservation to ensure that total *NBP* for the OR area during the runs from 1920 to 2005 equaled the sum of changes in above-ground living biomass (tree bole, branch, foliage, and understory) C (*AGC*) and in below-ground C (live roots, dead roots, and soil) plus surface dead organic C (standing dead, stumps, down woody debris, forest floor) (*BGC & SDC*).

4. Results

4.1. Seasonal effects of weather on forest productivity

4.1.1. CO_2 exchange modelled vs. measured during short-term changes in weather

EC measurements of CO_2 fluxes provide the best-constrained tests of the accuracy with which process-based models simulate short-term weather effects on forest productivity. Such tests have been conducted in previous studies (e.g. Grant et al., 2009a; Arain et al., 2006; Liu et al., 2005; Hember et al., 2010). *Ecosys* and *C-CLASS* have been tested at hourly or half-hourly timescales in the Oyster River DF49 flux tower fetch area (Figs. 2 and 8 in Grant et al., 2009a; Arain et al., 2006). The accuracy of these tests has been evaluated by regressing CO_2 fluxes from the models on those measured by EC. Regressions of hourly fluxes from *ecosys* on those measured by EC for each year from 1998 to 2006 had intercepts usually less than 0.5 μmol m^{-2} s^{-1}, slopes of 0.96-1.10, R^2 of 0.75-0.77 ($P < 0.0001$), and root mean square for differences (RMSD) of 3.1-3.8 μmol m^{-2} s^{-1}, comparable to uncertainty in measured fluxes (Table 2 in Grant et al., 2009a). A regression of ½-hourly fluxes from *C-CLASS* on those measured by EC from 1998 to 2002 had a slope of 0.84, and an R^2 of 0.76 (Table 3 in Arain et al., 2006).

In this study, we used *ecosys* and *C-CLASS* to investigate differing hypotheses in process models for simulating the effects of weather on CO_2 exchange at hourly and daily time scales during a particularly warm summer caused by an El Niño event in 2004. Modelled CO_2 fluxes were calculated as weighted averages of those from grid cells located in the DF49 flux tower fetch area (Figure 1), and compared with CO_2 fluxes measured at the flux tower. During a warming event in late June, midday T_a and vapour pressure deficit D rose from 8.3 ^oC and 0.4 kPa on DOY 166 to 28.2 ^oC and 3.4 kPa on DOY 171, then declined to 14.8 ^oC and 0.37 kPa on DOY 175 (Figure 4a). Midday CO_2 influxes measured by EC declined with warming from 27 μmol m^{-2} s^{-1} on DOY 166 to 6 μmol m^{-2} s^{-1} on DOY 171, then rose with cooling to 23 μmol m^{-2} s^{-1} on DOY 175

(Figure 4). Nocturnal CO_2 effluxes measured by EC rose with warming from 9 μmol m^{-2} s^{-1} on DOY 166 to 18 μmol m^{-2} s^{-1} on DOY 171, and then declined with cooling to ~13 μmol m^{-2} s^{-1} on DOY 175 (Figure 4b,c). Midday latent heat (*LE*) effluxes measured by EC rose with warming from 140 W m^{-2} on DOY 166 to 230 W m^{-2} on DOY 171, and then declined with cooling to 200 W m^{-2} on DOY 175 (Figure 5).

Both models simulated declines in CO_2 influxes and rises in CO_2 effluxes with warming that were consistent with those measured by EC (Figure 4). However these similar responses of CO_2 exchange to warming in the two models were simulated from different processes. In *ecosys*, increases in *D* with T_a caused rises in transpiration (A.1.3), and hence declines in ψ_c and root water potential (ψ_r). Declines in ψ_r raised root radial and axial resistances (Ω_r and Ω_a) to water transport from soil to canopy, thereby exacerbating declines in ψ_c, particularly in conifers which have lower Ω_a than do deciduous species (Tyree and Ewers, 1991). Declines in ψ_c forced declines in ψ_T, and hence in g_c (A.2.1), reducing CO_2 fixation (Grant and Flanagan, 2007) (A1.3) (Figure 4b) and limiting rises in *LE* (Figure 5a). Higher T_a also drove greater R_a (A.3.1), R_h (A.4.1), and hence CO_2 effluxes through highly sensitive Arrhenius functions. In *C-CLASS*, the empirical parameter D_0 caused g_c to decline sharply with increases in *D* (A.2.1) (Arain et al., 2002), forcing sharp declines in CO_2 influxes (Figure 4c) and in *LE* effluxes (Figure 5b) during warming, although declines in LE with warming were not apparent in the EC measurements. CO_2 effluxes rose less with warming in *C-CLASS* than in *ecosys*, driven by smaller rises in R_a (A.3.1) and R_h (A.4.1) from less sensitive Arrhenius functions.

Warming events such as that portrayed in Figure 4 had marked effects on daily *NEP*. Forest stands changed rapidly from sinks of 1-5 g C m^{-2} d^{-1} when T_a was less than 20 ^oC (e.g. DOY 165-167, DOY 175-198, DOY 214-217) to sources of 3-6 g C m^{-2} d^{-1} during warming events when T_a exceeded 20 ^oC (e.g. DOY 168-174, DOY 203-207, DOY 220-238) (Figure 6). August 2004 was unusually warm at OR, causing the Douglas-fir stand in the EC fetch area to remain a large source during most of the month. The modelled responses of CO_2 influxes and effluxes to warming and cooling (Figure 4) enabled *ecosys* and *C-CLASS* to simulate these large and rapid changes in *NEP* by reproducing 0.75 and 0.66 respectively of the variation in hourly CO_2 fluxes measured during 2004 (Table 2). Differences between modelled and measured fluxes were similar to uncertainty in the measured values.

4.1.2. Net ecosystem productivity modelled vs. measured from annual totals of CO_2 flux

These large changes in hourly and daily NEP during short-term changes in T_a would likely cause annual *NEP* to be affected by seasonal changes in T_a. To evaluate such effects at a longer time scale, annual NEP from the models and from gap-filled EC measurements were compared with mean daily maximum air temperature recorded during July - September (T_{amax}) from 1998 to 2005 (Figure 7). Modelled annual *NEP* was calculated as the average value for those from the 173 grid cells within the 85% *NEP* flux footprint of DF49 (Figure 1), weighted by the five-year flux probability density for that cell as discussed in Chen et al. (2009). During this period, T_{amax} varied from 16.4 to 20.1^oC with highest values in El Niño years 1998 and 2004.

Annual *NEP* derived from EC and averaged across models both declined under higher T_{amax} and rose under lower T_{amax} during this 8-year period (Figure 7),

consistent with the declines and rises in daily *NEP* with short-term warming and cooling (Figs. 4 and 6). Annual *NEP* from each process model was positively related to EC-derived values, as was the mean of all process models (R^2=0.6, P=0.03). Interannual variability of mean process model *NEP* was 65 g C m^{-2} $year^{-1}$, and that of the EC-derived values was 76 g C m^{-2} $year^{-1}$. However interannual variability varied among models, being smallest for *CBM-CFS3* in which weather effects on *NPP* were not represented, and largest for *C-CLASS* in which T_a exerted a particularly strong effect on CO_2 exchange as described earlier (Figure 4c; Figure 6b).

To further constrain model tests of annual *NEP*, values for annual *NPP* and R_h from the process models were compared with those derived from biometric and chamber measurements during 2003 - 2005 at the DF49 site by Jassal et al. (2007) (Table 3). Measured *NPP* was lowest and measured R_h highest during 2004 when the summer was warmest (Figure 7). Conversely, measured *NPP* was highest and measured R_h lowest during 2005 when the summer was coolest (Figure 7). Values of annual *NPP* from *ecosys* and *C-CLASS* were closest to the reported results, while those from the other models were considerably larger. Annual *NPP* from *ecosys* and *C-CLASS* in 2003-2005 (Table 3) were also within the range of 700-1000 g C m^{-2} $year^{-1}$ estimated by Hudiburg et al. (2009) for similarly-aged stands of Douglas-fir in the Coast Range of Oregon. All models except *Can-IBIS* gave annual R_h similar to that derived from measurements, although R_h from *ecosys* was slightly smaller.

4.2. Sensitivity of landscape NEP to summer temperature

Inventory models need to estimate weather effects on forest productivity over complex landscapes in which *NEP* is determined primarily by weather and disturbance. To evaluate weather effects for the OR landscape, modelled *NEP* (e.g.

Figure 7), *NPP* and R_h (e.g. Table 2) were examined for all models over the entire study area (Figure 1) during the undisturbed period 1963-1984, which followed recovery of modelled productivity during the 20 years after the 1928-1943 disturbances (Figure 3). Average T_{amax} during this period was 18.6 ^oC, including warm summers in 1967, 1974, 1978 and 1979 (20 $^oC < T_{amax} < 21$ ^oC) and cool summers in 1964, 1969 and 1976 (17 $^oC < T_{amax} < 18$ ^oC) (Figure 8a). In order to exclude stand age effects when modelling weather effects on forest productivity, annual deviations of *NPP* and *NEP* from 7-year moving-averages were derived for each model from all grid cells occupied by young to intermediate aged forest stands with closed canopies. This period was considered long enough to include most short-term weather variability caused by events such as El Niño, while excluding most long-term change in productivity caused by changes in forest age or nutrient status.

Deviations of annual *NEP* from moving averages were consistent in direction among all process models during each year of the comparison (Figure 8b). Correlations for *NEP* deviations among the process models *ecosys*, *Can-IBIS*, *C-CLASS* and *3PG* were significantly positive (R^2=0.7-0.9, P<0.001). Correlations between *CBM-CFS3* and the process models were weak (R^2=0.02-0.1) and not significant (P=0.1-0.6). *C-CLASS* gave the largest deviations of *NEP* (Figure 8b) as it did earlier (Figure 7), followed by *ecosys*, *Can-IBIS* and *3PG*, while *CBM-CFS3* gave the smallest. The range of deviations in annual *NEP* among the models was consistent with that of annual *NEP* modelled during 1998-2005 (Figure 7).

Deviations in annual *NEP* of all process models were more negative during years with warmer summers (1967, 1978 and 1979) and more positive during years with cooler summers (1964 and 1976) (Figure 8b). Regressions of

NEP deviations on T_{amax} for each model indicated that *NEP* declined with rises in summer T_{amax} by 36 - 89 g C m^{-2} y^{-1} $^{o}C^{-1}$ (R^2=0.4-0.7, P<0.001), depending on the sensitivity of *NEP* to T_a in each model (Figure 9). These declines could be attributed to declines in *NPP*, rises in R_h, or both.

4.3. Sensitivity of landscape NPP to summer temperature

Interannual variation modelled in *NEP* was resolved into that in *NPP* and R_h to determine their relative contributions to variation in *NEP*. Deviations of annual *NPP* from moving averages were also consistent in direction among all process models during each year of the comparison (Figure 8c). *Can-IBIS* simulated the largest deviations in annual *NPP* from its 7-year moving averages during the undisturbed period from 1963 to 1984, consistent with its larger values of *NPP* (Table 2), followed by *ecosys*, *C-CLASS*, *3PG* and *CBM-CFS3*. Deviations in *NPP* were well correlated among *ecosys*, *Can-IBIS*, *C-CLASS* and *3PG* (R^2=0.8-0.9, P<0.001). Correlations for *NPP* deviations between *CBM-CFS3* and process models were not significant (P=0.3-0.7) because *CBM-CFS3* did not simulate weather effects on *NPP*.

Deviations in annual *NPP* of process models declined during years with warmer summers (1967, 1978 and 1979) and rose during years with cooler summers (1964 and 1976) (Figure 8c), as did those in *NEP* (Figure 8b). Regressions of *NPP* deviations on T_{amax} for each process model indicated that *NPP* declined with rises in summer T_{amax} by 35 – 66 g C m^{-2} y^{-1} $^{o}C^{-1}$ (R^2=0.4-0.6) (Figure 10). These declines were remarkably similar among *ecosys*, *C-CLASS* and *Can-IBIS*.

4. 4. Sensitivity of landscape R_h to summer temperature

Deviations in modelled R_h were smaller than those in *NEP* and *NPP* (Figure 8d), and correlations among models were not as strong, indicating that modelled weather effects on annual *NEP* were caused mostly by those on *NPP*. Deviations in R_h from *ecosys* were positively correlated with those in *Can-IBIS*, *C-CLASS*, and *3PG* (R^2=0.2-0.7, P<0.05). Correlation for R_h deviations between *Can-IBIS* and *3PG* was significantly positive (R^2=0.5, P<0.001). Correlations of *CBM-CFS3* with *ecosys* and *C-CLASS* were positive (R^2=0.3-0.6, P<0.05), which was attributed to the annual temperature modifier used for calculating R_h in *CBM-CFS3* (Kurz et al., 2009). Correlations of *C-CLASS* with *Can-IBIS* and *3PG* were not significant (P=0.3-0.4).

Regressions of R_h deviations on T_{amax} for each process model indicated that deviations from *CBM-CFS3* and *C-CLASS* were positively related to summer T_{amax} (R^2=0.3-0.6) while those from *Can-IBIS* showed a weak negative response to summer T_{amax} (R^2=0.1, P=0.09) (Figure 11). Deviations from *ecosys* and *3PG* were not significantly related to summer T_{amax} (P=0.7-0.9).

The different responses of deviations in annual *NPP* and R_h to T_{amax} among models (Figs. 10 and 11) accounted for the different responses of deviations in annual *NEP* to T_{amax} (Figure 9). Annual *NPP* in *ecosys*, *Can-IBIS* and *C-CLASS* responded similarly to T_{amax} (Figure 10b,c,d). However annual R_h in *C-CLASS* increased with T_{amax} (Figure 11d), causing *NEP* to decline more with warming than did *NPP* (Figs. 9d and 10d). Annual R_h in *Can-IBIS* decreased with T_{amax} (Figure 11c), causing *NEP* to decline less with warming than did *NPP* (Figs. 9c and 10c). Annual R_h in *ecosys* and *3PG* showed no significant relationships with T_{amax} so that *NEP* declined similarly to *NPP* with warming (Figs. 9b,e and 10b,e).

4.5. Long-term forest carbon balance under historical climate and disturbances.

The modelled effects of weather on *NPP*, R_h and hence *NEP* (Figs. 4 – 11) need to function in complex landscapes in which *NPP*, R_h and *NEP* are also strongly affected by disturbances such as fire and harvest. Weather effects on productivity were therefore examined over the entire study area from 1920 to 2005, during which productivity was adversely affected by fire and harvesting from 1928 to 1943, and by harvesting in 1990 and after 1997 (Figure 3). All models generated similar *AGC* prior to 1928 as a result of their initialization and spinup protocols (Section 3.3) and then applied the same transfer coefficients to *AGC* for each disturbance type (Figure 3). Thus the simulated annual losses in *AGC* during 1928 - 1943 were similar among models (Figure 12a) However annual losses in *BGC & SDC* during this period differed among models (Figure 12b). *CBM-CFS3* and *3PG* simulated the greatest annual losses, while *ecosys*, *Can-IBIS* and *C-CLASS* simulated smaller losses. These differences were caused by applying the same transfer coefficients to different amounts of *BGC & SDC* in each model during disturbances. In *CBM-CFS3* all *BGC* was represented in a single soil layer to which the transfer coefficients were applied, whereas in the process models *BGC* was represented in several organic and mineral soil layers, with the same transfer coefficients applied only to the uppermost organic layers liable to combustion. Further resolution of transfer coefficients for combustion of *BGC & SDC* stocks is needed for process models with multiple soil layers of differing combustibility. Consequently declines in cumulative *NBP* (= cumulative changes *AGC* + *BGC* + *SDC*) varied from 250 to 400 Mg C ha^{-1} during 1928 – 1943 (Figure 12c), reflecting declines in both above- and below-ground C stocks (Figure 12a, b).

Between the 1928 – 1943 and post-1990 disturbance periods (Figure 3), growth in *AGC* was more rapid in *CBM-CFS3*, *ecosys* and *3PG* (*ca*. 4 Mg C ha^{-1} y^{-1}) and slower in *C-CLASS* and *Can-IBIS* (*ca*. 2 Mg C ha^{-1} y^{-1}) (Figure 12a). *AGC* growth in *CBM-CFS3* was driven from inventory growth curves for the OR area, and so closely represented actual *AGC* growth. *AGC* growth covaried annually among the process models, but ranked differently from *NPP* (Table 3), indicating substantial divergence in allocating *NPP* to *AGC vs*. litterfall. This divergence needs to be resolved through further testing against measurements before process models can simulate *AGC* growth reliably. Most models simulated losses in *BGC & SDC* for some time following the1928 – 1943 disturbance period (Figure 12b) due to slow recovery of *NPP* and hence *AGC* growth (Figure 12a), and to increased R_h from stocks of fine, non-woody litter and coarse woody debris gained during the disturbances (Figure 12b). These losses were eventually followed by gains in *BGC & SDC* as declines in litter stocks from earlier disturbances slowed and litterfall from current forest growth increased. These gains remained slow in all models except *3PG* in which they approached those in *AGC*. These changes in *AGC* and in *BGC & SDC* combined to give gains in cumulative *NBP* between the 1928 – 1943 and post-1990 disturbance periods that were greatest in *3PG*, intermediate in *CMB-CFS3* and *ecosys*, and smallest in *C-CLASS* and *Can-IBIS* (Figure 12c). All models simulated declines in gains of *AGC* and *BGC & SDC* caused by the post-1990 harvests.

4.6. Representing weather effects on productivity in inventory models.

There is a need to modify the inventory-driven estimate of annual *NPP* in *CBM-CFS* to account for the effects of weather. Variation in *NEP* from the process models was robust, and consistent with that from EC measurements at hourly (Figure 4), daily (Figure 6) and annual (Figure 7) time scales. Variation in

NEP was driven primarily by that in *NPP* (Figure 8c *v*s. 8b) which drove *AGC* growth in a complex, disturbed landscape at rates that were in most cases consistent with those derived from inventory growth curves. The general agreement in sensitivity of *NPP* to T_{amax} among the process models, indicated by the regression slopes in Figure 10, led to a generalized algorithm for temperature effects on forest *NPP,* which could be integrated into the calculation of *NPP* in *CBM-CFS*:

$$NPP' = NPP - 57.1\ (T_{amax} - 18.6) \qquad (1)$$

where *NPP* and NPP' are, respectively, current and temperature-adjusted estimates of annual *NPP* from *CBM-CFS3*, -57.1 is the average slope for the process models, 18.6 is the historical mean daily maximum T_a in July–September, and T_{amax} is the mean daily maximum T_a in July–September for the current year.

5. Discussion

The modelled responses of annual *NPP* to T_{amax} from which Eq. (1) was derived (Figure 10) arose from direct effects of T_a on CO_2 fixation processes calculated from Arrhenius (*ecosys* and *Can-IBIS*) or Q_{10} (*C-CLASS* and *3PG*) functions of T_c, solved in the process models (except for *3PG*) from canopy energy balances (A.1.2). In these functions, higher T_c also raised Michaelis-Menten values and lowered aqueous CO_2:O_2 ratios for carboxylation, reducing carboxylation substrate specificity and thereby decreasing CO_2 fixation rates in the upper range of T_a in this study (Grant et al., 2009b). Parameters used by the process models in these temperature functions have been derived from a wide range of experiments (e.g. Bernacchi et al., 2001; 2003).

The modelled responses of *NPP* to T_a also arose from indirect effects of T_a on CO_2 fixation processes through *D* (Grant et al., 2007a; Chen et al., 2002; Jassal et al., 2009). In *ecosys*, higher *D* reduced g_c and CO_2 fixation indirectly through its effect on water potential gradients along a soil-root-canopy hydraulic pathway. In the other process models, higher *D* reduced g_c directly, as did soil water status (A.2.1), but without an explicit linkage with soil-root-canopy hydraulics. In *C-CLASS*, lower g_c directly reduced both CO_2 fixation (A1.3) (Figure 4c) and *LE* (Figure 5b), while in *Can-IBIS* g_c did not affect CO_2 fixation which rather responded directly to soil drying hastened by more rapid evapotranspiration under higher T_a. In this study, summer T_{amax} varied from 16 ^{o}C to 21^{o}C, below values at which direct adverse effects of T_a on CO_2 fixation might be expected (e.g. Medlyn et al., 2002), so that indirect effects of *D* on CO_2 fixation were likely the principal cause of these declines.

In spite of these differences, all process models gave similar declines in annual *NPP* with rises in T_{amax} (Figure 10), indicating that the relationship between *NPP* and T_{amax} summarized in Eq. (1) is a robust feature of process models. This equation could make useful contributions to the calculation of interannual variation in forest productivity if implemented in an inventory model. Equation (1) would reduce annual NPP estimated for a closed temperate Douglas-fir stand by 200 g C m^{-2} during a year with a particularly warm summer such as 2004 from that during a year with a particularly cool summer such as 2001 (Figure 7). This reduction is only slightly smaller than that in NEP derived from EC measurements at OR in 2004 *vs*. 2001 (Figure 7) which may have been augmented by a small rise in R_h (Table 3). Reductions annual *NPP* estimated from equation (1) in years with warm *vs*. cool summers would be only slightly smaller than reductions in annual *NEP* derived from EC measurements by Falk et al.

(2008) at an old growth Douglas-fir/hemlock stand about 450 km south of OR. Such declines in productivity with summer warming (Figure 6) have been measured and modelled at hourly and daily timescales in several earlier studies at OR and elsewhere (e.g. Chen et al. 2002; Falk et al., 2008; Grant et al., 2005; 2007b; 2009a,b), and appear to be a general feature of coniferous stands. Such declines may have caused the negative correlation between tree ring index and June – August maximum temperatures found in boreal black spruce by Dang and Lieffers (1989) and in other boreal conifers by Barber et al. (2000) and Wilmking et al. (2004).

The responses of annual R_h to T_{amax} (Figure 11) were smaller than those of *NPP* and tended to differ in direction among the process models. Rises in T_a and thereby in T_s raised R_a in the models by increasing canopy or root activity and autotrophic R_m (A.3.1), and raised R_h by increasing microbial activity and heterotrophic R_m (A.4.1). In some models, annual R_h rose with summer T_{amax} in the current year (*CBM-CFS3* and *C-CLASS* in Figure 11) while in others (*ecosys* and *3PG*) annual R_h in the current year rose with greater productivity and hence litterfall in the previous year. The lack of significant response of annual R_h to T_{amax} in *Can-IBIS* was attributed to simulated effects of decreased soil moisture content in summer, which interacted with temperature effects (A.4.2). Experimental evidence at OR indicates that annual R_h does rise during warmer years. Morgenstern et al. (2004) reported that high T_a during the 1997-1998 El Niño event resulted in the greatest annual R_e ($=R_a + R_h$) measured from 1998 to 2002. Similarly Jassal et al. (2007) reported the greatest annual R_h from 2003 to 2005 was measured during the warmest year in 2004 (Table 3). However there was insufficient consensus among the process models to derive a summary equation for temperature effects on annual R_h.

In the process models, declines in CO_2 fixation combined with rises in R_a and R_h (Figure 4), led to the sharp declines of daily *NPP* and *NEP* during short-term increases in summer T_a (Figure 6) and of annual *NPP* and *NEP* under higher T_{amax} (Figure 8). These declines were highly nonlinear with T_a, as apparent in the large changes from net C uptake to net C emission measured and modelled in response to rises in T_a and D above threshold values of ~20 ^{o}C and ~2.5 kPa (Figs. 4 and 6). Such nonlinearity indicates that the findings of this study should not be extrapolated to T_{amax} beyond the range in this study (16 – 21 ^{o}C) at OR, nor to climates with MAT outside the range of that at OR (8.1 – 9.1 ^{o}C). Furthermore, these findings apply to coniferous forests with large Ω_a, and not to deciduous forests with lower Ω_a, and hence less sensitive response of CO_2 fixation to higher T_a (Grant et al., 2009a).

We also studied correlations of *NPP* and *NEP* with spring T_a, and with spring and summer precipitation in this Douglas-fir stand using the same methodology as that for T_{amax} described above, but found no significant landscape-level relationships, suggesting that summer T_a was the weather attribute that most affected forest productivity at OR. However our methodology is capable of identifying other weather attributes that most affect productivity in other forest stands.

This study suggests that a long time series of climate, inventory and disturbance data are needed to test landscape-scale models due to the legacy effects of disturbance history and hence age-class structure on contemporary C fluxes. This study also highlights the need for continued EC flux measurements to support model validation at decadal timescales because of interannual variability in weather caused by El Niño, warming and drought events (Grant et al., 2009a).

6. Conclusions

Modeling historical forest carbon dynamics over a complex, disturbed landscape revealed sensitivities of *NPP*, R_h and *NEP* to seasonal and interannual temperature variations as well as disturbance effects on forest *NBP*. Variation in *NPP* and *NEP* during forest regrowth was positively correlated among process models and negatively related to T_{amax}. The process models generally agreed regarding climate sensitivity of *NPP* and *NEP*, suggesting that ecozone-specific response functions for *NPP* to T_{amax} such as that summarized in Eq. (1) could be incorporated in inventory-based models such as *CBM-CFS3* to capture effects of climate variability on forest C inventories. However there was less agreement among process models in the simulation of disturbance effects. During an intense disturbance period, divergences among simulated changes in *BGC & SDC* stocks were attributed to differences in the models' initial *BGC* stock sizes and in the application of disturbance coefficients to different amounts of *BGC* arising from different soil layering in inventory *vs*. process models. Further resolution of disturbance, and particularly combustion, coefficients for *BGC & SDC* stocks is needed for process models. After the disturbance period, divergences in *NBP* were mainly due to differences in the forest regrowth rates simulated by each model, attributed at least partly to differences in allocating NPP to forest growth *vs*. litterfall.

Acknowledgements

These results are part of the historical carbon modelling project of the Canadian Carbon Program (CCP) which is supported through funding from the Canadian Foundation for Climate and Atmospheric Sciences (CFCAS) and the National Sciences and Engineering Research Council (NSERC). We thank Colin Ferster, Brad Hawkes, Gurp Thandi with the Canadian Forest Service for updates of the historical inventory and disturbance GIS coverage for the Oyster River forest area. We thank John Parminter of the B.C. Ministry of Forests and Bill Grutzmacher of Timberwest and Ken Epps of Island Timberlands for providing access to additional historical and current records. We thank Dave Spittlehouse of the B.C. Ministry of Forests for preparing and access to the reconstructed historical daily weather records and Andy Black, UBC for the current weather and EC records for Fluxnet Canada DF49 site. We thank our colleagues Pierre Bernier, Jingming Chen, Ajit Govind, Luc Guindon, Changhui Peng and Jianfeng Sun for providing constructive comments on the earlier draft. *Ecosys* model runs were done on AICT Linux Cluster at University of Alberta and the WestGrid Glacier cluster, and C-CLASS model runs were performed at SHARCNET.

References

Arain, M.A., Black, T.A., Barr, A.G., Jarvis, P.G., Massheder, J.M., Verseghy, D.L. and Nesic, Z., 2002. Effects of seasonal and interannual climate variability on net ecosystem productivity of boreal deciduous and conifer forests. Canadian Journal of Forest Research, 32(5): 878-891.

Arain, M.A., Yuan, F., and Black, T.A., 2006. Soil-plant nitrogen cycling modulated carbon exchanges in a western temperate conifer forest in Canada. Agricultural and Forest Meteorology, 140:171-192.

Barber, V.A., G.P. Juday and B.P. Finney. 2000. Reduced growth of Alaska white spruce in the twentieth century from temperature-induced drought stress. Nature 405:668-673.

Barr, A.G., Griffis, T.J., Black, T.A., Lee, X., Staebler, R.M., Fuentes, J.D., Chen, Z. and Morgenstern, K., 2002. Comparing the carbon budgets of boreal and temperate deciduous forest stands. Canadian Journal of Forest Research, 32:813-822.

BC Air Photo Library, 2003. http://ilmbwww.gov.bc.ca/bmgs/airphoto/index.htm

BC Forest Service, Forest Surveys and Working Plans Division, 1938. Map of Area Burned by the ‘‘Bloedel Fire’’: 1938. Victoria, BC.

Bergeron, O., Margolis, H.A., Black, T.A., Coursolle, C., Dunn, A.L., Barr, A.G. and Wofsy, S.C., 2007. Comparison of carbon dioxide fluxes over three boreal black spruce forests in Canada. Global Change Biology, 13:89-107.

Bernacchi, C.J., Singsaas, E.L., Pimentel, C., Portis, A.L. and Long, S.P., 2001. Improved temperature response functions for models of rubisco-limited photosynthesis. Plant, Cell and Environment, 24:253-259.

Bernacchi, C.J., Pimentel, C. and Long, S.P., 2003. In vivo temperature response functions of parameters required to model RuBP-limited photosynthesis. Plant, Cell and Environment, 26:1419–1430.

Black, T.A., Chen, W.J., Barr, A.G., Arain , M.A., Chen, Z., Nesic, Z., Hogg, E.H., Neumann, H.H., Yang, P.C., 2000. Increased carbon sequestration by boreal deciduous forest in years with a warm spring. Geophysical Research Letters, 27, 1271-1274.

Boudewyn, P., Song, X., Magnussen, S., Gillis, M.D., 2007. Model-based, Volume-to-Biomass Conversion for Forested and Vegetated Land in Canada. Information Report BC-X-411. Natural Resources Canada, Canadian Forest Service, Pacific Forestry Centre, Victoria, BC.

CanSIS, 2006. Soil Survey Data for British Columbia: Southern Vancouver Island. Agriculture and Agri-Food Canada. http://sis.agr.gc.ca/cansis/nsdb/detailed/bc/southvani.zip

Chen, B., Black, T.A., Coops, N.C., Hilker, T., Trofymow, J.A., and Morgenstern, K., 2009. Assessing tower flux footprint climatology and scaling between remotely sensed and eddy covariance measurements. Boundary Layer Meteorology, DOI 10.1007/s10546-008-9339-1.

Chen, J.M., Ju, W., Cihlar, J., Price, D., Liu, J., Chen, W., Pan, J., Black, A. and Barr, A., 2003. Spatial distribution of carbon sources and sinks in Canada's forests. Tellus, Series B: Chemical and Physical Meteorology, 55:622-641.

Chen, J., Falk, M., Euskirchen, E., Paw U, K.T., Suchanek, T.H., Ustin, S.L., Bond, B.J., Brosofske, K.D., Phillips, N. and Bi, R., 2002. Biophysical controls of carbon flows in three successional Douglas-fir stands on eddy-covariance measurements. Tree Physiology, 22, 169-177.

Chertov, O., Bhatti, J.S., Komarov, A., Mikhailov, A., and Bykhovets, S., 2009. Influence of climate change, fire and harvest on the carbon dynamics of black spruce in central Canada. Forest Ecology and Management, 257: 941-950.

Ciais, Ph., Reichstein, M., Viovy, N., Granier, A., Ogée, J., Allard, V., Aubinet, M., Buchmann, N., Bernhofer, Chr., Carrara, A., Chevallier, F., De

Noblet, N., Friend, A.D., Friedlingstein, P., Grünwald, T., Heinesch, B., Keronen, P., Knohl, A., Krinner, G., Loustau, D., Manca, G., Matteucci, G., Miglietta, F., Ourcival, J.M., Papale, D., Pilegaard, K., Rambal, S., Seufert, G., Soussana, J.F., Sanz, M.J., Schulze, E.D., Vesala, T. and Valentini, R., 2005. Europe-wide reduction in primary productivity caused by the heat and drought in 2003. Nature, 437: 529-533.

Coops, N.C., Black, T.A., Jassal, R.S., Trofymow, J.A. and Morgenstern, K., 2007. Comparison of MODIS, eddy covariance determined and physiologically modeled gross primary production (GPP) in a Douglas-fir forest stand. Remote Sensing and Environment, 107: 385-401.

Dang, Q.L., and V.J. Lieffers. 1989. Climate and annual ring growth of black spruce in some Alberta peatlands. Can. J. Bot. 67: 1885.1889.

Dixon, R.K., Brown, S., Houghton, R.A., Solomon, A.M., Trexler, M.C. and Wisniewski, J., 1994. Carbon stocks and flux of global forest ecosystems. Science, 263, 185-190.

El Maayar, M., Price, D.T., Black, T.A., Humphreys, E.R.and Jork, E-M., 2002. Sensitivity tests of the Integrated BIosphere Simulator (IBIS) to soil and vegetation characteristics in a Pacific Coastal coniferous forest. Atmosphere–Ocean, 40 (3),313-332.

Falk, M., Wharton, S., Schroeder, M., Ustin, S., Paw U, K.T., 2008. Flux partitioning in an old-growth forest: seasonal and interannual dynamics. Tree Physiology 28, 509–520.

Farquhar, G.D., von Caemmerer, S. and Berry, J.A., 1980. A biochemical model of photosynthetic CO_2 assimilation in leaves of C3 species. Planta, 149, (1): 78-90.

Fluxnet-Canada, 2006. Data Information System. http://www.fluxnet-canada.ca/

Foley, J.A., Prentice, I.C., Ramankutty, N., Levis, S., Pollard, D., Sitch, S. and Haxeltine A., 1996. An integrated biosphere model of land surface

processes, terrestrial carbon balance, and vegetation dynamics. Global Biogeochemical Cycles, 10: 603-623.

Godwin, G., 1937. Regeneration study on the logged-off lands of the Comox Logging and Railway Co., Oyster River, Forest Survey No. R 72, Survey File No. 0124780. Forest Service, BC (39 pp. and Map).

Grant, R.F., Arain, A., Arora, V., Barr, A., Black, T.A., & Chen, J., Wang S., Yuan F., and Zhang Y., 2005. Intercomparison of techniques to model high temperature effects on CO_2 and energy exchange in temperate and boreal coniferous forests. Ecological Modelling, 188(2-4), 217-252.

Grant, R.F. and Flanagan, L.B., 2007. Modeling stomatal and nonstomatal effects of water deficits on CO_2 fixation in a semiarid grassland. Journal of Geophysical Research, 112:G03011, doi:10.1029/2006JG000302.

Grant, R.F., Barr, A.G., Black, T.A., Gaumont-Guay, D., Iwashita, H., Kidson, J., McCaughey, H., Morgenstern, K., Murayama, S., Nesic, Z., Saigusa, N., Shashkov, A. and Zha, T., 2007a. Net ecosystem productivity of boreal jack pine stands regenerating from clearcutting under current and future climates. Global Change Biology, 13(7), 1423-1440.

Grant, R.F., Black, T. A., Humphreys, E. R., & Morgenstern, K., 2007b. Changes in net ecosystem productivity with forest age following clearcutting of a coastal Douglas-fir forest: Testing a mathematical model with eddy covariance measurements along a forest chronosequence. Tree Physiology, 27(1), 115-131.

Grant, R.F., Barr, A.G., Black, T.A., Margolis, H.A., Dunn, A.L., Metsaranta, J. and Wang, S., 2009a. Interannual variation in net ecosystem productivity of Canadian forests as affected by regional weather patterns – a Fluxnet-Canada synthesis. Agricultural and Forest Meteorology, 149:2022–2039.

Grant, R.F., Margolis, H.A., Barr, A.G., Black, T.A., Dunn, A.L., Bernier, P.Y., and Bergeron, O., 2009b. Changes in net ecosystem productivity of boreal

black spruce stands in response to changes in temperature at diurnal and seasonal timescales. Tree physiology 29, (1): 1-17.

Grant, R.F. and Nalder, I.A., 2000. Climate change effects on net carbon exchange of a Boreal aspen-hazelnut forest: Estimates from the ecosystem model *ecosys*. Global Change Biology, 6:183-200.

Hember, R.A., Black, T.A., Coops, N.C., Guy, R.D., 2010. Simulating gross primary production across a chronosequence of coastal Douglas-fir forest stands with a production efficiency model. Agricultural and Forest Meteorology 150:238-253.

Hudiburg, T., Law, B., Turner, D.P., Campbell, J., Donato, D. and Duane, M., 2009. Carbon dynamics of Oregon and Northern California forests and potential land-based carbon storage. Ecological Applications: 19 (1), 163-180.

Humphreys, E.R., Black, T.A., Morgenstern, K., Cai, T., Drewitt, G.B., Nesic, Z. and Trofymow, J.A., 2006. Carbon dioxide fluxes in coastal Douglas-fir stands at different stages of development after clearcut harvesting. Agricultural and Forest Meteorology, 140:6-22.

Intergovernmental Panel on Climate Change (IPCC), 1997. Revised 1996 Guidelines for National Greenhouse Inventories. IPCC/OECD/IEA, Bracknell, UK.

Intergovernmental Panel on Climate Change (IPCC), 2003. In: Penman, J., et al. (eds), Good Practice Guidance for Land Use, Land-use Change and Forestry. Institute for Global Environmental Strategies, Hayama, Japan (available at http://www.ipcc-nggip.iges.or.jp)

Jassal, R.S., Black, T.A., Cai, T., Morgenstern, K., Li, Z., Gaumont-Guay, D., and Nesic, Z., 2007. Components of ecosystem respiration and an estimate of net primary productivity of an intermediate-aged Douglas-fir stand. Agricultural and Forest Meteorology, 144 (1-2): 44-57.

Jassal, R.S., Black, T.A., Spittlehouse, D.L., Brümmer, C. and Nesic, Z., 2009. Evapotranspiration and water use efficiency in different-aged Pacific Northwest Douglas-fir stands. Agricultural and Forest Meteorology, 149 (6-7): 1168-1178.

Jungen, J.R., 1985. Soils of Southern Vancouver Island, BC Soil Survey Report 44. MOE Technical Report 17, BC Ministry of Environment, Victoria, BC.

Kucharik, C.J., Foley, J.A., Delire, C., Fisher, V.A., Coe, M.T., Lenters, J.D., Young-Molling, C., Ramankutty, N., Norman, J.M. and Gower, S.T., 2000. Testing the performance of a Dynamic Global Ecosystem Model: Water balance, carbon balance, and vegetation structure. Global Biogeochemical Cycles, 14 (3), 795-825.

Kurz, W.A., and Apps, M.J., 2006. Developing Canada's National Forest Carbon Monitoring, Accounting and Reporting System to meet the reporting requirements of the Kyoto Protocol. Mitigation and Adaptation Strategies for Global Change, 11: 33-43.

Kurz, W.A., Dymond, C.C., White, T.M., Stinson, G., Shaw, C.H., Rampley, G.J., Smyth, C., Simpson, B.N., Neilson, E.T., Trofymow, J.A., Metsaranta, J. and Apps, M.J., 2009. CBM-CFS3: A model of carbon-dynamics in forest and land-use change implementing IPCC standards. Ecological Modelling, 220: 480-504.

Landsberg, J. J., and Waring R. H., 1997. A generalised model of forest productivity using simplified concepts of radiation-use efficiency, carbon balance and partitioning. Forest Ecology and Management, 95: 209-228.

Li, Z., Kurz, W.A., Apps, M.J. and Beukema, S.J., 2003. Belowground biomass dynamics in the carbon budget model of the canadian forest sector: Recent improvements and implications for the estimation of *NPP* and *NEP*, Canadian Journal of Forest Research, 33, (1): 126-136.

Liu, J., Price, D.T. and Chen, J.M., 2005. Nitrogen controls on ecosystem carbon sequestration: A model implementation and application to Saskatchewan, Canada, Ecological Modelling, 186, (2): 178-195.

Medlyn, B. E., E. Dreyer, D. Ellsworth, M. Forstreuter, P.C. Harley, M.U.F. Kirschbaum, X. Le Roux, P. Montpied, J. Strassemeyer, A. Walcroft, K. Wang and D. Loustau. 2002. Temperature response of parameters of a biochemically based model of photosynthesis. II. A review of experimental data. Plant, Cell Environ. 25:1167-1179,

Meterological Services Canada, 2006. http://www.msc-smc.ec.gc.ca.

Morgenstern, K., Black, T.A., Humphreys, E.R., Griffis, T.J., Drewitt, G.B., Cai, T., Nesic, Z., Spittlehouse, D.L., and Livingston, N.J., 2004. Sensitivity and uncertainty of the carbon balance of a pacific northwest douglas-fir forest during an El Niño/La niña cycle. Agricultural and Forest Meteorology 123, (3-4): 201-219.

National Air Photo Library, 2003. http://airphotos.nrcan.gc.ca/index_e.php

Peng, C., Liu, J., Dang, Q., Apps, M.J. and Jiang, H., 2002. TRIPLEX: a generic hybrid model for predicting forest growth and carbon and nitrogen dynamics. Ecological Modelling, 153, 109-130.

Pojar, J., Klinka, K. and Demarchi, D.A., 1991. Chapter 6: Coastal Western Hemlock Zone. In Meidinger D. and Pojar J. (eds.). Ecosystems of British Columbia. BC Special Report Series No. 6. Victoria: BC Ministry of Forests, 95-111.

Schwalm, C.R., C.A. Williams, K. Schaefer et al.. 2010. A model‐data intercomparison of CO_2 exchange across North America: Results from the North American Carbon Program site synthesis. *J. Geophys. Res.*, 115, G00H05, doi:10.1029/2009JG001229.

Taylor, S., 2002. British Columbia Natural Disturbance Database. http://cfs.nrcan.gc.ca/subsite/disturbance.

Thornton, P.E., Law, B.E., Gholz, H.L., Clark, K.L., Falge, E., Ellsworth, D.S., Goldstein, A.H., Monson, R.K., Hollinger, D., Falk, M., Chen, J. and Sparks, J.P., 2002. Modeling and measuring the effects of disturbance history and climate on carbon and water budgets in evergreen needleleaf forests. Agricultural and Forest Meteorology, 113: 185-222.

Trofymow, J.A., Stinson, G. and Kurz, W.A., 2008. Derivation of a spatially explicit 86-year retrospective carbon budget for a landscape undergoing conversion from old-growth to managed forests on Vancouver Island, BC. Forest Ecology and Management, 256, (10): 1677-1691.

Turner, D.P., Ritts, W.D., Law, B.E., Cohen, W.B., Yang, Z., Hudiburg, T., Campbell, J.L. and Duane, M., 2007. Scaling net ecosystem production and net biome production over a heterogeneous region in the western United States. Biogeosciences, 4: 597-612.

Tyree, M.T. and F.W. Ewers. 1991. The hydraulic architecture of trees and other woody plants. New Phytol. 119:345-360.

Verseghy, D.L., 2000. The Canadian Land Surface Scheme (CLASS): Its history and future. Atmosphere-Ocean, 38: 1-13.

Wilmking, M., G.P. Juday, V.A. Barber and H.J. Zald. 2004. Recent climate warming forces contrasting growth responses of white spruce at treeline in Alaska through temperature thresholds. Global Change Biol. 10:1724-1736.

Yuan F., Arain M.A., Barr A., Black T.A., Bourque P.-A., Coursolle C., Margolis H., McCaughey H., and Wofsy S.C., 2008. Modeling analysis of primary controls on net ecosystem productivity of seven boreal and temperate coniferous forests across an east-west continental transect in Canada. Global Change Biology, 14: 1–20, doi: 10.1111/j.1365-2486.2008.01612.x.

Table 1. Characteristics of the Oyster River area.

- Elevation: 120 m-460 m
- Soil types: Arrowsmith; Bower; Cassidy; Cullite; Dashwood; Fairbridge; Hawarth; Hiller; Honeymoon; Kye; Piggott; Quimper; Quinsam (CanSIS, 2006)
- Tree species: Douglas-fir (*Pseudotsuga menziesii*); Western redcedar (*Thuja plicata*); Western hemlock (*Tsuga heterophylla*); Red alder (*Alnus rubra*)
- Dominant disturbance periods: 1928-1943; 1997-2005
- Main disturbance types: harvesting, slash burn, human caused burn

Table 2. Intercepts (*a*), slopes (*b*), coefficients of determination (R^2), root mean square of differences (*RMSD*) from regressions of hourly modelled CO_2 fluxes *vs*. hourly-averaged EC CO_2 fluxes in 2004 in the fetch area of flux tower DF49 (n = 4362). Uncertainty in measured fluxes was estimated to be 4.0 μmol m^{-2} s^{-1}.

Model	***a*** †	***b***	**R^2**	**RMSD**
	μmol m^{-2} s^{-1}			μmol m^{-2} s^{-1}
ecosys	0.63	0.99	0.75	3.8
C-CLASS	0.11	0.75	0.66	4.7

† *a*, *b* and R^2 from regressions of modelled on measured fluxes, RSMD from regressions of measured on modelled fluxes.

Table 3. Measured and footprint-weighted modelled annual *NPP* and R_h in the fetch area of flux tower DF49.

NPP (g C m^{-2} yr^{-1})	Measured*	*CBM-CFS3*	*Ecosys*	*Can-IBIS*	*C-CLASS*	*3PG*
2003	855	1283	790	1867	807	1004
2004	804	1259	830	1946	839	1125
2005	869	1267	966			1206
R_h (g C m^{-2} yr^{-1})						
2003	549	649	492	1219	651	552
2004	610	671	504	1294	662	756
2005	596	675	477			705

* from Jassal et al. (2007)

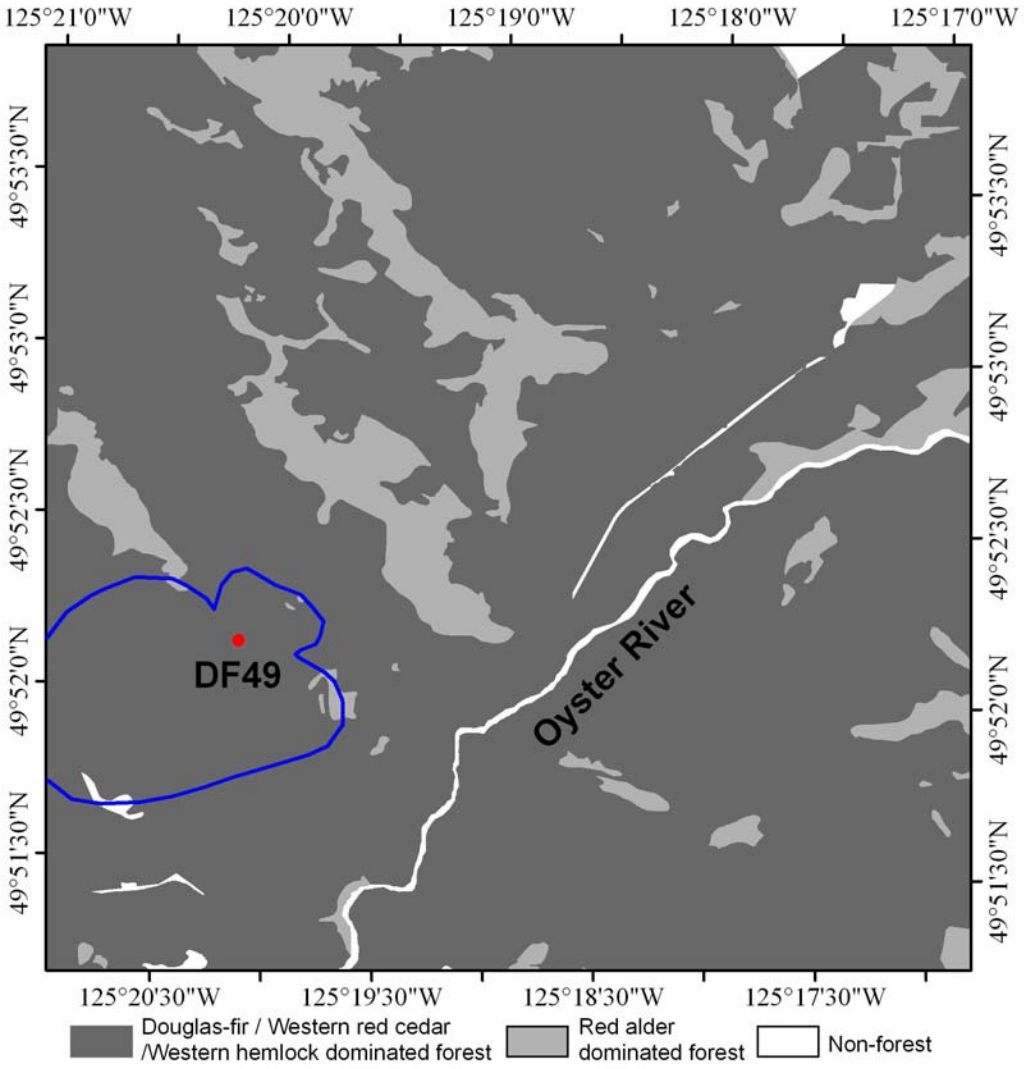

Figure 1. The location of the Oyster River area (5 km x 5 km) with the land cover in 1999. The DF49 flux tower (the 85% *NEP* flux footprint boundary was marked) is within this study area.

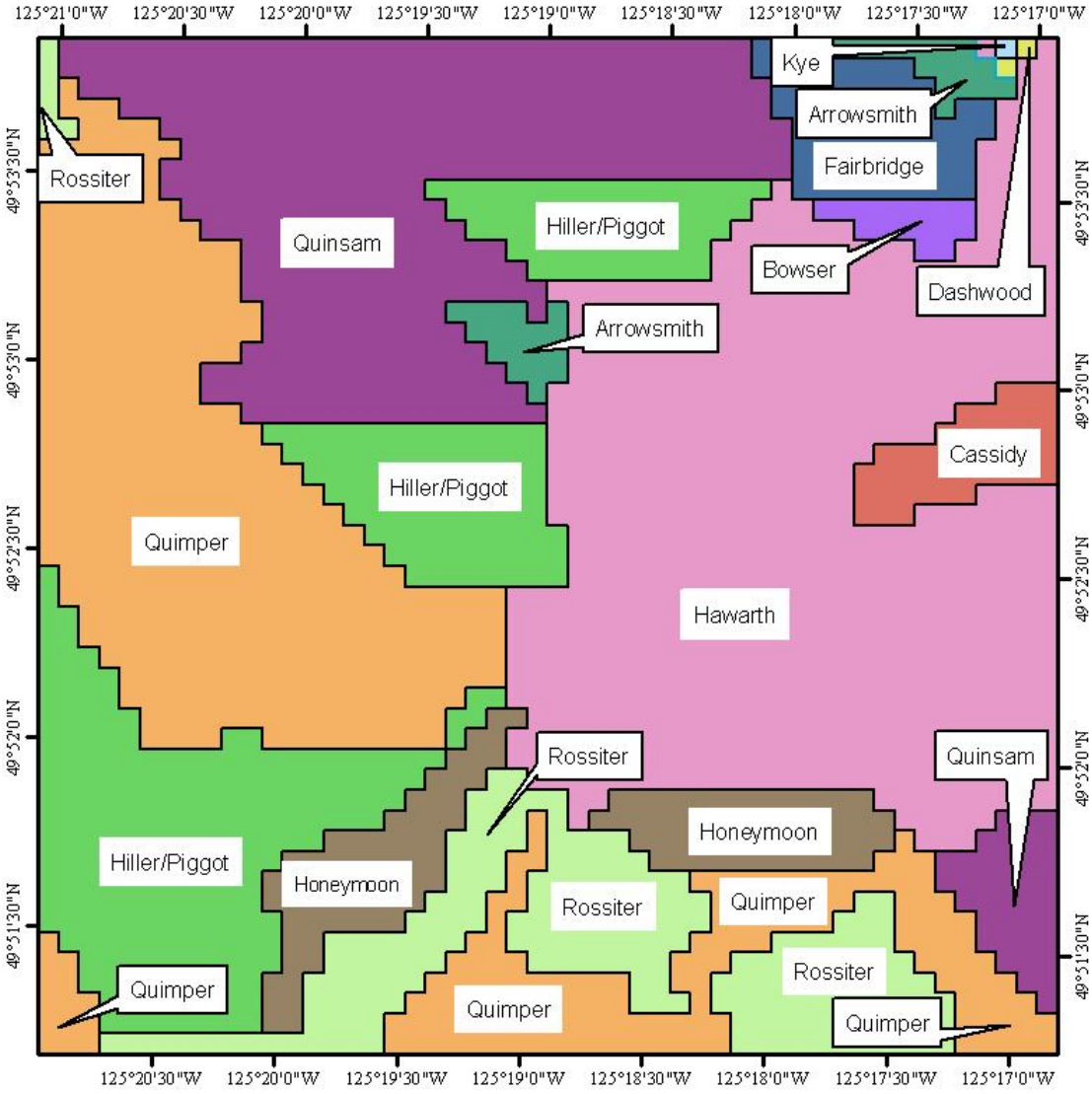

Figure 2. Distribution of soil types in the Oyster River area.

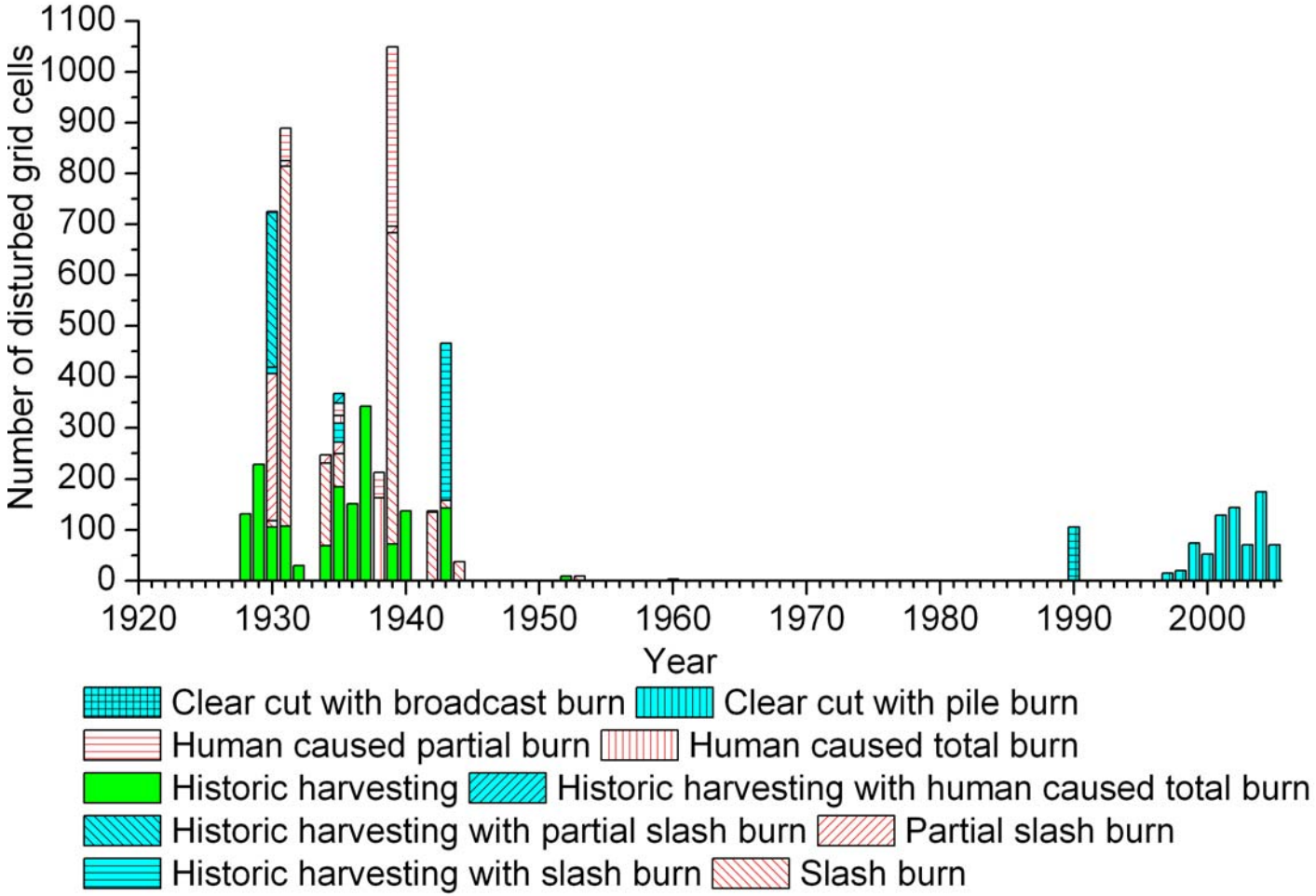

Figure 3. Temporal distribution of disturbed grid cells among the 2500 1 ha grid cells modelled at OR during 1920-2005.

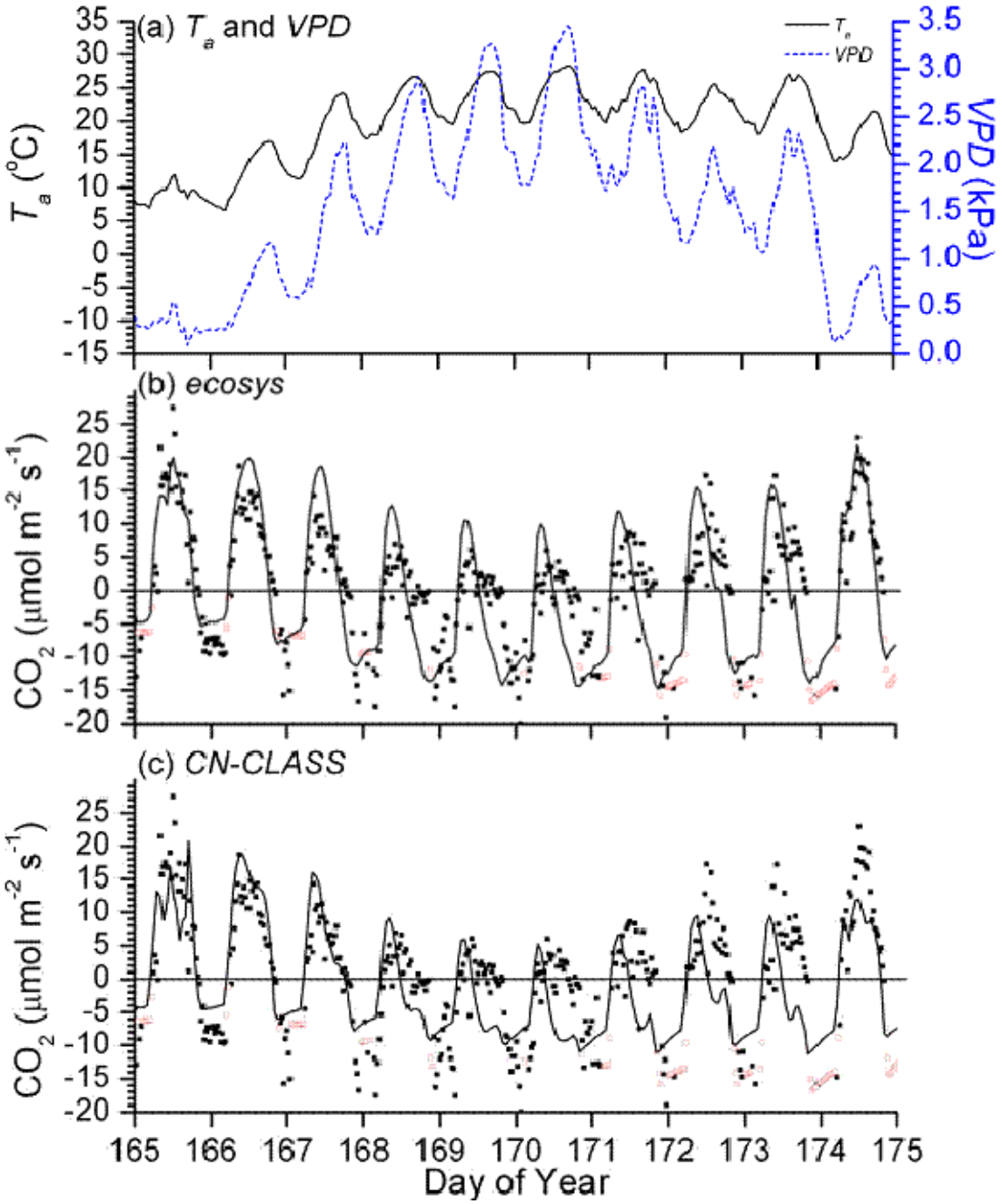

Figure 4. Hourly air temperature and vapor pressure deficit (a) and hourly CO_2 fluxes measured by eddy covariance (closed symbols) or gap-filled from eddy covariance measurements (open symbols) and modelled (lines) by *ecosys* (b) and *C-CLASS* (c) during DOY 166-175 of 2004 in DF49 flux tower fetch area. Positive fluxes represent net C uptake, negative fluxes represent net C emission.

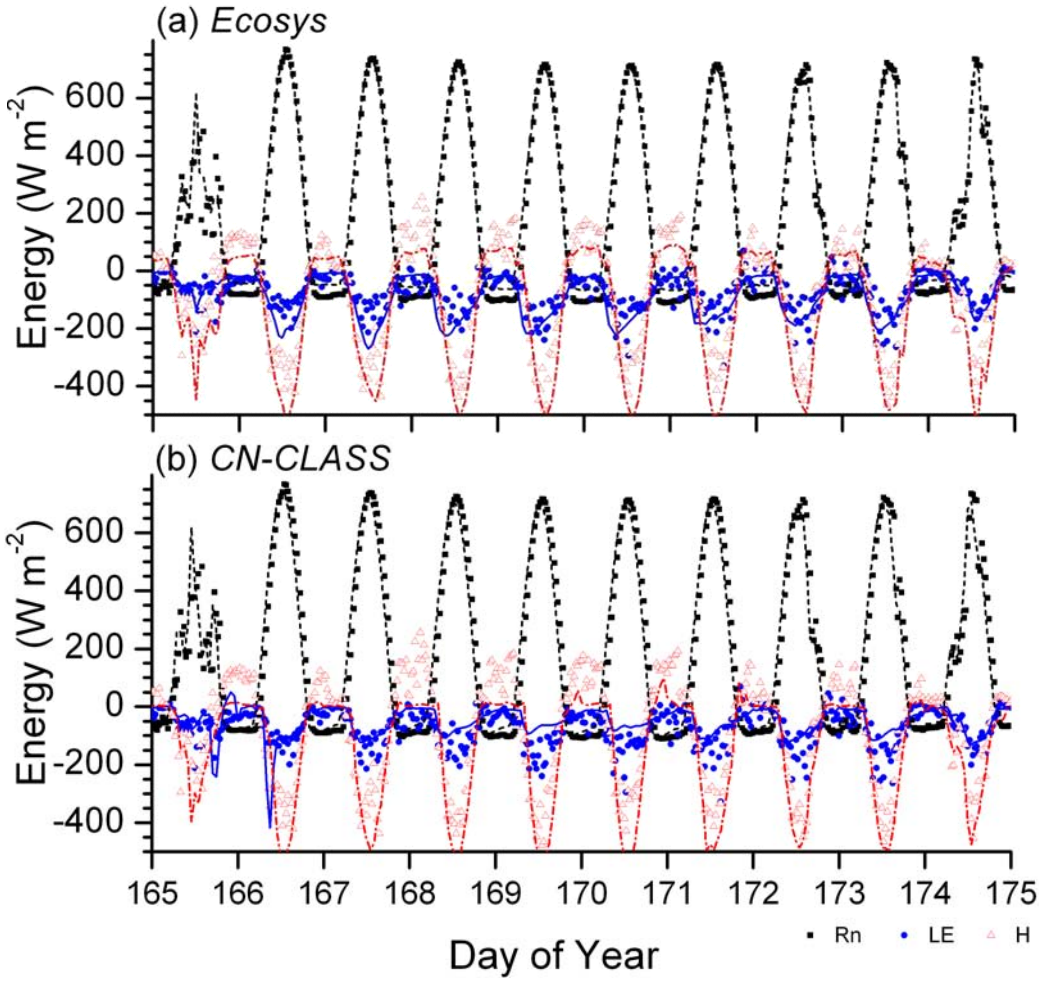

Figure 5. Net radiation (Rn), latent (LE) and sensible (H) heat fluxes measured by eddy covariance (symbols) and modeled (lines) by *ecosys* (a) and *C-CLASS* (b) during DOY 166-175 of 2004 in the DF49 flux tower fetch area.

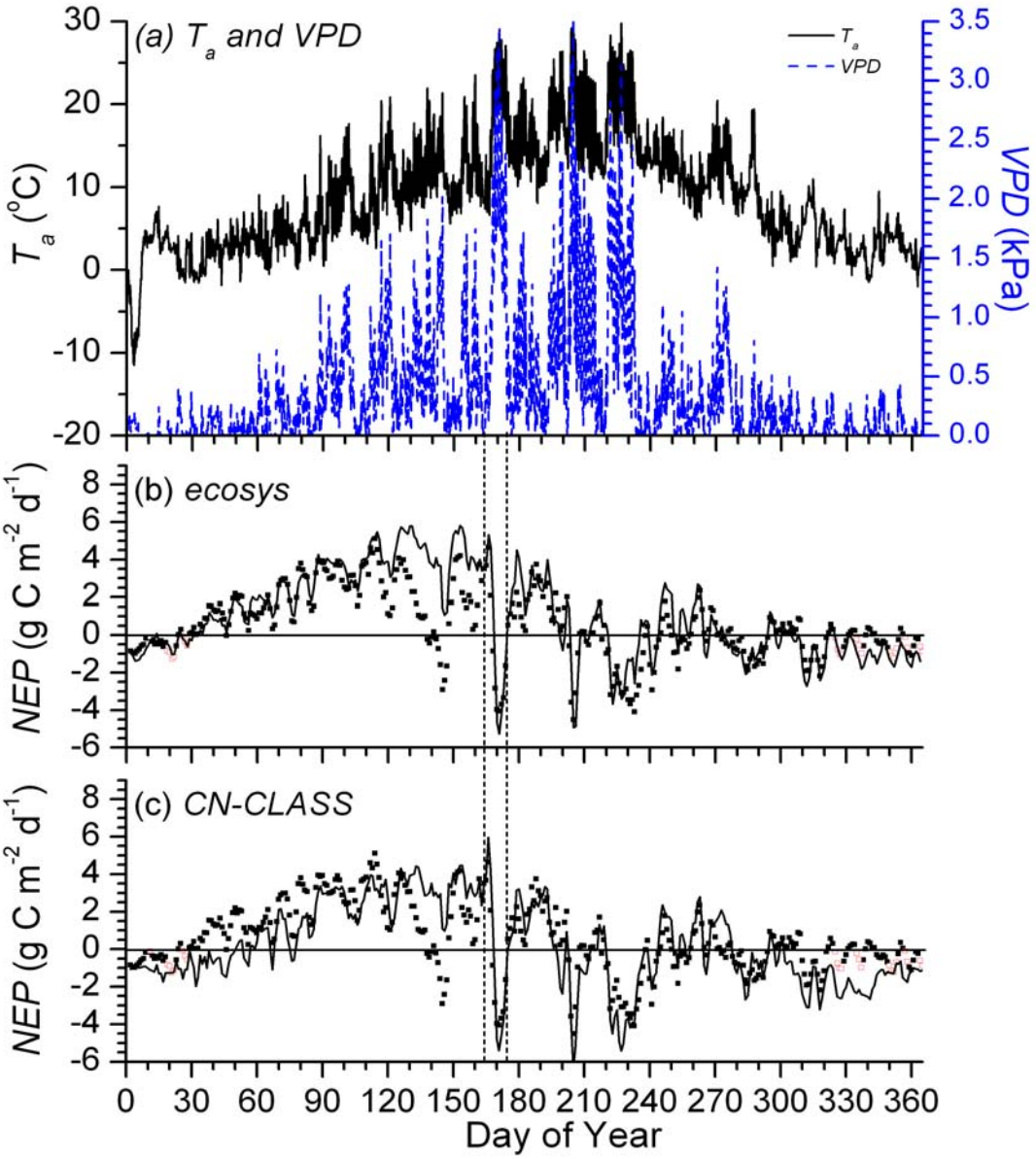

Figure6. Hourly air temperature and vapor pressure deficit (a) and 3-day average of net ecosystem productivity calculated from CO_2 fluxes measured by eddy covariance (closed symbols) or gap-filled from eddy covariance measurements (open symbols) and modelled (lines) by *ecosys* (b) and *C-CLASS* (c) for the year of 2004 in DF49 flux tower fetch area. Vertical lines indicate period shown in Figs. 4 and 5.

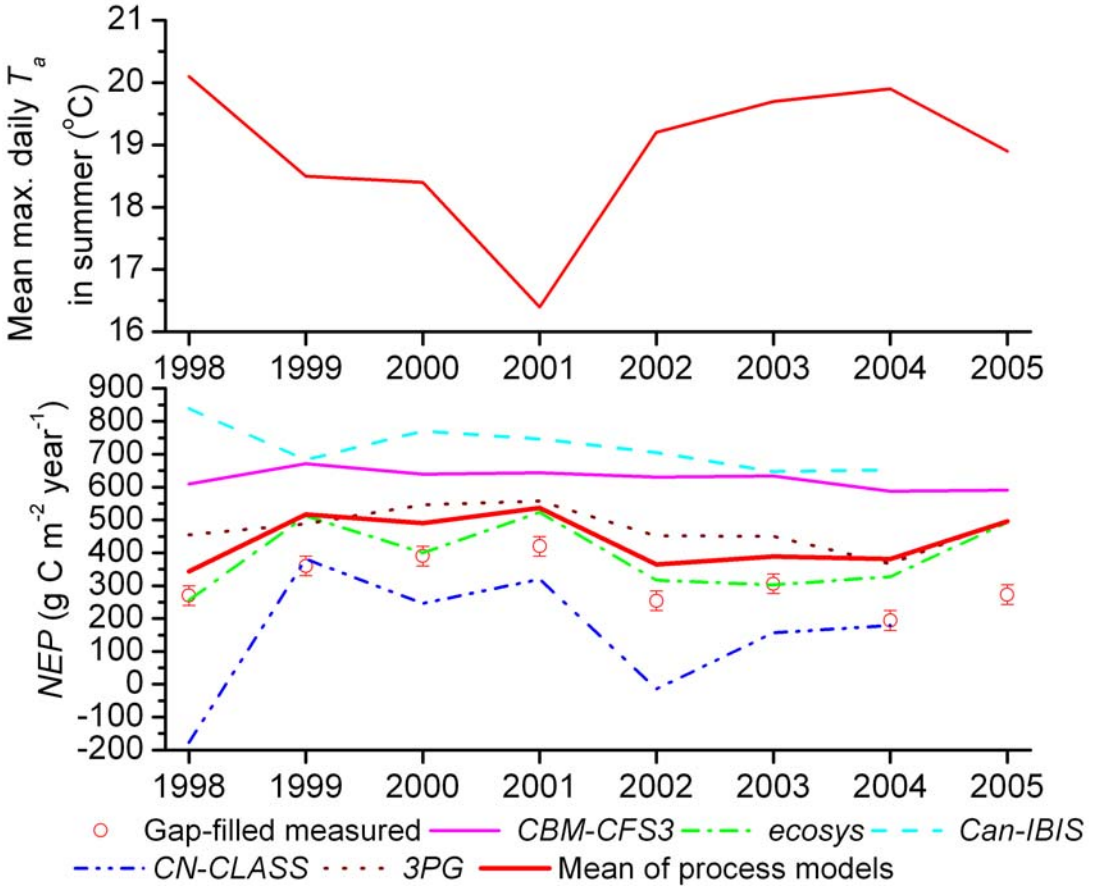

Figure 7. Variation in annual measured *NEP* (with uncertainty of ±30 g C m^{-2} $year^{-1}$ estimated by Morgenstern et al., 2004) and annual footprint-weighted modelled *NEP* with mean maximum daily air temperature in summer during 1998-2005 in the DF49 flux tower fetch area.

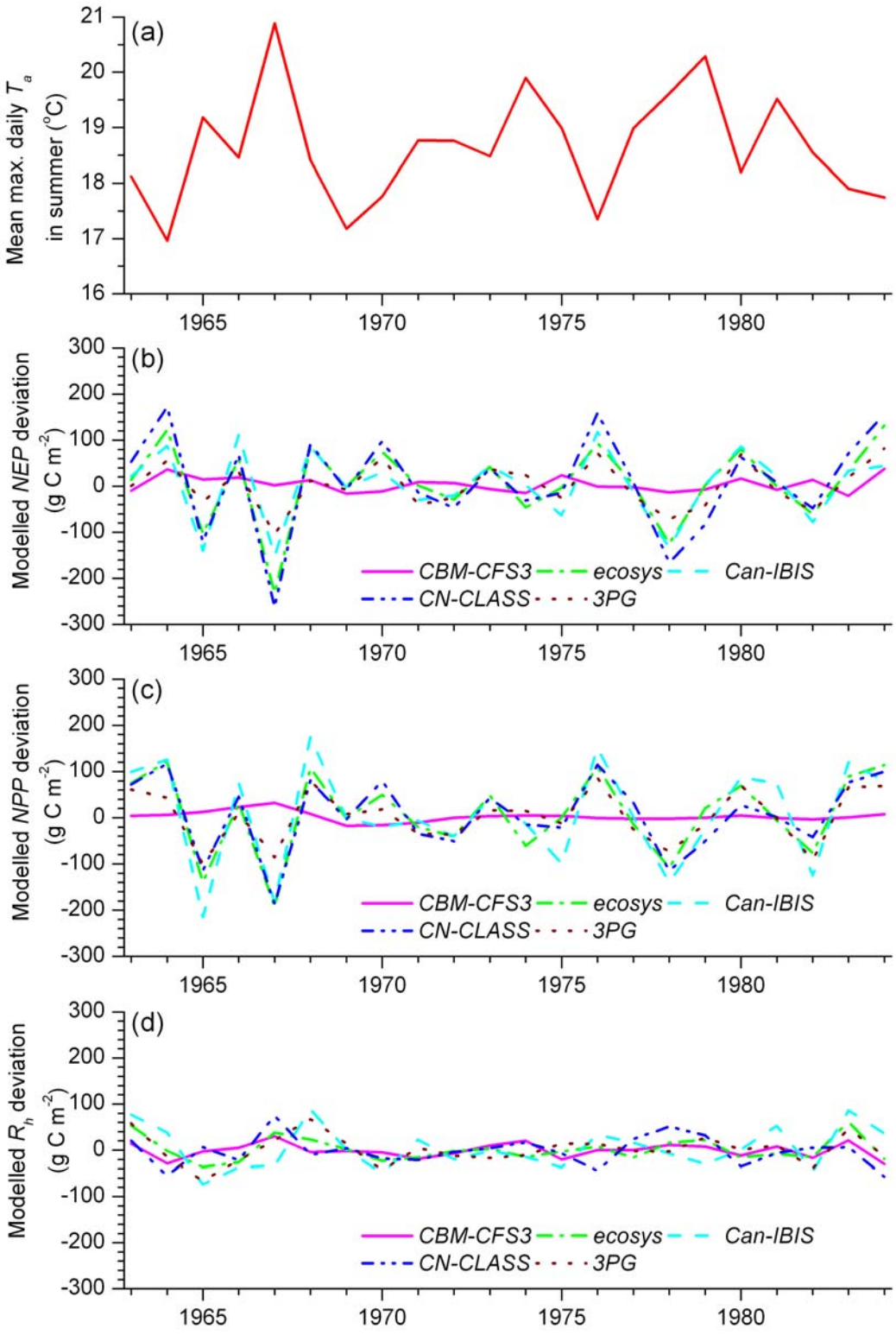

Figure 8. Responses of modelled *NEP, NPP* and R_h to mean daily maximum air temperature in summer during 1963-1984.

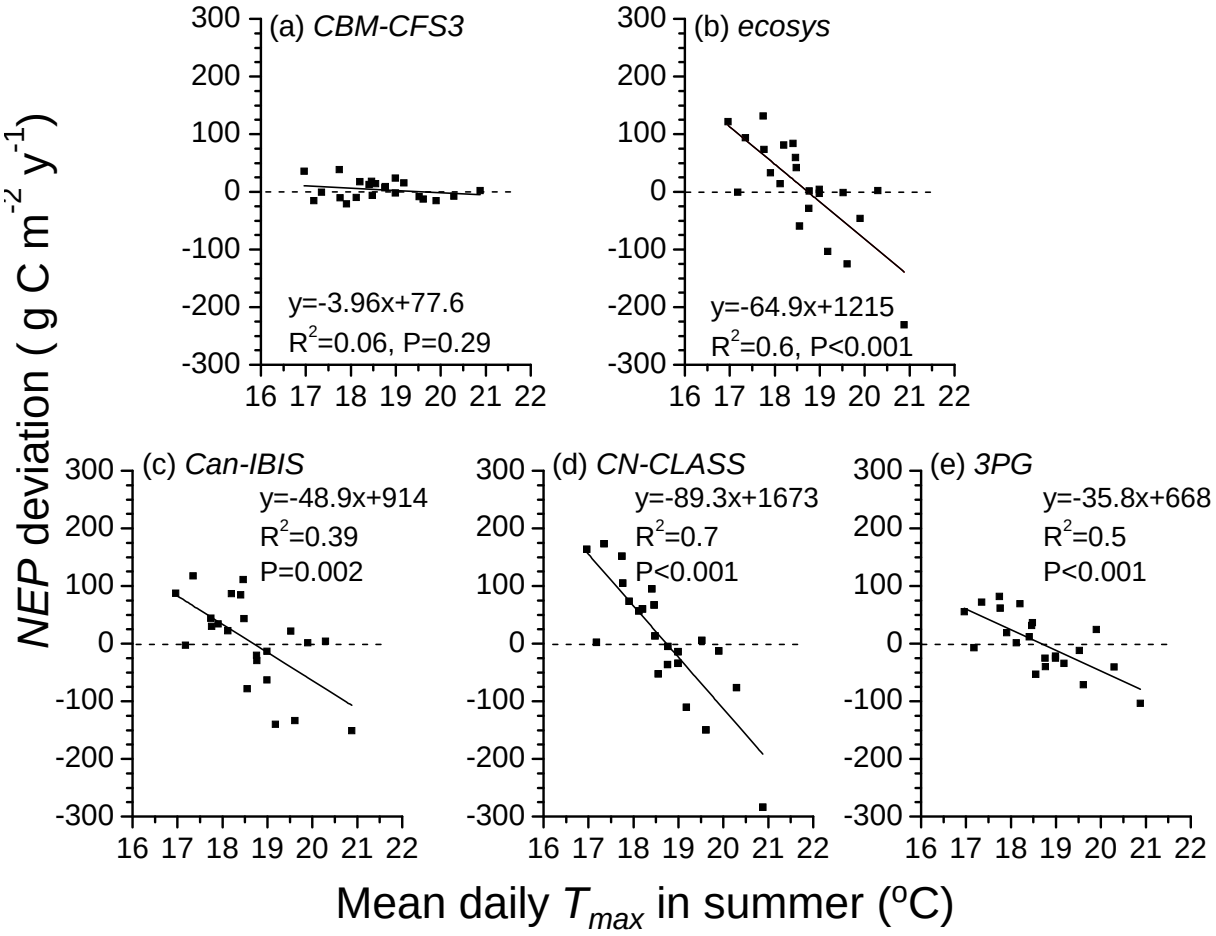

Figure9. Regressions of modelled *NEP* deviations on mean daily maximum temperature in summer during 1963-1984.

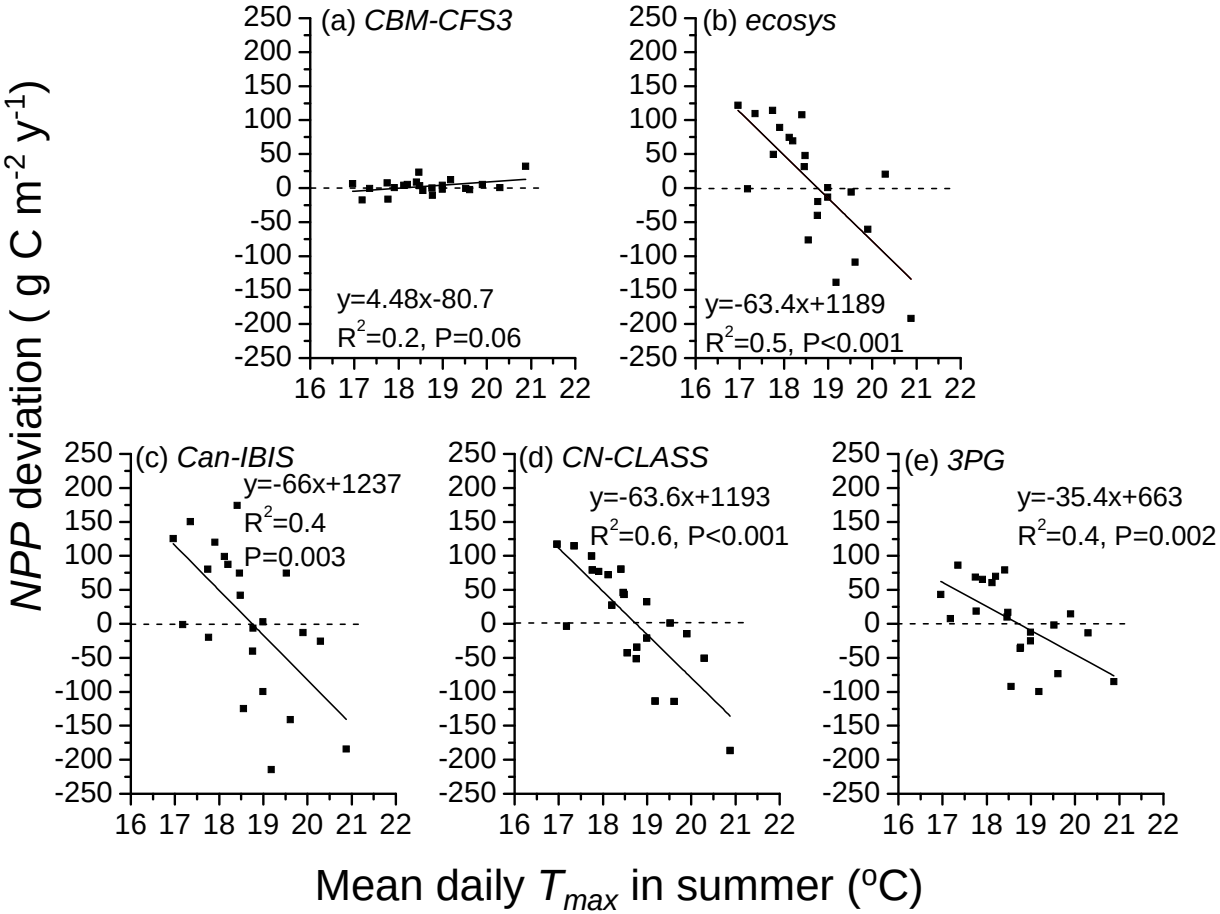

Figure10. Regressions of modelled *NPP* deviations on mean daily maximum temperature in summer during 1963-1984.

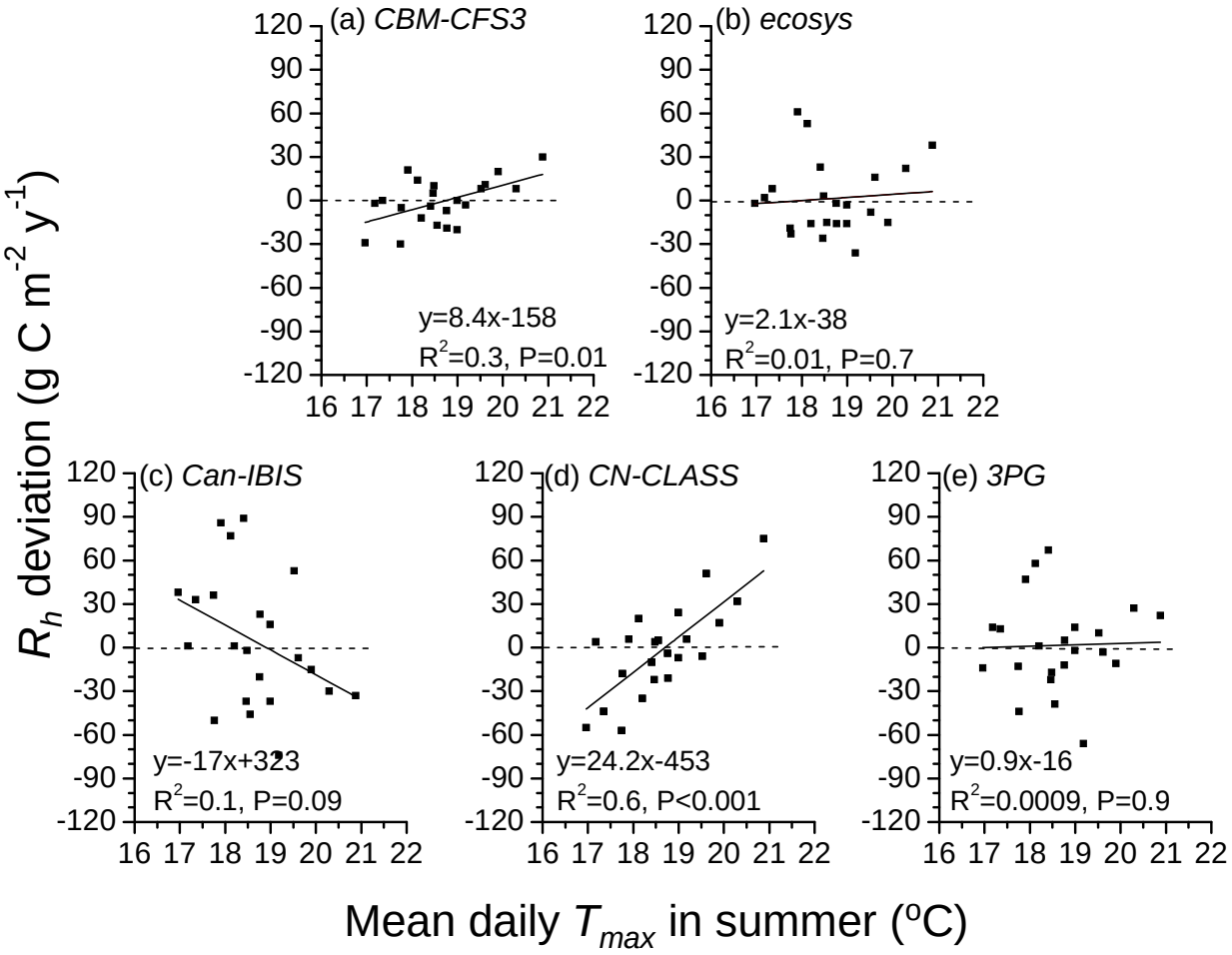

Figure11. Regressions of modelled R_h deviations to mean daily maximum temperature in summer during 1963-1984.

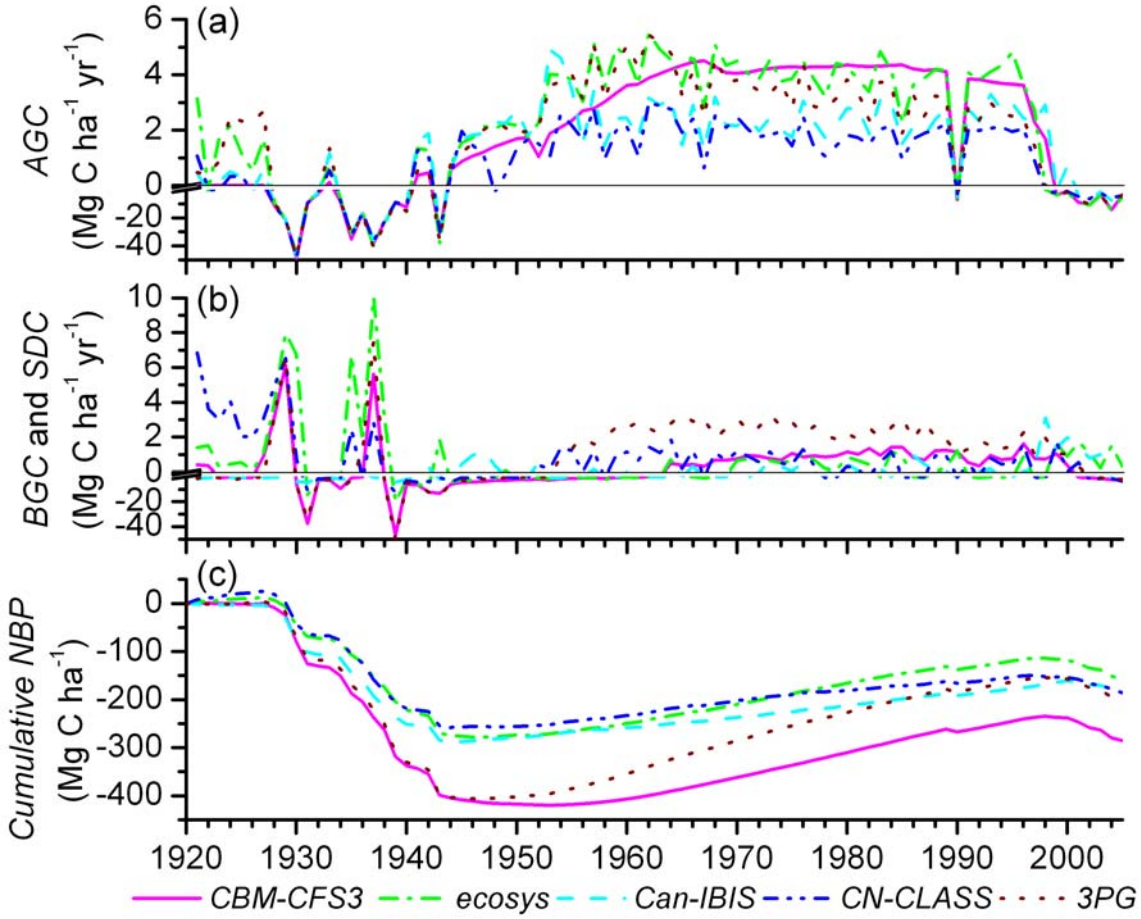

Figure 12. Annual changes in average above-ground living biomass C (*AGC*), below-ground C (*BGC*) and surface dead organic C (*SDC*), and cumulative net biome productivity (*NBP)* modelled in a 2500 ha landscape at OR during 1920-2005.

Appendix B

Model intercomparison to evaluate climate and disturbance effects on interannual variation in net ecosystem productivity of a boreal forest landscape

Z. Wang[a], R. F. Grant[a, ‡], A. Arain[b], P. Bernier[c], B. Chen[b], J. Chen[d], A. Govind[d, §], L. Guindon[c], W. A. Kurz[e], C. Peng[f], D. T. Price[g], G. Stinson[e], J. Sun[f], J. A. Trofymow[e] and J. Yeluripati[b, **]

[a]Department of Renewable Resources, University of Alberta, Edmonton, Alta., Canada, T6G 2E3;
[b]School of Geography and Earth Sciences, McMaster University, Hamilton, Ont., Canada;
[c]Canadian Forest Service, Laurentian Forestry Centre, Quebec City, QC, Canada;
[d]Department of Geography and Program in Planning, University of Toronto, Toronto, Ont., Canada;
[e]Canadian Forest Service, Pacific Forestry Centre, Victoria, BC, Canada;
[f]Institute of Environment Sciences, University of Quebec at Montreal, Montreal, QC, Canada;
[g]Canadian Forest Service, Northern Forestry Centre, Edmonton, Alta., Canada

Keywords: Ecosystem modelling; Carbon flux; Forest productivity; *CBM-CFS3; ecosys; Can-IBIS; C-CLASS; InTEC; TRIPLEX*

‡ Corresponding author. Tel.: +1 780 492 6609; fax: +1 780 492 1767.
E-mail address: Robert.grant@ales.ualberta.ca (R. Grant)
§ Present address: Unité EPHYSE, Institut national de la recherche agronomique (INRA), France.
** Present address: School of Biological Science, University of Aberdeen, Aberdeen, UK.

Abstract

A need has been identified for a simple, process-based algorithm to represent climate effects on annual productivity of forests for use in inventory-based models such as *CBM-CFS3* in which such effects are not currently represented. To develop this algorithm, landscape-level simulations and comparisons of forest productivity were conducted among one inventory model *CBM-CFS3* and five process models *ecosys*, *C-CLASS, Can-IBIS, InTEC* and *TRIPLEX* over a 6275 ha study area in the Chibougamau (CH) area of Quebec, Canada. Simulations of net primary productivity (*NPP*), net ecosystem productivity (*NEP*) and net biome productivity (*NBP*) were driven by daily weather data generated from meteorological records from the CH region from 1928 to 2003, then by hourly weather data recorded at CH from 2004 to 2005, and by data for soil properties, land cover and disturbance events generated from digital GIS layers. Tests of modeled CO_2 fluxes against eddy covariance (EC) measurements during 2004 and 2005 at CH indicated that climate effects on net CO_2 exchange could be summarized as gains in C uptake with warming in spring, but losses with warming in summer. The average annual *NEP* of all models was close to EC-derived values although that of individual models varied widely. Modelled *NEP* and disturbances drove changes in above-ground carbon (*AGC*) from 1928 to 1998 that were close to inventory values in most process models. During this period, variation of annual *NPP* in four of the five process models was positively correlated with mean maximum daily air temperature (T_a) in May-June (P<0.05). These correlations were used to formulate a simple algorithm to modify inventory-based estimates of *NPP* for spring T_a in the CH ecozone. However offsetting effects of summer warming on *NPP* and heterotrophic respiration (R_h) caused the correlation of annual *NEP* with spring T_a to be modelled less consistently.

1. Introduction

Boreal forests account for about 14% of the earth's vegetation cover (Kang et al., 2006) and sequester large amounts of carbon (C) (D'Arrigo, et al., 1987; Sun et al., 2008). The capability of boreal forests to capture C is governed by climate and disturbance (Amiro et al., 2001; Banfield et al., 2002; Rapalee et al, 1998). In Canada, the influence of climate and disturbance on boreal forests has aroused much attention (Chertov et al., 2009; Bergeron et al., 2007) since about 30% of the world's boreal forests are located in Canada (Canadian Forest Service, 2009). Understanding the responses of boreal forest productivity to climate and disturbance help us project future changes in forest C productivity and storage.

These responses may be studied with ecosystem models, which can be classified into inventory-based and process-based types. The most widely used inventory model in Canada is *CBM-CFS3* (Kurz et al., 2009), which constitutes the core component of Canada's national forest carbon monitoring, accounting, and reporting system (Kurz and Apps, 2006). However, as an inventory-based model, *CBM-CFS3* estimates forest productivity on the basis of forest growth curves and doesn't consider interannual variability in climate (Kurz et al., 2009). Process-based models such as *ecosys*, *Can-IBIS*, *C-CLASS, InTEC* and *TRIPLEX* can simulate the responses of forest productivity to different climate scenarios and disturbance regimes (Grant et al., 2007; Liu et al, 2005; Arain et al., 2006; Chen et al., 2003; Peng et al., 2002). One question that has been raised in the Canadian Carbon Program (CCP) was whether or not *CBM-CFS3* could capture climate effects on long-term C exchange of forest landscapes. Therefore, the CCP initiated a historical C model intercomparison project that included a coastal temperate forest landscape at Oyster River (OR) in

British Columbia (Wang et al., in review) and a boreal forest landscape at Chibougamau (CH) in Quebec reported here. The objectives of this intercomparison were (1) to simulate climate and disturbance effects on productivity of a boreal forest landscape using historical climate, disturbance and inventory data with *CBM-CFS3* and diverse process models; (2) to determine if climate effects on productivity in these process models are sufficiently supported by theory and observation to warrant adjusting estimates of annual productivity in *CBM-CFS3* for these effects to improve carbon accounting for boreal forest landscapes such as that at CH.

2. Model descriptions

Model comparisons were conducted among one inventory model *CBM-CFS3* and five process models: *ecosys*, *C-CLASS*, *Can-IBIS, InTEC* and *TRIPLEX*. These models are described in more detail below, with reference to key process algorithms in the Appendix.

2.1. Carbon Budget Model of the Canadian Forest Sector (CBM-CFS3)

2.1.1. Background

The inventory-based model *CBM-CFS3* (Carbon Budget Model of the Canadian Forest Sector, Kurz et al., 2009, http://carbon.cfs.nrcan.gc.ca/CBM-CFS3_e.html) was developed to serve as the key component of Canada's National Forest C Monitoring Accounting and Reporting System (NFCMARS, Kurz and Apps, 2006) and to provide forest managers with a national, regional and operational-scale modelling tool that implements Intergovernmental Panel on Climate Change (IPCC) standards. The *CBM-CFS3* modeling framework simulates the dynamics of all 5 IPCC forest ecosystem carbon pools (above- and below-ground biomass, litter, dead wood, and soils) in annual time steps by integrating forest inventory datasets and monitoring data with information describing dead organic matter and soil C dynamics. The model

inputs include forest inventory, merchantable wood volume yield curves, natural disturbance monitoring data, forest management, harvest and silvicultural activity schedules, land-use change monitoring data, and information describing disturbance impacts.

2.1.2. Ecosystem productivity simulations

CBM-CFS3 tracks C stocks and C stock changes in 10 biomass and 11 dead organic matter (*DOM*) C pools for each forest stand (Kurz et al., 2009). The living biomass pools are classified into merchantable stemwood, other wood, foliage, coarse roots and fine roots both for hardwoods and softwoods. Total live above-ground biomass is calculated from species and region specific volume-age curves of merchantable wood volume and then converted to component biomass pools using a national system of volume-to-biomass models (Boudewyn et al., 2007) and a curve-smoothing algorithm to estimate above-ground biomass at low merchantable wood volumes. Below-ground biomass C (fine and coarse roots) is estimated as a function of above-ground biomass (Li et al., 2003). *DOM* pools are divided into above-ground (snags, leaf and needle litter, fine woody debris, coarse woody debris, dead fine roots, forest floor humus) and below-ground (dead fine roots, dead coarse roots, humified soil C) components and compartmentalized according to their turnover rates. Carbon stock inputs to the *DOM* pools are computed according to biomass turnover and litterfall transfer rates as well as disturbance mortality (Kurz et al., 2009). Losses of *DOM* are explicitly modeled through a pool-type specific decay rate using a Q_{10} relationship based on mean annual air temperature with a fraction transferred to the atmosphere and another fraction to a humified slow *DOM* pool with its own Q_{10} decay rate. Net primary productivity (*NPP*) is calculated as the sum of net growth and litterfall at an annual time step. Heterotrophic respiration (R_h) is the sum of all *DOM*

pool decomposition losses to the atmosphere. Net ecosystem productivity (*NEP*) is estimated as the difference of *NPP* and R_h. Net biome productivity (*NBP*), or net ecosystem carbon balance (*NECB*) integrated over time and space, is calculated as *NEP* minus C losses to disturbances, such as direct emissions to the atmosphere in the event of fire, and transfers of C to the forest product sector in the event of timber harvesting. Losses as dissolved organic C (*DOC*) and dissolved inorganic C (*DIC)* are not estimated, but instead assumed to leave the ecosystem as part of R_h.

2.2. ecosys

2.2.1. Background

The process-based model *ecosys*

(https://portal.ales.ualberta.ca/ecosys/default.aspx; Grant, 2009a,b) was developed at the University of Alberta as a detailed, comprehensive model of terrestrial ecosystems. *Ecosys* is a multi-component model in which hourly rates of transfer processes or state changes are controlled by a set of hypotheses derived from basic chemical, biological and biological theories. The model uses inputs for weather, basic plant and soil properties, and plant and soil management events to simulate carbon, water, heat and nutrient cycling in terrestrial ecosystems at different timescales. *Ecosys* is used to estimate the impacts of weather, land use practices and soil quality on primary productivity, water and atmospheric quality and associated resource requirements (e.g. water, fertilizer) at hourly to centennial timescales.

2.2.2. Ecosystem productivity simulations

The CO_2 fixation rate of each leaf surface (A. 2.4 in Grant et al, 2005) is summed to arrive at a value for gross canopy CO_2 fixation (V_c = *GPP*), with set values for the maximum specific rubisco-limited CO_2 fixation rate (V_{rmax}) and the maximum specific electron transport rate (J_{max}) (A.1.1) (Grant et al., 2005). Canopy temperature effects on rubisco-limited CO_2 fixation rate (V_r) and electron transport

rate (J) follow Arrhenius functions with low and high temperature inactivation (A.1.2). Water stress effects on V_r and J are calculated using an exponential function of canopy turgor potential (ψ_T) from the canopy water potential (ψ_C) at which the difference between energy-driven canopy transpiration and hydraulically-driven total water uptake from all rooted soil layers equals change in plant water content (A.1.3). Nitrogen effects on V_r and J are estimated through functions of leaf structural and non-structural N:C ratios arising from uptake vs. assimilation of C and N (A.1.4). Water stress effect on leaf conductance (g_l) is calculated using an exponential function of ψ_T (A.2.1) related to that on V_r and J. Temperature effect on autotrophic respiration R_a follows an Arrhenius function of canopy or root temperature (A.3.1). Temperature effect on R_h is calculated using an Arrhenius function of soil temperature (T_s) (A.4.1) calculated from a solution to the general heat flux equation driven from surface energy exchange. Water effect on R_h is estimated from the ratio of O_2 uptake (Q_{O2}) and demand (Q'_{O2}) (A.4.2). Water stress effect on decomposition and therefore indirectly on R_h is modelled from competitive inhibition kinetics for specific microbial activity as affected by soil water content (A.4.2).

2.3. Modified version of Integrated Biosphere Simulator (Can-IBIS)

2.3.1. Background

Can-IBIS is a dynamic vegetation model developed by incorporating a soil nitrogen cycling model (Liu et al., 2005) and many other enhancements into the Integrated BIosphere Simulator (IBIS) of Foley et al. (1996). It features a hierarchical structure which simulates biophysical and physiological processes at hourly timescales, and generates outputs at daily to annual intervals over multiple centuries. Annual estimates of net primary productivity are allocated to vegetation C pools, with

accumulations in woody and foliar biomass used to determine dominant plant functional types (PFT) in upper (tree) and lower (shrub and herb) canopies, respectively. Model inputs are meteorological data and soil texture information, together with PFT-specific parameters for physiology, allocation and phenology.

2.3.2. Ecosystem productivity simulations

Photosynthesis is simulated following Farquhar et al. (1980; see also El Maayar et al., 2002), where V_{rmax} is specified for each PFT (A.1.1). Leaf temperature effect on V_r is calculated through a multiplier V_f (A.1.2). Water effects on V_r are estimated using an empirical function of available water content in rootable layers (A.1.3), while nitrogen effects are determined from the N:C ratio of leaves (A.1.4). Water effect on g_l is estimated through the effect on V_r (A.2.1). Temperature effects on R_a and R_h follow modified Arrhenius functions of canopy temperature (T_c) (A.3.1) and T_s (A.4.1), respectively. Soil temperature is simulated from energy balance and forcing climatology, including air temperature (T_a) and net radiation. Water effect on R_h is estimated through a function of the available water content of ice-free soil pore space (θ_s) (A.4.2).

2.4. Carbon and Nitrogen Coupled Canadian Land Surface Scheme (C-CLASS)

2.4.1. Background

The process-based model Canadian Land Surface Scheme (*CLASS*) was originally developed by the Meteorological Service of Canada for coupling into Canadian Global Climate Model (*CGCM*) and Regional Climate Model (Verseghy, 2000). The C- and N coupled version (*C-CLASS*) was developed by incorporating plant and soil carbon and nitrogen cycle algorithms in *CLASS* (Arain et al., 2006). *C-CLASS* simulates ecological, biophysical and physiological processes at half-hourly or

hourly time step (Yuan et al., 2008). Data inputs include meteorological variables, soil textures, vegetation parameters, and disturbance types and intensities.

2.4.2. Ecosystem productivity simulations

In *C-CLASS*, canopy CO_2 fixation is derived by integrating fractional coverage of sunlit and shaded photosynthesis rates (Farquhar et al., 1980), while soil processes are simulated for three soil layers. V_{rmax} is dependent on plant cover types and is a function of total rubisco-related nitrogen (N_{rub}), canopy N inverse decay distance (N_{id}), and leaf area index (*LAI*, with the threshold value of 1). J_{max} is estimated through V_{rmax}. (A.1.1). Leaf temperature effects on V_r and J are estimated through a function of the minimum, optimal and maximum leaf temperature (T_{min}, T_{opt} and T_{max}) (A.1.2). Water effects on V_r and J are estimated through effect on canopy conductance in A.2.1. Nitrogen effect on V_r is estimated through effect on V_{rmax} in A.1.1. Water effect on g_l is calculated using a function of root zone water content (θ), θ at wilting point and at field capacity (A.2.1). Temperature effect on R_a follows a function of Q_{10} values for leaf, wood and root (A.3.1). Temperature effect on R_h is computed using a function of T_s and its Q_{10} values (A.4.1). Water effect on R_h is estimated through a function of θ, one-half field capacity water content (a_1), and one-half porosity (a_2) (A.4.2).

2.5. Integrated Terrestrial Ecosystem C-budget model (InTEC)

2.5.1. Background

InTEC (Integrated Terrestrial Ecosystem C-budget model) was developed to simulate the integrated effects of disturbances, management practices, climate, and atmospheric factors at regional and global scales (Chen et al., 2000; Chen et al., 2003). The model simulates the dynamics of forest carbon stocks at an annual step through an up-scaling algorithm for the leaf-level model and combines the upscaled results with an age-NPP relationship. Inputs include climate, soil texture, nitrogen deposition,

forest stand age and vegetation parameters (e. g., leaf area index and land cover type which can be generated from remotely sensed data).

2.5.2. Ecosystem productivity simulations

InTEC retrospectively initializes C pools in a specified year using a reference year *NPP* generated from the process model *BEPS* then prospectively calculates annual *NPP* using response functions for disturbance and climate factors. In *BEPS*, the maximum rubisco-limited CO_2 fixation rate (V_{rmax}) is fixed (A.1.1). The maximum electron transport rate (J_{max}) is estimated as a linear function of V_{cmax} (A.1.1). Temperature effects on rubisco-limited CO_2 fixation rate (V_r) and electron transport rate (J) are estimated as an exponential function of temperature (A.1.2). Water effects on V_r and J are estimated through effect on canopy conductance (g_c) (A.1.3). Nitrogen effect on V_r is estimated using fixed V_r values for coniferous and broadleaf forests separately (A.1.4). Water effect on leaf conductance (g_l) is calculated using a function of soil water potential content (ψ) (A.2.1). In *InTEC*, temperature effect on autotrophic respiration R_a is estimated through effects on maintenance respiration (R_m) and CO_2 fixation rate by the canopy V_c (A.3.1). Temperature effect on heterotrophic respiration (R_h) is calculated using an exponential function of temperature (A.4.1). Water effect on R_h is estimated using a function of soil moisture (θ) (A.4.2).

2.6. TRIPLEX

2.6.1. Background

TRIPLEX was developed at the Ontario Forest Research Institute of Ontario Ministry of Natural Resources through collaboration with the Forestry and Forest Environment of Lakehead University. The model was developed on the basis of three models *3PG* (Landsberg and Waring, 1997), *TREEDYN* 3.0 (Bossel, 1996) and *CENTURY* 4.0 (Parton et al., 1993) to simulate forest growth and the dynamics of

carbon and nitrogen. Modelling processes of *TRIPLEX* has been described in details by Peng et al. (2002). Calculations were on a monthly time step for carbon flux and allocation, and an annual time step for tree growth, carbon, nitrogen, and water budget. Forest growth and C and N dynamics in the model are primarily driven by solar radiation. Other inputs include environmental factors (T_a, precipitation, soil water and N) and biological factors (forest age, biomass allocation, tree form, mortality).

2.6.2. Ecosystem productivity simulations

For CO_2 fixation, the maximum rubisco-limited CO_2 fixation rate (V_{rmax}) is fixed (A.1.1). The maximum electron transport rate (J_{max}) is estimated as a linear function of V_{cmax} (A.1.1). Temperature effects on rubisco-limited CO_2 fixation rate (V_r) and electron transport rate (J) are estimated as an exponential functions of temperature (A.1.2). Nitrogen effect on V_r is estimated using a function of V_{rmax} (A.1.4). Water effect on leaf conductance (g_l) is calculated using a function of *VPD* and a soil water modifier (A.2.1). Temperature effect on R_h is estimated using Q_{10} (A.4.1).

3. Modelling experiment

3.1. Experimental site

The Chibougamau boreal forest study area (49˚38’44” N - 49˚42’39” N, 74˚23’39” W - 74˚15’31” W, Figure 1) covers 6275 ha. Mean T_a at CH is 0 ^{o}C and annual precipitation is 961 mm (Fluxnet-Canada, 2006). Soils are derived from surficial deposits that are mainly glacial (well drained), fluvio-glacial and organic (poorly drained). Dominant tree species include black spruce (*Picea mariana* (Mill.), jack pine (*Pinus banksiana* Lamb.) and trembling aspen (*Populus tremuloides* Michx.) (Table 1 and Figure 1).

To support process model testing, a flux tower was set up in 2003 at the Eastern Old Black Spruce (EOBS) site within the CH study area at which CO_2 and energy fluxes have since been measured half-hourly as part of the CCP (Coursolle et al., 2006; Figure 1). Above-ground biomass from inventories in 1928 and 1998 at CH, available through the merchantable volume database (Bernier et al., 2010), was used for longer-term model tests. During this period, biomass was affected by disturbances including clearcut (>75% removal), clearcut with regeneration protection (>75% removal), partial cut (25%-75% removal), infrastructure development (100% removal), and light damage due to insect epidemy (Figure 2).

3.2. Model input data

3.2.1. Weather

Daily minimum and maximum T_a during 1928–2005 were calculated from historical weather records. Daily shortwave radiation during this period was generated from daily minimum and maximum T_a. Wind speeds measured at the EOBS flux tower in 2004 (http://fluxnet-canada.ccrp.ec.gc.ca/MeasuredData) were cycled through the simulation period (1928 - 2005). Half-hourly weather data (radiation, T_a, humidity, wind speed and precipitation) were acquired from the EOBS flux tower during 2004-2005 (Figure 1).

3.2.2. Soil types

Five soil types in the CH study area (fluvio-glacial, fine glacial till, coarse glacial till, deep organic and shallow organic) were identified from a vector map of surficial deposit type and soil texture properties. Soil types in each map polygon were allocated to 100 m x 100 m grid cells based on the soil type at the grid cell's centroid. Key properties for soil horizons (field capacity, wilting point, coarse fraction, pH, organic C, total N, and drainage) were derived from the Soil Landscapes of Canada

(SLC Version 3.1) in the CanSIS National Soil Database (CanSIS, 2006). The fluvio-glacial, deep organic and shallow organic soil types were poorly drained (water table depth 0.20 m in spring and 0.80 m in summer). Both fine and coarse glacial tills were well drained.

3.2.3. Forest types

Polygon-based forest cover in 1928 was generated from aerial photographs at the scale of 1:12 000 while forest cover in 1998 was extracted from the forest cover map at the scale of 1:20 000 (Bernier et al., 2010). Forest types in each map polygon were allocated to the 100 m x 100 m grid cells used for soil types based on the forest type at the grid cell's centroid.. The forest stand ages in 1928 were binned into classes of 10, 30, 50, 70, 90 and 120 years. To make the forested area consistent among models, only the 3825 grid cells forested both in 1928 and 1998 were modelled in this study.

3.2.4. Disturbances

Disturbances were identified from aerial photos taken in 1953-1954, 1958-1959, 1965, 1967-68, 1969-70, 1982 and 1998, while disturbances more recent than 1970 were identified from forest inventory maps. About 25% of the 3825 ha forested area was disturbed during 1928-2005 by clearcut, partial cut, or insect epidemy. The main disturbance periods were in 1950 and 1963 (Figure2). In 1950, 130 ha were partially cut, and in 1963, 608 ha were clearcut, 75 ha were partially cut, and 6 ha were slightly damaged by insect epidemy. These disturbances were allocated to the 100 m x 100 m grid cells used for forest and soil types for the years in which they occurred. Disturbance coefficients used in *CBM-CFS3* to estimate transfers of C among model pools for each disturbance type were applied in the process models.

3.3. Modelling protocol

The modelling protocol was similar to that described for an earlier intercomparison (Wang et al., in review). Briefly, the study area was resolved into 6275 grid cells of 100 m × 100 m, for which model runs were constructed using the attributes of the soil and plant types (3.2.2 and 3.2.3) and the disturbances (3.2.4) derived from maps of the study area. In *CBM-CFS3, Can-IBIS*, *InTEC* and *TRIPLEX*, a model run was conducted for each grid cell. In *ecosys* and *C-CLASS*, model runs were conducted for each unique combination of attributes, and results allocated to the grid cells in which these combinations occurred. Some model-specific protocols follow:

3.3.1. CBM-CFS3

Initial dead organic matter and soil (*DOM*) C stocks in 1928 were estimated using a model spin-up procedure (Kurz et al., 2009). The above-ground biomass C (*AGC*) in 1928 was calculated using the inventory-based merchantable volume through the model's built-in volume to biomass conversion algorithm. Softwood and hardwood volumes were calculated separately for each polygon and converted to biomass C. Annual *NPP* increments from 1928 onwards was calculated from growth curves for each forest inventory analysis unit, such as black spruce, jack pine, balsam fir and trembling aspen until a stand-replacing disturbance such as clear cut occurred. After the stand-replacing disturbance, the stand age was reset to zero and existing or, if planted, new growth curves were used to simulate *NPP* during forest regrowth. R_h was calculated as the sum of *DOM* pool decomposition losses which were functions of a temperature modifier (Kurz et al., 2009). *NEP* was calculated as *NPP* minus $R_{h.}$

3.3.2. Process models

Ecosys was seeded with black spruce and/or trembling aspen with a moss understory in the model year 1808, run to 1928 under repeated sequences of weather

data recorded at the EOBS flux tower, and then run to 2005 under the historical weather data (3.2.1). Clear cuts and replantings were modelled later in the 19th century so that stand ages modelled in 1928 agreed with those estimated from the 1928 inventory. Prescribed thinning was applied to simulate background mortality rate generally observed during forest regrowth. Profiles of different soil types were represented by 6 to 8 layers to depths of 0.6 – 1.0 m as indicated in SLC 3.1.

In *Can-IBIS*, a historical spin-up running to 1928 was conducted to stabilize ecosystem C pools. At the start of the simulation period (1928), the biomass densities on every grid cell were adjusted to agree with the *AGC* values inferred from the 1928 inventory. In *C-CLASS*, the 1928 *AGC* provided by *CBM-CFS3* was used to initialize the model. The initial wood biomass, heartwood biomass, root biomass and fine root biomass was assumed as 80%, 60%, 20% and 10% of *AGC* in 1928, respectively. The profile for each soil type was divided into 3 layers with thickness of 10 cm, 25 cm and 375 cm. In *InTEC*, C pools of biomass and soil were initialized assuming that the C and N exchanges between the terrestrial ecosystems and the atmosphere were in equilibrium for those stands at equilibrium age under the mean conditions of climate, CO_2 concentration and N deposition in the pre-industrialization period (Wang et al., 2007). In *TRIPLEX*, tree density, tree height and diameter at breast height (*DBH*) were initialized in 1928 for forest growth and yield simulations.

4. Results

4.1. Model testing against EC CO_2 fluxes

The ability of process models to simulate climate effects on *NEP* is supported by their ability to simulate CO_2 fluxes under changing seasonal weather. These abilities have been tested for boreal and temperate forests in previous studies (Bernier et al., 2010; Grant et al., 2005, 2009a,b; Arain et al., 2002; Liu et al., 2005; Chen et al., 2000; Sun et al., 2008). Here we use *ecosys* and *C-CLASS* as examples of how different

process models simulate daily CO_2 exchange in a cooler year (2004, MAT = -0.4 ^oC) *vs*. a warmer year (2005, MAT = +1.6 ^oC) (Figs. 3 and 4). Regression of daily *NEP* from *ecosys* on that from the EC measurements in 2004 indicated some agreement (slope = 1.01, R^2 = 0.54) (Figure 3b). The corresponding regression from *C-CLASS* indicated that *NEP* was underestimated (slope = 0.23, R^2 = 0.31) (Figure 3c). The regression of daily *NEP* from *ecosys* in 2005 also indicated some agreement (slope= 1.06, R^2 = 0.67) (Figure 4b) while that from *C-CLASS* also indicated underestimation (slope 0.22, R^2 = 0.16) (Figure 4c).

Different seasonal weather patterns caused daily *NEP* to follow different seasonal time courses in 2004 and 2005. Earlier spring warming in 2005 (Figure 4a *vs*. 3a) hastened the onset of net C uptake to DOY 118 from DOY 128 in 2004, raising spring *NEP* (Figure 4b *vs*. 3b). In *ecosys*, earlier net C uptake in spring 2005 vs. 2004 (Figure 5d vs. 5b) was enabled by initiating conifer dehardening and subsequent CO_2 fixation after accumulating a set number of hours (150) at $T_c > 0$ ^oC (e.g. Figure 5c vs. 5a) under lengthening photoperiods (Grant et al., 2009b). After initialization, CO_2 fixation in the model rose rapidly with warming because the Arrhenius functions governing key fixation processes rise sharply with temperature at lower T_a (A.1.2).

However higher summer T_a in 2005 vs. 2004 (e.g. DOY 185 - 195 in Figure 4a vs. 3a) caused greater declines in daily *NEP*, such that modelled and measured net C uptake was lost during days when maximum T_a exceeded 25 ^oC (Figure 4b,c vs. 3b,c). Under these conditions, higher T_a and D in *ecosys* (Figure 5g vs. 5e) forced lower ψ_c (A.1.3), g_l (A.2.1) and hence smaller midafternoon CO_2 influxes (A.1.3) (Figure 5h vs. 5f). Furthermore the Arrhenius functions for CO_2 fixation processes

rise little with temperature at higher T_a (A.1.2). Higher T_a also caused greater R_a (A.3.1), R_h (A.4.1), and hence greater CO_2 effluxes (Figure 5h vs. 5f). The sharp but brief declines of daily *NEP* under higher T_a in *ecosys* thus arose from the combined effects of smaller influxes and larger effluxes (see also Figure 5 in Grant et al., 2009b). In *C-CLASS*, prolonged declines in daily *NEP* with warming in 2005 (Figure 4c) were attributed to the small D_0 value that caused g_l, and hence CO_2 influxes, to decline sharply under rising D (A.2.1) (Arain et al., 2002), and to the large Q_{10} value for R_h that caused CO_2 effluxes to rise sharply with T_s in cooler soils (A.4.1).

The effects of T_a on seasonal CO_2 exchange in the models partly determined their annual *NEP*. These were compared among models for grid cells within the EOBS flux tower fetch during the undisturbed period from 1965 to 2005 (Figure 2), and compared with aggregated gap-filled EC flux measurements at EOBS during 2004-2005 (Figure 6). The models gave low values for annual *NEP* (mostly 0 – 100 g C m^{-2} y^{-1}) with substantial interannual variability caused by weather, overlaying a longer-term trend to lower *NEP* with advancing forest age. However little covariation in annual NEP was apparent among the models, indicating different responses to interannual variation in weather (e.g. Figure 5). Averages of simulated *NEP* from all process models were close to EC-derived values, although *NEP* from individual models diverged.

4.2. Model comparisons with AGC inventory

Decadal-scale *NEP* in the models (Figure 6) was constrained by comparing changes in *AGC* simulated between 1928 and 1998 for all grid cells in the study area with those from forest inventories presented in Bernier et al (2010) (Figure 7). *AGC* modelled in 1928 was determined by model spinup protocols (3.3.2) in which *AGC* of

some models was set to that of the inventory, while *AGC* of others was regenerated from stand-replacing disturbances set to reproduce estimated stand ages in 1928. From 1928 to 1998, rises in modelled *AGC* were driven by *NEP* (Figure 6), but declines were caused by C transfers during disturbances (Figure 2). Changers in below-ground C (*BGC*), also driven by *NEP*, were much smaller than those in *AGC*. The inventory-based *AGC* change during this period was 13.67 Mg C ha^{-1}, while modelled *AGC* changes were 11.03 Mg C ha^{-1} (*CBM-CFS3*), 17.11 Mg C ha^{-1} (*ecosys*), 7.28 Mg C ha^{-1}(*Can-IBIS*), 26.22 Mg C ha^{-1} (*C-CLASS*), 11.02 Mg C ha^{-1} (*InTEC*), and 10.73 Mg C ha^{-1}(*TRIPLEX*). *AGC* changes in *C-CLASS* and *Can-IBIS* deviated above and below the inventory value, while those in the other models were closer (Figure 7).

4.3. Intercomparison of landscape-level NEP and its sensitivity to spring and summer temperature

Temperature effects on interannual variability of *NEP* and its components *NPP* and R_h among the models were further examined for all undisturbed grid cells during 1965-2004 (Figure 8), following intensive disturbance in 1963 (Figure 2). To remove age effects on productivity during this period (Figure 6), *NEP*, *NPP and* R_h were expressed as annual deviations from 7-year moving-averages from all undisturbed grid cells for each model. Most process models gave positive deviations of *NPP* (i.e. *NPP* greater than average) when spring T_a, summarized as mean maximum daily T_a during May and June, exceeded 16 ^{o}C (e.g. in 1968, 1971, 1998, 1999, 2001, 2003, although not in 1975 or 1982), and negative deviations of *NPP* when spring T_a fell below 14 ^{o}C (e.g. in 1969, 1974, 2004). *NPP* deviations from *CBM-CFS* remained zero because this inventory model does not represent weather

effects on *NPP*. However there was no apparent agreement among the process models for interannual variation in R_h and hence *NEP* (Figure 8).

Deviations in annual *NEP*, *NPP* and R_h were regressed on both spring and summer T_a to determine if seasonal effects of T_a on *NEP* (e.g. Figs. 3, 4 and 5) could be identified at an annual time scale (Figure 9). Deviations in annual *NEP* were positively correlated to mean daily maximum T_a during spring in *ecosys* and *InTEC* (R^2 = 0.2 and 0.1 respectively in Figure 9), arising in *ecosys* from the earlier onset of C uptake with earlier spring warming (Figure 4b vs. 3b). These correlations were improved if expressed as partial coefficients in multiple regressions of *NEP* deviations on both spring and summer T_a (R^2 = 0.4 for both models), indicating that the effects on *NEP* of spring T_a could have been partially offset by those of summer T_a as shown for *ecosys* in Figure 5. No significant correlations of annual *NEP* deviations with spring T_a were observed in the other models.

Deviations in annual *NEP* were negatively correlated to mean daily maximum T_a during summer only in *C-CLASS* (R^2 = 0.4 in Figure 10), arising from the prolonged adverse response of daily *NEP* to summer warming in this model (Figure 4c). This correlation was improved if expressed as a partial coefficient in a multiple regression of *NEP* deviations on both spring and summer T_a (R^2 = 0.7), indicating that the effects on *NEP* of summer T_a could have been partially offset by those of spring T_a. No significant correlations of annual *NEP* deviations with summer T_a were observed in the other models. In *ecosys*, this lack of correlation was attributed to the brief duration of the adverse effects of summer warming on daily NEP (Figs. 4b, 5d)

4.4. Intercomparison of landscape-level NPP and its sensitivity to spring and summer temperature

Deviations in annual *NEP* were resolved into those in *NPP* and R_h. No interannual variability in *NPP* was modelled by *CBM-CFS3* as observed earlier. *NPP* deviations were positively correlated to mean maximum T_a during spring in *ecosys, C-CLASS, InTEC* and *TRIPLEX* (R^2 = 0.2, 0.1, 0.3 and 0.2, respectively), but not significantly so in *Can-IBIS* (Figure 11). The stronger correlations of *NPP* with spring T_a in *ecosys* and *InTEC* drove those of *NEP* (Figure 9). *NPP* deviations were negatively correlated to mean maximum T_a during summer in *C-CLASS* (R^2=0.2) (Figure 12), driving the negative correlation of summer T_a with *NEP* (Figure 10). However this correlation was not found in the other models (Figure 12).

4. 5. Intercomparison of landscape-level R_h and its sensitivity to spring and summer temperature

Deviations in annual R_h were positively correlated to mean daily maximum T_a during spring in *C-CLASS* and *TRIPLEX* (R^2 = 0.2 and 0.1 respectively), but negatively correlated in *ecosys* (R^2 = 0.2) (Figure 13). These deviations were positively correlated to mean daily maximum T_a during summer only in *C-CLASS* (R^2=0.3) (Figure 14), contributing to the strongly negative correlation of annual *NEP* to summer T_a in this model (Figure 10). Model deviations in annual R_h were partly affected by *NPP* and hence litterfall in years immediately prior to those on which the deviations were regressed, weakening the correlations.

5. Discussion

Higher spring T_a in boreal forests have been reported to hasten snowmelt (Jarvis and Linder, 2000) and leaf emergence (Black et al., 2000), lengthen the

growing season (Barr et al., 2004), cause higher growing season T_s (Goulden et al., 1998) and lower soil moisture, and hence affect C and water balances. Rises in spring T_a have also caused rises in spring net CO_2 uptake (Barr et al., 2004) as modelled in this study (Figure 5). These rises (e.g. Figure 4 vs. Figure 3; Grant et al., 2009b) caused four of the five process models in this study to simulate positive relationships of spring T_a with annual *NPP* (Figure 11), although only *ecosys* and *InTEC* simulated ones with annual *NEP* (Figure 9). Collectively, this relationship could be summarized for use in inventory models as:

$$NPP_{adj} = NPP_{base} + 9.5 \text{ (avg. spring } T_{a\max} - 16.5)$$

where NPP_{adj} is the temperature-adjusted annual *NPP* (g C m^{-2} y^{-1}), NPP_{base} is the unadjusted *NPP* currently estimated in the inventory model (g C m^{-2} y^{-1}), 9.5 is the average slope of the four significant regressions in Figure 11 (g C m^{-2} y^{-1} $^oC^{-1}$), avg. spring $T_{a\max}$ is the average daily maximum T_a in May and June in a given year (^oC), and 16.5 is the long-term avg. spring $T_{a\max}$ at CH (^oC). The reliable use of this relationship is confined to the site conditions in the CH ecozone and to climatic conditions recorded during the period in which the relationship was developed.

Higher summer T_a in boreal conifers has been reported to lower *NEP* by decreasing net CO_2 fixation (e.g., Grant et al., 2005). Consequently, boreal conifers experience pronounced mid-season declines in *NEP* due to larger R_e and reduced *GPP* (Griffis et al., 2003), as seen in Figs. 3 and 4. These mid-season declines may offset gains in *NEP* with higher spring T_a if spring and summer T_a are correlated, as found for the 1965-2004 period in this study, although the correlation was weak ($R^2 = 0.1$). Consequently variation in spring and summer T_a explained little of the variation in annual *NEP* in most models (Figure 9, 10).

Interannual variability in *NEP* caused by weather in the models was superimposed on longer-term changes in net biome productivity (*NBP*) caused by disturbance and consequent changes in forest age (Chen et al., 2002). *NBP* in the models was adversely affected by *AGC* losses of 5.4-10.9 Mg C ha^{-1} yr^{-1} (Figure 15a) during intensive cutting in 1963 (Figure 2). These losses were partially offset by temporary gains in *BGC* and *SDC* while residues left from the cutting decomposed (Figure 15b), causing declines in *NBP* (Figure 15c). During 1963, these declines varied among the models from 2.7 to 7.5 Mg C ha^{-1}, indicating that greater convergence in modelling *NBP* will require greater consistency in modelling the effects of both weather and disturbances on forest productivity.

Acknowledgements

These results are part of the historical carbon modelling project of the Canadian Carbon Program which is supported through funding from CFCAS and NSERC grants. We thank Robbie Hember for providing constructive comments on the earlier draft. e*cosys* model runs were done on AICT Linux Cluster at University of Alberta and WestGrid Glacier.

References

Amiro, B.D., Stocks, B.J., Alexander, M.E., Flannigan, M.D., Wotton, B.M., 2001. Fire, climate change, carbon and fuel management in the Canadian boreal forest. International Journal of Wildland Fire, 10, 405–413.

Arain, M.A., Black, T.A., Barr, A.G., Jarvis, P.G., Massheder, J.M., Verseghy, D.L. and Nesic, Z., 2002. Effects of seasonal and interannual climate variability on net ecosystem productivity of boreal deciduous and conifer forests. Canadian Journal of Forest Research, 32 (5): 878–891.

Arain, M.A., Yuan, F., and Black, T.A., 2006. Soil-plant nitrogen cycling modulated carbon exchanges in a western temperate conifer forest in Canada. Agricultural and Forest Meteorology, 140:171-192.

Banfield, G.E., Bhatti, J.S., Jiang, H., and Apps, M.J., 2002. Variability in regional scale estimates of carbon stocks in boreal forest ecosystems: results from west-central Alberta. Forest Ecology and Management, 169(1–2): 15–27.

Barr, A.G., Black, T.A., Hogg, E.H., Kljun, N., Morgenstern, K., and Nesic, Z., 2004. Inter-annual variability in the leaf area index of a boreal aspen–hazelnut forest in relation to net ecosystem production. Agricultural and Forest Meteorology, 126(3–4): 237–255.

Bergeron, O., Margolis, H.A., Black, T.A., Coursolle, C., Dunn, A.L., Barr, A.G. and Wofsy, S.C., 2007. Comparison of carbon dioxide fluxes over three boreal black spruce forests in Canada. Global Change Biology, 13:89-107.

Bernier, P.Y., Guindon, L., Kurz, W.A. and Stinson, G., 2010. Reconstructing and modelling 71 years of forest growth in a Canadian boreal landscape: a test of the CBM-CFS3 carbon accounting model. Canadian Journal of Forest Research, 40(1): 109–118.

Black, T.A., Chen, W. J., Barr, A.G., Arain , M.A., Chen, Z., Nesic, Z., Hogg, E.H., Neumann, H.H., Yang, P.C., 2000. Increased carbon sequestration by boreal deciduous forest in years with a warm spring. Geophys. Res. Lett. 27, 1271-1274.

Bossel, H., 1996. *TREEDYN3* Forest Simulation Model. Ecological Modelling, 90: 187–227.

Boudewyn, P., Song, X., Magnussen, S., Gillis, M.D., 2007. Model-based, Volume-to-Biomass Conversion for Forested and Vegetated Land in Canada. Information Report BC-X-411. Natural Resources Canada, Canadian Forest Service, Pacific Forestry Centre, Victoria, BC.

Canadian Forest Service, 2009. The State of Canada's Forests 2009. Natural Resources Canada, Ottawa.

CanSIS, 2006. Soil Survey Data for British Columbia: Southern Vancouver Island. Agriculture and Agri-Food Canada. http://sis.agr.gc.ca/cansis/nsdb/detailed/bc/southvani.zip

Chen, J.M., Ju, W., Cihlar, J., Price, D., Liu, J., Chen, W., Pan, J., Black, A. and Barr, A., 2003. Spatial distribution of carbon sources and sinks in Canada's forests. Tellus, Series B: Chemical and Physical Meteorology, 55:622-641.

Chen, W., Chen, J. and Cihlar, J., 2000. An integrated terrestrial ecosystem carbon-budget model based on changes in disturbance, climate, and atmospheric chemistry. Ecological Modelling 135: 55–79.

Chen, W., Chen, J.M., Price, D.T., and Cihlar, J., 2002. Effect of stand age on net primary productivity of boreal black spruce forest in Ontario, Canada. Canadian Journal of Forest Research 32, 833–842.

Chertov, O., Bhatti, J. S., Komarov, A., Mikhailov, A. and Bykhovets, S., 2009. Influence of climate change, fire and harvest on the carbon dynamics of black spruce in central Canada. Forest Ecology and Management, 257: 941-950.

Coursolle, C., Margolis, H.A., Barr, A.G., Black, T.A., Amiro, B.D., McCaughey, J.H., Flanagan, L.B., Lafleur, P.M., Roulet, N.T., Bourque, C.P.-A., Arain, M.A., Wofsy, S.C., Dunn, A., Morgenstern, K., Orchansky, A.L., Bernier, P.Y., Chen, J.M., Kidston, J., Saigusa, N. and Hedstrom, N., 2006. Late-summer carbon fluxes from Canadian forests and peatlands along an east–west continental transect. Can. J. For. Res. 36(3): 783–800.

D'Arrigo, R., Jacoby, G.C. and Fung, I.Y., 1987. Boreal forests and atmosphere-biosphere exchange of carbon dioxide. Nature, 329, 321–323.

El Maayar, M., Price, D.T., Black, T.A., Humphreys, E.R.and Jork, E-M., 2002. Sensitivity tests of the Integrated BIosphere Simulator (IBIS) to soil and vegetation characteristics in a Pacific Coastal coniferous forest. Atmosphere–Ocean, 40 (3): 313-332.

Farquhar, G.D., von Caemmerer, S. and Berry, J.A., 1980. A biochemical model of photosynthetic CO_2 assimilation in leaves of C3 species. Planta, 149, (1): 78-90.

Fluxnet-Canada, 2006. http://www.fluxnet-canada.ca/

Foley, J.A., Prentice, I.C., Ramankutty, N., Levis, S., Pollard, D., Sitch, S. and Haxeltine A., 1996. An integrated biosphere model of land surface processes, terrestrial carbon balance, and vegetation dynamics. Global Biogeochemical Cycles, 10: 603-623.

Goulden, M.L., Wofsy, S.C., Harden, S.E., Trumbore, S.E., Crill, P.M., Gower, S.T., Fries, T., Daube, B.C., Fan, S.-M., Dutton, D.J., Bazazz, A. and Munger, J.W.,

1998. Sensitivity of boreal forest carbon balance to soil thaw. Science, 279: 214–217.

Grant, R. F., Arain, A., Arora, V., Barr, A., Black, T. A., & Chen, J., Wang S., Yuan F., and Zhang Y., 2005. Intercomparison of techniques to model high temperature effects on CO_2 and energy exchange in temperate and boreal coniferous forests. Ecological Modelling, 188(2-4), 217-252.

Grant, R. F., Barr, A. G., Black, T. A., Gaumont-Guay, D., Iwashita, H., & Kidson, J. et al., 2007. Net ecosystem productivity of boreal jack pine stands regenerating from clearcutting under current and future climates. Global Change Biology, 13(7), 1423-1440.

Grant, R.F., Barr, A.G., Black, T.A., Margolis, H.A., Dunn, A.L., Metsaranta, J. and Wang, S., 2009a. Interannual variation in net ecosystem productivity of Canadian forests as affected by regional weather patterns – a Fluxnet-Canada synthesis. Agricultural and Forest Meteorology, 149:2022–2039.

Grant, R.F., Margolis, H.A., Barr, A.G., Black, T.A., Dunn, A.L., Bernier, P.Y., and Bergeron, O., 2009b. Changes in net ecosystem productivity of boreal black spruce stands in response to changes in temperature at diurnal and seasonal timescales. Tree physiology 29, (1): 1-17.

Griffis, T.J., Black, T.A., Morgenstern, K., Barr, A.G., Nesic, Z., Drewitt, G.B., Gaumont-Guay, D. and McCaughey, J.H., 2003. Ecophysiological controls on the carbon balances of three southern boreal forests. Agric. For. Meteorol. 117: 53–71.

Jarvis, P. and Linder, S., 2000. Constraints to growth of boreal forests. Nature, 405: 904–905.

Kang, S., Kimball, J. and Running, S., 2006. Simulating effects of fire disturbance and climate change on boreal forest productivity and evapotranspiration. Science of the Total Environment, 362, 85–102.

Kurz, W.A., and Apps, M.J., 2006. Developing Canada's National Forest Carbon Monitoring, Accounting and Reporting System to meet the reporting requirements of the Kyoto Protocol. Mitig. Adapt. Strategies Glob. Change, 11(1): 33–43.

Kurz, W.A., Dymond, C.C., White, T.M., Stinson, G., Shaw, C.H., Rampley, G.J., Smyth, C., Simpson, B.N., Neilson, E.T., Trofymow, J.A., Metsaranta, J., and Apps, M.J., 2009. CBM-CFS3: A model of carbon-dynamics in forest and land-use change implementing IPCC standards. Ecological Modelling, 220: 480-504.

Landsberg, J. J., and Waring R. H., 1997. A generalised model of forest productivity using simplified concepts of radiation-use efficiency, carbon balance and partitioning. Forest Ecology and Management, 95: 209-228.

Li, Z., Kurz, W.A., Apps, M.J. and Beukema, S.J., 2003. Belowground biomass dynamics in the carbon budget model of the canadian forest sector: Recent improvements and implications for the estimation of *NPP* and *NEP*, Canadian Journal of Forest Research, 33, (1): 126-136.

Liu, J., Price, D. T. and Chen, J. M., 2005. Nitrogen controls on ecosystem carbon sequestration: A model implementation and application to Saskatchewan, Canada, Ecological Modelling, 186, (2): 178-195.

Parton, W.J., Scurlock, J.M., Ojima, D.S., Gilmanov, T.G., Scholes, R.J., Schimel, D.S., Kirchner, T., Menaut, J-C., Seastedt, T., Garcia Moya, E., Kamnalrut, A. and Kinyamario, J.I., 1993. Observations and modelling of biomass and soil

organic matter dynamics for the grassland biome worldwide. Global Biogeochem. Cycles 7, 785–809.

Peng, C., Liu, J., Dang, Q., Apps, M. J. and Jiang, H., 2002. TRIPLEX: a generic hybrid model for predicting forest growth and carbon and nitrogen dynamics. Ecological Modelling 153, 109-130.

Rapalee, G., Trumbore, S.E., Davidson, E.A., Harden, J.W. and Veldhuis, H., 1998. Soil carbon stocks and their rate of accumulation and loss in a boreal forest landscape. Global Biogeochemical Cycle 12, 687–701.

Sun, J., Peng, C., McCaughey, H., Zhou, X., Thomas, V., Berninger, F., St-Onged, B. and Hua, D., 2008. Simulating carbon exchange of Canadian boreal forests II. Comparing the carbon budgets of a boreal mixedwood stand to a black spruce forest stand. Ecological Modelling, 219, 276–286.

Verseghy, D.L., 2000. The Canadian Land Surface Scheme (CLASS): Its history and future. Atmosphere-Ocean, 38: 1-13.

Wang, S., Chen, J., Ju, W., Feng, X., Chen, M., Chen, P., and Yu, G., 2007. Carbon sinks and sources in China's forests during 1901–2001. Journal of Environmental Management, 85: 524–537.

Wang, Z., Grant, R. F., Arain, M. A., Chen, B., Coops, N., Hember, R., Kurz, W. A., Price, D. T., Stinsond, G., Trofymowd, J.A. and Yeluripatib, J., in review. Model intercomparison to evaluate climate effect on interannual variation in net ecosystem productivity of a coastal temperate forest landscape. Ecological Modelling.

Yuan F., Arain M.A., Barr A., Black T.A., Bourque P.-A., Coursolle C., Margolis H., McCaughey H., and Wofsy S.C., 2008. Modeling analysis of primary controls on net ecosystem productivity of seven boreal and temperate coniferous

forests across an east-west continental transect in Canada. Global Change Biology, 14: 1–20, doi: 10.1111/j.1365-2486.2008.01612.x.

Table 1. Site characteristics of the Chibougamau area.

Mean annual temperature: 0 ^{o}C
Annual precipitation: 961 mm
Average elevation: 239.9 m
Surficial deposits: glacier deposit; fluvio-glacial deposit; organic deposit
Tree species: black spruce (*Picea mariana* (Mill.); Jack pine (*Pinus banksiana* Lamb.); Trembling Aspen (*Populus tremuloides* Michx.)
Main disturbance types: clearcut; clearcut with regeneration protection; partial cut; infrastructure; light damage due to insect epidemy

Table 2. Responses of modelled NEP in the undisturbed grid cells to mean daily maximum air temperature in May-June and July-August during 1965-2004.

Model	Mean daily maximum T_a in May-June	Mean daily maximum T_a in July-August
Ecosys	0.4	ns
Can-IBIS	ns*	ns
C-CLASS	ns	-0.7
InTEC	0.4	ns
TRIPLEX	ns	ns

* ns stands for not significant.

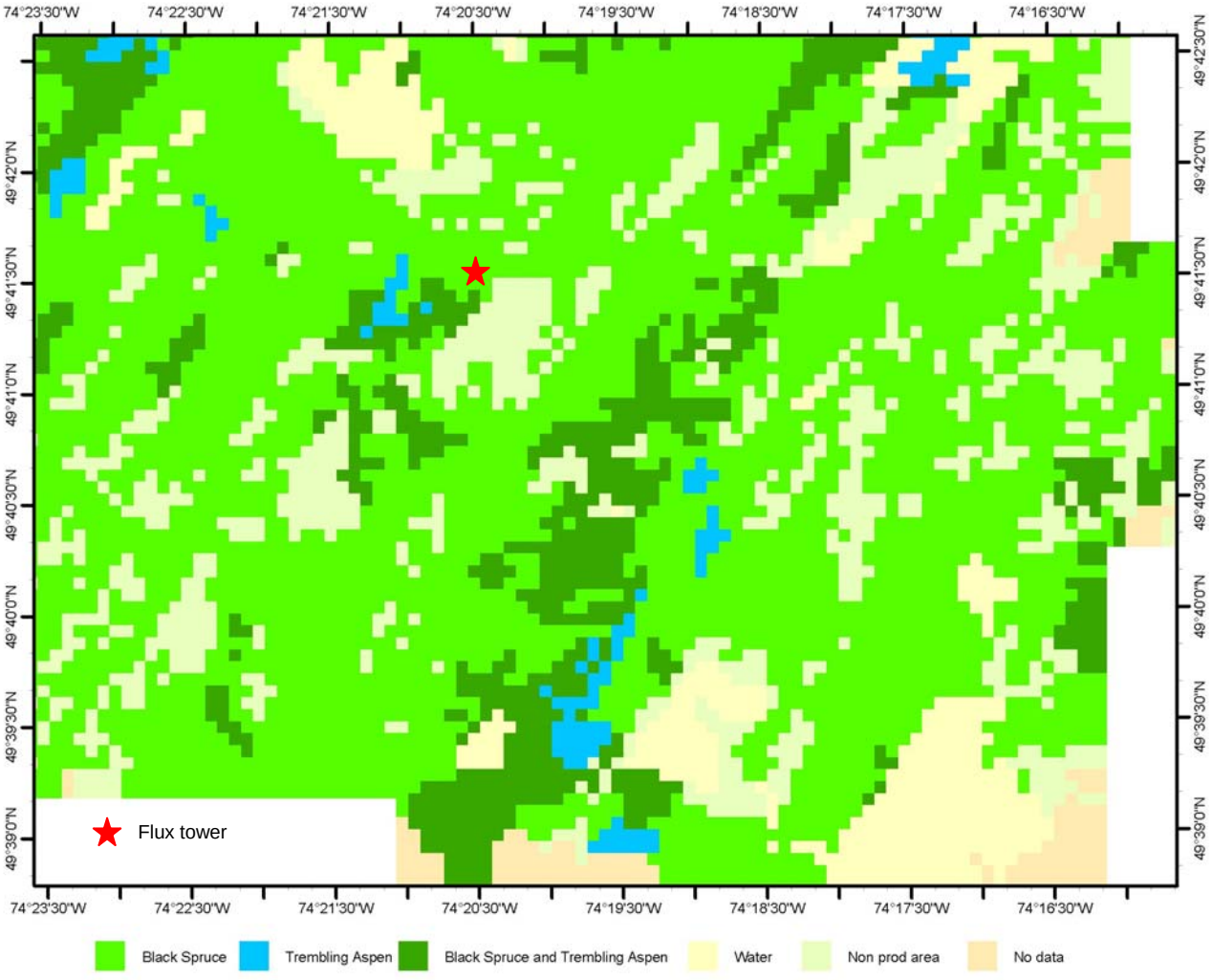

Figure 1. Location of Chibougamau study area and spatial distribution of tree species in 1998. For simplification, the species was grouped into three categories: black spruce, trembling aspen, and the mixed black spruce and trembling aspen. The EOBS flux tower is within this study area.

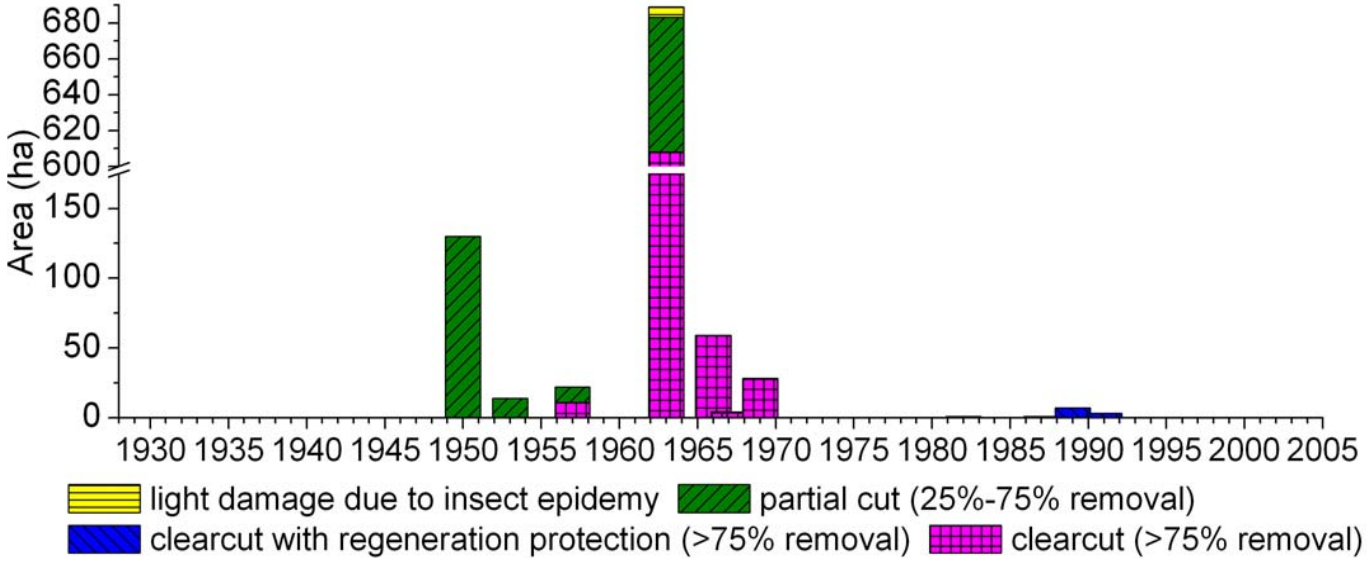

Figure 2. Temporal distribution of disturbances during 1928-2005.

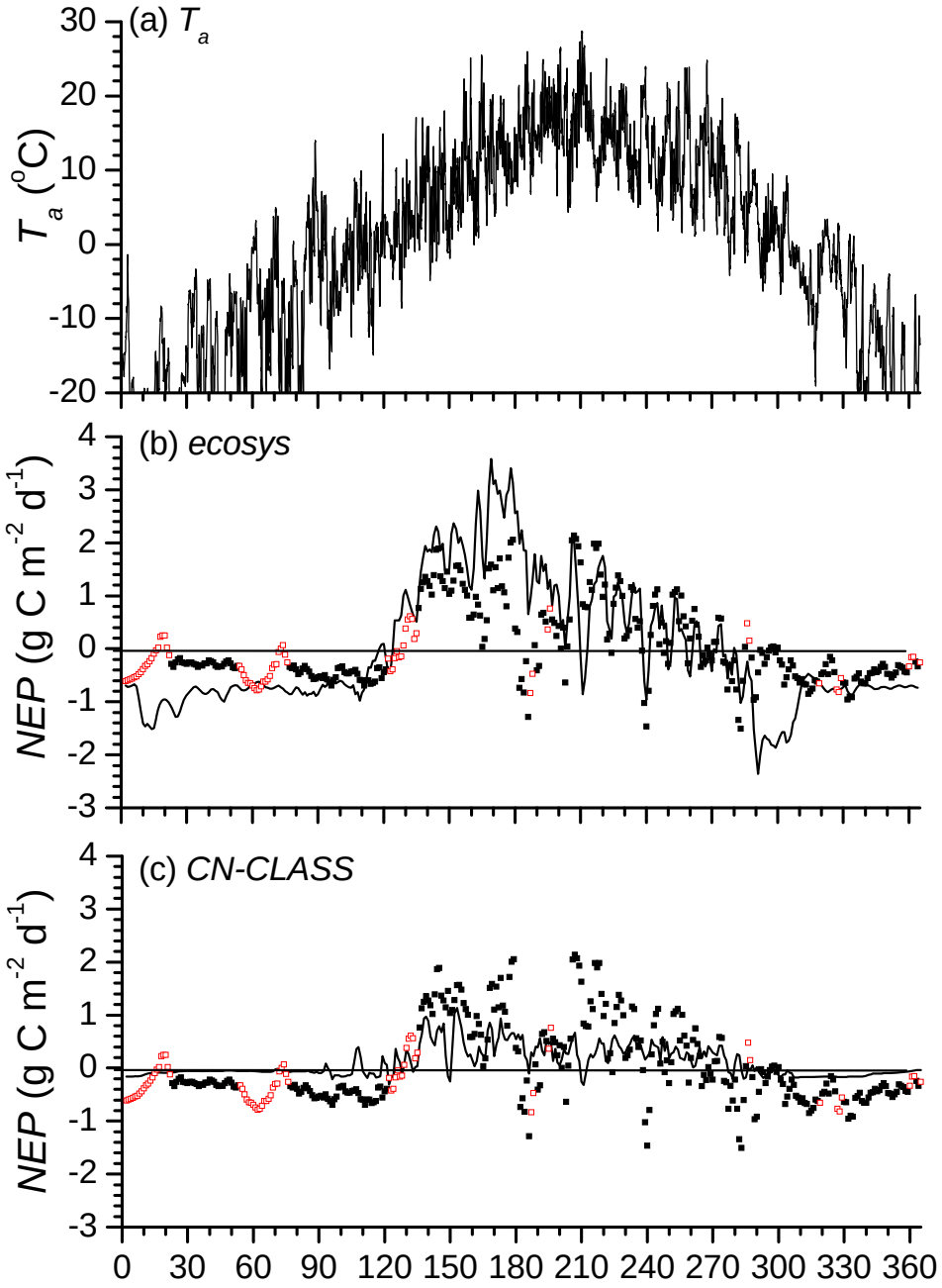

Figure 3. Hourly air temperature (a) and 3-day average of net ecosystem productivity calculated from CO_2 fluxes measured by eddy covariance (closed symbols) or gap-filled from eddy covariance measurements (open symbols) and modelled (lines) by *ecosys* (b) and *C-CLASS* (c) for the year of 2004 in flux tower fetch area.

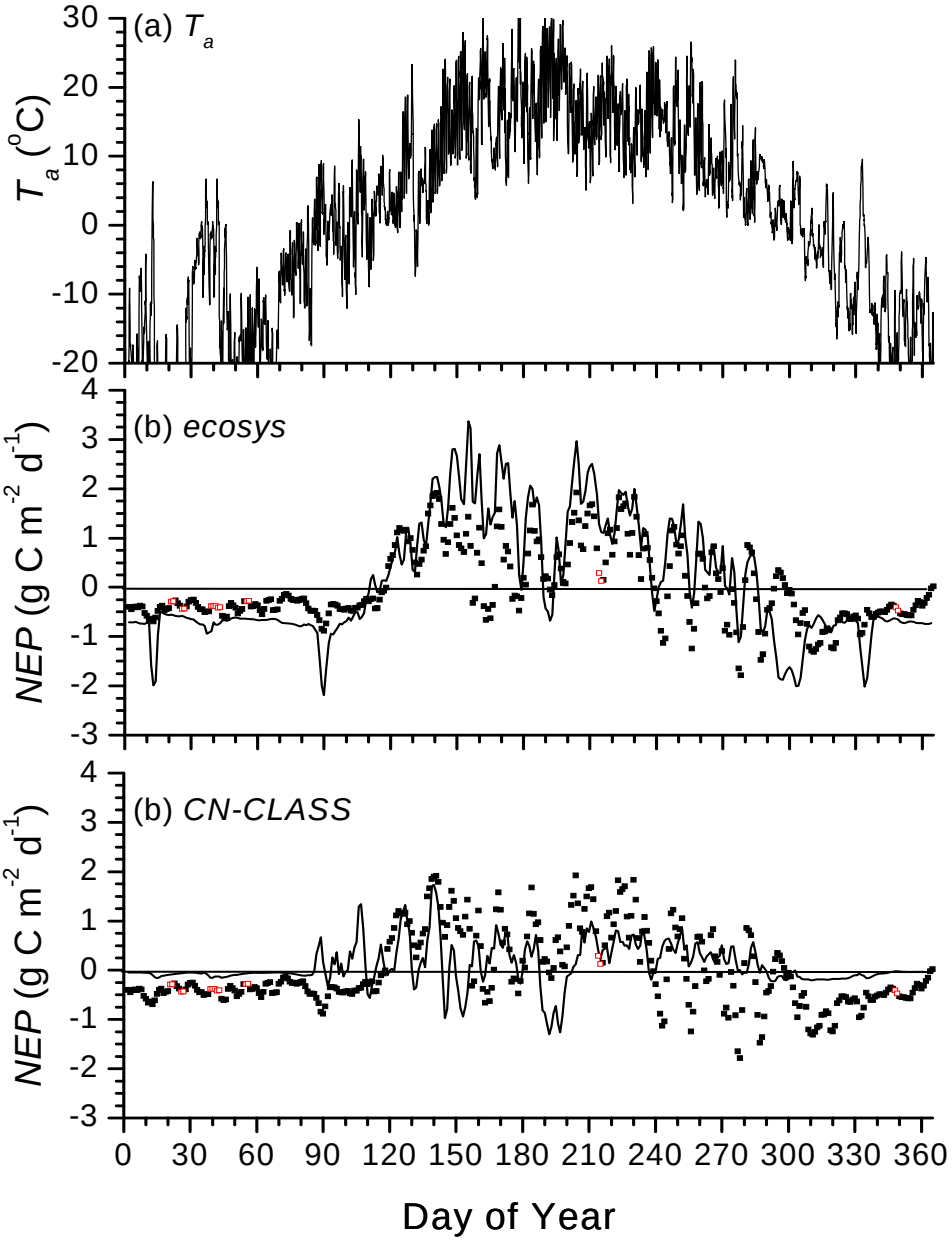

Figure 4. Hourly air temperature (a) and 3-day average of net ecosystem productivity calculated from CO_2 fluxes measured by eddy covariance (closed symbols) or gap-filled from eddy covariance measurements (open symbols) and modelled (lines) by *ecosys* (b) and *C-CLASS* (c) for the year of 2005 in flux tower fetch area.

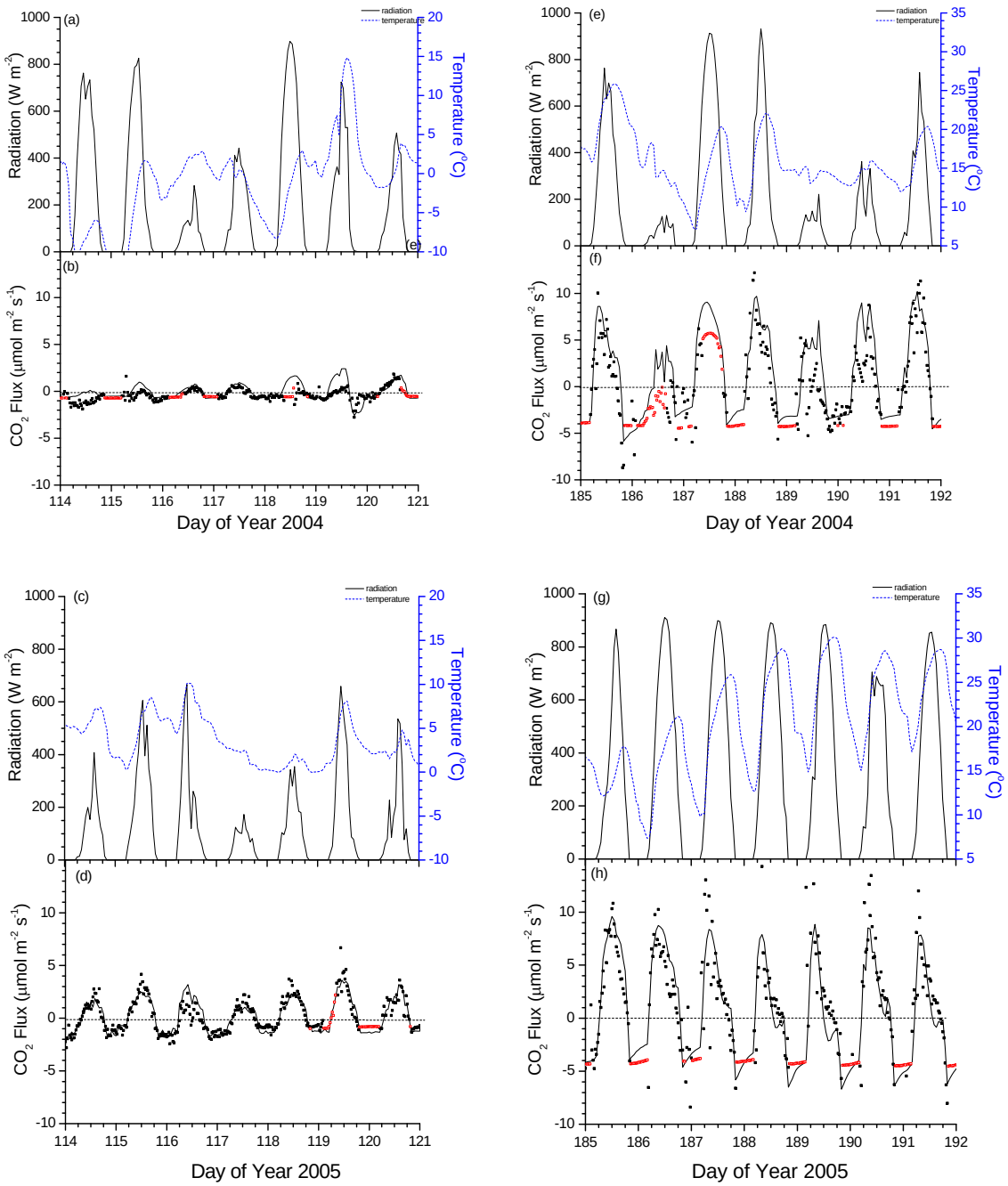

Figure 5. Radiation, temperature and CO_2 exchange measured or gap-filled (solid or open symbols) and modelled by *ecosys* (lines) at EOBS during (a-d) spring (DOY 115 – 121) and (e-h) summer (DOY 186-192) in 2004 and 2005

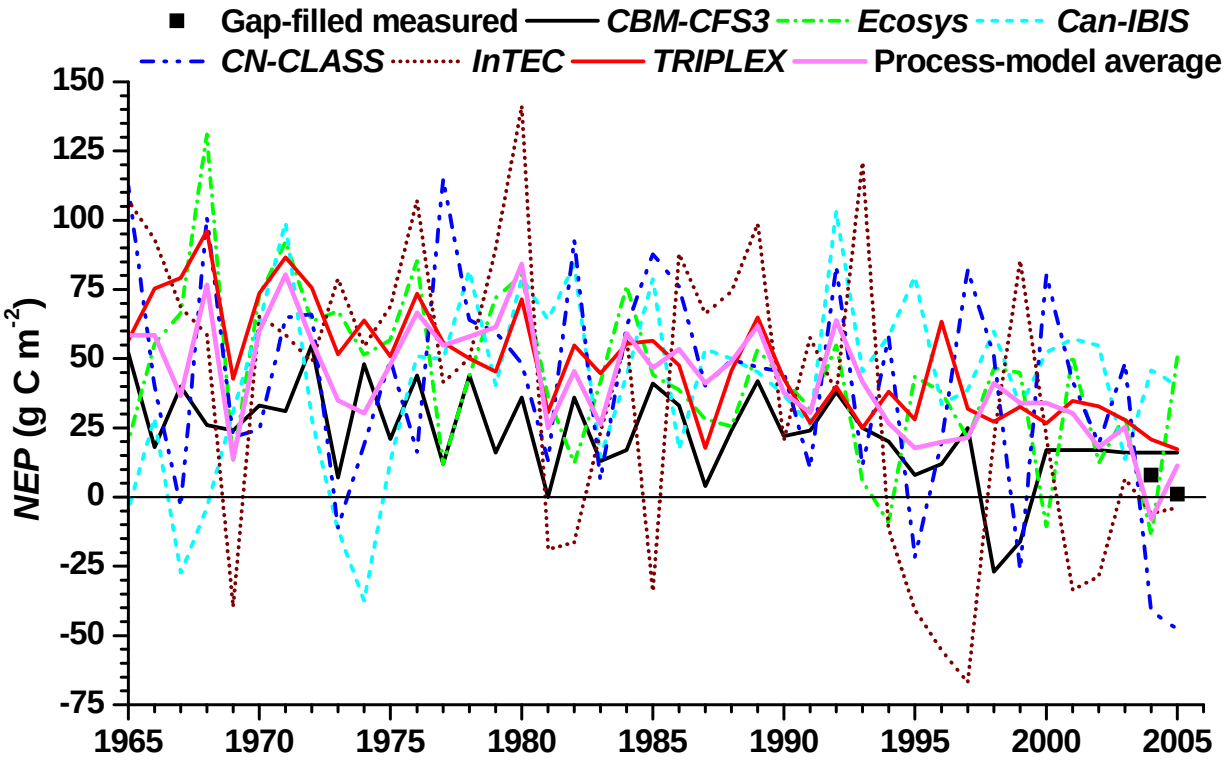

Figure 6. Modelled NEP during 1965-2005 and measured values in 2004-2005 in the fetch area of the EOBS flux tower.

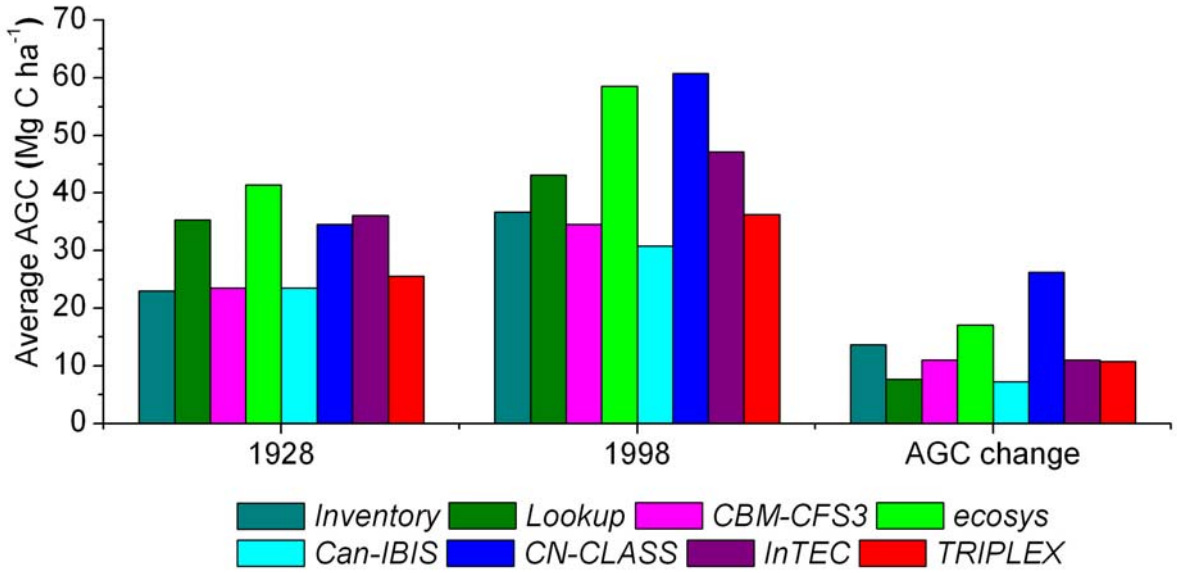

Figure 7. Above-ground C (AGC) change between 1928 and 1998 for all grid cells in the Chibougamau study area.

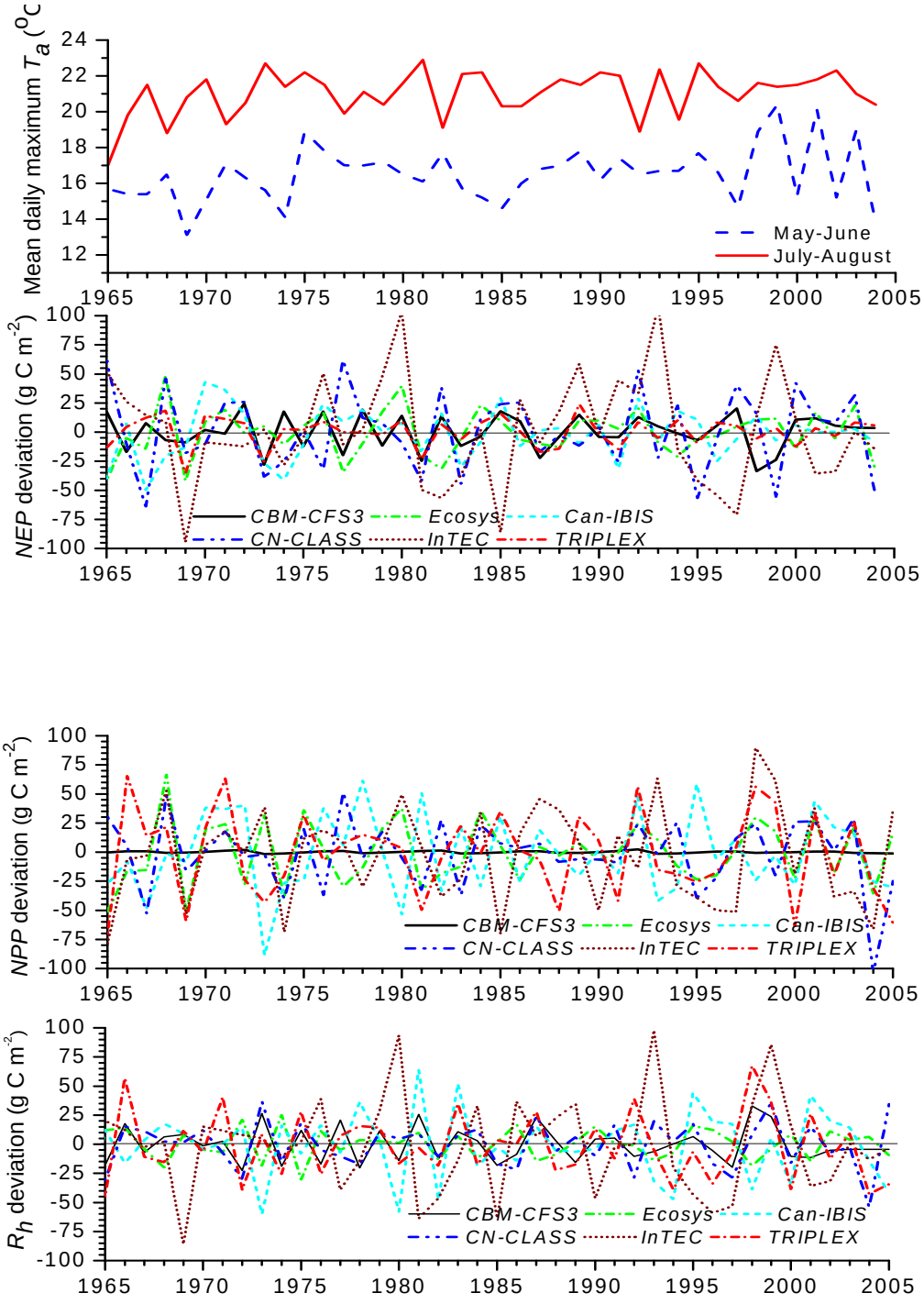

Figure 8. Responses of modelled *NEP, NPP* and R_h to mean daily maximum air temperature in summer (July-August) and spring (May-June) during 1965-2004.

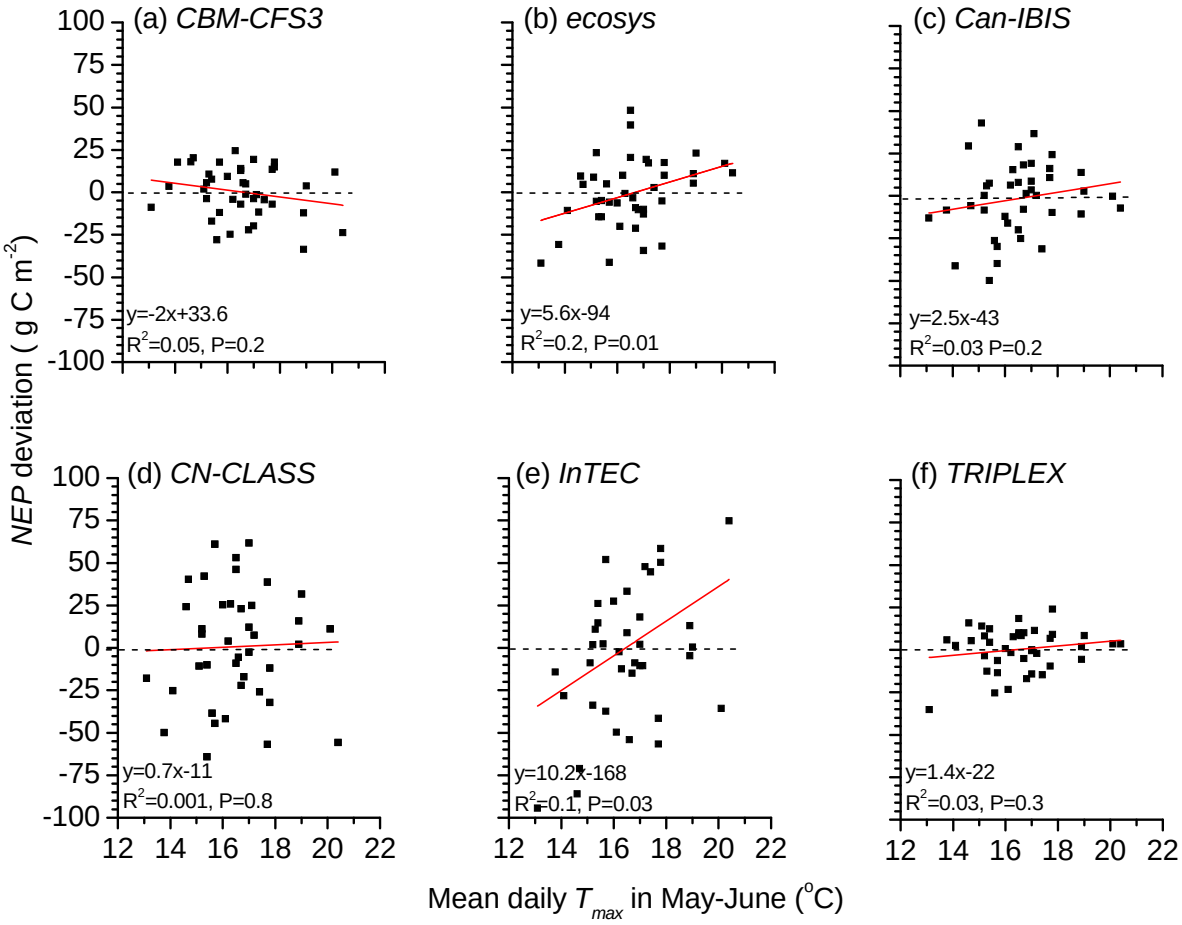

Figure9. Regressions of modelled *NEP* deviations to mean daily maximum temperature in spring during 1965-2004.

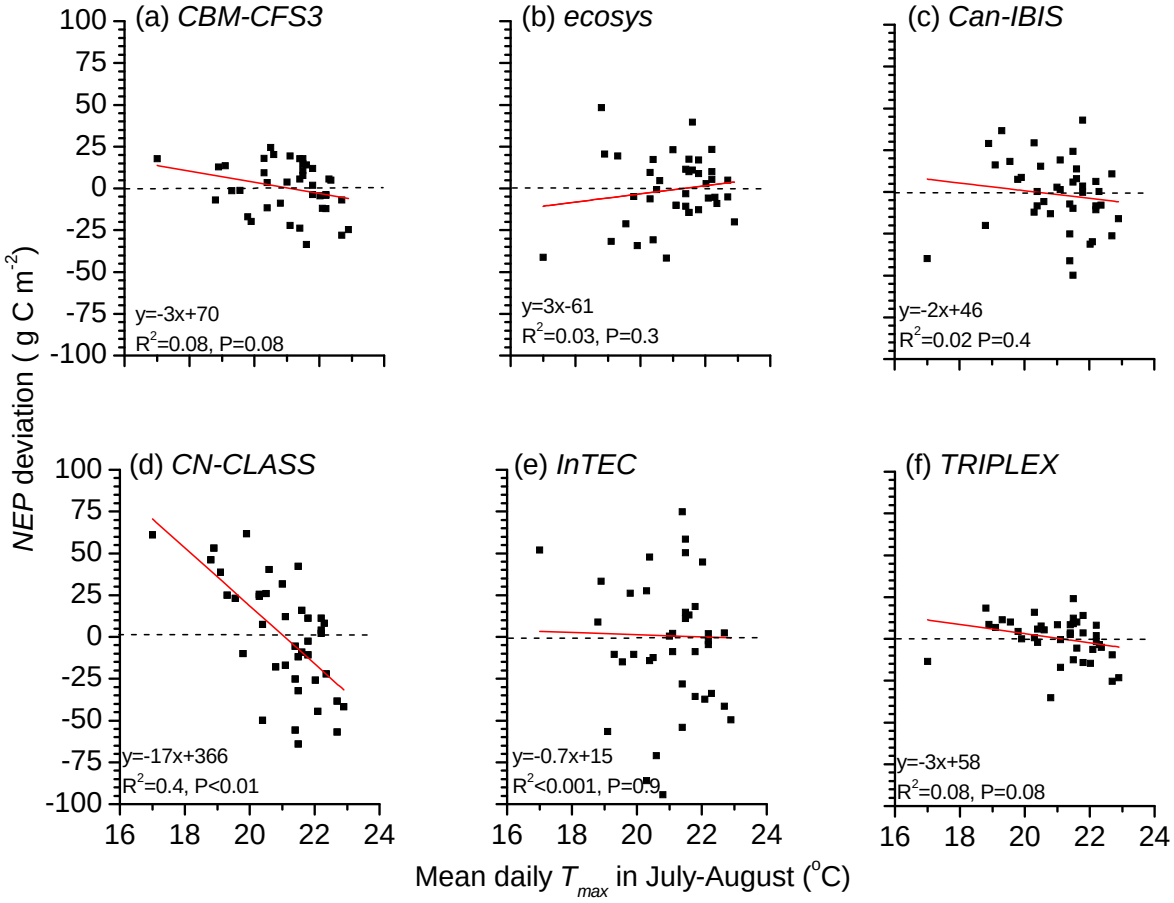

Figure 10. Regressions of modelled NEP deviations to mean daily maximum temperature in summer during 1965-2004.

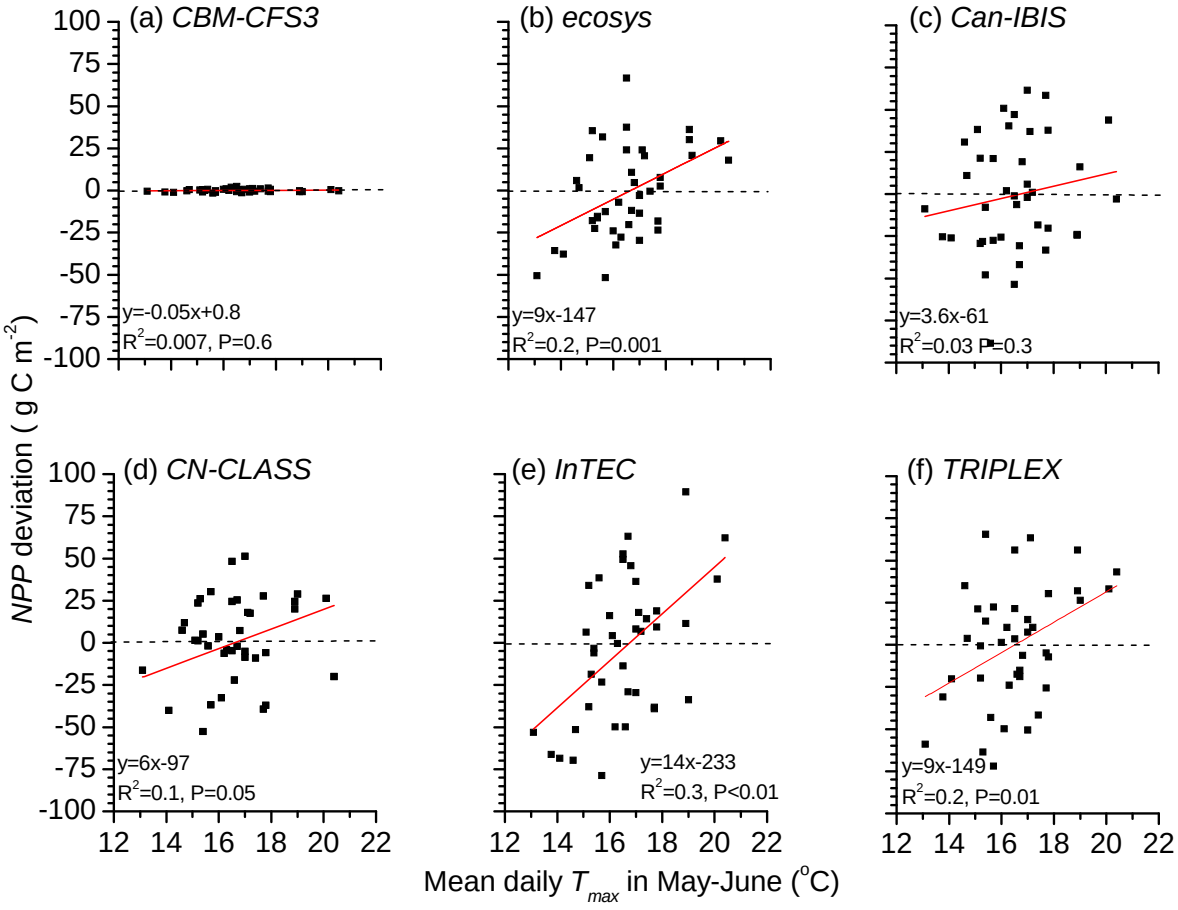

Figure 11. Regressions of modelled NPP deviations to mean daily maximum temperature in spring during 1965-2004.

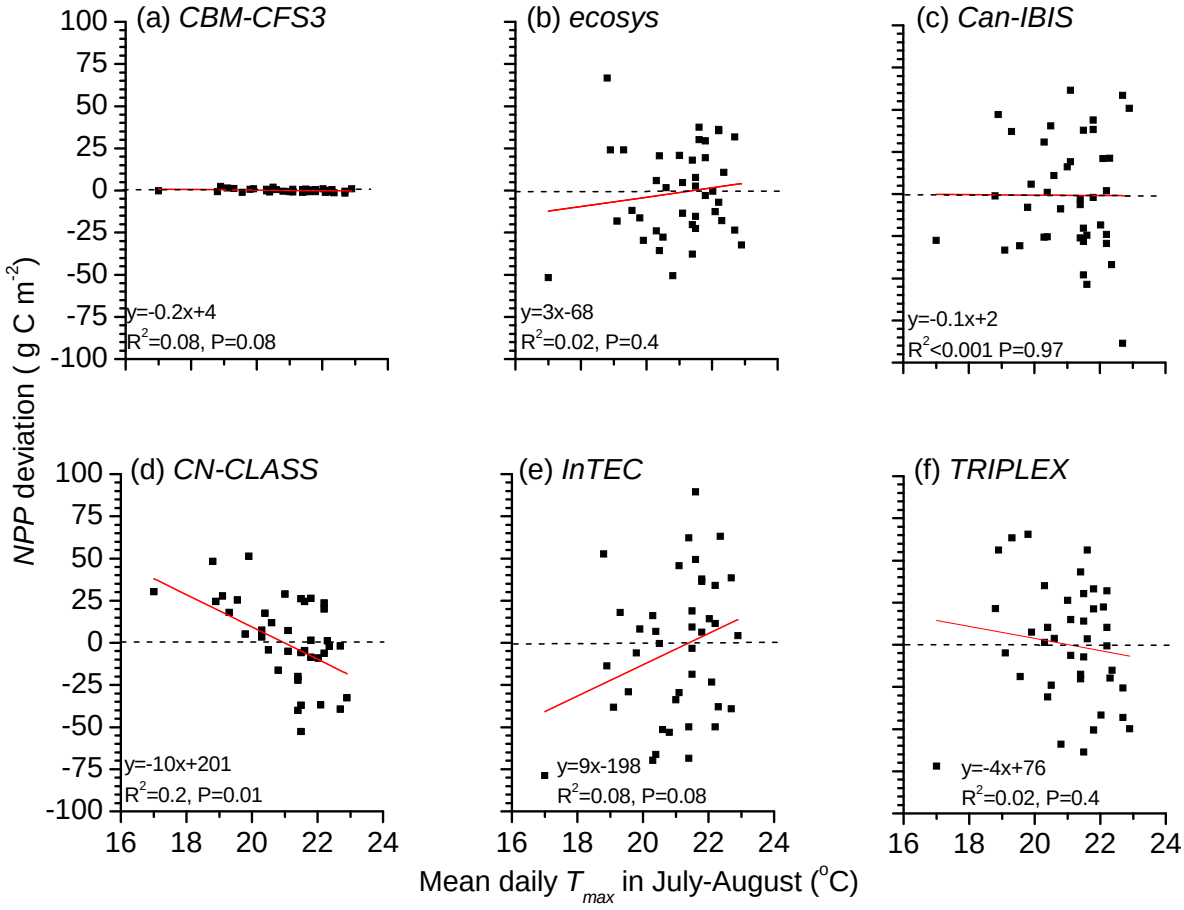

Figure 12. Regressions of modelled *NPP* deviations to mean daily maximum temperature in summer during 1965-2004.

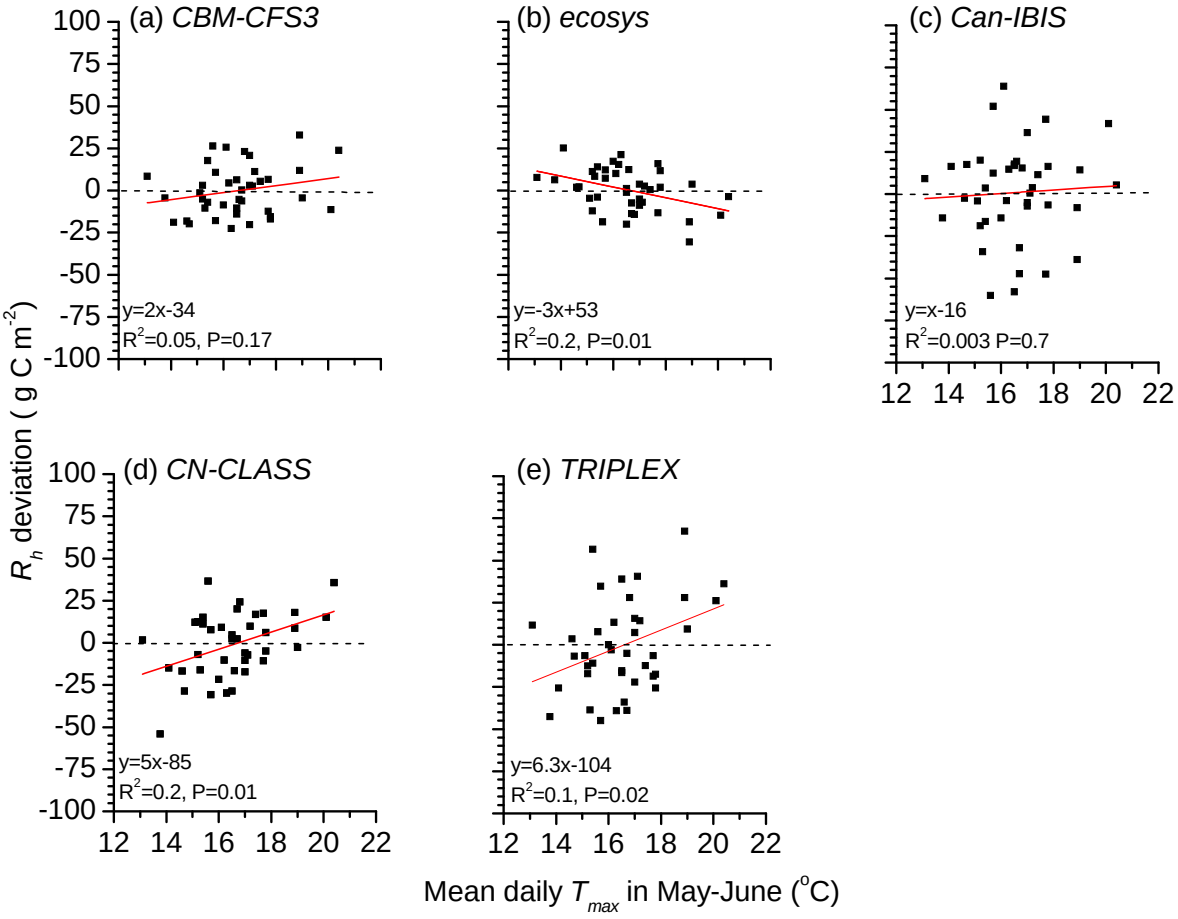

Figure 13. Regressions of modelled R_h deviations to mean daily maximum temperature in spring during 1965-2004.

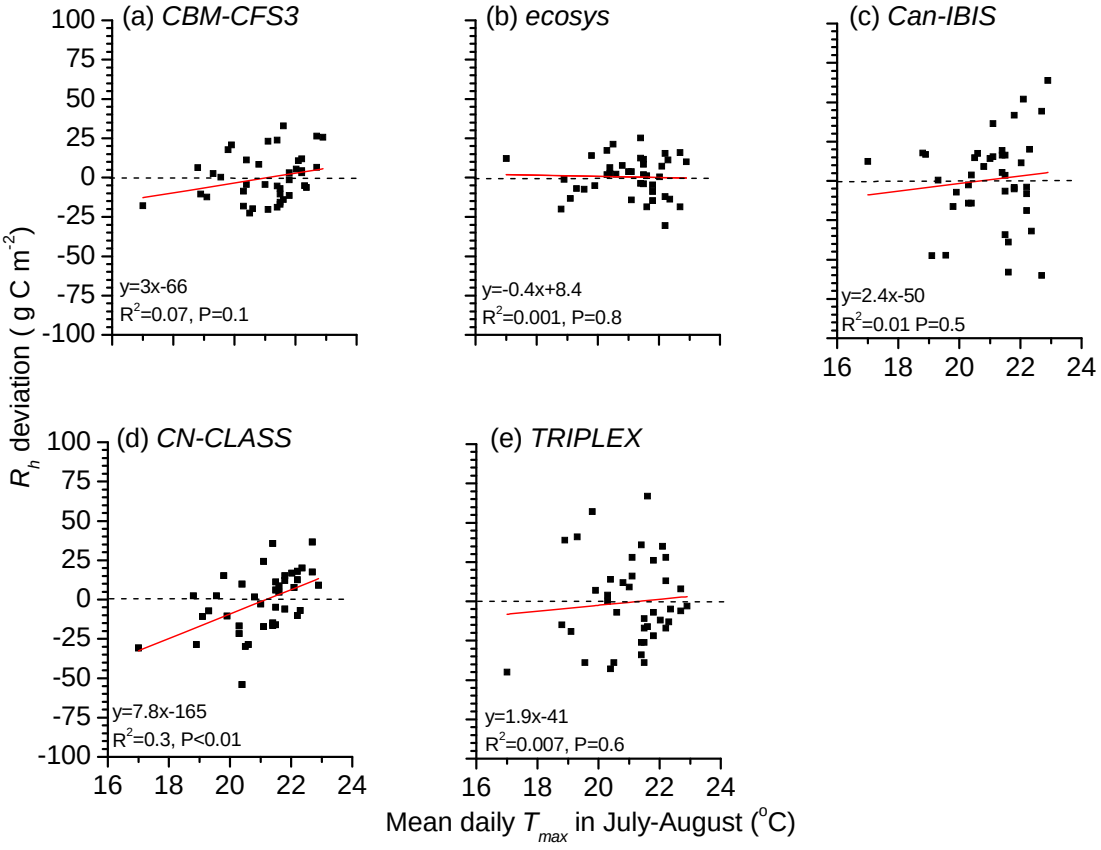

Figure 14. Regressions of modelled R_h deviations to mean daily maximum temperature in summer during 1965-2004.

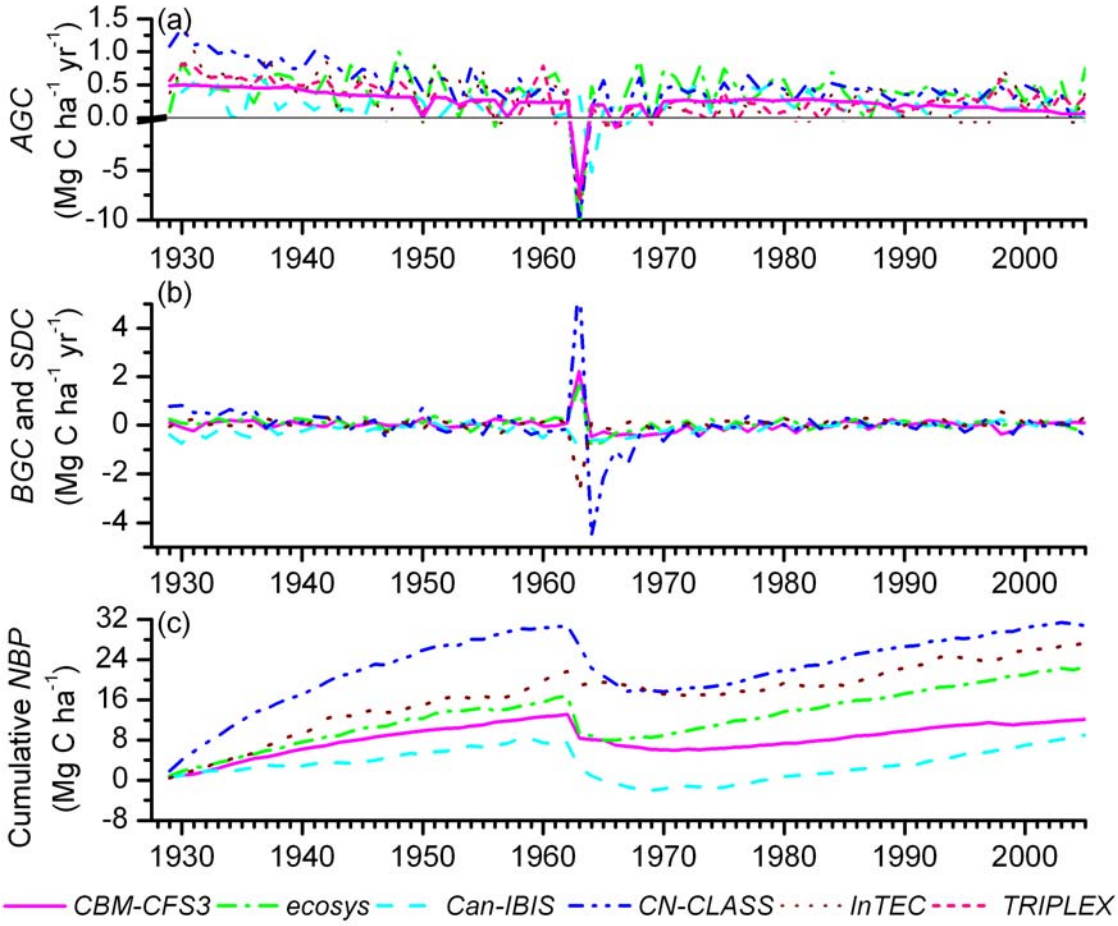

Figure 15. Average above-ground living biomass C (*AGC*), below-ground C (*BGC*) and surface dead organic C (*SDC*), and cumulative net biome productivity (*NBP*) modelled in the forested grid cells at CH during 1929-2005

Appendix: Key algorithms used in the models. (N/A = not applicable or available)

A.1 CO_2 Fixation	***ecosys***	***Can-IBIS***	***C-CLASS***	***InTEC***	***TRIPLEX***
A.1.1 maximum rubisco-limited CO_2 fixation rate V_{rmax} and maximum electron transport rate J_{max}	V_{rmax} = 45 μmol g^{-1} activated rubisco s^{-1} at 25ºC for all C_3 plants; J_{max} = 450 μmol g chlorophyll s^{-1} at 25ºC for all C_3 plants	V_{rmax} varies with plant functional types (PFT): cool temperate needleleaf evergreen (CTNE, Oyster River): 85 μ mol m^{-2} (leaf area) s^{-1} at 15 °C; J_{max}: N/A	$V_{rmax}(N_{rub0}) = \alpha[1-\exp(-1.8N_{rub0})]$ ***Where*** $\alpha = 39.0\,\mu molm^{-2}s^{-1}$; $N_{rub0} = \frac{N_{rub}N_{id}}{1-\exp(-k_nL)}$ ***N_{rub} is total Rubisco-related nitrogen (g N m^{-2} ground area) in the canopy; N_{id} is canopy N inverse decay distance; k_n is exponential coefficient for N_{rub} decline from top to bottom canopy. L is LAI (>1).*** ***J_{max}=2.7*V_{rmax}***	V_{rmax}= 60 μmol m^{-2} s^{-1} at 25ºC for all forest types; $J_{max} = 29.1+1.64*V_{cmax}$	V_{rmax}= 45 μmol m^{-2} s^{-1} at 25ºC for all forest types; $J_{max} = 29.1+1.64*V_{cmax}$
A.1.2 temperature effect on photosynthesis	For V_r and J, Arrhenius function of canopy temperature: E_a = 57.5 kJ mol^{-1} with low and high temperature inactivation where E_a is the energy of	For V_r, Follows Leuning (2002) Arrhenius function: for T_l > -10 ºC, else 0.0. $V_f = \frac{C\exp[(E_a/RT_0)(1-T_0/T_l)]}{1+\exp[(S_vT_l-H_d)/(RT_l)]}$ where V_f is the multiplier	For V_r and J, $\left(\frac{T_{max}-T_l}{T_{max}-T_{opt}}\right)\left(\frac{T_l-T_{min}}{T_{opt}-T_{min}}\right)^{(T_{opt}-T_{min})/(T_{max}-T_{opt})}$ T_{min} = 0ºC; T_{opt}= 35ºC;	$2.3^{\frac{25-T}{10}}$ for V_r and J	$2.4^{\frac{25-T}{10}}$ for V_r and J

	activation (Bernacchi et al., 2001; 2003)	applied to V_r and $C = 1 + \exp[(S_v T_0 - E_d)/(RT_0)]$ E_a, E_d, S_v are PFT-specific parameters, T_0 is a reference temperature (normally 298.16 K), T_l is average leaf temperature (K), R is the gas constant; For J, N/A	T_{max}= 45°C.		
A.1.3 water effect on photosynthesis	$V_r\, f(e^{-b\psi_T}) = g_l\,(C_a - C_i)$ where b =3; $\psi_T = \psi_c - \psi_\pi$ where ψ_T is the canopy turgor potential, ψ_c is the canopy water potential, ψ_π is the osmotic potential. ψ_c is solved when transpiration – uptake = change in water content: $(e_a - e_{ciTci})/(r_{ai} + r_{ci}) - \Sigma_l \Sigma_z (\psi_{ci} - \psi_{sl})/(\Omega_{s_{i,l,z}} + \Omega_{ri,l,z} + \Sigma_x \Omega_{ai,l,z,x}) = M_{c(t)}\theta_{ci\psi ci(t)} - M_{c(t-1)}\theta_{ci\psi ci(t-1)}$ where e^a is atmospheric vapor density at T^a and ambient humidity; e_{ciTci} is canopy vapor density at T^c for plant species i; r^a is aerodynamic resistance; r^c is stomatal resistance; l is for canopy layer; z is for root; ψ^c is canopy water potential; ψ^s is soil water potential; Ω^s is radial resistance to water transport from soil to surface of roots; Ω^s is radial resistance to water transport from surface to	Empirical function of available water content, θ_{avail}, in rootable soil layers. S is a water stress coefficient (between 0 and 1.0 where 1.0 implies no stress), computed as a root-fraction-weighted average of values for each soil layer, k, according to PFT-specific parameters. When $\theta_{avail}(k)$ is below field capacity $\theta_{fc}(k)$, (ice-free pore space): $S_{dry}(k) = 1.582 F_{root}(k) \times [1 - \exp(-\theta_{avail}(k) S_j)]$ where S_j is a PFT-specific drought tolerance factor (1.05 for CTNE). The factor 1.582 ($\approx 1/(1-e^{-1.0})$) normalizes the stress function. F_{root} is the fraction of total root biomass computed following Jackson et al. (1996, 1997) separately for upper and lower plant canopies. For $\theta_{avail}(k)$ above field capacity: $S_{wet}(k) = F_{root}(k) \times [1 - 2.0(\theta_{avail}(k) - \theta_{fc}(k) S_j)^2]$ and $S(k) = \min\{S_{dry}(k), S_{wet}(k)\}$ otherwise	Through effect on canopy conductance as shown in A. 2.1	through effect on canopy conductance $g_c = g_{l,sunlit} A_{l,sunlit} + g_{l,shaded} A_{l,shaded}$	N/A

	axis of roots; Ω^a is axial resistance to water transport along axes of primary (x=1) or secondary (x=2) roots; M^c is phytomass C; θ is canopy water content. (Grant and Flanagan, 2007)	$S(k) = S_{dry}(k)$			
A.1.4 nitrogen effect on V_r and J	rubisco concentration = *f*(leaf structural N:C) rubisco activation = *f*(leaf non-structural N:C) chlorophyll concentration = *f*(leaf structural N:C) chlorophyll activation = *f*(leaf non-structural N:C) (Grant et al., in press)	$V_r = V_{\tau max}$ * min{1.0, N:C_{leaf} / N:$C_{V\tau max}$} N:$C_{V\tau max} \approx 0.036$ (CTNE); For *J,* N/A	Through effect on V_{rmax} as shown in A.1.1	V_r=0.75 for coniferous forests V_r=1.0 for broadleaf forests	$V_r = V_{\tau max}$ * f(N) f(N) =(N / N_{max}) ≈ 0.8
A.2 Canopy Conductance	***ecosys***	***Can-IBIS***	***C-CLASS***	***InTEC***	***TRIPLEX***
A.2.1 water effect on leaf conductance g_l	$r_l = r_{l\min} + (r_{l\max} - r_{l\min})e^{-b\psi_T}$, $r_l = g_l^{-1}, r_{l\min} = g_{l\max}^{-1}$, $g_{l\max} = V_l/(C_a - C_i), \psi_T = \psi_c - \psi_\pi$, b = 5 where g_l is stomatal conductance, V_l is CO_2 fixation rate of leaf surface, c_a is atmospheric CO_2 concentration, c_i is the intercellular CO_2 concentration, r_l is the leaf diffusive resistance (Grant and Flanagan, 2007)	Ball–Berry model of leaf conductance (e.g. Ball et al. 1987) with water stress effects applied both to V_{rmax} and leaf stomatal conductance, (g_l), for separate sunlit and shaded canopy fractions: $g_l = (mA_nH_r)/C_S + bS$ where A_n is the calculated net photosynthesis rate, H_r is relative humidity at the leaf surface, C_s is the computed CO_2 concentration at the leaf surface and linearization coefficients m and b are set to 5.0 and 0.01, respectively, for conifer PFTs. Note that A_n is also a function of S, due to effect on V_{rmax} (See A.1.3). Total canopy conductance is weighted by the *LAI* fractions simulated for each PFT and expressed as a canopy water	$g_c = g_{lmin} + mf_w V_l / \{(C_i - \Gamma)(1+D/D_0)\}$ g_{lmin} = 0.01 mol m^{-2} s^{-1} m = 3, D_0 = 1 kPa $f(\theta_s) = \min\left(1, \frac{3(\theta_s - \theta_{\min})}{\theta_{\max} - \theta_{\min}}\right)$ θ_s is root zone θ; θ_{min} is θ at wilting point; θ_{max} is θ at field capacity (Arain, et al., 2006)	*if* $\psi < -100\,kPa$ $f(\psi i) = 1 + (\frac{-\psi i - 100}{100})^{0.75}$ *else* $f(\psi_l) = 1$ ψ is soil water potential (kPa)	$G_c = g_l^*$ * LAI *min(VPD,fsw) fsw is modifier soil water on forest growth

		vapor transfer coefficient. Values of *S(k)* are used to allocate root water uptake from each soil layer, $Q_t(k)$, contributing to total evapotranspiration for each canopy, c (1=lower, 2=upper): $Q_t(k) = E_{tc} L_c f_c S(k) / S_{tc}$ where E_{tc} and S_{tc} are total transpiration and total S, and L_c and f_c are *LAI* and fractional cover, respectively, for canopy c.			
A.3 Autotrophic Respiration	***ecosys***	***Can-IBIS***	***C-CLASS***	***InTEC***	***TRIPLEX***
A.3.1 temperature effect on R_a	Arrhenius function of canopy or root temperature: E_a = 57.5 kJ mol^{-1} with low and high temperature inactivation. R_a first meets maintenance respiration R_m calculated from an exponential function of T_c (Q_{10} = 2.25), then growth respiration which drives plant growth	Follows Lloyd and Taylor (1994): Arrhenius function of tissue temperature T_i (leaves, stem, fine roots) $f(T_i) = \exp\left[E_0\left(\frac{1}{15-T_0} - \frac{1}{15-T_i}\right)\right]$ T_0 = 15 °C E_0 = 3500.0 (gives $Q_{10} \approx 1.5$)	Through a Q_{10} function of canopy temperature as follows: $f_l(T_l) = Q_{10,l}^{(T_l-15)/10}$ $Q_{10,leaf}$ = 2.0 (T_l > 5 °C) $Q_{10,froot}$ = 2.0 (T_l > 5 °C) $Q_{10,wood}$ = 1.5 (T_l > 5 °C) $Q_{10,croot}$ = 1.5 (T_l > 5 °C) Q_{10} = 4.0 ($0 < T_l < 5$ °C) T_l, leaf or canopy temperature Subscript *froot,* fine root Subscript *croot,* coarse root	***through effects on maintenance respiration R_m and CO_2 fixation rate by the canopy V_c*** ***For R_m,*** $2.3^{\frac{T-25}{10}}$	***N/A***
A.4 Heterotrophic Respiration	***ecosys***	***Can-IBIS***	***C-CLASS***	***InTEC***	***TRIPLEX***
A.4.1 temperature effect on R_h	Arrhenius E_a = 57.5 kJ mol^{-1} with low and high temperature inactivation. R_h first meets maintenance respiration R_m calculated from an exponential function of T_s (Q_{10} = 2.25) , then growth respiration which drives microbial growth	Follows Lloyd and Taylor (1994) : Arrhenius function, computed hourly and averaged daily, where soil temperature T_s > -36 °C and baseline T_0 = 15 °C $f(T_s) = \exp\left[T_c\left(\frac{1}{T_0-227.13} - \frac{1}{T_s-227.13}\right)\right]$ T_c =344.0 and T_0 in K. Soil decomposition is calculated using average temperature of all rootable soil layers; litter decomposition is calculated	Through a Q_{10} function for organic matter decomposition as shown below: $f(T_s) = Q_{10soil}^{(T_s-10)/10}$ Q_{10} = 2.0 (T_s>10 °C) Q_{10} = 4.0 (T_s<10 °C) T_s is the temperature at the upper soil layer (10 cm)	$e^{308.56\left(\frac{1}{35+46.032} - \frac{1}{T+46.32}\right)}$	Q_{10} = 2.0

		using T_s for top soil layer only.		
A.4.2 water effects on R_h	$R_h = R_h' Q_{O2}/Q'_{O2}$ Where R_h'=0.125 g C gmicr. C^{-1} h^{-1} at 25 °C Q_{O2} = O_2 uptake Q'_{O2} = O_2 demand $D'_{Si,j,C}$ = $\{D'_{Sj,C}[S_{i,C}]\}/\{[S_{i,C}] + K_{mD}(1.0 + [\Sigma_n M_{i,n,a}]/K_{iD})\}$ Where $D'_{Si,j,C}$ is specific decomposition of S by microbial biomass M at 25 °C and ambient solid organic matter S; K_{mD} is Michaelis-Menten constant for D_s. (Grant and Flanagan, 2007)	For available water content (AWC) of ice-free soil pore space %, $f(\theta) = \exp\left[\frac{(\theta - 60)^2}{-800.0}\right]$ when AWC < 60%, $f(\theta) = 0.000371\theta^2 - 0.0748\theta + 4.13$ when AWC ≥ 60% Where θ is soil water content	$f(\theta_s) = (\frac{\theta_s}{a_1 - \theta_s})(\frac{a_2}{a_2 - \theta_s})$ Where θ_s is volumetric soil water content of the root zone, a_1 is one-half field capacity water content, a_2 is one-half porosity	For coarse soil, $5.44(\frac{\theta}{\theta_s}) - 5.03(\frac{\theta}{\theta_s})^2 - 0.472$ For medium to fine soil, $5.63(\frac{\theta}{\theta_s}) - 4.64(\frac{\theta}{\theta_s})^2 - 0.710$